UNIVERSIDAD AUTÓNOMA DE MADRID
FACULTAD DE CIENCIAS
Departamento de Ingeniería Química

SISTEMAS AVANZADOS BASADOS EN LÍQUIDOS IÓNICOS PARA LA CAPTURA Y CONVERSIÓN DE GASES

ADVANCED SYSTEMS BASED ON IONIC LIQUIDS FOR GAS CAPTURE AND CONVERSION

Tesis Doctoral

RUBÉN SANTIAGO LORENZO

Madrid, 2019

UNIVERSIDAD AUTÓNOMA DE MADRID
FACULTAD DE CIENCIAS
Departamento de Ingeniería Química

SISTEMAS AVANZADOS BASADOS EN LÍQUIDOS IÓNICOS PARA LA CAPTURA Y CONVERSIÓN DE GASES

ADVANCED SYSTEMS BASED ON IONIC LIQUIDS FOR GAS CAPTURE AND CONVERSION

MEMORIA

para optar al grado de

Doctor con Mención Internacional

y al sello

International PhD

que presenta

Rubén Santiago Lorenzo

bajo la dirección de:

Dr. José Francisco Palomar Herrero

Dr. Jorge Bedia García Matamoros

Madrid, 2019

D. José Francisco Palomar Herrero, Profesor Titular de Universidad y **D. Jorge Bedia García Matamoros**, Profesor Contratado Doctor Interino, ambos profesores del Departamento de Ingeniería Química, de la Universidad Autónoma de Madrid,

HACEN CONSTAR: que el presente trabajo, titulado: *"Sistemas avanzados basados en líquidos iónicos para la captura y conversión de gases",* presentado por D. Rubén Santiago Lorenzo, ha sido realizado bajo su dirección, en los laboratorios del Departamento de Ingeniería Química, de la Universidad Autónoma de Madrid y que, a su juicio, reúne los requisitos de originalidad y rigor científico necesarios para ser presentados como Tesis Doctoral mediante compendio de artículos conforme al artículo 8 del Procedimiento relativo al tribunal, defensa y evaluación de la tesis doctoral en la Universidad Autónoma de Madrid.

Y para que conste a efectos oportunos, firmamos el presente informe en Madrid, a 3 de septiembre de 2019.

José Francisco Palomar Herrero Jorge Bedia García Matamoros

La realización de este trabajo ha sido posible gracias al apoyo económico del Ministerio de Economía y Competitividad (MINECO) a través de los proyectos **CTQ2014-52288-R** y **CTQ2017-89441-R,** de la Comunidad de Madrid (Referencia **P2013/MAE-2800** y **P2018/EMT4348**), así como a la concesión de una beca de Formación de Personal Investigador (FPI) del MINECO (Referencia **BES-2015-075555**).

A mi madre, mi padre y mi hermano

AGRADECIMIENTOS

En primer lugar, me gustaría comenzar agradeciendo a mis directores de tesis, Dr. José Palomar y Dr. Jorge Bedia por dirigirme y tutelarme durante estos últimos años para la consecución del objetivo. Gracias Pepe por darme la oportunidad de poder trabajar en tu magnífico grupo de investigación y por apostar y confiar en mí, incluso ni cuando yo mismo lo hacía. Estoy seguro de que el trabajo de estos últimos años no es más que el principio de todo lo que nos queda por delante. Gracias también a ti Jorge por tu plena disponibilidad para ayudarme y guiarme en las numerosas dudas y cuestiones que me han surgido durante el transcurso de esta tesis. Gracias a los dos, porque habéis hecho que todo resulte mucho más fácil. Ha sido un verdadero placer trabajar con vosotros.

Gracias al Dr. Juan José Rodríguez por sus consejos y las fructíferas reuniones científicas mantenidas a lo largo de los últimos años. La verdad es que es una gran suerte poder disfrutar de ti en este Departamento.

I would also like to thank Professor Rasmus Fehrmann for giving me the opportunity to work on his wonderful investigation group on ionic liquids. There were three wonderful months at Technical University of Denmark that I will never forget. Of course, I would also want to thank Dr. Susanne Mossin for her help and support during my stay there at DTU. I cannot forget thanking the entire Centre for Sustainable Chemistry & Catalysis. Specially, thanks to Kjartan, David and Anders for their great support, for becoming more friends than colleagues. Thanks to Christina, Joey and Mathilde for becoming my new Danish family. I will never forget you all.

Por supuesto no puedo olvidarme de todos mis compañeros del ya Departamento de Ingeniería Química. Gracias, Cris por tu gran acogida, por convertirte en gran compañera desde mi llegada. Gracias también a ti Carlos, por acompañarme en este duro viaje desde el primer día, por las "chops" y por los innumerables momentos de risas dentro y fuera de la UAM. Gracias Anita por ser como eres, por contagiar esa sonrisa y ese ánimo que te caracteriza. Gracias también a Alicia por ser compi de mesa y apoyo durante estos últimos casi 4 años, por estar siempre dispuesta a echar una mano y por cuidarnos y alimentarnos en el IQ3. Gracias Gonzalo por aportarme tanto en tan poco tiempo. Gracias Inés por convertirte también en más amiga que compañera, por las risas y los momentos desconexión en el IQ3. Por supuesto no puedo olvidarme de mis compis de la planta. Gracias Esther por como eres, por tu imborrable sonrisa, por entenderme más que nadie, por las risas dentro y fuera de la UAM. Gracias Javi por ser mi segundo yo, por las incontables conversaciones de fútbol y tonterías varias, por tu gran apoyo. Gracias a todos, sin vosotros nada hubiera sido lo mismo.

Gracias a todos los miembros de los laboratorios del módulo C6 y planta piloto, Antonio, Pablo, Jeff, Lucía, Sandra, Pepelu, Alejandro H., Cris G., Andrés, Adriana, Dani H., Jose, María, Jaime, Manu, Almudena, Gonzalo, Manu, Álvaro, Isma, Inés S. Gracias también a Luis y Javi, nuestros técnicos de laboratorio, gracias por vuestra incalculable ayuda.

Mención especial merece el equipo "LIs". Creo que no puedo estar más agradecido de haber compartido estos últimos años de trabajo con vosotros tres. Gracias Cristian, por tanto. Gracias por enseñarme todo lo que ha estado en tu mano desde el día 1, por ser un apoyo diario, por convertirte en un gran amigo. Gracias Dani por tu siempre disposición para ayudar, por ser un gran compañero. Es imposible no aprender de ti

cada día. Especialmente, me gustaría dar las gracias a Jesús, por ser apoyo y referente, por convertirse en un gran amigo, por enseñarme tanto cada día, por escucharme y ayudarme. Gracias a los tres por formar un verdadero equipazo, por los viajes, por los momentos fuera y dentro de la UAM, por las “chops” y los “anisillos”. Sin duda, sin vosotros tres todo hubiera sido mucho más difícil.

No puedo olvidarme de todos los estudiantes que decidieron trabajar con nosotros en sus TFG y TFM. Gracias Irene, Virginia, Ana, April, Javi. Guardo un gran recuerdo de todos vosotros.

Gracias a mis amigos por su apoyo incondicional hoy y siempre. Especialmente gracias, Nacho, Pérez, Gil, Llanos y Gonxo. Gracias también a mis abuelos, tíos y primos por estar conmigo en cada decisión que he tomado, por quererme y apoyarme.

Si hay tres personas a las que estoy especialmente agradecido son mis padres y mi hermano. Gracias, papá, por ser mi referente, por enseñarme que con trabajo duro puedo conseguir todo lo que me proponga. Gracias, mamá, por el día a día, por el amor incalculable que me das, por tu apoyo incÏ ÎÄÉÃÉÏ ÎÁÌ cada día. Gracias Mario por quererme por transmitirme esa paz y tranquilidad, por ser apoyo en la sombra. No hay día que no aprenda algo de ti. Gracias a los tres, por dármelo todo sin pedir nada a cambio.Si este logro significa algo, no dudéis que es tan mío como vuestro.

Por último, tengo que darte las gracias a ti Claudia, mi compañera de vida. Gracias por aparecer en mi vida para quedarte definitivamente en ella. Gracias por tu apoyo, tus consejos, tu infinita paciencia, pero sobre todo por el día a día, por cuidarme y quererme. Estoy seguro de que esto sólo es el comienzo de todo el camino que nos queda por recorrer juntos.

INDEX

1. ABSTRACT/RESUMEN 1

2. INTRODUCTION 17

2.1 IONIC LIQUIDS 19

2.1.1 Ionic liquid properties *20*

2.1.2 Ionic liquid process engineering *22*

2.1.3 Industrial applications of ionic liquids *23*

2.2 GAS ABSORPTION WITH IONIC LIQUIDS 26

2.2.1 Carbon dioxide (CO_2) *26*

2.2.1.1 CO_2 emissions 26

2.2.1.2 CO_2 capture configurations 28

2.2.1.3 Available CO_2 capture technologies 31

A. Chemical absorption with aqueous amines 31

B. Other absorption systems 34

C. Adsorption 36

D. Other technologies 37

2.2.1.4 CO_2 capture with ionic liquids 38

A. Physical absorption 39

B. Chemical absorption 40

2.2.2 Acetylene (C_2H_2) *42*

2.2.2.1 Importance of acetylene 42

2.2.2.2 Production of acetylene 44

2.2.2.3 Available technologies for acetylene treatment 45

2.2.2.4 Acetylene capture with ionic liquids 46

2.2.3 Hydrogen Sulfide (H_2S) *47*

2.2.3.1 H_2S as contaminant 47

2.2.3.2 Available technologies for H_2S treatment 49

2.2.3.3 H_2S capture with ionic liquids 51

2.2.4 Nitrogen Oxide (NOx) *52*

2.2.4.1 NOx emissions 52

2.2.4.2 Available technologies for NOx treatment 53

2.2.4.3 NOx capture with ionic liquids 55

2.3 ADVANCED MATERIALS BASED ON IONIC LIQUIDS 56
2.3.1 Supported Ionic Liquid Phase (SILP) *56*
2.3.2 Encapsulated Ionic Liquids (ENILs) *57*

2.4 COMPUTATIONAL TOOLS FOR DESIGN SEPARATION PROCESSES BASED ON IONIC LIQUIDS 58
2.4.1 COSMO-RS method *59*
2.4.2 Process simulation *60*

2.5 MULTISCALE APPROACH FOR THE DESIGN OF PROCESSES BASED ON IONIC LIQUIDS 63

3. AIM & SCOPE 65

4. CONCLUSIONS/CONCLUSIONES 71

5. APPENDIX 81

5.1 ACETYLENE ABSORPTION BY IONIC LIQUIDS: A MULTISCALE ANALYSIS BASED ON MOLECULAR AND PROCESS SIMULATION 83

5.2 ASSESSMENT OF IONIC LIQUIDS AS H_2S PHYSICAL ABSORBENTS BY THERMODYNAMIC AND KINETIC ANALYSIS BASED ON PROCESS SIMULATION 85

5.3 FROM KINETICS TO EQUILIBRIUM CONTROL IN CO_2 CAPTURE COLUMNS USING ENCAPSULATED IONIC LIQUIDS (ENILS) 87

5.4 ENCAPSULATED IONIC LIQUIDS TO ENABLE THE PRACTICAL APPLICATION OF AMINO ACID-BASED IONIC LIQUIDS IN CO_2 CAPTURE 89

5.5 CO_2 CAPTURE BY SUPPORTED IONIC LIQUID PHASE (SILP): HIGHLIGHTING THE ROLE OF THE PARTICLE SIZE 91

5.6 METHANOL PROMOTED OXIDATION OF NITROGEN OXIDE (NOX) BY ENCAPSULATED IONIC LIQUIDS (ENILS) 93

REFERENCES 95

Publications related to this PhD Thesis 111

Other publications 113

1. ABSTRACT/RESUMEN

ABSTRACT

Nowadays, it is important to develop new technologies able to substitute traditional ones to avoid the emissions of toxic or harmful gases to the atmosphere. In this sense, it should be noted that CO_2, H_2S, NOx and C_2H_2 are among gases typically removed by absorption processes in the chemical industry. ILs are receiving great attention as potential solvents due to their unique properties, such as low vapor pressure, high thermal and chemical stability, and high solvent capacity, among others. Moreover, the fact that ILs are formed by a cation and an anion offers a great number of possible combinations, which allows to design the solvent for specific applications. This research work aims to the development and evaluation of systems based on ILs to capture C_2H_2, H_2S and CO_2 by chemical and physical absorption. Moreover, the last part of the work opens a new application of ILs to, not only capture, but also convert NO to value-added compounds.

This PhD thesis is divided in six different works, each one published in a scientific journal (see Appendix section).

The first work of this thesis studies the potential application of ILs as acetylene absorbents. COSMO-based/Aspen Plus multiscale simulation methodology was employed as computational tool to select and evaluate ILs for the task. First, molecular simulation using COSMO-RS method was used to select the potential ILs presenting most suitable thermodynamic and kinetic properties among more than 300 ILs for C_2H_2 capture. For comparison purposes, N,N-dimethylformamide (DMF) was used as benchmark industrial solvent. Molecular simulations showed ILs with competitive properties in molar and mass terms in relation with those of DMF. The analysis of the solute-ILs interactions revealed that absorption

is governed by the anion nature. Specifically, ILs with hydrogen bond acceptor character will have stronger interactions due to the acidic character of acetylene. On the other hand, diffusivity results showed the kinetic limitations of ILs compared to DMF due to their higher viscosity. Second, Aspen Plus process simulator was used to evaluate the performance of the ILs with competitive characteristics compared to those of DMF in both the absorption operation and regeneration stage. Thermodynamic analysis concluded that at least two of the studied ILs were competitive with the benchmark solvent, with even lower solvent consumption and less separation stages. However, kinetic analysis in a packed column showed that operation with ILs is governed by mass transfer kinetics, resulting in higher solvent consumption, higher operating temperatures, and higher absorption column dimensions compared to those of DMF. Lastly, the analysis of the regeneration stage concluded the great advantage of using ILs, reaching higher C_2H_2 purities and recoveries and less energy consumption than when using DMF in the process.

Second work aims to the evaluation of ILs as potential H_2S absorbents. It used the same methodology described for first work. In this case, ILs screening among more than 700 ILs revealed that H_2S physical absorption is mainly controlled by the anions able to form hydrogen bond with the acidic character of the solute. A collection of ILs with favorable properties for H_2S absorption was selected for their application as absorbents in packed column by means of Aspen Plus process simulations. Equilibrium based calculations in absorption column were in good agreement with those of molecular simulation, revealing higher efficiencies in terms of solvent consume by decreasing Henry's law constants of H_2S in ILs. However, rigorous absorption

column simulation showed the strong mass transfer kinetic control in packed columns using ILs. Consequently, ILs with the best performance in thermodynamic aspect, become worse for the operation. On the contrary, those ILs with lower viscosities require less solvent consumption, lower operating temperatures and lower absorption column sizes.

These first two works demonstrated the great mass transfer limitations of ILs in gas capture due to their high viscosity. For this reason, in the third work Encapsulated Ionic Liquids (ENILs) are presented to overcome the kinetic limitations in CO_2 physical capture with ILs. First, COSMO-based/Aspen Plus methodology was used to select four ILs with high and similar CO_2 absorption capacity but markedly different transport properties for their experimental evaluation. Simulations of packed absorption columns showed very high CO_2 recoveries (50 – 98%) when only thermodynamic equilibrium is taken into account for the majority of the ILs, and very different behaviors when mass transfer kinetics is considered (0.3 – 62%). In fact, CO_2 recoveries were ordered in decreasing order of ILs viscosity. This let us analyze the thermodynamic and kinetic behavior of ILs with very different viscosities when being encapsulated (ENILs). Experimental gravimetric results using pure ILs as absorbents reflected high and similar CO_2 absorption capacities but different kinetic behavior. Then, ENILs were prepared and their porous texture, elemental analysis and morphology characterized. Characterization results confirmed IL loadings around 80% in each material. Experimental results showed that CO_2 absorption capacity of ILs was maintained after encapsulation, whereas CO_2 absorption mass transfer kinetics was increased 50 times for ENILs in relation with that of pure ILs. Lastly, fixed-bed experiments

at different temperatures revealed that bed efficiency depends on the CO_2 solubility in ENIL, in contrast of the behavior of neat IL in CO_2 absorption, which is controlled by the unfavorable kinetic. Therefore, this work presents ENILs as a solution for problems of pure ILs in CO_2 physical capture processes. Therefore, the IL selection criteria moves from kinetics to CO_2 solubility aspects.

ENILs demonstrated to present a solution for problems of pure ILs in CO_2 physical capture processes. However, it has been widely reported the low absorption capacities that ILs with CO_2 physical absorption present compared to traditional amines. For this reason, the fourth work presents ENILs loaded with ILs that have CO_2 chemical absorption characteristics. In this sense, the performance of three amino acid based ILs (aa-ILs) was studied due to their low cost, abundant availability and high biodegradability. First, CO_2 chemical absorption by pure aa-ILs was experimentally analyzed by infrared spectroscopy. DFT calculations allowed proposing a reaction mechanism by comparing IR characteristic vibrational signals with those experimentally obtained. Then, CO_2 absorption capacity of pure ILs was analyzed by gravimetric measurements at three different temperatures, revealing that absorption was rather slow, because of their high viscosities, and solid formation while reacting with CO_2. Therefore, ENILs were prepared and characterized to enable the application of aa-ILs. Gravimetric results demonstrated the possibility of using ENILs to allow CO_2 absorption in these aa-ILs at three different temperatures. Lastly, a thermodynamic model was proposed to quantify physical (Henry's law constants) and chemical (equilibrium constants) contributions of CO_2 absorption for each IL. Enthalpies of reaction found were low compared to amines,

which would favor the reaction reversibility and sorbent regeneration and imply lower energy duty.

The two previous works reported the improvement on CO_2 absorption rate of ILs by the incorporation of ILs on a solid support. The fifth work of the Thesis studies the influence of the support particle size on CO_2 chemical absorption. In this case, Supported Ionic Liquids Phase (SILP) sorbents, using an acetate-based IL and silica as support, were used. First, SILPs with remarkably different particle sizes were prepared and characterized by analyzing their porous texture, morphology, thermal stability, and elemental composition. It was checked that IL nominal load for each particle size was almost the same and close to 40%. Second, experimental gravimetric CO_2 isotherms of the SILPs with three particle sizes were evaluated at three different sorption temperatures, revealing that equilibrium sorption capacity is only attributed to the IL incorporated on silica support. Langmuir-Freundlich model was used to successfully fit experimental CO_2 sorption isotherms. Third, kinetics of the process was evaluated by means of fixed-bed experiments at three different temperatures, gas flow rates, CO_2 partial pressures and SILP particle sizes. A linear driving force model successfully described experimental breakthrough curves. The analysis of kinetic coefficients revealed faster mass transfer rates by decreasing SILP particle size and increasing temperature and CO_2 partial pressure. Moreover, no external diffusion was found, obtaining same kinetic coefficients while increasing the gas flow rate through the fixed-bed. Lastly, Aspen Adsorption was used to model the operation thanks to a found relationship between the kinetic coefficients and the experimental variables of study. Simulations revealed that at low CO_2 partial pressures, chemical reaction is the controlling stage, whereas at higher

ones, diffusion into SILP is governing the process. This methodology allows designing CO_2 sorption systems based on SILPs at given conditions, minimizing SILP needing by optimizing particle size and type of IL.

The sixth and last work was able thanks to an international stay on Fehrmann's group at the Technical University of Denmark. This work tries to open the application of ENILs to catalysis in gas phase. It aims to evaluate the use of ENILs as NO oxidation catalysts at humid conditions and low temperatures. First, ENILs were prepared and characterized using the same techniques as in previous works. In this work, the performance of ENILs was compared to that of empty carbon capsules. Experimental conditions consisted of initial NO concentrations of 2,000 ppm, changing IL loading, O_2 and water content in a fixed-bed reactor. Experiments in dry conditions revealed higher activities of empty carbon capsules than those of ENILs, because reaction was occurring in the pores of the material. However, experiments in humid conditions concluded that reaction is not affected by the presence of water for ENILs. In the case of empty carbon capsules, the reaction was completely inhibited at high relative humidity. Then, methanol was tested to promote the reaction, being the MeOH/NO ratio optimized between 0.2 – 0.4. In sum, ENIL with 40% of IL loading exhibited the best performance on NO oxidation reaction to nitric acid.

RESUMEN

En la actualidad está adquiriendo importancia el desarrollo de nuevas tecnologías capaces de sustituir las ya presentes para evitar las emisiones de gases a la atmósfera. En este sentido, caben destacar el CO_2, H_2S, NOx y C_2H_2 entre los gases tradicionalmente eliminados por procesos de absorción en la industria química. Los líquidos iónicos (LIs) están recibiendo gran atención como disolventes alternativos debido a sus favorables propiedades, como son su baja presión de vapor, alta estabilidad térmica y química y alta capacidad disolvente, entre otras. Además, dado que están formados enteramente por un catión y un anión, existen un gran número de combinaciones posibles, que permiten el diseño de los mismos para aplicaciones específicas. El presente trabajo tiene como objetivo el desarrollo y evaluación de sistemas basados en LIs para la captura de C_2H_2, H_2S y CO_2 por absorción física y química. Además, la última parte del trabajo abre la posibilidad de una nueva aplicación para capturar y convertir NO a compuestos de alto valor añadido empleando LIs encapsulados.

La presente tesis doctoral está dividida en seis trabajos, cada uno de ellos publicado en una revista científica.

En el primer trabajo se estudia la posible aplicación de los LIs como absorbentes de acetileno. La metodología COSMO/Aspen Plus, desarrollada por el grupo de investigación en el que se enmarca esta tesis, se empleó como una herramienta computacional para seleccionar y evaluar un gran número de LIs. En primer lugar, se utilizó el simulador molecular COSMO-RS para seleccionar LIs que presenten propiedades adecuadas tanto termodinámicas como cinéticas (entre más de 300) para la captura de acetileno. N,N-dimetilformamida (DMF) se empleó

como disolvente industrial de referencia. Los resultados de la simulación molecular mostraron LIs con propiedades de absorción competitivas en unidades molares y másicas, comparadas con el DMF. El análisis de las interacciones soluto-LI reveló que el proceso de absorción está gobernado por la naturaleza del anión. Específicamente, aquellos LIs que presenten gran carácter aceptor de enlace de hidrógeno tendrán interacciones más fuertes con el acetileno, debido a su naturaleza ácida. Por otro lado, los resultados de medidas de difusión gas-LI mostraron las limitaciones cinéticas que los LIs presentan debido a sus altos valores de viscosidad. En segundo lugar, el simulador de procesos Aspen Plus se empleó para evaluar el comportamiento de los LIs seleccionados en la etapa anterior y que presentan características competitivas en comparación con el DMF en la operación de absorción y regeneración. El análisis termodinámico permitió concluir que al menos dos LIs son competitivos con el disolvente de referencia, con menores consumos de disolvente y menos etapas de separación. Sin embargo, el análisis cinético en columnas de relleno con LIs demostró que la operación de absorción está controlada por la cinética de transferencia de materia. Como consecuencia, se encontraron mayores consumos de disolvente, temperaturas de operación más altas, y columnas de absorción más grandes en comparación con el DMF. Por último, el análisis de la etapa de regeneración permitió concluir la gran ventaja en el uso de LIs, alcanzando mayores purezas y recuperaciones de acetileno y consumos energéticos más bajos que el proceso con DMF.

El segundo trabajo tiene como objetivo la evaluación de LIs como potenciales absorbentes de H_2S. Se empleó la misma metodología descrita en el primer trabajo. En este caso, un barrido entre más de 700 LIs reveló que la absorción física de H_2S está controlada por la naturaleza

del anión. De esta forma, aquellos capaces de formar enlaces de hidrógeno con el carácter ácido del soluto fueron los LIs que presentaron interacciones más fuertes. Se seleccionó una colección de LIs con propiedades favorables para la captura de H_2S para su aplicación como absorbentes en columnas de relleno utilizando el simulador de procesos Aspen Plus. Los resultados de las simulaciones en las que sólo se tiene en cuenta el equilibro termodinámico están en concordancia con aquellos extraídos de la etapa de simulación molecular, obteniendo eficiencias más altas en términos de consumo de disolvente cuando se disminuye la constante de Henry del H_2S en los LIs. Sin embargo, los resultados en columnas más rigurosas mostraron un alto control de la cinética de transferencia de materia del proceso. Como consecuencia, los LIs con mejores resultados desde el punto de vista termodinámico son los peores para la operación. Por el contrario, aquellos LIs con viscosidades más bajas requieren un consumo de disolvente más bajo, temperaturas de operación más bajas y dimensiones de columna más pequeñas.

Los dos primeros trabajos mostraron las grandes limitaciones de transferencia de materia que los LIs presentan en procesos de captura de gases, debido a sus altos valores de viscosidad. Por esta razón, en el tercer trabajo, los líquidos iónicos encapsulados (ENILs) se presentan para vencer esas limitaciones cinéticas en la absorción física de CO_2 con LIs. En primer lugar, la metodología COSMO/Aspen Plus fue usada para seleccionar cuatro LIs con capacidades de absorción de CO_2 altas y similares, pero propiedades de transporte muy diferentes, para su posterior evaluación experimental. Los resultados de la simulación mostraron altas recuperaciones de CO_2 considerando únicamente el equilibrio termodinámico para la mayor parte de LIs (50 - 98% de recuperación). Sin embargo, se encontraron comportamientos muy

diferentes en columnas más rigurosas en las cuales también se considera la cinética de transferencia de materia (0.3 - 62% de recuperación). De hecho, las recuperaciones de CO_2 se ordenan en orden decreciente de viscosidad de LI. Esto permitió analizar el comportamiento cinético y termodinámico de LIs con distintos valores de viscosidad tras ser encapsulados (ENILs). Los resultados gravimétricos experimentales con LI puro mostraron las altas y similares capacidades de absorción de CO_2 de los LIs seleccionados, pero distinto comportamiento cinético para cada uno de ellos. Tras ello, los ENILs fueron preparados y caracterizados analizando su estructura porosa, análisis elemental y morfología. Los resultados de la caracterización confirmaron cargas de LI alrededor del 80% en cada material. Los ensayos de sorción de CO_2 demostraron que la capacidad de absorción de los LIs se mantiene tras su encapsulación, mientras que la cinética de transferencia de materia se incrementó en un factor de 50 para el caso de los ENILs en comparación a las del LI puro. Por último, experimentos de lecho fijo a distintas temperaturas revelaron que la eficiencia del proceso de captura de CO_2 en el lecho depende de la solubilidad de CO_2 en el ENIL, en contraste con el comportamiento de la operación con LIs puros, el cual está controlado por las desfavorables cinéticas de transferencia de materia. Por tanto, la selección del LI para la captura física de CO_2 se mueve desde criterios cinéticos (viscosidad) en el caso de LIs puros, a termodinámicos (solubilidad de CO_2) en el caso de ENILs.

Los ENILs han demostrado ser una solución a los problemas de los LIs en procesos de captura física de CO_2. Sin embargo, la baja solubilidad de CO_2 por parte de LIs de absorción física en comparación con las aminas, ha sido ampliamente demostrada. Por esta razón, el cuarto trabajo presenta los ENILs con LIs que presentan absorción química de CO_2. En

este sentido, fue evaluado el comportamiento de tres LIs derivados de aminoácido (aa-LIs), debido a su bajo precio, abundante disponibilidad y alta biodegradabilidad. En primer lugar, se analizó experimentalmente la absorción química de CO_2 por parte de los aa-LIs mediante espectroscopia infraroja (IR). Cálculos DFT permitieron proponer un mecanismo de reacción comparando las señales características del espectro de IR con aquellas obtenidas experimentalmente. A continuación, la capacidad de absorción de CO_2 de los LIs puros fue analizada mediante ensayos gravimétricos a tres temperaturas, revelando procesos de absorción muy lentos, debido a sus altos valores de viscosidad, y la formación de un complejo sólido cuando el aa-LI reacciona con el CO_2. Por tanto, los ENILs se prepararon y caracterizaron para permitir la aplicación de los aa-LIs. Los resultados mostraron la posibilidad de emplear los ENILs para permitir la saturación de los aa-LIs a tres temperaturas distintas. Por último, se propuso un modelo termodinámico para cuantificar la contribución física (constante de Henry) y química (constante de equilibrio) de la absorción de CO_2 para cada LI. Se encontraron entalpías de reacción bajas en comparación a las aminas, lo que favorecería la reversibilidad del proceso y la regeneración del sorbente, implicando consumos energéticos más bajos.

Los dos trabajos previos mostraron la mejora en la velocidad del proceso de absorción de los LIs mediante su incorporación a un soporte sólido. El quinto trabajo de la tesis estudia la influencia del tamaño de partícula del soporte en el proceso de absorción química de CO_2. En este caso, se emplearon líquidos iónicos soportados (SILPs) utilizando un LI basado en el anión acetato y SiO_2 como soporte. En primer lugar, se prepararon y caracterizaron SILPs de tamaños de partícula muy diferentes analizando sus propiedades texturales, morfología,

estabilidad térmica y composición elemental. Los resultados de esta caracterización permitieron comprobar que la cantidad de LI para cada tamaño de partícula es prácticamente 40% en los tres casos. En segundo lugar, se evaluaron las isotermas de CO_2 experimentales del SILP para cada tamaño de partícula a tres temperaturas. La comparación de estos datos con aquellos obtenidos para el LI puro demostró que la capacidad de sorción es únicamente debida al LI que permanece en el interior del ENIL. Las isotermas experimentales fueron ajustadas empleando el modelo de Langmuir-Freundlich. En tercer lugar, se evaluó la cinética de sorción del proceso mediante experimentos en lecho fijo a tres temperaturas, caudales de gas, presiones parciales de CO_2 y tamaños de partícula. Se empleó un modelo basado en fuerza impulsora para la descripción de las distintas curvas de rotura. El análisis de los coeficientes cinéticos obtenidos permitió concluir que al disminuir el tamaño de partícula y aumentar la temperatura y presión parcial de CO_2, se obtienen cinéticas de transferencia de materia más rápidas. Además, se puede concluir que el sistema no presenta problemas de difusión externa debido a que los coeficientes cinéticos son prácticamente idénticos al aumentar el caudal de gas. Por último, se empleó el simulador Aspen Adsorption para modelar la operación tras encontrar una relación entre los coeficientes cinéticos obtenidos y las variables de estudio experimentales. Los resultados permitieron concluir que a bajas presiones parciales de CO_2, la reacción química es la etapa controlante del proceso, mientras que a mayores presiones parciales la difusión del gas en el SILP es la etapa dominante. Esta metodología permite el diseño de procesos de sorción de CO_2 basados en SILPs, minimizando los consumos de SILP mediante la optimización del tamaño de partícula y el tipo de LI.

El sexto y último trabajo fue posible gracias a la estancia internacional en el grupo del Prof. Fehrmann en la Universidad Técnica de Dinamarca. Este trabajo trató de buscar una nueva aplicación a los ENILs hacia la catálisis en fase gas. El objetivo fue evaluar el uso de ENILs como catalizadores de la reacción de oxidación de NO en condiciones de humedad a bajas temperaturas. En primer lugar, los ENILs fueron preparados y caracterizados empleando las técnicas descritas en los trabajos anteriores. En este trabajo, se comparó el comportamiento de los ENILs con el de las cápsulas vacías sin LI. Las condiciones experimentales empleadas fueron una concentración de NO de 2.000 ppm, cambiando la cantidad de LI en el ENIL, y el contenido de oxígeno y agua. Los ensayos en condiciones secas revelaron altas conversiones empleando las cápsulas vacías en comparación con los ENILs, debido a que la reacción ocurre en los poros del material. Sin embargo, los ensayos en condiciones húmedas concluyen que la reacción no se ve afectada en presencia de agua cuando se emplean ENILs como catalizadores. En el caso de emplear las cápsulas de carbón vacías, la reacción se inhibe completamente a altas humedades relativas. A continuación, se demostró que la adición de metanol mejora el comportamiento de la reacción en términos de conversión. Se obtuvo una relación optimizada metanol/NO entre 0,2 y 0,4. En resumen, ENILs con cargas del 40% de LI mostraron el mejor comportamiento para la reacción de oxidación de NO a ácido nítrico en condiciones de humedad.

2. INTRODUCTION

2.1 IONIC LIQUIDS

Ionic Liquids (ILs) are salts formed entirely by ions with melting points below 100 °C [1]. This definition comprises a broad group of salts that are solids at normal conditions. Therefore, the most part of ILs are liquids at room temperature conditions, and are usually defined as *room temperature ionic liquids (RTILs)* [2]. The main difference between conventional ionic salts (i.e. NaBr) and ILs is the presence of asymmetric and voluminous ions (specially the cation). Moreover, the interaction between the cation and the anion does not allow the formation of crystalline structures. These characteristics facilitate the liquid state of ILs at normal conditions. Commonly, ILs present an organic cation of different nature (aromatic, such as imidazolium and pyridinium, or chains attached to phosphorus or nitrogen, such as phosphonium or ammonium, among others) and anions also of different nature (inorganic, such as Cl^-, I^-… or organic structures, such as NTf_2, DCN…) [3].

The availability of such great number of cations and anions results in more than 10^6 ILs combinations [4]. Thus, the chance of tuning the cations and anions properties for specific applications makes ILs to be considered as "designer solvents" [5]. Furthermore, ILs properties make them being known as new solvents in the chemical industry [6]. The most remarkable of these properties are the low vapor pressure, which means an almost negligible volatility, high thermal and chemical stability or high solvent capacity, among others.

For all these reasons, ILs have attracted great attention among the scientific community in last decades [7]. This has been reflected in the gradual growth of number of publications related to ILs in last two decades (Figure 1).

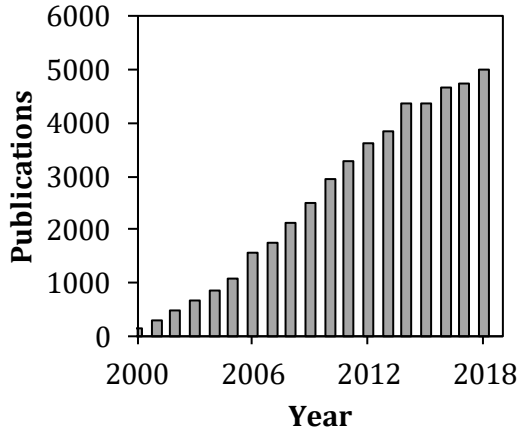

Figure 1: Number of publications related to "ionic liquids" in last two decades. Source: *Web of Science*

2.1.1 Ionic liquid properties

The consideration of ILs as potential solvents for chemical industrial applications is due to their remarkable properties when compared with traditional solvents. In this sense, the main characteristics of ILs are:

- Negligible vapor pressure, which means these solvents are considered non-volatiles at normal conditions. ILs do not evaporate, so vacuum systems can be developed without significant solvent losses [8]. This property makes them specially interesting against traditional solvents in separation processes [9].
- Relatively high thermal stability depending on the ions that contain. In this sense, aromatic based cations present higher thermal stability than other head groups. Regarding the anions, usually organic ones ($[NTf_2]^-$, $[DCN]^-$) possess the highest decomposition temperatures usually between 300

and 400 °C [10, 11]. They also present high chemical stability, being non-flammable.

- Low melting points. Most of them are RTILs. The presence of big cations or anions leads to lower melting points [12].
- High viscosity values (30 – 300 cP at room temperature) [13], as a consequence of the strong interactions between the cation and the anion (electrostatic interactions, Van der Waals forces and hydrogen bonds) [14]. Long alkyl chains of the cation usually leads to more viscous ILs [15]. Regarding the anion effect on viscosity, those of inorganic nature (Cl^-, Br^-, I^-…) present the highest viscosity values (even solids), while those organic ($[NTF_2]^-$,$[DCN]^-$…), which are more voluminous, are low viscous.
- Density values between 1.0 and 1.6 g/cm^3 [16], slightly higher than that of water. An increase on the alkyl chain of the cation derives on lower densities [17].
- Surface tension between 30 and 60 N/m at room temperature [18], which increases with shorter alkyl chain lengths of the cation [19].
- Variable solubility of water depending on the nature of the IL. In this sense, those ILs presenting high polar ions (nitrates, sulfates, among others) are essentially hydrophilic. On the contrary, ILs containing fluorinated ions can be completely hydrophobic [20]. It is important to point that all the ILs are hygroscopic, in spite of their hydrophobicity (as in the case of fluorinated ions).
- Environmental concerns regarding ILs. Although they are known as “green solvents”, ILs are proved to be potentially

toxic [21]. Despite that, some are easily biodegradable by different methods [22].

2.1.2 Ionic liquid process engineering

The versatility of ILs makes possible their application in several fields. Figure 2 shows the different research areas in which ILs are applied [23].

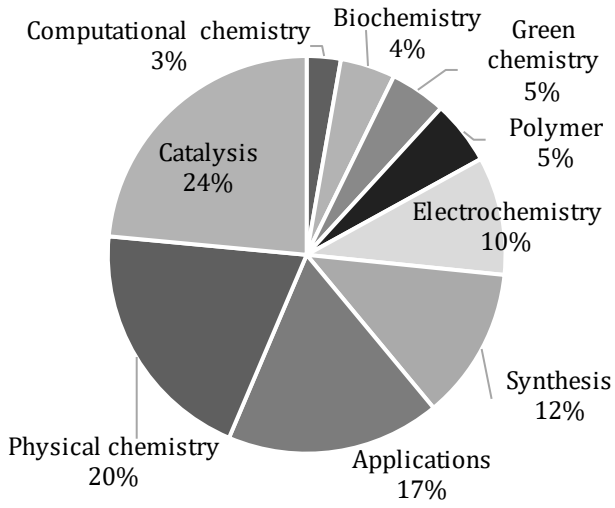

Figure 2: Distribution of research areas of ILs a function of publications in last years [23]

The catalytic application is the one most explored by scientific community, comprising the 24% of the total number of related publications. ILs are used as catalysts, solvents or catalyst supports [24]. This application comes not only by their unique properties, but also by the improved selectivities when introducing ILs in the reaction media [25]. More recently, efforts have been centered on CO_2 conversion to value-added compounds using ILs as catalysts [26-28].

Then, physical properties measurements are also found relevant, contributing to 20% of the total publications. In this sense, pure properties of ILs and their mixtures were evaluated, such as viscosity [13, 29-31], density [29-32], refractive index [30, 32], electrical conductivity [32], surface tension [33, 34] or heat capacity [35], among others.

One of the major research lines of ILs is their application to different systems and processes. Specially attention have been focused on separation processes including: gas absorption [36-38], liquid-liquid extraction [38-40], membranes [41, 42] or chromatography [43].

Synthesis of new ILs is always in continuous improvement, so several research groups dedicate their efforts to synthetize new ILs or use them to new synthesis processes [44, 45].

The good electrical properties of ILs have been important to develop new electrochemical applications, such as electro-catalysis, electro-synthesis… [46-48]. Polymer technologies based on ILs are also been investigated [49]. Specially, ILs are used in membranes field by different ways, including immobilization of IL in a porous solid [50, 51] or by using polymeric ILs (PILs) [49, 52]. It is well known the use of ILs to green chemistry applications (contributing to 5% of the publications) [53, 54]. The application of ILs to biochemistry was also found of relevance between the published articles [55, 56]. Last, several papers related to computational chemistry using ILs were also found [57, 58].

2.1.3 Industrial applications of ionic liquids

In recent years, an increasing number of companies are betting for industrial processes based on ILs [59, 60]. The first operating pilot plant

was developed by IFP ("Institute Français du Pétrole") in 1996 [61]. Dimersol process consists of the dimerization of alkenes and butenes to value-added hexenes and octenes. The traditional process employs a cationic nickel complex as catalyst without solvent. The addition of IL as solvent of the catalyst leads to a reduction in the catalyst disposal, lower cost of the process, better dimer selectivity and higher yield.

BASF is the company that more promotes the implementation of ILs processes in the industry. In fact, it was the first company that commercialized the first IL process. **BASIL** (Biphasic Acid Scavenging using Ionic Liquids) was implemented in a plant in Ludwigshafen (Germany) in 2002 [62, 63]. The main goal of this process is to obtain alkoxyphenylphosphines (a generic photo-initiator precursor). In the original process, an insoluble paste was generated as by-product (triethylammonium chloride) while triethylamine was used to scavenge the formed acid during the reaction. The replacement of triethylamine by 1-methylimidazole forms an IL (1-methylimidazolium chloride) as by-product, which is easily separated out of the reaction mixture as discrete phase. The main advantages of the **BASIL** process are the much smaller reactor needed and the increased yield (from 50% to 98%). Nowadays, it operates with a capacity up to 1,000 tons/year on the plant in Germany. Other process developed by the company (BASF) is the use of ILs as entrainers to break common azeotropes (water-ethanol, water-tetrahydrofuran). The main advantage of the substitution of traditional solvent by ILs is the significant reduction of the costs of separation and recycling. The replacement of phosgene also attracted the attention of the company in last years. In this sense, phosgene is substituted by an IL-hydrogen chloride solution, avoiding the well-known phosgene

problems. Other processes developed by the company include the cellulose solution or aluminum electro-deposition [59].

Eastman Chemical Company developed a 3,4-epoxybutene isomerization plant, which was working from 1996 until 2004 with a capacity of 1,400 tons/year. ILs were introduced in the process as catalysts (Lewis acid ILs). The plant is idle because of the reduction in the product demand [59].

Degussa utilizes ILs in different processes, including hydrosilylation of polydimethylsiloxane. In this case, ILs are used as solvent media for the catalyst, in which no significant leaching is observed. Moreover, the company incorporates ILs to their processes of paint additives or lithium batteries production.

Air Products company uses ILs for the transport and distribution at small scale of acid gases of high toxicity, such as PH_3 or AsH_3 [59]. *Petronas* commercializes their adsorbent "HycaPure Hg" for the elimination of mercury from gas natural streams [64]. It consists of the immobilization of an IL with anions based on cupper salts over a silica support [65].

IoLiTec (Ionic Liquid Technologies) studies the use of ILs in industrial applications among which stands out the CO_2 capture. Regarding this application, they produced 200 kg of a mixture of three different ILs using continuous micro flow reactor technology for their future incorporation in a pilot plant in Greece, which is currently being built [66].

PetroChina develops the Harbin Petrochemical Alkylation Unit, which is the first IL alkylation unit. The process employs chloroaluminate ionic

liquid as catalyst, substituting the HF typically used in this kind of processes [67]. The advantages of the technology are the reduction of the operating temperature, simplification of the process (avoiding the use of HF that is a high dangerous compound), the achievement of higher efficiencies and RON,… In November 2017, the 150,000 ton/year plant passed the preliminary feasibility and it is working from 2018 [68].

2.2 GAS ABSORPTION WITH IONIC LIQUIDS

ILs application to the absorption of gases of different nature was studied in several works in last decades [69]. It is of special interest the use of ILs aimed to CO_2 and NOx capture processes emitted from traditional thermo-electrical plants. Moreover, due to the easy design of ILs for specific applications, they are typically studied to absorb other different gases. In this introduction section, it is detailed the importance of capturing CO_2, C_2H_2, H_2S and NOx. Moreover, available technologies to eliminate these solutes are also detailed. Lastly, current research on the use of ILs was also provided.

2.2.1 Carbon dioxide (CO_2)

2.2.1.1 CO_2 emissions

Carbon dioxide (CO_2) is one of the well-known "greenhouse gases" (GHG). The presence of these gases in the atmosphere blocks the emission of infrared radiation to the space, absorbing and reflecting the radiation from the Earth's surface, and causing the global warming effect. CO_2 is the most important greenhouse gas, constituting the 84% of the greenhouse gas emissions to the atmosphere [70]. The European Union (EU) has committed to achieving a reduction in its GHG emissions of at least 20% by 2020 and 80% by 2050 (compared with 1990 levels) [71]. GHG emissions from 1990 are decreasing according to EU exigence's (see

Figure 3). In last years, different agreements have been carried out to keep controlling the GHG emissions. Kyoto Protocol (1997) and United Nations Climate Change Conference (2015) are considered as great achievements against the climate change.

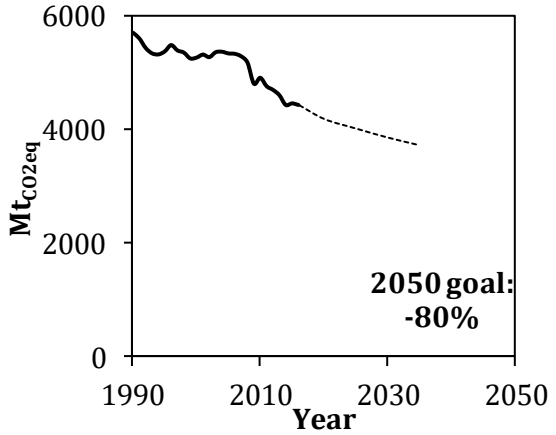

Figure 3: Greenhouse gas (GHG) emission trends, projections and targets in the European Union [71]

Although CO_2 is present naturally in the atmosphere, its normal concentration is being affected by the human activity. Thus, Figure 4 presents the GHG emissions by the main different sectors [72]. It is clearly seen how the main contribution to GHG emissions is related to the energy supply sector (power plants) constituting more than one third of the total. Moreover, the decrease in the emissions follows the same trend of the energy supply one, which means that great efforts have been carried out in this direction. In this sense, the simplest way to avoid the emission of CO_2 is mitigating this great source of emissions.

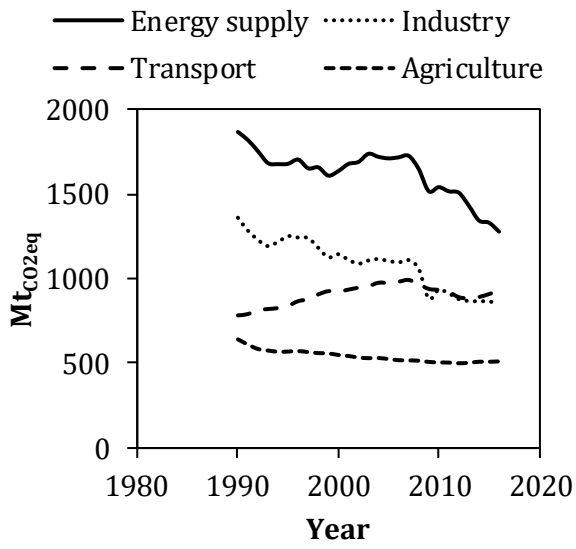

Figure 4: Greenhouse gas (GHG) emissions by m sectors in the European Union. [72]

2.2.1.2 CO_2 capture configurations

CO_2 capture, transport and storage systems constitute one of the areas with most development in R&D. The main objective of these systems is to concentrate a stream with high CO_2 purity, for its subsequent transport and store. As described before, the simplest way to mitigate the CO_2 emissions is to develop systems integrated on power plants. In this sense, different configurations for the CO_2 capture can be classified in post-combustion, pre-combustion and oxy combustion [73, 74].

Post-combustion: In this system, CO_2 capture is accomplished at the outlet of the combustion process. It is the most extended strategy traditionally employed in power plants from fossil fuels. First, the fuel (carbon, petrol, gas…) is burnt in an air atmosphere, being the released energy employed to generate electricity. The combustion outlet gas, after removing suspension particles and sulfur compounds, comprises N_2 (70-

75%), CO_2 (10-15%), H_2O (5-10%) and O_2 (3-4%). The gas leaves the process at 40-70 °C and near atmospheric pressure. Then, CO_2 is selectively removed before the gas emission. In this sense, it is important to develop systems that can selectively retain CO_2 from N_2, water and O_2. The main advantage of this system is the easy implementation in any existent power plant without great modifications. However, it presents some disadvantages, such as the low CO_2 partial pressure and the low total pressure compared to sequestration requirements, which increment the energetic cost of the operation [73].

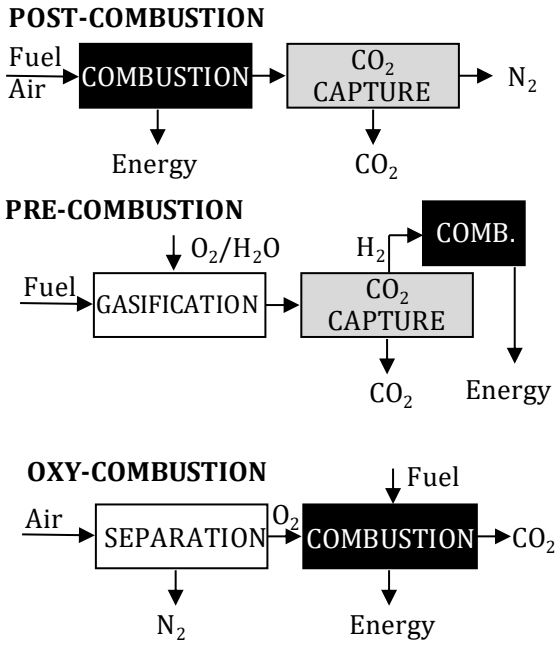

Figure 5: Scheme of different CO_2 capture systems in power plants

Pre-combustion: In this system, the fuel is gasified, instead of burnt, in presence of pure O_2 and H_2O vapor, and converted into syngas (CO + H_2). Then, this syngas will be got in contact with H_2O, in the well-known "Water Gas Shift" reaction to convert CO into H_2, releasing CO_2. At this point, the CO_2 capture system is located to selectively capture the CO_2 from H_2. The generation of electricity is produced by the released energy in the H_2 combustion stage. The streams to be treated usually contain concentrations of 40% of CO_2, more than 55% of H_2 and total pressures of 15-40 bar. In this case, it is important to look for systems able to selectively retain CO_2 from H_2. The main advantages of this kind of systems are the concentrated CO_2 achieved at high total pressures, which will mean an increase driving force for separation and a potential reduction in energy costs due to the compression stages.

Oxy combustion: In this technology, which is still under development, pure O_2 is fed to the system instead of air for the combustion stage. Therefore, a previous separation stage of the main components of the air is necessary. Then, only CO_2 and H_2O are generated during the combustion stage, with absence of N_2. The main advantage of the system is the very high CO_2 concentration in the flue gas, which partially avoid the capture stage (separation of water by condensation). However, it presents the disadvantages of high cost associated to the cryogenic O_2 production step and a decrease in the process efficiency due to the cooled CO_2 recycle required to maintain temperatures for combustor materials.

The US Department of Energy provided a detailed economic comparison between the three technologies [75-77]. They conclude that pre-combustion CO_2 capture is the most favorable one in economic terms, mainly due to the high CO_2 operating pressures that would reduce

the compression costs. However, the investment needed for this process is higher than those of the other two systems. In fact, the only one able to work in actual power plants is post-combustion treatment. In this case, the factors that determine the cost of the process are the CO_2 absorption/desorption and, especially, the solvent regeneration stage [78]. The necessity of developing CO_2 capture processes in current power plants makes post-combustion treatment the most studied in the literature, which will result in an increasing number of plants using this technology.

2.2.1.3 Available CO_2 capture technologies

The challenge is to develop CO_2 capture technologies able to work efficiently on the configurations explained before, especially on the post-combustion one. In this sense, the main problem is to get technologies that can work at low CO_2 partial pressures. Therefore, big efforts are being centered on the development of new systems that can improve the performance of the available technologies. Some of these technologies are detailed below.

A. Chemical absorption with aqueous amines

Chemical absorption with amines (alkanolamines) is the most extended technology to capture CO_2 in post-combustion configuration. In fact, it has been used for decades in different plants [79]. Amines react rapidly with CO_2 at low partial pressures. They present great advantages for using as absorbents, such as their great CO_2 absorption capacity and their low cost. However, they also present some disadvantages that make the scientific community to explore new technologies. The most employed amine is monoethanolamine (MEA), considered as benchmark solvent due to its great ability for CO_2 capture [80]. Other amine-based

solutions have been traditionally used, such as diethanolamine (DEA) or triethanolamine (TEA), among others. In fact, amines are classified depending on their structure and they present different CO_2 reaction mechanisms and properties. Primary amines (i.e. MEA) present a 2:1 stoichiometry and possess fast chemical reaction kinetics. Secondary amines present a 1:1 stoichiometry, which means that CO_2 absorption capacity is higher than that of primary ones. A typical chemical absorption scheme of CO_2 capture plant using aqueous amines as absorbent is shown in Figure 6 [81]. MEA reacts with CO_2 following the mechanism of reaction (Eq. 1):

$$CO_2 + 2R_1R_2NH \leftrightarrow R_1R_2NCOO^- + R_1R_2NH_2^+ \qquad Eq.1$$

The reaction occurs by forming a zwitterion that ends in a carbamate [82]. Then, the carbamate is hydrated to form the corresponding carbonate.

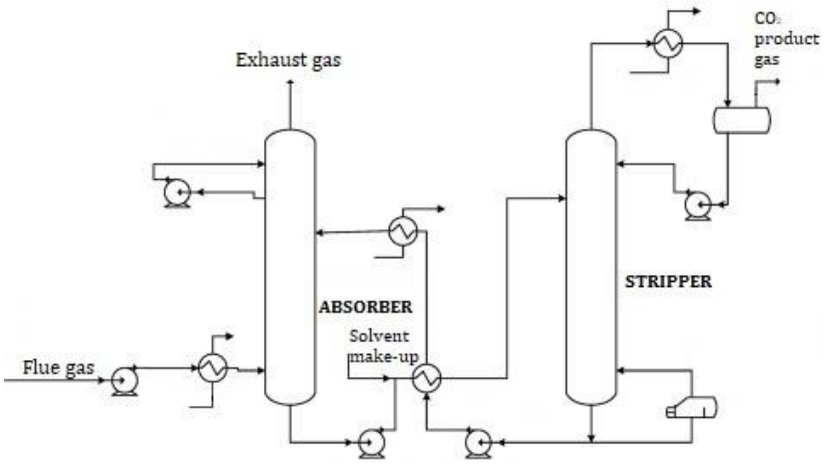

Figure 6: Typical scheme of CO_2 capture plant using aqueous amines as absorbent. *Source*: Adapted from Liang et. *al. [81]*

Following the scheme on Figure 6, the low partial pressure CO_2 in the flue gas is introduced to the absorber after a conditioning stage of temperature. The gas is fed to the system at the bottom of the column (50-55 °C and atmospheric pressure) in crosscurrent flow with lean solvent that comes from the desorber. Clean gas is released to the atmosphere by the top of the absorber. On the contrary, while CO_2 is being absorbed, "rich amine" goes to the stripper. The saturated liquid goes first to a heat exchanger to raise its temperature prior to the regeneration stage. The hot fluid is the "lean amine" that comes from the desorber. The stripper operates at 120-150°C and the pressure is increased until 5 bar. A CO_2 stream saturated of water is released from the top of the stripper and can be properly storage or transported. "Lean amine" without CO_2 can be easily returned to the absorber.

The drawback of this technology is the high-energy consumption in the amine regeneration stage, due to the severe operating conditions needed. Moreover, solvent degradation, loss and corrosion are again issues to be solved in the future [83]. In fact, MEA process is used as reference in new solvents for CO_2 capture. Energy Department of the United States (DOE) uses the aqueous MEA solution (30%) as reference with a 90% of CO_2 recovery and 95% of purity at the outlet stream. In that case, it would suppose an energetic consume of 4.2 GJ/t_{CO2} considering the whole process [84]. This energetic cost contributes to the 80% of the total cost of the kWh of electricity when compared to the process without capture. For all these reasons, it is important to develop new systems and processes that can decrease not only the associated costs but also the operating problems of amine solutions. Next sections will introduce other emerging technologies that may be alternative to amine process.

B. Other absorption systems

Although amine solvents continue being the most extended technology in the chemical industry, other systems are now implanted to treat the CO_2 from gas natural, hydrogen or other streams. In this sense, other absorbents try to solve the well-known operating problems that amines present. Some physical absorbents are used that require less energy consumption in the regeneration stage due to the physical interaction with CO_2. Moreover, these solvents are favored when high CO_2 partial pressures are present in the stream to be treated. Physical absorbents overcome amines absorption capacity at high pressures [85]. Therefore, some companies are developing and patenting physical absorbents for CO_2 capture that consist of mixture of commercial solvents [86].

Rectisol is a solvent that retains CO_2 physically based on chilled methanol. It presents the advantage of working at low temperatures (below 0 °C) to avoid the vaporization of the methanol at normal process conditions. At this low temperature, absorption process is favored. However, it presents a low CO_2 selectivity when H_2S is present in the stream. The companies that commercialize this solvent are *Linde AG* and *Lurgi AG [86].*

Selexol is mainly composed of dimethyl ether of polyethylene glycol (DPEG). It presents the highest CO_2 solubility compared to the other physical absorbents. It is able to operate in a broad temperature range (0 – 175 °C). It is less expensive than *Rectisol* and presents less volatility. The limitations are its high viscosity compared to traditional solvents, which will result in low mass transfer kinetics. The companies that develop this solvent are *Norton, Dow Chemical* and *UOP [86].*

Sepasolv-MPE consists of a mixture of polyethylene glycol and dialkyl ethers. It presents almost the same properties as *Selexol* because main compounds are essentially the same. Therefore, the broad temperature range and low volatility are the main advantages of the solvent. *BASF* company commercialize it [86].

Fluor company gives its name to this solvent, which is mainly constituted of propylene carbonate (PC). It has been used since late 1950s so it is a compound well studied. Solvent losses are low despite presenting higher vapor pressure than *Selexol.* However, it is not recommended when H_2S is present in the system because it reacts with water and become unstable at high temperatures. For this reason, operating temperatures are always below 65 °C [86].

Purisol is mainly formed by N-methyl-2-pyrrolidone (NMP). It is necessary to wash it with water for a proper solvent recovery. It presents higher vapor pressure than other physical solvents, so operating temperatures are always below 25 °C. Moreover, it is hardly selective to H_2S, so it must be avoidable when this compound is present in the stream. *Lurgi GmbH* company commercialize this technology [86].

Morphysorb was developed by *ThyssenKrupp* Company and it is mainly based on N-formyl-morpholine (NFM) and N-acetyl-morpholine (NAM). It has been industrially used since 2002 and it was developed for its high selectivity of acid gases when heavy hydrocarbons are present.

On contrast with the described physical absorbents, some other solvents composed of functionalized amino groups are used. In this sense, amino acid salts [87], carbonate systems [88], or aqueous ammonia [89] are also employed to absorb CO_2.

C. Adsorption

Main disadvantages of absorption processes comprise low contact area between gas and liquid, low CO_2 capacity, solvent loss and corrosion. For all these reasons, solid adsorption may be an alternative for CO_2 capture process [90]. First, it is important to take into account the benchmark to have a suitable adsorbent for CO_2 capture [91, 92]. These works conclude that a good adsorbent must satisfy: 1) low-cost raw materials, 2) low heat capacity, 3) fast kinetics, 4) high CO_2 adsorption capacity, 5) high CO_2 selectivity and 6) thermal, chemical and mechanical stability under extensive cycling. Many research groups have been working, in last decades, on developing solid materials able to satisfy these requirements. Different classifications can be done attending to physical or chemical adsorption, or material origin, among others.

Physical adsorbents: Carbonaceous materials have been used in last years due to availability, low cost and high thermal stability [93]. The main problem of these materials is the weak CO_2 adsorption in a range of 50-120 °C, which is high sensitivity in temperature and low selectivity in the operation. Consequently, new research is focused on solving these issues by: 1) improving surface area and pore structure using different precursors and 2) increasing alkalinity by chemical modification on surface. Zeolites materials are also used as CO_2 physical adsorbents. In this case, adsorption efficiency is affected by their size, charge density, and chemical composition of the porous structure [94]. In this sense, current work is focused on zeolites with crystalline structure, high surface area, and 3-dimensional pore structures changing their Si/Al ratio. Zeolite materials present some disadvantages such as low CO_2/N_2 selectivity and adsorption competition in moisture conditions [90].

Mesoporous silica was also studied due to its high surface area, high pore volume, tunable pore size and good thermal and mechanical stability. However, CO_2 adsorption capacity is not enough at atmospheric pressure, which hinders its application. Metal-organic frameworks (MOFs) have also being studied in recent years due to their high surface area, controllable pore structure and tunable pore surface properties. MOFs present high adsorption capacities but low selectivity when gas mixtures are present [90].

Chemical adsorbents: Different new adsorbents try to improve CO_2 adsorption and selectivity modifying chemically the surface. The addition of basic organic groups (amine) and inorganic metal oxide (alkali metal or alkali-earth metal) are widely reported [90]. In these cases, the interaction between CO_2 molecules and basic active sites on the surface enhances CO_2 adsorption forming covalent bonds. Amine-based adsorbents present the advantage of having low heat of regeneration. However, low CO_2 adsorption capacity and high cost are still drawbacks to solve. New studies are focused on preparing supports with high amine loading, using amines with high nitrogen content, and introducing amines with effective methods. Alkali metals (Li, Ca…) are considered as effective for CO_2 capture because of their high adsorption capacity. However, diffusion problems are found to difficult their industrial application [90].

D. Other technologies

Emerging technologies are also being studied to selectively retain CO_2 apart from the already mentioned. Membranes technology is one of the most studied. It comprises on the preferential pass of a gaseous stream through the membrane. One option is to use membranes based on polymers, zeolites, or silica functionalized with amines. Research efforts

are focused on the development of membranes that present a very efficient CO_2 separation, so high CO_2 selectivity and permeability are the aims of the design. However, these membranes are not stable due to the evaporation and high degradation of the solvent [95]. Moreover, it is usually necessary more than one pass through the membrane to reach high efficiencies, which is translated into higher cost of the process.

Other emerging technologies are systems based on carbonates that take advantage of the reactivity of CO_2 with the carbonate to form bicarbonate. Then, a simple heating can easily desorb the reacted CO_2. This results in a less expensive regeneration process when compared with traditional amines. However, problems related to corrosion and solvent loss are not solved with this system [96].

Ammonia systems present great similarities with amine process. Their advantages are less energy consumption in regeneration stage, less degradability and high absorption capacity. However, these compounds are more volatile, which is translated into lower operating temperatures to avoid the evaporation of the solvent [97].

In last decades, the use of ILs as CO_2 absorbents have attracted the attention of the scientific community [98]. They try to solve the problems regarding the regeneration stage taking advantage of the low vapor pressure of ILs. This technology will be described in next sections of the introduction.

2.2.1.4 CO_2 capture with ionic liquids

This section presents the most relevant contributions on the research developed on CO_2 capture with ILs. The processes are divided in two great groups: physical and chemical absorption.

A. Physical absorption

In last years, many investigation groups studied the CO_2 physical absorption with ILs. This section is focused on the operating variables that more affect to CO_2 solubility.

First, physical absorption using ILs is favorable from the energetic point of view since less consume is achieved in the regeneration stage, compared to the chemical one. Therefore, it is important to develop ILs with high CO_2 solubility. Inherent with the type of the IL, CO_2 physical absorption with ILs follows the behavior observed in traditional physical solvents. Therefore, an increase in the temperature leads to lower CO_2 absorption capacities [99]. The effect of the CO_2 partial pressure presents an opposite behavior. At low partial pressures, the solubility is relatively low while as increasing the pressure, the solubility is increased [100].

Second, the anion is the main factor influencing the CO_2 solubility [101]. Among the studied ILs, those that contain an anion with fluoroalkyl group present the highest CO_2 absorption molar capacity [102]. They follow the trend: nitrate (NO_3) < dicyanamide (DCN) < tetrafluoroborate (BF_4) < hexafluorophosphate (PF_6) < trifluoromethanesulfonate (TfO) < bis(trifluoromethylsulfonyl)imide (NTf_2) [102]. Regarding the cation, it presents a lower contribution to the CO_2 physical absorption with ILs. Among the studied cations, those that contain imidazolium cation with longer alkyl chains exhibit a higher CO_2 absorption molar capacity, so they are the most common for the task [103].

Despite the great attention given to CO_2 physical solubility by ILs, very recent studies suggest that mass transfer kinetics is even more determinant than thermodynamics in commercial separation equipment

[104, 105] Thus, ILs with the most favorable mass transfer properties are those that exhibit the best CO_2 capture performance in absorption columns.

B. Chemical absorption

All the mentioned ILs present high CO_2 absorption capacity at high pressure. On the contrary, comparing the capacities with traditional amines at low partial pressures (typical post-combustion configuration), they are still quite lower. For this reason, and taking into advantage one of the properties of ILs ("designer solvents"), functionalized ILs were designed to chemically retain CO_2. In this sense, depending on the functionalization carried out, different groups can be distinguished:

ILs functionalized with amines: they are synthesized by introducing amino groups to the cation and/or the anion. The first amino-functionalized IL was 1-butyl-3-propylamineimidazolium tetrafluoroborate, reporting an absorption mechanism that forms carbamate by reaction of CO_2-amino group [106]. This IL achieved a ratio of CO_2/IL about 0.5, which is similar to those reached by traditional MEA [107]. Later works studied ILs based on imidazolium cations functionalized with primary and ternary amines and hydroxyl groups [108]. These ILs achieved similar absorption capacities to conventional amines. At this point, it emerged the idea of functionalizing ILs with amino acids giving rise to amino acid based ILs [109-111]. In this case, the stoichiometry of the reaction changes to 1:1 and absorption capacity is decreased due to the physical contribution. Typical anions are derived from glycine, methionine, proline, lysine… These ILs are easily biodegradable. However, they present high viscosity, becoming solids when reacting with CO_2, which hinders their practical application [111].

ILs functionalized with acetates: the functionalization of the anion of ILs with acetate groups has been extensively studied improving significantly the CO_2 absorption capacity [112-114]. All these studies demonstrated the chemical reaction of the IL with CO_2. The most extended mechanism of reaction suggests that CO_2 is joint to the imidazolium ring forming a carboxylate (stoichiometry 1:1). Regarding absorption capacities and energy consumes, they present moderate absorption capacities (25 m^3/m^3) and lower enthalpies of reaction than traditional amines (-40 kJ/mol), which will be translated into lower energy consumptions. Process simulation studies conclude that systems based on these ILs present similar efficiencies than MEA process but significantly slower mass transfer kinetics, due to their high viscosities [115]. All of it results in problems associated to the kinetics of the process and regeneration stage.

ILs based on Aprotic Heterocyclic Anions (AHAs): these ILs consist of an anion with a functionalized heterocycle [116]. The nitrogen of the heterocycle presents a 1:1 stoichiometry. The reaction is completely displaced to products. These ILs are specifically designed to chemically retain CO_2, so they present high absorption capacity and relatively low enthalpy of reaction (40 – 55 kJ/mol [117]). Therefore, regeneration stage will be less energy demanding compared to traditional amines processes. One advantage of these ILs is that their performance is not affected by the presence of water in the system [117]. However, it provokes a slight increase in the viscosity of the media, due to the formation of hydrogen bonds [117]. In this sense, the selection of the cation is important, being long chain phosphoniums, those with lower viscosity values. On the contrary, the use of imidazolium cations leads to the competition between the anion and the cation with CO_2 giving as a

result a non-stable IL [117, 118]. Therefore, the viscosity range is between 100- 500 cP at 25 °C [119], not as high as other "Task Specific ILs", which facilitates the CO_2 absorption kinetics.

2.2.2 Acetylene (C_2H_2)

Acetylene or ethyne is the simplest alkyne. It is a colorless gas with no odor. It is a lightweight and flammable compound with high combustion temperature [120]. In next sections, importance of acetylene and actual technologies to remove it from gaseous effluents are collected. Last research on the use of ILs to treat acetylene are also provided.

2.2.2.1 Importance of acetylene

Pure acetylene is relatively not toxic to human health. It can only act as asphyxiant when displacing the available oxygen. A concentration of 10% produces a slight intoxication, and no adverse effects were found from chronic exposure. Moreover, acetylene does not seem to be a significant component for air pollution, so actions are not required from this point [121]. However, chemical applications of acetylene are diverse, so its separation and purification are important for the chemical industry. In fact, *Zion Research* has published a report collecting the global demand of acetylene in last years and future prospects [122]. Figure 7 presents the global acetylene gas market (2014-2020).

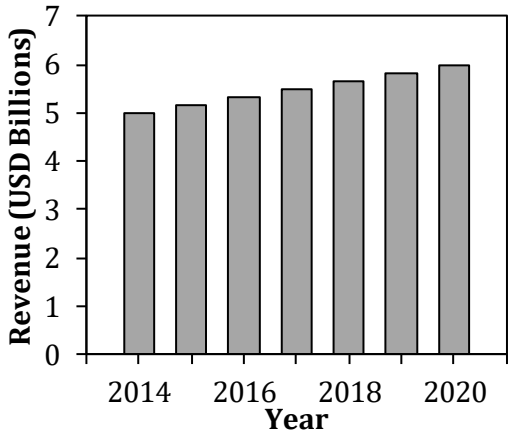

Figure 7: Global acetylene gas market (2014-2020).
Source: Zion Research Analysis 2015 [122]

As shown, demand of acetylene is growing in last years. The high demand of the compound is due to the chemical, welding & cutting applications [122]. Taking advantage of the great flammable properties that acetylene possesses, it is widely used in welding, brazing, cutting, hardening, texturing, and thermal spraying of many materials [123].

Besides the mentioned applications, acetylene is used industrially as reactive in important reactions. Vinylation reactions consist of the addition of compounds such as water, alcohols, amines… to acetylene to form vinyl compounds used for polymerization [124]. First industrial vinylation products were acetaldehyde, vinyl chloride and vinyl acetate. Other example is ethynylation reactions, which consist of the additions of carbonyl compounds to acetylene remaining the triple bond intact [123]. The most important products from these reactions are propargyl alcohol and butynediol. Carbonylation are reactions between acetylene and carbon monoxide using water, alcohols or amines. Traditional products of this reaction are acrylic acid, ethyl acrylate, hydroquinone, among others [124]. Cyclization and polymerization of acetylene

consists of the reaction of acetylene with itself to form cyclic and linear polymers. In this sense, products synthetized are polyacetylene, 1,3,5,7-cyclooctatetraene, among others [125].

2.2.2.2 Production of acetylene

Traditionally, acetylene is produced from hydrocarbons through reactions that require very high temperatures and short reaction times. Due to the severe operating conditions needed, the correct hydrocarbon: oxygen ratio, which also determines the reaction temperature, is essential to obtain good acetylene yields [123]. Among all the hydrocarbons used, methane is of particular interest, but all of them follow similar reaction schemes. In this sense, the formation of acetylene is carried out at reaction temperatures in the range of 800 – 1500 °C. Oil is used at cooling down stage for being more thermally efficient than water. All the acetylene processes yield a number of by-products (H_2 or CO, among others), which may cause problems if acetylene is the only desired product, so its separation and purification is essential. BASF process for the production of acetylene from gas natural is applied since 1950 [126]. Some plants around the world use this technology to produce acetylene. The main idea of these plants is to use the flame reaction on hydrocarbons and oxygen. In this case, the amount of oxygen is the key to the production of high amount of acetylene [126]. In this process, acetylene needs to be recovered from the mixture of by-products formed during the reaction.

Production of acetylene from calcium carbide is of primary importance for welding applications. The reaction consists of calcium carbide with water to form acetylene and calcium hydroxide. This reaction is highly exothermic so, it is important to dissipate the

generated heat. During the reaction, other gaseous compounds, such as sulfur and phosphorus compounds are formed with acetylene and they must be removed due to harmful effects to the synthesis process [123].

It is important to mention the production of acetylene as by-product of steam cracking. In this kind of processes, hydrocarbons are converted into olefins such as ethylene and propene. However, undesired compounds such as acetylene are formed. Typical concentrations of acetylene on these streams are between 0.25 – 2.1 wt%. Therefore, it is important to develop technologies to recover acetylene from these streams.

It is clear that acetylene production present undesired compounds during the synthesis process. In addition, acetylene was also found as by-product of other synthesis processes. Therefore, next section presents the traditional technologies for acetylene removal or recovery.

2.2.2.3 Available technologies for acetylene treatment

The most extended industrial application to remove acetylene is selective hydrogenation. However, due to the great number of industrial applications that acetylene presents, absorption using traditional solvents is also employed. In this case, acetylene is recovered with high purity.

Acetylene selective hydrogenation: this technology consists of the selective hydrogenation of acetylene to ethylene using a Pd-based catalyst [127]. This technology is normally implemented at ethylene production plants because acetylene is produced as by-product during the synthesis stage. Thus, selective hydrogenation makes possible to produce more ethylene, which is the aim of this kind of plants [123].

Typical operating conditions are 40 – 120 °C and 15 – 40 bar of pressure. Different options are found depending on the type of feed to the plant: i) front-end hydrogenation (streams usually contain H_2, CO, methane, C_2H_2, C_2H_4 and C_2H_6), ii) raw-gas hydrogenation (before C_2/C_3 separation, streams contain H_2, CO and hydrocarbons) and iii) tail-end (pure C_2 stream) [123].

Acetylene Absorption: it typically uses traditional solvents such as N,N-dimtehylformamide (DMF) and N-methylpyrrolidinone (NMP). In these processes, the operating pressure is between 0.8 – 3.0 MPa. Other compounds involved in the gas mixture may be harmful to the traditional solvents [123]. *Linde Engineering* commercializes a technology for efficient acetylene production [128]. Linde process uses DMF as solvent, with plant capacities up to 15,000 metric tons per year. However, typical problems associated to traditional volatile solvents are promoting the search of new solvents that can overcome their limitations. In this sense, new solvents should show melting points lower than the dew point of feed gas, high solubility and selectivity of acetylene, high thermal and chemical stability, low toxicity and low vapor pressure at the operating temperature [123]. ILs have attracted the attention to scientific community because they satisfy the requirements as suitable solvents for acetylene recovery. Next section will evaluate the state of the art of ILs as acetylene absorbents.

2.2.2.4 Acetylene capture with ionic liquids

First work regarding acetylene absorption with ILs studied the acetylene/ethylene separation using computational and experimental measurements [129]. They concluded that basic anions interact with hydrogen atom(s) of acetylene, resulting in higher acetylene solubility

and selectivity. In this sense, anions based on phosphate and phosphonate groups presented the best performance. Then, further research was done following the previous publication, correlating the hydrogen bond basicity with acetylene solubility of those previous selected ILs [130]. The experimental and theoretical conclusions of this work are in good agreement with previous ones, reporting higher acetylene absorptions by selecting ILs with high hydrogen-bond acceptor ability of the anions.

Later, two theoretical studies [131, 132] employing molecular dynamics simulation reported again the higher solubility and selectivity by anions able to accept hydrogen bonds. Finally, COSMO-RS has been used to design new functionalized ILs able to separate efficiently acetylene/ethylene mixtures [133]. In this case, anions based on acetate anions with long alkyl chains are suggested to absorb acetylene.

2.2.3 Hydrogen Sulfide (H_2S)

H_2S is a colorless, flammable, corrosive and toxic gas with a characteristic odor. In this section, the problematic of H_2S emissions is shown. Then, available technologies to avoid its emission and emerging technologies based on ILs are collected.

2.2.3.1 H_2S as contaminant

Exposure to H_2S can cause health problems comprising inflammation and irritation of eyes, dizziness, headache, nausea or even death if concentration goes up to 300 ppm. H_2S combination with water or oxygen produces SO_2, one of the responsible of the well-known “acid rain”, so it can produce extremely negative effects to the atmosphere [134]. In fact, SO_2 is one of the called greenhouse gases (more

information about its emission can be found in section 1.2.1.1 of the introduction of this PhD thesis). Figure 8 presents the distribution of sulfur emissions by main sectors [135].

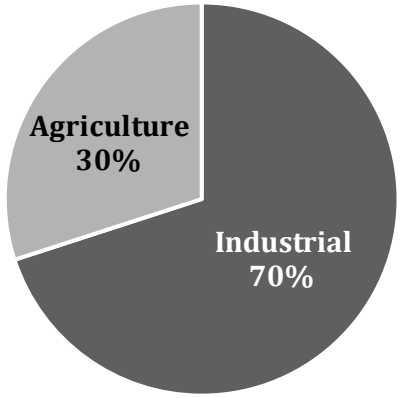

Figure 8: Distribution of sulfur emissions. *Source: Convention on Long-range Transboundary Air Pollution [135]*

As can be seen, agriculture source presents a great contribution with H_2S form, but industry is the sector that more sulfur compounds produces. In this sense, it is important to develop systems to remove H_2S present in the industry prior to its release to the atmosphere.

Specifically, gas natural has become one of the most promising alternatives to the traditional and pollutant energy sources due to its cleanliness [136]. Unfortunately, natural gas streams often contain sulfur compounds, being H_2S the most important one. In fact, streams that present sulfur compounds impurities are called “sour gas”. The gas is considered sour when H_2S content is more than 4 ppm by volume [137]. Therefore, the removal of acid gases from these streams is commonly called “sweeting” process. For all these reasons, it is important to completely remove the H_2S present in natural gas streams.

Moreover, the removal of H_2S increases the calorific value of the natural gas [138].

2.2.3.2 Available technologies for H_2S treatment

A huge number of technologies are available for H_2S treatment. However, the most extended one in the industry is chemical absorption with amines [139].

Chemical absorption with aqueous amines: packed or plate columns are used at operating temperatures from 30 to 50 °C and pressures between 5 – 205 atm [140]. The process is essentially the same as the homologue for CO_2 capture with amines (see details in section 1.2.1.3.A) using MEA and DEA. They, again, present good H_2S absorption capacities at low partial pressures but high energy demanding consumptions in the regeneration stage due to the high volatility of the absorbent. Moreover, the presence of CO_2 in the streams result in competitive absorption with amine solutions [141].

Physical absorption was also accomplished using the same commercial solvents than for CO_2 physical absorption (see details in section 1.2.1.3.B). In this sense, Rectisol, Selexol and Morphysorb are those more employed [142]. Previous works reported that methanol process requires the lowest circulation rate and lowest net power to absorb H_2S [142]. A comparison between Rectisol and Selexol suggested that Selexol treating to be less costly than Rectisol [143]. Their high volatility values hinder, once again the regeneration process.

Membrane contactor: it has been introduced to enhance the absorption performance and solve some problems such as foaming, corrosion [144]. In this case, the membrane is used as a barrier between

the liquid and the gas phase, allowing the transport of species of gas into the liquid. Hollow fiber polymeric membranes are usually employed to accomplish the task. In acid gas removal, the gas goes inside the tube while liquid solvent goes from the shell [139]. Industrial application of this technology is difficult because polymeric membranes does not tolerate high temperature off-gases containing H_2S.

Adsorption: different adsorbents have been tested for H_2S capture. Commonly, active carbons are used due to their high specific surface area and pore volume. Modifications of the activated carbon surface by treatments with NaOH and KOH can promote reactive adsorption [145]. Metal-oxide adsorbents are also employed covering a wide range of operating temperatures (25 – 1600 °C) and can reduce H_2S concentrations to 10 ppm [146]. However, high energy demanding consumption in the regeneration operation reduces their potential industrial application.

Claus process: this system is employed to remove H_2S in high concentrations. It consists of two steps: thermal oxidation and catalytic reaction [147]. It presents the main limitation that, due to thermodynamic restrictions, 3 – 5% of H_2S remains untreated, so selective catalytic oxidation has to be used to completely remove the remaining gas.

Next section presents the state of the art of H_2S absorption using ILs, which is an emerging technology that may overcome the limitations of traditional solvents.

2.2.3.3 H_2S capture with ionic liquids

In the last decade, different ILs have been evaluated as H_2S absorbents by physical absorption [148]. First work regarding H_2S capture with ILs reported the performance of hexafluorophoshpate based IL [149]. In this case, it exhibits moderate absorption capacity, but due its viscosity and low stability in moisture conditions, the practical application of this IL is difficult. However, it was stablished as reference to compare the performance of other ILs. Anions based on $[NTf_2]^-$ present higher absorption capacities, which are increased with increasing the length of the alkyl chain of the imidazolium cation, probably due to the increased free volume [150, 151]. Then, ILs based on tris(perfluoroalkyl)trifluorophosphate $[FAP]^-$ anion exhibited higher H_2S affinity [152], but less selectivity than others studied.

Later, anions based on Cl^- and Br^- exhibited a great ability to selectively separate H_2S from CO_2 [153], even better than those reported for MDEA-based solvents. This is due to the small and highly coordinated anion, able to give strong hydrogen bond interactions. Until then, all the research was focused on H_2S physical absorption. On the other hand, ILs based on carboxylate anions were proved [154] to present a non-ideal profile. This behavior is attributed to the ability of carboxylate anions to chemically absorb H_2S, showing good hydrogen bond acceptors. As demonstrated, hydrogen bond capacity marks H_2S absorption, and in most of the cases it is carried out by the anion, so it is important to select anions with ability to form hydrogen bonds with H_2S.

2.2.4 Nitrogen Oxide (NOx)

In this section, problem of NOx emissions and the actual technologies to remove them are described. Then state of the art regarding NOx capture with ILs is reported.

2.2.4.1 NOx emissions

Nitrogen oxides (NOx) term includes nitric oxide (NO), nitrogen dioxide (NO_2), and other oxides of nitrogen. NOx play an important role in environmental and human health effects [155]. Harmful human health effects comprise respiratory problems causing inflammation of the airways at high NOx concentrations. Long term exposure can affect lung function, increase the risk of respiratory problems and increases the response to allergens [155]. Among the concerns regarding the presence of NOx in the troposphere, it is found smog formation, acid rain, and ozone layer depletion [155]. In addition, problems regarding global warming are the same exposed for CO_2 on Section 1.2.1.1 of Introduction.

The trend of NOx emissions by different sectors in last years is shown in Figure 9 [155]. NOx emissions follow the same trend as the rest of greenhouse gases. Their emissions are decreasing since 2006 according to the International Energy Agency. The distribution of emissions by sectors reflects that transport contributes notoriously. In this sense, transition from classic petrol vehicles to hybrid and electric in next years will contribute to the decrease in the emissions of that sector [156]. Regarding rest of the sectors, all derived from industrial and power stations contribute to more of the 50% of the emissions. In this case, we can divide the formed NOx in: i) fuel NOx (formed by nitrogen-containing compounds), ii) thermal NOx (formed in combustion process at high temperatures), and iii) prompt NOx (formed by the reaction of

hydrocarbon fragments with atmospheric N_2) [157]. Some of them are unavoidable due to the formation when nitrogen is present. For this reason, it is important to develop technologies able to capture the undesired NOx.

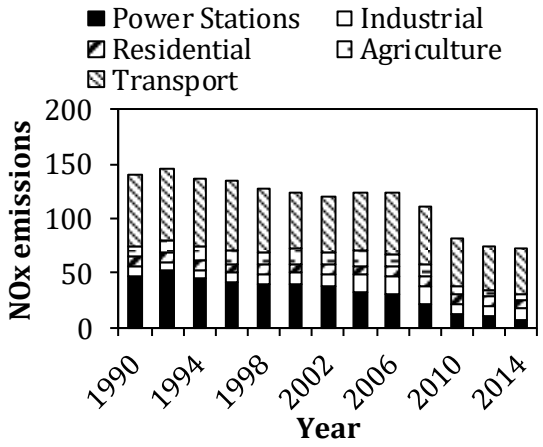

Figure 9: NOx emissions sources and trends. *Source: Environmental Protection Agency (EPA) [155].*

2.2.4.2 Available technologies for NOx treatment

Technologies for NOx abatement are divided in two great groups: primary and secondary techniques. Primary techniques are devoted to reducing the emissions at source to avoid formation of NOx. Secondary techniques are those that treat the formed NOx in the flue gases, commonly named as post-combustion treatments. This section presents the most typical technologies to treat NOx comprising both primary and secondary techniques.

Low-NOx Burners. They are considered a primary technique and are specially designed to reduce the formation of the three NOx types. They are based on the principles of *staged air combustion, flue gas recirculation* and *staged fuel combustion*. New low-NOx burners combine

the three reduction techniques [158]. The staged air combustion technique creates two distinct combustion zones, one with low oxygen concentrations (formation of N_2 instead of NO) and the other with excess of oxygen (end of combustion) [159]. Flue gas can be recirculated into combustion chamber. The case of staged fuel combustion technique consists of the reduction of NOx already formed creating three combustion zones: primary as secondary, and a post-combustion zone. 80% of the fuel is injected into primary zone where combustion takes place in excess of air. The remaining fuel is injected into secondary zone. This generates a reducing environment, as hydrocarbon radicals produced in this zone reduce thermal NOx to N_2 [160]. Drawbacks of this technology are the formation of CO as by-product and the necessity to pulverize solid fuel prior to the inlet in combustion chamber.

Selective Non-Catalytic Reduction (SNCR): it is considered a secondary technique and uses ammonia, urea, and isocyanic acid as reducing agents at high temperatures [161]. Being catalyst-free, SNCR is simply and easy to implant on existing plants, so it is widely applied in the industry. Due to prize, safety, and convenient transportation, urea has been prioritized as reducing agent in SNCR processes [162]. However, it presents the disadvantages of high operating temperatures (above 600 °C), while temperatures above 750 °C reduce selectivity and efficiency. In this sense, results of practical applications of SNCR reported efficiencies between 30 – 40% [163].

Selective Catalytic Reduction (SCR): limitations of SNCR make relevant the development of catalysts to improve efficiency and selectivity, reducing the operating temperature. In fact, this is the most extended technology used nowadays in the industry. SCR with ammonia was identified as the most promising method for the reduction

technology in spite of the strong contaminant character of ammonia [164]. The reaction comprises equimolar concentrations of NH_3 and NO with a few percent of oxygen to form N_2 and water at operating temperatures between 300 – 400 °C [165]. Different catalysts have been proved in SCR reaction, but those using noble metal catalysts are very effective, and simultaneously very active NH_3 oxidation catalyst [166]. Vanadium-tungsten-titanium catalysts are also analyzed, operating efficiently at temperatures between 200 – 450 °C [167]. Typical content of V_2O_5 is 5-10 wt%, acting over AlO_2 support. SCR can be placed in different positions of the process, beginning (high dust), medium (low dust) and end position (tail-end). The technology presents disadvantages regarding deactivation of the catalyst due to the presence of alkali hydroxides formed in combustion processes and the high operating temperatures needed to reach good efficiencies. For these reasons, new technologies with different catalysts are being investigated to reduce operating temperatures maintaining high efficiency in the NO removal.

2.2.4.3 NOx capture with ionic liquids

Few works reported NOx capture using ILs. However, they are promising IL absorbers that can selectively retain flue gas components. First work related to NOx absorption with ILs, presented the first functional IL able to capture NO [162]. They reported a molar capacity of 4.52 mol NO per mol IL. However, this kind of ILs presents the difficulties on synthesis stage, which would limit its industrial application. Then, a metallic functional IL, $[bmim]_2[FeCl_4]$, was synthetized. This IL was able to chemically absorb NO [168]. An absorption capacity up to 0.8 mol NO captured per mol IL was observed. When testing cyclic absorption-desorption experiments, a lower capacity of 0.3 mol NO per mol IL was

obtained without loss of capacity after 4 consecutive cycles. Deep eutectic solvents (DES) were also proved as NO absorbents, reaching capacities of 4.25 mol NO per mol DES [169].

It is important to develop systems able not only to remove NOx but also to convert them into value added products. In this sense, an interesting work developed at the Technical University of Denmark reported [bmim][NO_3] as successful catalyst for NO oxidation to higher NOx species, and HNO_3 in last term, in presence of water [170].

2.3 ADVANCED MATERIALS BASED ON IONIC LIQUIDS

Evaluation of ILs as solvents of different gases (CO_2, C_2H_2, H_2S and NOx) concluded the high affinity and absorption capacities that these systems present by the different solutes of interest. However, one conclusion is repeated along the analysis: high viscosity of ILs limits the mass transfer diffusion over the ILs. Especially in those that present chemical absorption and are particularly viscous, which would hinder their practical application when compared with processes based on amines. Therefore, it is necessary to develop advanced systems based on ILs able to overcome the kinetic restrictions of pure ILs. Thus, Supported Ionic Liquids and Encapsulated Ionic Liquids were defined.

2.3.1 Supported Ionic Liquid Phase (SILP)

One way to overcome gas absorption kinetic limitations is by using SILPs (*Supported Ionic Liquid Phase*). It consists of the distribution of a thin layer of IL over the surface of a porous support. SILP concept was introduced for the first time with an Rh catalyst suspended in IL, for its use in a slurry type reactor for hydroformylation [171]. The study concluded that SILP formulation was not ideal for liquid phase reactions

because partial dissolution of the IL into the liquid phase leading to leaching of the Rh catalyst. Then, it was introduced SILP for heterogeneous gas phase reactions [172]. Again, Rh was used as active phase over the IL, but this time in a gas phase reaction: hydroformylation of propene in a continuous gas flow. Supports of different nature can be used to create SILPs, but all of them presenting high surface, such as activated carbons [173], SiO_2 [174], or MOFs [175], among others.

The general procedure to synthetize SILP is to dissolve the IL in a low boiling-point solvent (usually methanol or acetone) and introduce the support to the dissolved IL prior to gentle evaporation of the solvent to ensure evenly dispersion of the IL on the support. The resulting SILP appearance is completely dry. It was concluded that using this material, mass transfer limitations over the IL surface become negligible, so they are able to overcome the restrictions observed when using pure ILs [176]. On the contrary, these materials present a great limitation, which is the IL loading that are able to contain. In this sense, the amount of IL depends on the porosity of the material but it usually stays below 20% in weight [177], although, in some cases the loading reaches 50% [175, 178]. This fact reduces the absorption capacity in relation to that of the pure IL. In order to incorporate a larger amount of IL on the support, the use of Encapsulated Ionic Liquids (ENILs) is considered.

2.3.2 Encapsulated Ionic Liquids (ENILs)

ENIL materials consists of a solid support with the IL incorporated in form of micro drops. In this sense, the main difference respect to SILPs is the distribution of the IL on the support. Different ENIL materials have been synthetized aimed to different applications. Different types of

supports can be used, such as polymers [179-181] or zeolites [182] with a high IL loading.

The research group in which is framed this PhD thesis has developed ENIL materials based on carbon sub-microcapsules [183]. This support consists of hollow carbon capsules of diameters between 400 – 700 nm with a great central hollow and a mesoporous shell. The IL is located covering the completely specific surface of the support (central hollow and porous shell) [184] with IL loadings up to 80%w, much higher than those reached when using SILPs. Therefore, ENILs gather the advantages acquired by SILPs (overcoming mass transfer kinetic problems of pure ILs) but also are able to retain a high load of IL, and therefore high absorption capacities.

These materials have been successfully applied to different gas capture applications, such as ammonia [184, 185] and CO_2 [186-188]. In fact, this PhD thesis presents a continuation of Dr. Moya's research in the field of CO_2 capture using ENILs [189].

2.4 COMPUTATIONAL TOOLS FOR DESIGN SEPARATION PROCESSES BASED ON IONIC LIQUIDS

The use computational tools can facilitate very significantly the ILs selection before experimental tests due to the huge number of potential combinations cation-anion. For this reason, COSMO-RS method is an useful tool because it allows analyzing interactions between ILs and solutes of interest without the needing of any experimental data [190, 191]. Moreover, industrial applications of ILs can be analyzed more realistically by means of process simulation using AspenONE®. The

combination of both computational tools can be very helpful in order to develop and evaluate new processes based on ILs.

2.4.1 COSMO-RS method

COSMO-RS method (**CO**nductor-like **S**creening **MO**del for **R**eal **S**olvents) is a predictive quantum chemistry method with the purpose of predicting chemical potential in liquids created by A. Klamt in 1995 [190]. Then, a refined version was developed in 1998 [192]. Newer developments and re-implementations were later carried out [193, 194].

COSMO-RS is based on COSMO continue solvation method, in which a molecule in solution is described as an isolated molecule in a cavity of a solvent. The model calculates the charge density polarity (σ) produced in the solute-solvent context [191].Then, the molecule is treated as different segments of the polarized charge surface, which is easily collected in a histogram called *σ-profile*. Then, it is possible to calculate the chemical potential of each segment, visualized on *σ-profile*. It describes the affinity of the system to a determined polarized segment. Using *σ-potential* and thermodynamic relationships, it is possible to determine the chemical potential of a solute in a solvent. This is how activity coefficients are calculated.

Different quantum-chemical software generates the required information for COSMO-RS calculations. Thus, Turbomole, Gaussian, DMOL3, ORCA, Molpro… are able to generate the relative information related to the surface of polarized charge distribution used by COSMO-RS method (*.cosmo file) [190].

COSMO-RS method has been demonstrated to be a useful tool for the property predictions of ILs. In this sense, pure properties predictions

[195-197], vapor-liquid equilibria [198-201], liquid-liquid equilibria [200, 202, 203], among other characteristics are evaluated. Moreover, interactions between solutes and ILs, with each contribution can be easily analyzed by this methodology [195, 196]. Related to the aim of this PhD thesis, COSMO-RS method was applied to gas capture applications of different nature. In this sense, the investigation group in which this PhD thesis is framed carried out different works related to ILs-based systems for separation processes [204], CO_2 capture [205-207], aromatic extraction [208], toluene absorption [209], propane/propylene separation [210], volatile organic compounds absorption [211], or ammonia capture [212, 213], among others.

2.4.2 Process simulation

The use of process simulators can be helpful to design new processes based on ILs but also to minimize experimental tests by selecting the IL attending to its performance at process. In this sense, process simulation can be used to estimate the real viability of the process, the unit operations design, complete process, costs or process optimization. Among commercial process simulators traditionally employed, Aspen Plus, Aspen HYSYS, Promax, UniSIM… are broadly used. The introduction of chemical and physical properties of components involved in the simulation are required to successfully simulate the operation [214]. In this sense, the accuracy of the information introduced to the simulator affects directly to the reliability of the results obtained from process simulation [215]. In simulations with conventional compounds involved, physical and chemical information of the compounds is included on large databases of the process simulator. However, until the date, ILs are not conventionally included on databases of commercial process simulators. Therefore, different options to include ILs as compounds are available.

Conventional compounds: Conventional process simulators allow the incorporation of ILs as conventional compounds. Pure component properties must be introduced to the simulator, such as density, viscosity, molar volume, boiling point, surface tension, heat capacity, and their dependence with the temperature, among many others. Then, using the thermodynamic models as default in process simulator (Peng-Robinson, PRSV, NRTL, UNIQUAQ…), experimental data is modeled. This methodology presents the advantage of the great precision of the modeling. However, the necessity of collecting such amount of experimental data is hardly time and cost demanding. In fact, taking into account, the number of existing ILs, their prize, and the extreme difficulty to measure some properties, such as boiling point, use of this methodology to study the viability of new processes based on ILs is in clear doubt. One example of the application of this methodology are the inclusion of 1-ethyl-3-methyilmiidazolium tris(pentafluoroethyl) trifluorophosphate ([emim][FAP]) to perform thermodynamic calculations using Peng-Robinson model, involving CO_2 and hydrocarbons solubility on ILs [216]. The use of NRTL thermodynamic model was also accomplished, modelling the liquid-liquid equilibria of ternary mixtures: heptane-toluene and 1-ethyl-3-methylimidazolium ethylsulfate to accomplish the extraction unit operation [217]. Both works reported the high accuracy of the methodology used but it is important to remark that in both cases only an individual operation was studied. For this reason, the application of this methodology to select ILs as potential components in industrial processes is difficult.

Group Contribution Methods (GCM): they are used to estimate pure component and its mixtures properties. UNIFAC (UNIQUAC Functional-group Activity Coefficients) [218] is the most extended one among

commercial process simulators. Originally, it was developed for the prediction of activity coefficients in nonelectrolyte liquid mixtures. Regarding the compounds of interest of this PhD thesis, group parameters of UNIFAC model were extended for its application to ILs systems [219]. The main advantage of the use of this methodology is that its formulation is simple and can be directly incorporated into commercial process simulators. However, the large number of ILs possibilities may mean the expansion of the UNIFAC groups, which will difficult its "simple" application. One example of the application of this methodology in Aspen Plus process simulator is the evaluation of ILs for n-hexano-methylcyclopentane extractive distillation [220]. In this work, a large number of experimental data were collected. Then a combination of UNIFAC-IL model with a mixed integer nonlinear program was applied to compare the performance of ILs with benchmark solvent employed in the industry. Moreover, extractive desulfurization of fuel oils using ILs with UNIFAC groups was also studied [221]. They used Aspen Plus simulator to optimize the liquid-liquid extraction performance of ILs in a given multicomponent model.

The aforementioned methodologies to simulate ILs in commercial process simulators present drawbacks, such as the necessity of introducing experimental data or the development of contribution groups. For this reason, ILs group of the Chemical Engineering Department of Universidad Autónoma de Madrid developed a multiscale methodology, in which no experimental data is required to perform process simulations with ILs [222-224].

2.5 MULTISCALE APPROACH FOR THE DESIGN OF PROCESSES BASED ON IONIC LIQUIDS

Multiscale approach aims to the development of new processes based on ILs using simultaneously molecular and process simulation. In this sense, COSMO-based property methods, such as COSMO-RS [190] or COSMO-SAC [193] are able to solve the problems derived to the incorporation of ILs into commercial process simulators. These methods can predict thermo-physical properties of ILs without the necessity of adding any experimental data. AspenONE process simulators have included COSMO-based methods to estimate activity coefficients through the called COSMOSAC property model [225].

ILs are introduced to the simulator as pseudo-components. The required properties to completely define ILs from this way are density, normal boiling point (NBP), and molecular weight. All these pure component properties are calculated by using COSMOtherm software (see more details in Section 1.4.1 of this PhD thesis). Then, remaining properties necessary to define COSMOSAC thermodynamic model are σ-profile and molecular volume. Once again, these properties are calculated by COSMO-RS method. In order to have accurate results on mass transfer kinetic calculations, viscosity and its dependence with the temperature is also provided to the simulator [13]. The scope of this methodology is the conceptual design of new processes based on ILs. In this sense, new contributions are found using it: i) evaluation of ILs as solvents in processes at industrial scale, ii) introduction of additional criteria for the selection of ILs as potential absorbents, iii) study of the viability of processes based on ILs comparing with available technologies traditionally employed.

This methodology has been applied to different processes in last years, such as toluene absorption [209], absorption refrigeration cycles using ILs [226, 227], regeneration of ILs in separation processes [228], CO_2 capture [229, 230], aliphatic-aromatic separation [231-233], among others. Recently, ILUAM database was created, including 100 ILs for its use in AspenONE process simulators [234]. The database is available online and free of charge for scientific community.

3. AIM & SCOPE

AIM & SCOPE

The aim of this PhD thesis is the development and evaluation of advanced materials based on ILs devoted to gas treatment.

In the first stage of the study, the potential application of ILs in the separation of acetylene and hydrogen sulfide from gas streams is evaluated using COSMO-based/Aspen Plus computational methodology. To achieve this task, molecular and process simulation are simultaneously used to analyze the possible advantages and disadvantages of using ILs in absorption operations for separating these solutes of industrial interest. Different steps were accomplished for the consecution of this objective:

1. Screening of suitable ILs as absorbents of specific gas solute from a huge database of solvents using COSMO-RS method.
2. Analysis of solute-ILs interactions using COSMO-RS method.
3. Evaluation of solvent performance of selected ILs in industrial absorption column using Aspen Plus process simulator, by means of equilibrium and rate-based models.
4. Evaluation of IL regeneration stage using Aspen Plus simulations, to estimate the separation efficiency and energy consumption and to compare with available industrial technology.

In the second stage, problems related to absorption mass transfer rates in ILs tried to be solved by their immobilization on solid supports. In this case, CO_2 capture was analyzed due to the well-known problematic associated to its emissions. The following partial objectives were found to be essential to the achievement of the main goal:

1. Synthesis, characterization and evaluation of Encapsulated Ionic Liquids (ENILs) as CO_2 physical sorbents.
    a. Selection of ILs with similar thermodynamic but different kinetic behaviors using COSMO-based/Aspen methodology to study the influence of the ILs in the CO_2 capture process with ENILs.
    b. Experimental evaluation of ENILs to solve the mass transfer kinetic problems of ILs.
    c. Experimental evaluation of selected ENILs by means of gravimetric and fixed-bed tests to demonstrate the thermodynamic control of CO_2 capture operation using ENIL sorbent.
2. Synthesis, characterization and evaluation of ENILs as CO_2 chemical sorbents using amino acid based ILs (aa-ILs).
    a. Evaluation of a more realistic approach of aa-ILs for CO_2 capture by both thermodynamic and kinetic analysis. ENILs are proposed to overcome the kinetic limitations of pure aa-ILs.
    b. Study of the mechanism of reaction by DFT calculations and infrared spectroscopy tests.
    c. Thermodynamic model approach to obtain characteristic physical and chemical contributions to CO_2 absorption by aa-ILs.
3. Synthesis, characterization and evaluation of Supported Ionic Liquids (SILPs) as CO_2 chemical sorbents using an acetate-based IL.
    a. Evaluation of the influence of SILP particle size on thermodynamic and kinetic behavior of CO_2 capture by means of gravimetric and fixed-bed tests, at

different operating conditions (temperature, CO_2 partial pressure and gas flow).

b. Modeling of experimental thermodynamic and kinetic curves using Aspen Adsorption process simulator.
c. Proposal of an empirical model to describe the kinetics of the operation.
d. Design of CO_2 capture processes based on SILPs at given conditions by optimizing SILP particle size.

Last stage was able due to the international stay with Prof. Fehrmann's group at the Technical University of Denmark. In this case, ENILs materials were tested for NOx treatment:

1. Evaluation of ENILs as NOx oxidation catalysts in dry and humid conditions.
2. Evaluation of the effect of IL loading on the oxidation process.
3. Study of the promotion of the reaction by the addition of methanol.

4. CONCLUSIONS/CONCLUSIONES

CONCLUSIONS

Results extracted from this PhD thesis contribute to the potential application of ILs as solvents in the industry. This work joins the results of both computational tools and experimental tests to develop efficient advanced systems based on ILs for gas treatment. For one side, different experimental techniques were employed, such as gravimetry, IR spectroscopy and fixed-bed to evaluate the thermodynamic and kinetic behavior of the proposed materials in gas separation and conversion. For other side, COSMO-based/Aspen Plus methodology was used to select and evaluate ILs as absorbents of different gases. Lastly, Encapsulated Ionic Liquids (ENILs) and Supported Ionic Liquids (SILPs) were developed and evaluated in physical and chemical CO_2 capture, demonstrating that allow overcoming the mass transport limitations of ILs. These materials were also successfully proved as catalysts for NOx oxidation.

The main conclusions extracted from this PhD thesis are divided in three great blocks:

1. ILs as potential acetylene and hydrogen sulfide absorbents.
    - Molecular simulation using COSMO-RS allows the reliable selection of those ILs with most favorable thermodynamic and kinetic characteristics for the separation among a wide number of cation-anion combinations.
    - Process simulation using Aspen Plus concludes that no thermodynamic restrictions are observed among selected ILs compared to benchmark solvents in absorption unit operation. Mass transfer kinetics is found to control the operation using ILs due to high ILs viscosity. Therefore, higher

absorption column dimensions are needed. Consequently, those ILs that present more favorable mass transfer properties are those more suitable for the task. Regeneration stage demonstrates the advantage of using ILs reaching a total recovery with high solute purities, due to their low vapor pressures.

2. Immobilization of ILs on solid supports for CO_2 physical and chemical capture.
    - ENILs in CO_2 physical absorption are proved to solve the kinetic restrictions of pure ILs, preserving the CO_2 absorption capacity of the latter. Fixed-bed experiments reveal that there are no significant differences in absorption rates between tested ENILs with different ILs. Bed efficiencies are determined by the solubility of CO_2 in ILs. Therefore, selection of IL for CO_2 capture moves from kinetic criteria (viscosity) in the case of pure ILs to thermodynamic criteria (CO_2 solubility) in ENILs.
    - ENILs in CO_2 chemical absorption with amino acid based ILs are shown to solve the problems of pure aa-ILs as CO_2 chemical absorbents (very viscous and solid formation when reacting with CO_2). It was proposed a reaction mechanism based on DFT calculations and experimental infrared spectra. Physical (Henry's law constant) and chemical (equilibrium constant) contributions to CO_2 absorption are calculated from experimental data. Their associated enthalpies of reaction reveal an easy reaction reversibility and sorbent regeneration under mild conditions.
    - Thermodynamic and kinetic behavior of SILPs of different particle sizes on CO_2 chemical absorption is

evaluated. Gravimetric measurements show that CO_2 sorption capacity is only attributed to the IL regardless of the SILP particle size. Experimental breakthrough curves are fitted revealing that kinetics of the process are hardly affected by a reduction of SILP particle size. Aspen Adsorption is used to evaluate SILP behavior at different conditions of those experimentally tested. Results conclude that at low CO_2 partial pressures, chemical reaction is the controlling stage and higher CO_2 partial pressures lead to mass transfer control. This methodology allows optimizing sorption operation at given conditions selecting the adequate SILP particle size.

3. ENILs as catalysts for NO oxidation.

   - ENILs are proved as successful catalysts for NO oxidation at low temperatures. Experimental results compare the behavior of empty carbon capsules with ENILs with different IL loading. Results in dry conditions suggest that reaction is favored at low IL loadings. Experiments in humid conditions reveal that NO oxidation reaction is not being inhibited in presence of water, opposite behavior of that observed for empty carbon capsules. The reaction is promoted by the addition of methanol (in presence of water). An increase in 20% of conversion is observed when temperature is increased up to 60 °C. ENILs exhibit the best catalyst performance among those tested in humid conditions.

CONCLUSIONES

Los resultados extraídos de la presente tesis doctoral contribuyen a la potencial aplicación de los LIs como disolventes en la industria química. Este trabajo reúne los resultados obtenidos mediante herramientas computacionales y ensayos experimentales en el desarrollo de sistemas avanzados basados en LIs para el tratamiento de gases. Por una parte, se emplearon distintas técnicas experimentales, como gravimetría, espectroscopia de infrarrojo y lecho fijo para evaluar el comportamiento termodinámico y cinético de los materiales propuestos para la separación y conversión de gases. Por otra parte, se utilizó la metodología COSMO/Aspen Plus para seleccionar y evaluar los LIs como absorbentes de distintos gases. Por último, se desarrollaron los líquidos iónicos encapsulados (ENILs) y soportados (SILPs) para su evaluación en la captura física y química de CO_2. Estos materiales permiten vencer los problemas de transferencia de materia que los LIs puros presentan. Estos materiales se probaron como catalizadores en la reacción de oxidación de NOx.

Las principales conclusiones extraídas de esta tesis doctoral están divididas en tres grandes bloques:

1. LIs como potenciales absorbentes de acetileno y sulfuro de hidrógeno.
    - Simulaciones moleculares empleando el método COSMO-RS permiten la selección de los LIs con características termodinámicas y cinéticas favorables para la separación de gases entre un gran número de cationes y aniones.

- Simulaciones de procesos empleando Aspen Plus concluyen que no existen limitaciones termodinámicas entre los LIs seleccionados comparados con el disolvente industrial de referencia. Sin embargo, la cinética de transferencia de materia controla el proceso de absorción empleando LIs debido a sus altos valores de viscosidad. Como consecuencia, mayores alturas de columna son necesarias para alcanzar la separación. En este sentido, aquellos LIs que presentan las propiedades de transporte más favorables son aquellos más adecuados para la separación. Simulaciones de la operación de regeneración demuestran la clara ventaja de emplear LIs, alcanzando recuperaciones totales con altas purezas de soluto.

2. Inmovilización de LIs en soportes sólidos para la captura física y química de CO_2.
    - Los ENILs son capaces de superar las limitaciones cinéticas en la captura física de CO_2 que los LIs puros presentan, manteniendo las capacidades de absorción de los mismos. Experimentos en lecho fijo revelan que no existen diferencias significativas en la velocidad de sorción de CO_2 entre los ENILs preparados con distintos LIs. El aprovechamiento del lecho viene determinado por la solubilidad del CO_2 en los LIs. Por tanto, la selección del LI para la captura de CO_2 se mueve desde criterios cinéticos (viscosidad) en el caso de los LIs puros a criterios termodinámicos (solubilidad de CO_2) en el caso de los ENILs.
    - Se ha demostrado la capacidad de los ENILs para resolver los problemas que los LIs derivados de aminoácido (aa-LIs) presentan para la captura química de CO_2, como son su alta

viscosidad y la formación de un complejo sólido al reaccionar con el CO_2. Se ha propuesto un mecanismo de reacción basado en cálculos DFT y espectros de infrarrojo experimentales. A continuación, se calcularon la contribución física (constante de Henry) y química (constante de equilibrio) a la absorción de CO_2, a partir de los datos experimentales. Las entalpías de reacción calculadas revelaron una fácil reversibilidad de reacción y sencilla regeneración de sorbente en condiciones de operación suaves.

- Se ha evaluado el comportamiento termodinámico y cinético de SILPs de distintos tamaños de partícula en la captura química de CO_2. Ensayos gravimétricos demostraron que la capacidad de sorción de CO_2 es únicamente debida al LI contenido en el SILP, independientemente del tamaño de partícula de éste. Las curvas de rotura experimentales fueron ajustadas a un modelo cinético basado en fuerza impulsora, revelando que la cinética del proceso está muy afectada por el tamaño de partícula del SILP. Se empleó el simulador Aspen Adsorption para la evaluación del comportamiento del SILP de distintos tamaños en condiciones de operación distintas a las estudiadas experimentalmente. Los resultados permitieron concluir que la reacción química es la etapa controlante cuando se emplean bajas presiones parciales de CO_2. Por el contrario, la cinética de transferencia de materia es la etapa controlante cuando se trabaja a altas presiones parciales. Esta metodología permite optimizar la operación de sorción basada en SILPs, seleccionando el tamaño de partícula y tipo de LI adecuado para las condiciones planteadas.

3. ENILs como catalizadores de la reacción de oxidación de NO.

- Se han evaluado los ENILs como catalizadores en la reacción de oxidación de NO a bajas temperaturas. Los resultados experimentales permitieron comparar el comportamiento de las cápsulas vacías con el de los ENILs a distintas cargas de LI. Los experimentos en condiciones secas mostraron que la reacción está favorecida a bajas cargas de LI. Experimentos en condiciones de humedad revelaron que la reacción de NO no se ve afectada por la presencia de agua, al contrario de lo ocurrido para las cápsulas vacías. La reacción se ve favorecida mediante la adición de metanol (en presencia de agua). Se observó un aumento del 20% en términos de conversión a temperaturas de 60 °C. Por tanto, los ENILs mostraron el mejor comportamiento catalítico entre los catalizadores probados en presencia de agua.

5. APPENDIX

5.1 Acetylene absorption by ionic liquids: A multiscale analysis based on molecular and process simulation

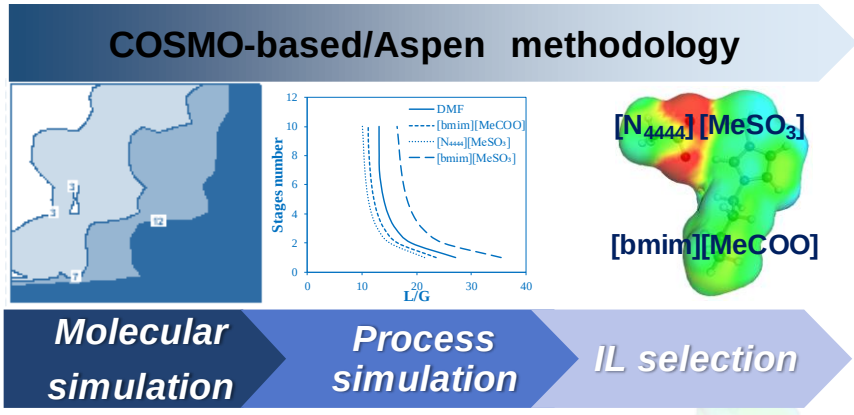

Separation and Purification Technology 204 (2018) 38–48

Contents lists available at ScienceDirect

Separation and Purification Technology

journal homepage: www.elsevier.com/locate/seppur

Acetylene absorption by ionic liquids: A multiscale analysis based on molecular and process simulation

R. Santiago, J. Bedia, D. Moreno, C. Moya, J. de Riva, M. Larriba, J. Palomar*

Sección de Ingeniería Química, Universidad Autónoma de Madrid, 28049 Madrid, Spain

ARTICLE INFO

Keywords:
Acetylene
Absorption
Ionic liquids
COSMO-RS
Aspen Plus
ILUAM

ABSTRACT

A COSMO-based/Aspen Plus multiscale simulation methodology was used to evaluate a wide variety of ionic liquids (ILs), more than 300, as potential acetylene absorbents. First, by means of Conductor-like-Screening Model for Real Solvents (COSMO-RS) method, molecular simulations were conducted to select ILs with adequate thermodynamic (Henry's law constants) and kinetic (diffusion coefficients) properties as acetylene absorbents, using N,N-dimethylformamide (DMF) as benchmark industrial solvent for such solute absorption. Then, the operating units of acetylene absorption of an acetylene and argon mixture, and exhausted solvent regeneration were modeled in Aspen Plus. Simulations of absorption column using equilibrium based design model demonstrated that at least two ILs (1-butyl-3-methylimidazolium cation and acetate and sulfonate anions) present competitive solvent performance in acetylene absorption respect to DMF. In contrast, process analyses with a more realistic rate-based column model revealed that the mass transfer rate clearly controls the acetylene absorption with ILs compared to DMF, due to their viscosity differences. Finally, modeling solvent regeneration stage showed clear advantages of using ILs as acetylene absorbents since efficient acetylene recovery is achieved by flash distillation (vacuum pressure and temperature increase), operation hindered in the case of DMF due to is high volatility, requiring the solvent regeneration by a distillation equipment with higher operating and investment costs. Current COSMO-based/Aspen Plus approach has been demonstrated useful to perform preliminary analyses of the potential application of ILs in new separation processes, before starting with experimental essays, highly demanding in cost and time.

1. Introduction

Acetylene (C_2H_2) is an important organic raw material used in different industrial applications such as soldering or illumination and heat source [1]. The low yield of acetylene synthetized (between 5 and 30% of the total acetylene commercialized) in the chemical industry (by cracking naphtha or natural gas and plasma pyrolysis of coal) makes its separation and purification necessary [2]. The acetylene produced is accompanied with ethylene (C_2H_4), an essential chemical compound in the production of polymers such as polyethylene [3]. The presence of acetylene in the polymerization reactions of ethylene is undesired, since it can produce the catalyst poisoning influencing directly in the quality of the product [4]. Furthermore, during the polymerization reactions, an explosion can happen if acetylenic compounds are converted into solids and block the fluid stream. For these reasons, it is important to eliminate efficiently the acetylene from the ethylene feed streams [5]. The removal of acetylene from ethylene streams is commercially carried out by partial hydrogenation of acetylene over a supported noble metal catalyst such as Pd [6]. This process presents some disadvantages like the potential production of ethane by overhydrogenation of acetylene, causing the loss of the desirable reactive (ethylene). In addition, Pd catalyst can be deactivated by the formation of carbonaceous deposits, directly affecting the economy of the process. Physical separation by absorption using an organic solvent is an alternative commercial process used for the separation of acetylene [7]. Traditional organic absorbents, like N,N-dimethylformamide (DMF) and N-methylpyrrolidinone (NMP), present some typical disadvantages such as absorbent loss, difficult regeneration due to organic solvents' volatility and environmental pollution. For these reasons, big efforts have been focused on looking for new environmentally friendly solvents that overcome these disadvantages. In this sense, ionic liquids (ILs) have received attention as potential new solvents for gas separation processes [8]. The interest of using ILs to the task comes from their good properties: high and tunable solvent capacity, very low-vapor pressure, non-flammability, relatively high chemical and thermal stability and low corrosivity [8,9]. An additional peculiarity of ILs is that they are known as "designer

* Corresponding author.
E-mail address: pepe.palomar@uam.es (J. Palomar).

https://doi.org/10.1016/j.seppur.2018.04.060
Received 22 December 2017; Received in revised form 28 February 2018; Accepted 21 April 2018
Available online 23 April 2018
1383-5866/

solvents" since the cation and anion can be modified/permuted to design an IL with specific properties for a particular application [10]. Several groups have centered their research on the application of ILs as absorbents in different gas separation processes [11–13] including several solutes as CO_2 [14–17], NH_3 [18–21] or volatile organic compounds (VOCs) [22,23]. Several experimental studies have demonstrated that ILs present a wide range of mass absorption capacity depending on both their cation-anion chemical properties and molecular weights. In addition, it was reported that an important mass transfer kinetic control might occur in the absorption process using ILs [24], especially considering that these solvents present relatively high viscosity compared to conventional solvents. Recently, experimental and theoretical studies on the gas separation of C_2H_2/C_2H_4 by ILs have also been reported [13,25–29]. In those works, solubility measurements of acetylene in ILs of imidazolium or pyrrolidinium families with different anions have been carried out, obtaining higher capacities for acetylene absorption than those of traditional organic solvents [26]. It was experimentally demonstrated that the acetylene solubility increases in the IL with a stronger hydrogen-bond-acceptor (HBA) character [25,26]. Molecular dynamics studies also investigated the behavior of acetylene-ILs mixtures, comparing the theoretical and experimental results [27,28,30]. In a recent study, Zhao et al [29] used the Conductor-like-Screening Model for Real Solvents (COSMO-RS) method to predict the Henry's constants of acetylene and ethylene in ILs. In general, it was concluded that ILs with hydrogen bond acceptor groups are promising candidates to selectively separate acetylene, at least from a thermodynamic point of view.

Recently, our group has developed a multiscale research strategy oriented to develop new gas capture processes based on ILs systems [22,31], based on molecular simulation, experimental tests, and process simulation. In the first stage, COSMO-RS a priori computational method [32] is applied to obtain a preliminary selection of ILs with favorable thermodynamic/kinetic properties for the absorption of the required solute, minimizing the long and difficult experimental studies. Thus COSMO-RS method is applied to perform systematic screenings of Henry's law constants of gas solutes in ILs, among a huge database of ions (more than 500), to evaluate the cation and anion effect on the gas–liquid equilibrium (GLE) of the system. In addition, the intermolecular interactions in the fluid mixture can be analyzed by COSMO-RS, providing a guide for the selection of ILs with improved characteristics for the task. In the second stage, experimental absorption tests are carried out at different temperatures and pressures; employing a high-pressure microbalance, with the aim of evaluating the thermodynamics and kinetics of gas absorption in ILs [14,17,24]. As a result, key parameters for the design of absorption columns at industrial scale are obtained, such as absorption capacities and diffusivities. In the last stage of multiscale research methodology, the gas separation processes based on ILs are modeled by using the Aspen Plus commercial process simulator, including both the absorption and solvent regeneration stages. For this purpose, an integrated COSMO-based/Aspen Plus approach is applied to create components that are not in Aspen's database, as it is the general case of ILs [33]. Once the ILs have been included in Aspen Plus's database, the individual separation operations and global processes involving ILs can be modeled, easily carrying out sensitivity analyses of different design variables [22,24,31,34–37]. One main contribution of using process simulation analyses in the development of potential applications of ILs is that it allows introducing new technical and economic criteria in the selection of optimized ILs for specific separations [38]. In addition, professional process simulators can be used to perform viability analyses of the technology based on ILs (through the estimation of energy consumptions, operating and capital cost, etc.) by comparison to available commercial technologies that use conventional solvents [24,34].

In this work, the potential application of ILs in the separation of acetylene by absorption is evaluated by means of COSMO-based/Aspen Plus multiscale research strategy. However, one main modification on

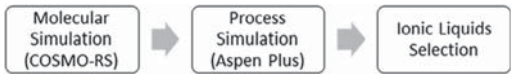

Fig. 1. Alternative multiscale research strategy diagram.

above described multiscale methodology is introduced: in this study, both molecular and process simulation are firstly and sequentially applied (Fig. 1) to preliminary select the ILs with better performance in the global gas separation processes. The use of the integrated molecular + process simulations allows performing a more rigorous selection of ILs from the view of the practical application at industrial scale, considering not only thermodynamic or kinetic properties but also technical, energetic and economic criteria. In addition, the performance of selected ILs is compared to that obtained using dimethylformamide (DMF), a conventional solvent industrially used to absorb acetylene. For this purpose, the COSMO-RS method is firstly applied to perform an IL property screening among a large database of ions (more than 300 ILs included). Henry's constant of acetylene in the IL solvent is predicted as thermodynamic parameter of reference to select ILs with high gas solute solubility, as it was successfully done previously [20,22]. The COSMO-RS approach is also used to estimate the viscosities for the calculation of the diffusion coefficient of acetylene in the studied ILs, by using Wilke-Chang model; i.e., molecular simulations also contribute to anticipating the kinetic behavior of the system. Additionally, COSMO-RS analysis allows better understanding the acetylene-IL mixture behavior from a molecular point of view, in terms of the intermolecular interactions happening in the fluid mixture. As a result, an initial selection of commercial ILs by means of thermodynamic and kinetic is carried out, comparing to the properties of DMF, which is used as benchmark industrial acetylene absorbent. Secondly, the unit operations for acetylene absorption and desorption are modeled using the selected ILs and DMF using the professional Aspen Plus process simulator. A sensitivity analysis of operating variables is carried out using rigorous equilibrium and rate-based models for the absorption operation in commercial packed columns, in order to evaluate the role of thermodynamics and kinetics in the separation efficiency. Lastly, the regeneration of the exhausted solvent is studied with a flash distillation, analyzing, for each solvent used, the temperature and pressure effect on the product purity and solvent losses. Current computational analysis contributes as a preliminary evaluation of the potential application of IL for acetylene absorption, as an alternative to the DMF conventional solvent, providing a set of ILs with favorable absorbent properties, contributing to minimize the number of experimental tests needed at laboratory or pilot plant scale.

2. Computational details

2.1. COSMO-RS calculations

Firstly, the geometry of gaseous compounds (acetylene and argon) involved in the work were optimized at BP86/TZVP computational level in gas phase. Two molecular models were used to describe de IL compounds: the ion-pair (CA) and the independent counter ions (C + A) models, optimizing the corresponding structures at BP86/TZVP computational level with solvent effect through the COSMO continuum solvation method. Once all the molecules were optimized until its minimum energy level, the polarized charge distribution on the molecular surface -obtained by a COSMO single point calculation- was saved in a .cosmo file. All these quantum-chemical calculations and .cosmo file generation were carried out in Turbomole 7.0 software. COSMOtherm program package (version C30_1501) and its parametrization BP_TZVP_C30_1501 was used, afterward, for the COSMO-RS calculations, obtaining the σ-profiles and σ-potentials of the pure compounds as well as the Henry's law constants of acetylene in ILs and detailed contributions to excess enthalpies in equimolar acetylene-IL

mixtures. Henry's law constants are calculated by means of the following expression:

$$K_H = \gamma_i^{\infty} \cdot p_0^{vap} \quad (1)$$

Where K_H is Henry's law constant, γ_i^{∞} is the activity coefficient of the solute at infinite dilution in the IL calculated by COSMOtherm and p_0^{vap} is the vapor pressure of the pure gas, estimated by both COSMOtherm and the Antoine equation (obtained from reference [39]). A complete description of the procedure for the activity coefficient calculation could be found in the work developed by Klamt [40].

In order to accomplish the kinetic screening among the huge number of ILs (more than 300), viscosities at 298.15 K were calculated by using COSMOtherm (full description in the Supplementary Information). The key kinetic parameter employed in our calculations is the diffusion coefficient (D). The widely used Wilke-Chang correlation [41] was used to estimate the diffusion coefficients of acetylene solute in ILs and DMF absorbent:

$$D = 7.4 \cdot 10^{-8} \cdot \frac{(\phi \cdot M_{IL})^{0.5} \cdot T}{\mu_{IL} \cdot V_{Acetylene}^{0.6}} \quad (2)$$

Where ϕ is the association parameter (with value of 1, considering in this case IL as unassociated solvent), M_{IL} is the molar weight of ILs, T is temperature (K), μ_{IL} is the viscosity of ILs (calculated by COSMOtherm with its later correction) and $V_{Acetylene}$ is the molar volume of acetylene at the corresponding temperature (calculated by COSMOtherm).

2.2. Component definition and property model specification in Aspen

In process simulation, the ILs are created as pseudo-components in Aspen Plus v8.8 using the ion-paired model (CA). For this purpose, molecular weight, normal boiling point and density (at 60 °F) predicted by COSMO-RS were used to define IL as pseudo-component in Aspen Plus property system. In addition, to complete the component definition, the viscosity-to-temperature dependence was specified, using an Arrhenius type equation, employed by default in Aspen Plus. The experimental viscosity-to-temperature data was first regressed and then refined in a previous publication carried out by our group [42]. The gaseous compounds of the work (acetylene and argon) were included in the simulation as conventional compounds, and their parameters and properties were loaded from Aspen Plus database. The COSMOSAC property model was selected to estimate the activity coefficients of the components in mixture. There are three modifications of the property model: (i): the original COSMO-SAC model proposed by Lin and Sandler [43];(ii): the original COSMO-RS model proposed by Klamt [40]; and (iii): the modification to the Lin and Sandler model developed by P. Mathias et. al. The COSMOSAC property model in Aspen Plus needs the following additional molecular information of the compounds provided by COSMO-RS, required to complete the specifications of ILs, acetylene, and argon: molecular volumes (COSMO volume) and σ-profiles. This information is included within the simulator in six parameters: CSACVL (compounds molecular volume in angstroms) and SGPRF1 to SGPRF5 (five sigma profile parameters, each containing 12 segments of the σ-profile). All the values related to the creation of the ILs as pseudo-components are included in Table S3 (Supplementary Information). More information on this computational approach was reported in the documentation of the ILUAM database, which will be soon published with information available for 100 common ILs [33].

2.3. Acetylene absorption

The acetylene absorption column was modeled using the *RADFRAC* model implemented in Aspen Plus v8.8, employing equilibrium and Rate-Based modes. The gas inlet was fed with an initial composition of 2 mol% of acetylene (typical composition studied in the literature [44,45] between 0.5 and 3 mol%) and 98 mol % of argon and a constant gas flow of 10 kg/h (almost 100 L/min) (as reference for a pilot plant). Initially, the inlet temperature and pressure of the gas and absorbent streams were 40 °C and 1 atm, respectively. Different simulation cases were developed to analyze the absorption stage: *Case 1:* The equilibrium column was simulated with one theoretical stage as reference varying the inlet liquid mass flow (L/G). As a result, acetylene recoveries for each selected IL were calculated as a function of the L/G ratio. *Case 2:* Using the equilibrium mode of RADFRAC column, the theoretical stage number was changed between 1 and 10 with the aim of estimating the needed liquid flow of absorbent for achieving 80% of acetylene recovery in each case. *Case 3:* Using the Rate-Based mode, the temperature of the gas and liquid inlets was varied from 293 to 363 K with the aim of studying the possible mass transfer limitations of the operation. For this purpose, it has been selected Raschig Rings packing (15–25 mm depending on column diameter) with a column height of 1 m as a reference. The column diameter was calculated using the "Packing Sizing" utility of the RADFRAC column for a fractional approach to maximum capacity of 62% and then transferred to the "Packing Rating" utility of the RADFRAC model. The calculations provide different acetylene recovery as a function of the temperature. *Case 4:* Using the Rate-Based mode, different column designs (with Raschig Rings packing of 25 mm and a maximum capacity of 62%) were calculated fixing an acetylene recovery of 80% when using ratio L/G ratio (in mass) in the range of 60–160, obtaining the needed diameter and height for the separation in each case.

The conditions for all the cases are summarized in Table 1:

2.4. Solvent regeneration

The regeneration unit was modeled using the *FLASH2* model implemented in Aspen Plus v8.8. The constant flow treated, which includes the absorbed gas in saturated DMF or IL, was 1300 kg/h, which was previously selected by modeling the absorption column that was inside the range of typical pilot plant columns (in terms of height/diameter ratio and pressure drop per meter of column). The regeneration was studied by decreasing the pressure at temperatures between 313 and 393 K. Thus, it could be analyzed the acetylene recovery and the acetylene purity of the clean gas stream.

3. Results

3.1. Molecular simulation: prediction of the interactions based on σ-profiles

COSMO-RS methodology calculates the thermodynamic properties of fluid mixtures using the molecular surface polarity distributions (σ-surface) of their individual compounds, obtained from quantum

Table 1
Conditions for the cases of study of the process simulation section.

	Pressure (atm)	T (K)	G (kg/h)	L (kg/h)	Recovery	Mode	Stages
Case 1	1	313	10	10–1200	–	EQ	1
Case 2	1	313	10	–	80%	EQ	1–10
Case 3	1	293–393	10	100	–	EQ/RB	5/1 m
Case 4	1	313	10	600–1600	80%	RB	–
Reg.	$1–10^{-5}$	313–393	–	–	–	–	–

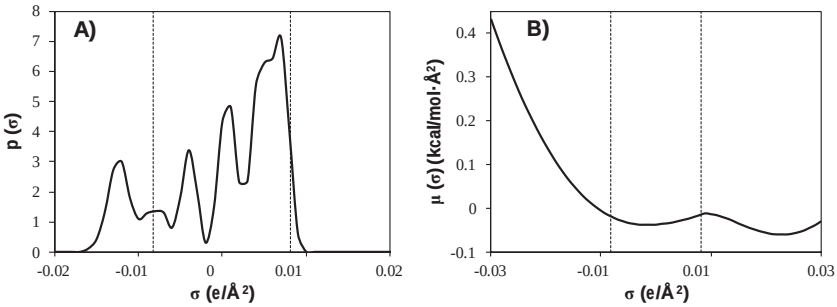

Fig. 2. σ-profile and σ-potential of acetylene obtained by COSMO-RS.

chemical calculations, which is easily visualized by the σ-profile histogram (σ-profile) [32]. Based on COSMO-RS theory, the σ-profile includes the main chemical information necessary to predict possible interactions of a compound in a fluid phase. Furthermore, COSMO-RS provides the σ-potential as an additional tool for analyzing the affinity of the solvent to interact with compounds that present charge density [μ (σ)] with polarity (σ). Fig. 2 presents the σ-surface, σ-profile, and σ-potential of acetylene. Both, σ-profile and σ-potential can be qualitatively divided in three main regions upon the following cut-off values: hydrogen bond donor ($\sigma < -0.0082\,e/Å^2$) and acceptor ($\sigma > +0.0082\,e/Å^2$) regions and the non-polar region ($-0.0082 < \sigma > +0.0082\,e/Å^2$). The σ-profile of acetylene is dominated by a series of peaks located in the non-polar region. Furthermore, the peak located at $-0.012\,e/Å^2$, which corresponds to the hydrogen atoms of acetylene molecule indicates their ability to act as hydrogen bond donor (acidic character). The σ-potential of acetylene reflects its strongly repulsive interactions with acidic groups. On the contrary, it presents weak attractive interactions with basic groups (hydrogen bond acceptor region of the histogram) and non-polar compounds.

To anticipate the possible intermolecular interactions between acetylene and IL absorbents, σ-profiles and σ-potential of common anions (Fig. 3) and cations (Fig. 4) of common ILs are also analyzed. For instance, in the case of anions, the σ-profile of $[MeCOO]^-$ (Fig. 3A) shows a main peak at the positive polar region ($0.021\,e/Å^2$) which indicates a strong basic character (hydrogen bond acceptor) associated to the carboxylate oxygen atoms. These evidence can also be seen in the σ-potential in which high exothermic mixtures (strongly attractive interactions) are expected with acidic species and weak exothermic mixtures with non-polar compounds. The $[MeSO_3]^-$ anion shows a peak at $0.017\,e/Å^2$ due to the oxygen atoms, with also strong hydrogen bond acceptor character and some weak peaks at the non-polar region which corresponds to the methyl group and S atom. A similar description can be done for the $[MeSO_4]^-$ anion, but in this anion lower basic character is observed. In both cases, σ-potential indicates higher exothermic mixtures with acidic compounds than with non-polar compounds. The $[BF_4]^-$ anion shows a peak at $0.012\,e/Å^2$ which indicates a relatively weak hydrogen bond acceptor character, in agreement with its σ-potential curve. Lastly, the σ-profile related to $[NTf_2]^-$ anion presents its main peak at the non-polar region and an additional weaker peak at $0.01\,e/Å^2$, describing a big anion with low polarized charge and low basic character. In this case, the σ-potential indicates that high exothermic mixtures are not expected with acidic groups. Analyzing the σ-potential of common anions (Fig. 3B), repulsive interactions (endothermic mixtures) are expected when basic groups are involved in the operation. Due to the acidic character of acetylene, it is expected that better interaction will be accomplished using ILs with basic anions. In this sense, the basicity trend of anions would be $[MeCOO]^- > [MeSO_3]^- > [MeSO_4]^- > [BF_4]^- > [NTf_2]^-$.

The same analysis is carried out for common cations, in this sense, the σ-surfaces, σ-profiles, and σ-potentials of some studied cations can be seen in Fig. 4. It is observed that the σ-profiles of cationic species are dominated by a main peak with an electronic density distribution in the non-polar region, corresponding to the alkyl substituents and the aromatic ($[bmim]^+$ and $[hxpy]^+$ cases) and aliphatic ($[N_{4444}]^+$ and $[P_{4444}]^+$ cases) head groups. In addition, for imidazolium cations as $[bmim]^+$, a weak peak is located at lower values than the cut off, $-0.0082\,e/Å^2$, associated to the hydrogen atoms of the aromatic ring in $[bmim]^+$ case. A similar description may be done for pyridinium cations like $[hxpy]^+$ which presents a weak peak located at $-0.011\,e/Å^2$ corresponding to the hydrogen atoms of the aromatic ring. This indicates some acidic character of hydrogen atoms of imidazolium and pyridinium cations, stronger for the case of C_2-H. In order to complete this analysis, the σ-potential of cations is also evaluated (Fig. 4B). From the results of the σ-potential, all the cations present repulsive interactions with acidic groups (as can be seen the endothermicity at the hydrogen bond donor region). In addition, some weak exothermic mixtures appear in the non-polar region. As studied above, $[bmim]^+$ and

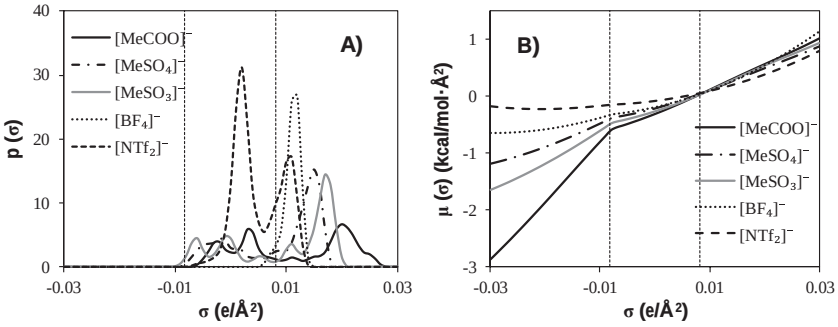

Fig. 3. σ-profile and σ-potential of different anions obtained by COSMO-RS.

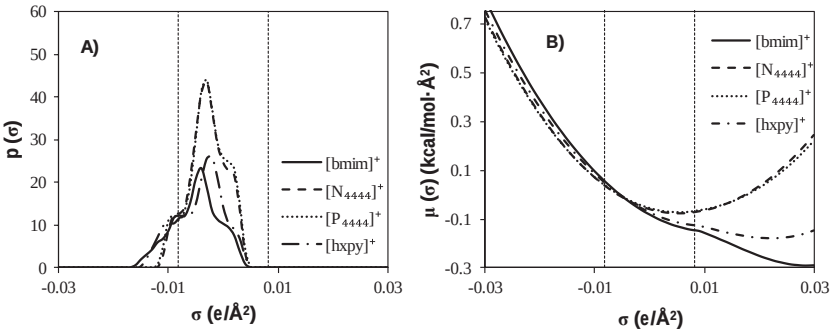

Fig. 4. σ-profile and σ-potential of different cations obtained by COSMO-RS.

$[hxpy]^+$ cations may provide weak exothermic mixtures with compounds, present hydrogen bond acceptor groups. In fact, the hydrogen bond donor capacity of the cation families decreases in the following order: $[bmim]^+ > [hxpy]^+ > [P_{4444}]^+ > [N_{4444}]^+$. Therefore, looking for favorable acetylene-IL intermolecular interactions, it is expected that those cations with absence of acidic groups will be a better selection, since it may avoid cation-anion hydrogen bond interactions, competing with acetylene-anion interactions.

3.2. Henry's law constants validation

Following, the capability of COSMO-RS to predict the gas solubility in ILs is evaluated by comparing experimental and calculated Henry constants ($K_H = \gamma_i^{\infty} \cdot p_i$) for more than 50 solute-IL systems collected in Gonzalez-Miquel's work [46] (including 11 solutes and 15 ILs), using both a molecular ion-paired model (CA) and an independent ions (C + A) model to simulate the IL solvent when experimental vapor pressure is employed and vapor pressure predicted by COSMO-RS is used. Compounds of very different nature such as CO_2, H_2, inert gases, aromatics, alkanes, alkenes and alkynes are included, involving a wide range of Henry's law constant values (from 0.1 bar for benzene in [hxmim][NTf_2] to 4500 bar for H_2 in [bmim][NTf_2]) at nearly room temperature. In order to assure the good predictions of Henry's law constants for acetylene, the available acetylene experimental vapor pressure values and their temperature dependence are included [39]. It is obtained that the best results are obtained (slope = 0.99, square correlation coefficient $R^2 = 0.98$) when experimental vapor pressure (p_i^*) and C + A model are used (Fig. 5). However, it should be noted that COSMO-RS does not predict adequately the acetylene's vapor pressure ($p_{i\,\text{COSMO-RS}}^* = 16.8$ bar, $p_{i\,\text{experimental}}^* = 51.2$ bar at 300 K) when *.energy file is used. For this reason, experimental vapor pressure fitted to Antoine Equation was introduced by means of A, B and C coefficients which allows comparing the new Henry's law constants with experimental data. Figures that represent the rest of the cases are shown in Supplementary Material (Figs. S2 and S3). The best results are obtained when experimental vapor pressures of acetylene are used, by introducing the Antoine parameters in the *.vap file (A = 4.66; B = 909.08; C = 7.95) and C + A model will be used for next K_H calculations by COSMO-RS in this work.

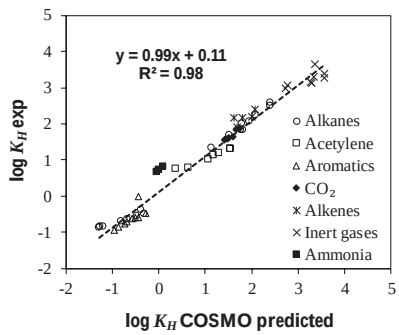

Fig. 5. Experimental vs COSMO-RS Henry's law constants of solutes in ILs using experimental vapour pressure of the different solutes at near temperatures from 20 to 30 °C (C + A model).

3.3. Ionic liquids selection

Thermodynamic analysis. In order to select optimized ILs for acetylene absorption, COSMO-RS method was applied for predicting Henry's law constants (K_H) of acetylene in 306 LIs at 298.15 K. Hence, a computational screening was performed over ILs based on different cations and anions (see Table S1 in the Supplementary Material). The results from the COSMO-RS screening of Henry's law constants of acetylene in ILs (C + A model) are presented in Fig. 6 (data available in Table S2 of the Supplementary Material). Firstly, it is concluded that suitable selection of ILs plays an important role in acetylene absorption, attending to the wide range of K_H (1–50 bar) for acetylene-IL systems obtained from COSMO-RS analysis. It is observed that the acetylene

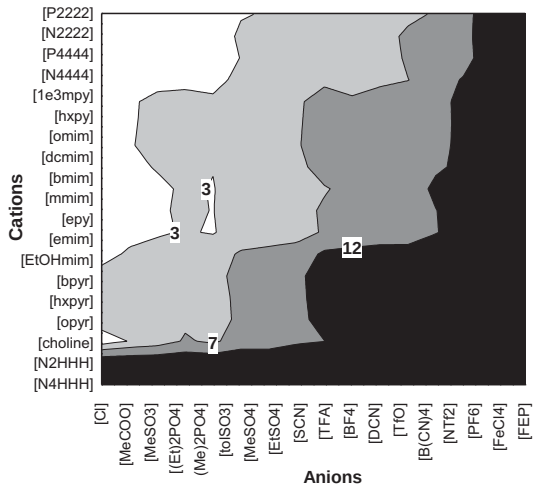

Fig. 6. Screening of predicted Henry's law constants (bar) of acetylene in 306 ILs (C + A model using experimental vapor pressure) at T = 298.15 K calculated by COSMO-RS.

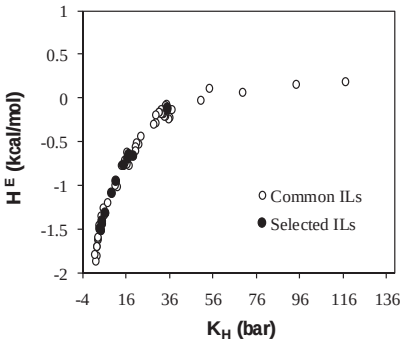

Fig. 7. Excess molar enthalpies (H^E) of equimolar acetylene-IL mixtures versus Henry's law constants (K_H) for acetylene in 70 ILs (C + A model and experimental vapour pressure), both computed by COSMO-RS at 298.15 K.

absorption capacity of ILs is more determined by the anion than by the cation, increasing the acetylene gas solubility in the IL solvent when increasing the hydrogen bond acceptor character of the anion, in good agreement with conclusions achieved from the σ-profiles and σ-potential of these species. Regarding the cation effect, tetra-substituted long chain phosphonium and ammonium cations seem to be the best selection for the task, followed by pyridinium and imidazolium cations. It is important to notice that ILs based on hydroxyl functionalized cations such as $[EtOHmim]^+$ or $[choline]^+$ are undesirable selections since the acetylene absorption capacity of IL decreases due to competitive hydrogen bond cation-anion interactions.

To obtain further insights on the absorption mechanism from a molecular point of view, COSMO-RS estimations of excess enthalpy (H^E) of acetylene-IL mixtures have been calculated to analyze the GLE data in terms of the intermolecular interactions in the liquid fluid, according to Eq. (3):

$$H^E = H^E(HB) + H^E(MF) + H^E(vdW) \quad (3)$$

Where excess enthalpies are obtained from hydrogen bonding (HB), electrostatic-misfit (MF) and van der Waals (vdW) contributions. Fig. 7 compares H^E for equimolar acetylene-IL mixtures to Henry's law constant values at 298.15 K for 70 ILs calculated by COSMO-RS. As a general trend, higher solubility (decreasing K_H values) of acetylene in ILs is associated to higher exothermicity (decreasing H^E values) of the mixture, while the lower solubility of acetylene in the ILs is related with enthalpy values of the mixtures close to zero. Fig. 8 allows analyzing the absorption of acetylene in a representative sample of ILs in terms of the contributions of different intermolecular interactions to the H^E values of acetylene-IL mixtures. It shows that a significant increase of the acetylene solubility in ILs with anions presenting a strong basic character, such as $[MeCOO]^-$ or $[MeSO_3]^-$, can be mainly ascribable to hydrogen bond interaction between acetylene solute and IL solvent. It is also noted that attractive electrostatic (MF) energies also contributes to the properties of the mixture, favoring the acetylene solubility in ILs.

Kinetic analysis. It is important to consider the relatively high values ILs viscosities and, correspondingly, their effect on the absorption rate. For this reason, Wilke-Chang correlation was applied in order to evaluate the diffusion coefficients of acetylene in ILs using the information computed by COSMO-RS. Therefore, in Fig. 9, a computational screening of diffusion coefficients is performed for all the cations and anions involved in this work (data available in Table S3 of the Supplementary Material). As can be seen, the differences between diffusion coefficients of acetylene in different ILs are significant (up to two orders of magnitude), depending on these values on both the IL cation and anion. Therefore, it may be important to consider kinetic properties when selecting adequate ILs for the absorption of acetylene.

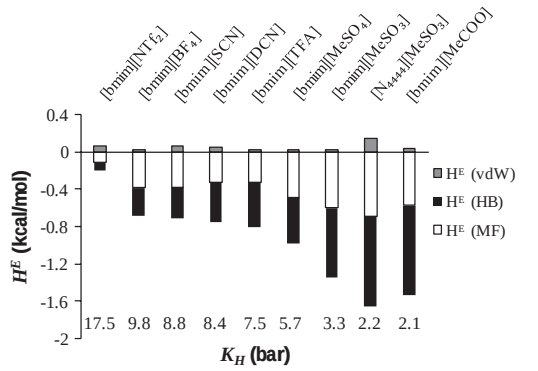

Fig. 8. Description of the solvent effect on K_H of acetylene, at 298.15 K by using the interaction energies contributions [electrostatic (MF); Van der Waals (VdW); and hydrogen-bonding (HB)] to excess molar enthalpies of acetylene-IL (C + A model and experimental vapour pressure) mixture computed by COSMO-RS.

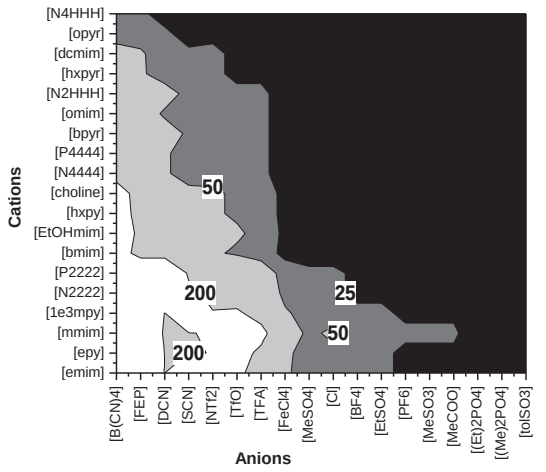

Fig. 9. Screening of predicted diffusion coefficients ($\times 10^{12}$ m^2/s) of acetylene in 306 ILs (C + A model) at T = 313 K calculated by Wilke-Chang correlation.

Analyzing the computational results, we preliminary select 9 commercial ILs, mainly attending to their favorable thermodynamic properties for acetylene absorption. This sample includes some ILs previously studied in the bibliography as a reference and others with low K_H values predicted by COSMO-RS (Table 2). As it has been noted, the selection of adequate ILs for a specific gas separation should also consider their transport properties. The ILs included in Table 2 present a wide range of molar weights, viscosities and consequently diffusivity values of acetylene in ILs.

Analyzing the Table 2, it is observed that there are three ILs with Henry's law constants (in molar terms) of acetylene lower than DMF. Conversely, when the solubility is expressed in mass terms, only the [bmim][MeCOO] IL presents an acetylene solubility slightly higher than DMF. This is due to the high ILs molecular weight compared to DMF's. Regarding the kinetic properties, it is important to notice that DMF presents an acetylene diffusivity two or three order of magnitude higher than the selected ILs, because of its remarkably lower viscosity.

Table 2
Properties of selected ILs/DMF or IL/DMF-acetylene system.

ILs	MW	K_H (bar) 298.15 K	Mass Fraction 298.15 K, 1 atm	Viscosity (cP) 298.15 K	Diffusivity (m^2/s) 298.15 K
[bmim][NTf_2]	419.4	17.5	0.004	51.4 [42]	$4.1{\cdot}10^{-11}$
[bmim][BF_4]	226.0	9.8	0.013	114.2 [42]	$1.6{\cdot}10^{-11}$
[bmim][SCN]	197.3	8.8	0.017	55.7 [42]	$3.3{\cdot}10^{-11}$
[bmim][DCN]	205.3	8.4	0.017	31.1 [42]	$5.7{\cdot}10^{-11}$
[bmim][TFA]	252.2	7.5	0.016	77.5 [47]	$3.9{\cdot}10^{-11}$
[bmim][$MeSO_4$]	250.3	5.7	0.022	184.6 [42]	$8.7{\cdot}10^{-12}$
[bmim][$MeSO_3$]	234.3	3.3	0.047	713.1*	$8.5{\cdot}10^{-12}$
[N_{4444}][$MeSO_3$]	337.6	2.2	0.060	1560.7*	$1.8{\cdot}10^{-12}$
[bmim][MeCOO]	198.3	2.1	0.105	447.2 [42]	$3.5{\cdot}10^{-12}$
DMF	73.1	4.5	0.091	0.9 [48]	$1.5{\cdot}10^{-9}$

* Calculated by COSMO-RS.

3.4. Process simulation results

GLE validation. Firstly, gas–liquid equilibria (GLE) calculations by COSMO-based/Aspen Plus approach were validated using experimental data collected from the literature. Calculations were carried out employing the three COSMO-based equations (codes 1–3) available in COSMOSAC property model as implicit in Aspen Plus (Table S4 of Supplementary Information). Attending relative mean deviations (MRD) when changing COSMOSAC models, COSMO-RS equation (code 2) reproduces better the GLE than the others two. Calculations performed using CA model to describe IL compounds provide better predictions of GLE for acetylene-IL systems (9%) than those obtained using C + A model. The compared and calculated P-x diagram at 313 K for acetylene-ILs systems involved in this work to the available experimental data [25] can be found in the Fig. S4 of the Supplementary Material.

Acetylene absorption. The role of thermodynamics of acetylene absorption when using selected ILs and DMF absorbents was evaluated using RADFRAC column simulations in equilibrium model (*Case 1*). Fig. 10 presents the acetylene recovery using different absorbent feed mass flows (different L/G) at fixed number of equilibrium stages (5). As expected, acetylene separation performance improves when increasing the solute solubility in ILs at fixed operating conditions (Table 2), observing that 3 ILs present solvent capabilities competitive with DMF from a thermodynamic standpoint. Thus, the ILs [bmim][MeCOO], [N_{4444}][$MeSO_3$] and [bmim][$MeSO_3$] allow reaching recoveries of more than 99% in the modeled *Case 1*, similar than DMF; whereas a maximum acetylene recovery of 90% is obtained with the [bmim][$MeSO_4$] IL. The other ILs present lower separation efficiencies in the operating conditions of *Case 1*.

Case 2 simulations were carried out -using the 3 most favorable ILs and DMF- in order to evaluate liquid mass flow necessary (L/G) to achieve 80% acetylene recovery at different equilibrium stages (Fig. 11). As can be seen, similar relationship between the number of equilibrium stages and needed L/G mass ratio for a specified separation is obtained for DMF and [bmim][MeCOO] and [N_{4444}][$MeSO_3$], whereas the IL [bmim][$MeSO_3$] shows slightly worse absorbent performance. The operating range was between 12 and 20 L/G ratio (Fig. 11). For its good thermodynamic properties, [bmim][MeCOO] and [N_{4444}][$MeSO_3$] were selected for the next steps of the study.

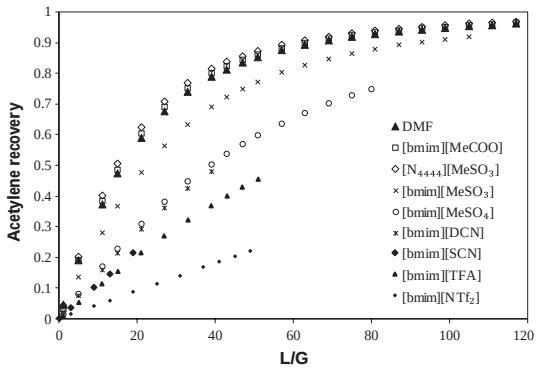

Fig. 10. Acetylene recovery changing L/G ratio (in mass terms) using DMF and selected ILs, calculated using RADFRAC column in equilibrium mode (Case 1).

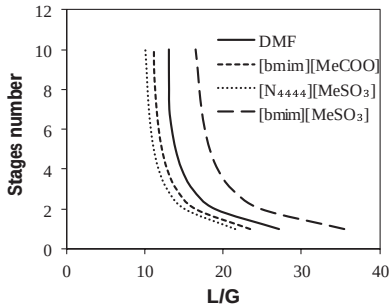

Fig. 11. Mass liquid flow necessary for reaching 80% acetylene recovery changing the stages number of the absorption column using DMF and 3 selected ILs, calculated using RADFRAC column in equilibrium mode (Case 2).

The potential kinetic control of acetylene absorption by ILs and DMF was evaluated modeling the absorption in a commercial packing column using the RADFRAC model in rate-based mode (*Case 3*). A L/G ratio of 10 was used since it allows obtaining a wide range of acetylene recoveries. Fig. 12 compare the acetylene recovery obtained using Rate-Based and equilibrium modes of the RADFRAC column when the temperature of both the gas and liquid inlet streams is varied simultaneously from room temperature to 353 K. It can be observed that the acetylene absorption by ILs (Fig. 12A and 12B) is clearly controlled by the mass transfer rate at near to room temperatures, reaching near a 50% of recovery loss when equilibrium and Rate-Based modes are compared. On the contrary, the results obtained with the traditional organic solvent DMF (see Fig. 12C), reflects just a 10% of recovery loss, according to the short gap between equilibrium and Rate-Based curves. When the inlet temperature is increased, the kinetic control progressively diminishes until 333–343 K, temperature range where equilibrium starts to control the process. This is directly related to the high viscosity of ILs at near room temperatures compared to traditional solvents such as DMF, difference that decreases at higher temperatures [42].

Finally, simulations using Case 4 were performed to size the absorption column required to achieve a specific separation at fixed operating conditions (*Case 4*). Fig. 13 presents the results of the column height needed to reach an 80% acetylene recovery when L/G ratio is

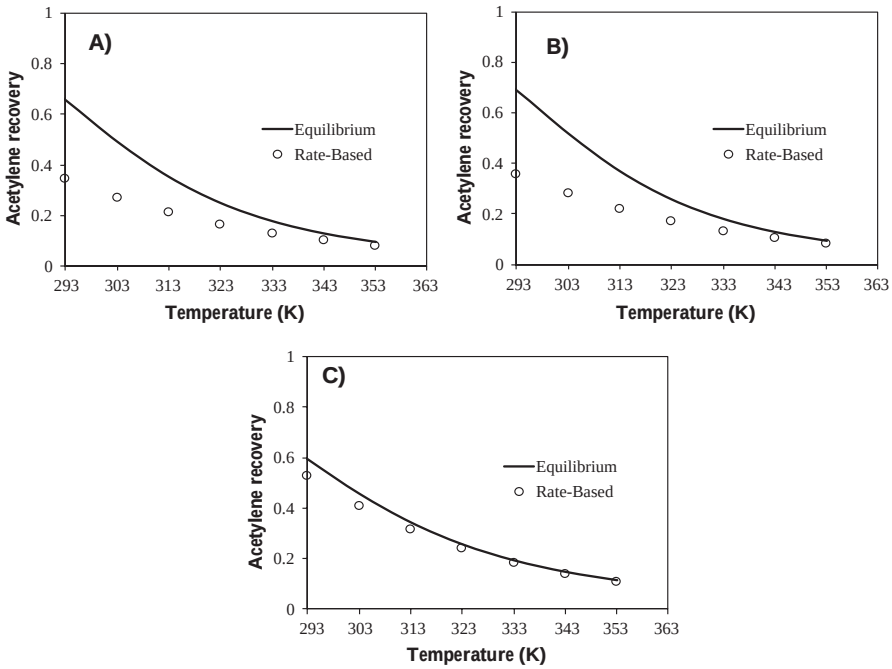

Fig. 12. Acetylene recovery as a function of the gas and liquid inlet temperature when Rad-Frac model is operating in equilibrium and Rate-Based models for (A) [bmim][MeCOO], (B) $[N_{4444}][MeSO_3]$, and C) DMF absorbents (Case 3).

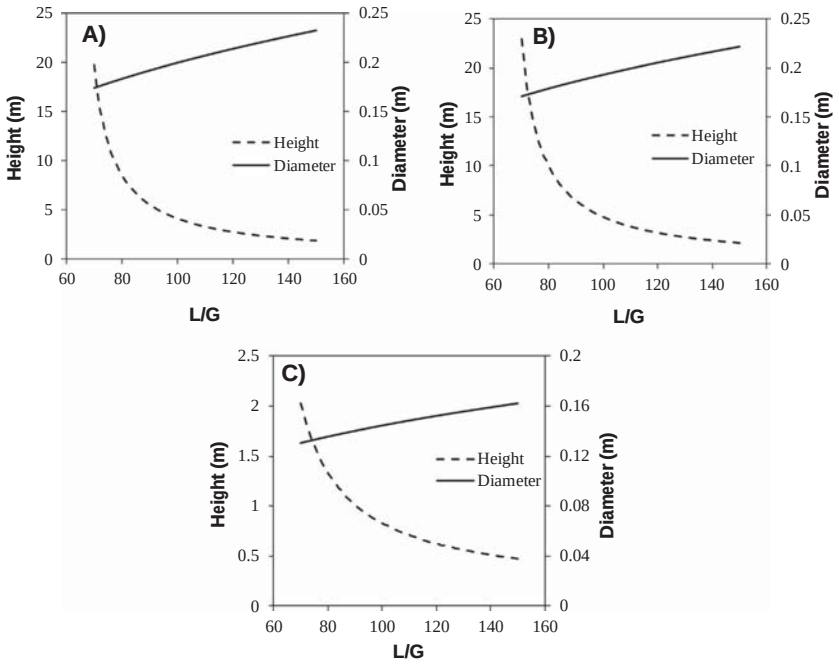

Fig. 13. Absorption column design for different L/G ratios (in mass units) using (A) [bmim][MeCOO], (B) $[N_{4444}][MeSO_3]$, and (C) DMF as absorbents (Case 4).

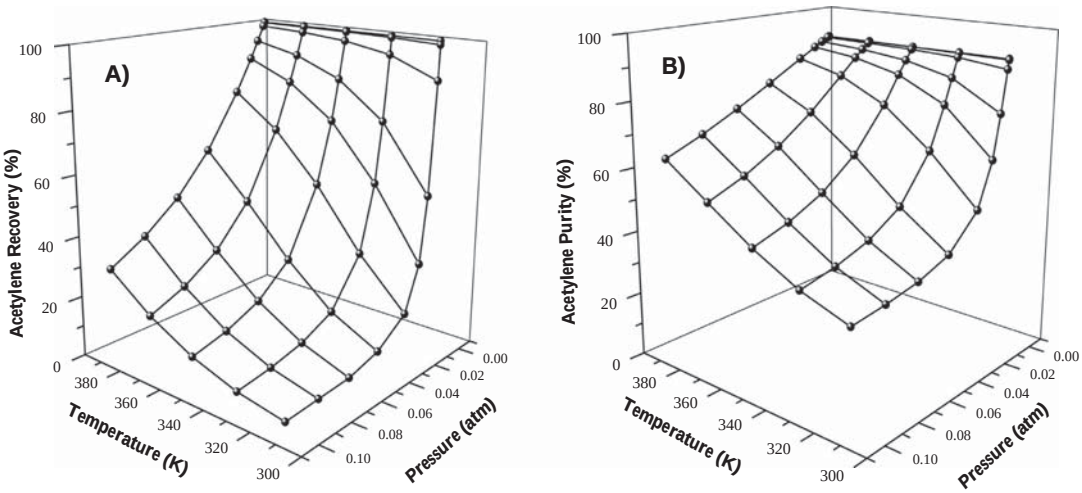

Fig. 14. (A) Acetylene recovery and (B) Acetylene purity as a function of the temperature and pressure in the regenerator unit when IL is used.

varied from 60 to 160. As can be seen, remarkably higher packing column heights are required when using ILs (from 2 to 22 m) than when using DMF (0.5–2 m) at same operating conditions. In contrast, the diameter designed to fix a capacity factor of 62% is similar for ILs and DMF, since it is mainly determined by L/G ratios at the fixed design specifications. Summarizing, the mass transfer rates play a crucial role in the solvent performance of ILs in acetylene absorption, limiting their potential use as alternative to volatile organic solvents as DMF in the studied separation.

Absorbent regeneration. Once evaluated the performance of ILs and DMF in absorption stage, it is also needed to simulate the regeneration unit of exhausted absorbent, since this later operation determines the operating costs of global acetylene separation processes [49]. For this purpose, a flash distillation by vacuum pressure with a temperature increase is proposed to regenerate the ILs and recovery the acetylene compound, based on previous results in the bibliography [24,36,38].

First, Fig. 14A presents the acetylene recovery in the vapor stream at different operating pressures and temperatures when the IL is used as absorbent. As can be seen, when the temperature is increased and the pressure of the system is decreased, the highest acetylene recoveries are obtained. In fact, total acetylene recoveries were carried out at different conditions. The key parameter of the desorption operation seems to be the vacuum pressure required, reaching 100% acetylene recoveries from 10^{-3} atm. In addition, in Fig. 14B is shown the acetylene purity obtained. The data follow the same trend as the acetylene recovery one, reaching the maximum acetylene purity values when the vacuum pressure are minimum and the operation temperatures are maximum. Therefore, it has been demostrated the posibility of recovering the total amount of acetylene by a simple flash distillation by combining both a temperature increase and a pressure decrease.

Second, Fig. 15A shows the results of acetylene recovery for the DMF absorbent while Fig. 15B analyzed the acetylene purity in the clean gas stream. The data follow the same trend as the IL case i.e. the maximum acetylene recoveries and purities are achieved for low values of pressure and high values of temperature. In this case, a wider range with total acetylene recovery than the IL case was found in different conditions. Nonetheless, when the acetylene recoveries are 100%, the acetylene purity of the clean gas stream is almost zero. This is directly atributed to the evaporation of the DMF solvent and the later loss in the vapor stream. In addition, if soft conditions are carried out in the regenerator, the maximum acetylene purity reached is 10% (clearly lower than the IL case in the same conditions). Therefore, a simple flash distillation operation cannot be used to regenerate the exhausted DMF absorbent without solvent loss, and much more costly multistage distillation is required. These results reveals a clear advantage of using ILs in the regeneration stage, since total acetylene recoveries and purities were reached by single stage distillation when ILs are employed.

4. Conclusions

In the present work, ILs were selected and evaluated for their potential application in acetylene absorption using a COSMO-based/Aspen Plus multiscale methodology. Molecular simulations were successfully carried out over a wide number of ILs in order to preliminary select a sample of absorbents with adequate thermodynamic and kinetic characteristics for such separation, competitive with those reported for conventional acetylene absorbents as DMF. It was observed a strong influence of the anion on the IL solvent properties, obtaining higher acetylene absorption capacity in ILs formed by anions with strong hydrogen bond acceptor character, due to the favorable solute-solvent interactions with acidic acetylene compound. In contrast, the diffusivity of acetylene in IL media is relatively low when comparing to the DMF case and it is observed that thermodynamics and mass transfer kinetics are strongly influenced by the selection of cation and anion. Then, the performance of ILs as acetylene absorbent was evaluated by modeling the absorption and IL regeneration units involved in the separation processes, using the Aspen Plus process simulator. From the thermodynamic point of view, at least two ILs are competitive with the DMF. However, when absorption operation is modeled in a more realistic scenario (commercial packed column, rigorous Rate-Based theoretical treatments), the acetylene absorption by selected ILs was found severely controlled by the mass transfer rate at near to room temperatures, in contrast to the case of DMF, whose absorption capacity is much properly exploited. Consequently, the necessary packing height for reaching an 80% acetylene recovery is one order of magnitude greater than in DMF-based process. In contrast, the analysis of regeneration operation reveals the clear advantage of ILs as absorbent, since their depreciable volatility allows the efficient regeneration of the exhausted solvent and the acetylene recovery by using a simple flash distillation. On the contrary, using volatile DMF absorbent requires more energy demanding and costly distillation processes, in order to prevent the solvent loss through the gas stream. Current COSMO-based/Aspen Plus approach has been demonstrated useful to perform preliminary analysis of the potential application of ILs in new separation processes,

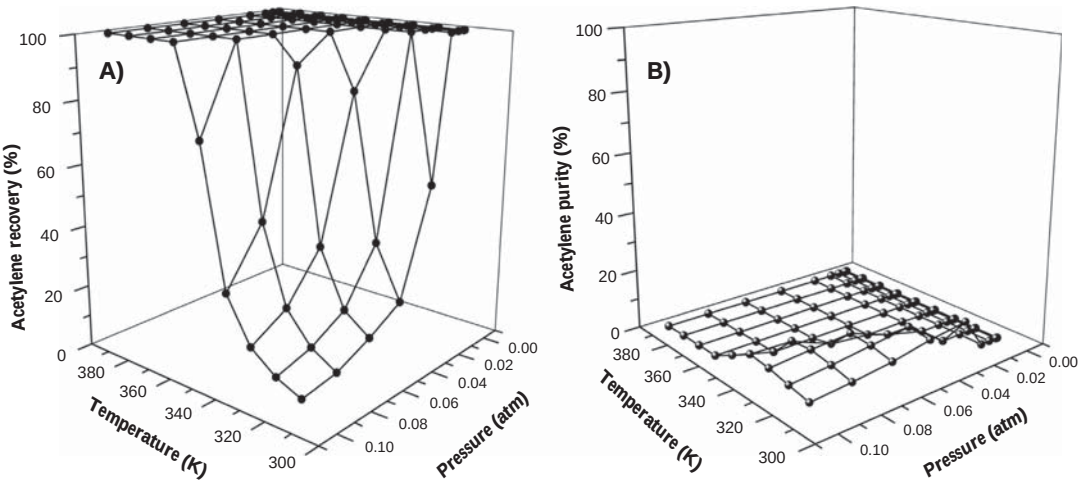

Fig. 15. (A) Acetylene recovery and (B) Acetylene purity as a function of the temperature and pressure in the regenerator unit when DMF is used.

providing relevant insights regarding the solvent selection and the viability of the new processes based on IL from comparison to conventional technologies, before starting with experimental essays, more cost and time demanding.

Acknowledgments

The authors are grateful to Comunidad Autónoma de Madrid (Project S2013/MAE-2800) and to Ministerio de Economía y Competitividad (MINECO) of Spain (Project CTQ2017-89441-R) for financial support. We are very grateful to Centro de Computación Científica de la Universidad Autónoma de Madrid for computational facilities.

Appendix A. Supplementary material

Supplementary data associated with this article can be found, in the online version, at https://doi.org/10.1016/j.seppur.2018.04.060.

References

[1] T.F. Xia, J.F. Cai, H.Z. Wang, X. Duan, Y.J. Cui, Y. Yang, G.D. Qian, Microporous metal-organic frameworks with suitable pore spaces for acetylene storage and purification, Micropor. Mesopor. Mater. 215 (2015) 109–115.
[2] X.X. Wang, J. Gao, J.S. Zhang, X.P. Zhang, R.L. Guo, Theoretical and experimental studies on acetylene absorption in a polytetrafluoroethylene hollow-fiber membrane contactor, Chem. Eng. Technol. 38 (2) (2015) 215–222.
[3] K.M. Sundaram, M.M. Shreehan, E.F. Olszewski, Ethylene, in Kirk-Othmer Encyclopedia of Chemical Technology. 2000, John Wiley & Sons, Inc.
[4] W. Huang, J.R. McCormick, R.F. Lobo, J.G. Chen, Selective hydrogenation of acetylene in the presence of ethylene on zeolite-supported bimetallic catalysts, J. Catal. 246 (1) (2007) 40–51.
[5] J.M. Lee, J. Palgunadi, J.H. Kim, S. Jung, Y.S. Choi, M. Cheong, H.S. Kim, Selective removal of acetylenes from olefin mixtures through specific physicochemical interactions of ionic liquids with acetylenes, PCCP 12 (8) (2010) 1812–1816.
[6] M. Ruta, G. Laurenczy, P.J. Dyson, L. Kiwi-Minsker, Pd nanoparticles in a supported ionic liquid phase: Highly stable catalysts for selective acetylene hydrogenation under continuous-flow conditions, J. Phys. Chem. C 112 (46) (2008) 17814–17819.
[7] K. Weissermel, H.-J. Arpe, Acetylene, in Industrial Organic Chemistry. 2008, Wiley-VCH Verlag GmbH. p. 91–105.
[8] J.S. Wilkes, P. Wasserscheid, T. Welton, Introduction, in Ionic Liquids in Synthesis. 2008, Wiley-VCH Verlag GmbH & Co. KGaA. p. 1–6.
[9] J.G. Huddleston, A.E. Visser, W.M. Reichert, H.D. Willauer, G.A. Broker, R.D. Rogers, Characterization and comparison of hydrophilic and hydrophobic room temperature ionic liquids incorporating the imidazolium cation, Green Chem. 3 (4) (2001) 156–164.
[10] J. Palomar, J.S. Torrecilla, J. Lemus, V.R. Ferro, F. Rodriguez, A COSMO-RS based guide to analyze/quantify the polarity of ionic liquids and their mixtures with organic cosolvents, PCCP 12 (8) (2010) 1991–2000.
[11] D. Han, K.H. Row, Recent applications of ionic liquids in separation technology, Molecules 15 (4) (2010) 2405.
[12] X. Han, D.W. Armstrong, Ionic liquids in separations, Acc. Chem. Res. 40 (11) (2007) 1079–1086.
[13] Y.S. Zhao, R. Gani, R.M. Afzal, X.P. Zhang, S.J. Zhang, Ionic liquids for absorption and separation of gases: an extensive database and a systematic screening method, Aiche J. 63 (4) (2017) 1353–1367.
[14] C. Moya, J. Palomar, M. Gonzalez-Miquel, J. Bedia, F. Rodriguez, Diffusion coefficients of CO_2 in ionic liquids estimated by gravimetry, Ind. Eng. Chem. Res. 53 (35) (2014) 13782–13789.
[15] J.E. Bara, T.K. Carlisle, C.J. Gabriel, D. Camper, A. Finotello, D.L. Gin, R.D. Noble, Guide to CO_2 separations in imidazolium-based room-temperature ionic liquids, Ind. Eng. Chem. Res. 48 (6) (2009) 2739–2751.
[16] S. Zeng, X. Zhang, L. Bai, X. Zhang, H. Wang, J. Wang, D. Bao, M. Li, X. Liu, S. Zhang, Ionic-liquid-based CO_2 capture systems: structure interaction and process, Chem. Rev. 117 (14) (2017) 9625–9673.
[17] C. Moya, N. Alonso-Morales, M.A. Gilarranz, J.J. Rodriguez, J. Palomar, Encapsulated Ionic liquids for CO_2 Capture: using 1-butyl-methylimidazolium acetate for quick and reversible CO_2 chemical absorption, ChemPhysChem 17 (23) (2016) 3891–3899.
[18] J. Palomar, M. Gonzalez-Miquel, J. Bedia, F. Rodriguez, J.J. Rodriguez, Task-specific ionic liquids for efficient ammonia absorption, Sep. Purif. Technol. 82 (1) (2011) 43–52.
[19] A. Yokozeki, M.B. Shiflett, Ammonia solubilities in room-temperature ionic liquids, Ind. Eng. Chem. Res. 46 (5) (2007) 1605–1610.
[20] J. Bedia, J. Palomar, M. Gonzalez-Miquel, F. Rodriguez, J.J. Rodriguez, Screening ionic liquids as suitable ammonia absorbents on the basis of thermodynamic and kinetic analysis, Sep. Purif. Technol. 95 (2012) 188–195.
[21] J. Lemus, J. Bedia, C. Moya, N. Alonso-Morales, M.A. Gilarranz, J. Palomar, J.J. Rodriguez, Ammonia capture from the gas phase by encapsulated ionic liquids (ENILs), Rsc Adv. 6 (66) (2016) 61650–61660.
[22] J. Bedia, E. Ruiz, J. de Riva, V.R. Ferro, J. Palomar, J.J. Rodriguez, Optimized ionic liquids for toluene absorption, AIChE J. 59 (5) (2013) 1648–1656.
[23] M.J. Salar-Garcia, V.M. Ortiz-Martinez, F.J. Hernandez-Fernandez, A.P. de los Rios, J. Quesada-Medina, Ionic liquid technology to recover volatile organic compounds (VOCs), J. Hazard. Mater. 321 (2017) 484–499.
[24] J. de Riva, J. Suarez-Reyes, D. Moreno, I. Diaz, V. Ferro, Ionic liquids for post-combustion CO 2 capture by physical absorption: Thermodynamic, kinetic and process analysis, Int. J. Greenhouse Gas Control 61 (2017) 61–70.
[25] J. Palgunadi, H.S. Kim, J.M. Lee, S. Jung, Ionic liquids for acetylene and ethylene separation: Material selection and solubility investigation, Chem. Eng. Process. Process Intensif. 49 (2) (2010) 192–198.
[26] J. Palgunadi, S.Y. Hong, J.K. Lee, H. Lee, S.D. Lee, M. Cheong, H.S. Kim, Correlation between hydrogen bond basicity and acetylene solubility in room temperature ionic liquids, J. Phys. Chem. B 115 (5) (2011) 1067–1074.
[27] H. Xu, Z. Han, D.J. Zhang, J.H. Zhan, Interface behaviors of acetylene and ethylene molecules with 1-butyl-3-methylimidazolium acetate ionic liquid: a combined quantum chemistry calculation and molecular dynamics simulation study, ACS Appl. Mater. Interfaces 4 (12) (2012) 6646–6653.
[28] X. Zhao, H.B. Xing, Q.W. Yang, R.L. Li, B.G. Su, Z.B. Bao, Y.W. Yang, Q.L. Ren, Differential solubility of ethylene and acetylene in room-temperature ionic liquids: a theoretical study, J. Phys. Chem. B 116 (13) (2012) 3944–3953.
[29] X. Zhao, Q. Yang, D. Xu, Z. Bao, Y. Zhang, B. Su, Q. Ren, H. Xing, Design and screening of ionic liquids for C_2H_2/C_2H_4 separation by COSMO-RS and experiments, AIChE J. 61 (6) (2015) 2016–2027.

[30] H. Xing, X. Zhao, Q. Yang, B. Su, Z. Bao, Y. Yang, Q. Ren, Molecular dynamics simulation study on the absorption of ethylene and acetylene in ionic liquids, Ind. Eng. Chem. Res. 52 (26) (2013) 9308–9316.
[31] E. Ruiz, V.R. Ferro, J. de Riva, D. Moreno, J. Palomar, Evaluation of ionic liquids as absorbents for ammonia absorption refrigeration cycles using COSMO-based process simulations, Appl. Energy 123 (2014) 281–291.
[32] A. Klamt, F. Eckert, W. Arlt, COSMO-RS: an alternative to simulation for calculating thermodynamic properties of liquid mixtures, in: J.M. Prausnitz, M.F. Doherty, and R.A. Segalman (Eds.), Annual review of chemical and biomolecular engineering, Annual Reviews: Palo Alto. 1 (2010) pp. 101–122.
[33] V.R. Ferro, C. Moya, D. Moreno, R. Santiago, J. de Riva, G. Pedrosa, M. Larriba, I. Diaz, J. Palomar, Enterprise Ionic Liquids Database (ILUAM) for use in Aspen ONE programs suite with COSMO-based property methods, Ind. Eng. Chem. Res. 57 (3) (2018) 980–989.
[34] J. de Riva, V.R. Ferro, D. Moreno, I. Diaz, J. Palomar, Aspen Plus supported conceptual design of the aromatic-aliphatic separation from low aromatic content naphtha using 4-methyl-N-butylpyridinium tetrafluoroborate ionic liquid, Fuel Process. Technol. 146 (2016) 29–38.
[35] V.R. Ferro, J. de Riva, D. Sanchez, E. Ruiz, J. Palomar, Conceptual design of unit operations to separate aromatic hydrocarbons from naphtha using ionic liquids. COSMO-based process simulations with multi-component “real” mixture feed, Chem. Eng. Res. Des. 94 (2015) 632–647.
[36] M. Larriba, J. de Riva, P. Navarro, D. Moreno, N. Delgado-Mellado, J. Garcia, V.R. Ferro, F. Rodriguez, J. Palomar, COSMO-based/Aspen Plus process simulation of the aromatic extraction from pyrolysis gasoline using the {4empy NTf2 + emim DCA} ionic liquid mixture, Sep. Purif. Technol. 190 (2018) 211–227.
[37] D. Moreno, V.R. Ferro, J. de Riva, R. Santiago, C. Moya, M. Larriba, J. Palomar, Absorption refrigeration cycles based on ionic liquids: Refrigerant/absorbent selection by thermodynamic and process analysis, Appl. Energy 213 (2018) 179–194.
[38] V.R. Ferro, E. Ruiz, J. de Riva, J. Palomar, Introducing process simulation in ionic liquids design/selection for separation processes based on operational and economic criteria through the example of their regeneration, Sep. Purif. Technol. 97 (2012) 195–204.
[39] D. Ambrose, R. Townsend, Vapour pressure of acetylene, Trans. Faraday Soc. 60 (1964) 1025–1029.
[40] A. Klamt, Conductor-like screening model for real solvents: a new approach to the quantitative calculation of solvation phenomena, J. Phys. Chem. 99 (7) (1995) 2224–2235.
[41] C.R. Wilke, P. Chang, Correlation of diffusion coefficients in dilute solutions, Aiche J. 1 (2) (1955) 264–270.
[42] J. de Riva, V.R. Ferro, L. del Olmo, E. Ruiz, R. Lopez, J. Palomar, Statistical refinement and fitting of experimental viscosity-to-temperature data in ionic liquids, Ind. Eng. Chem. Res. 53 (25) (2014) 10475–10484.
[43] S.-T. Lin, S.I. Sandler, A priori phase equilibrium prediction from a segment contribution solvation model, Ind. Eng. Chem. Res. 41 (5) (2002) 899–913.
[44] A.J. McCue, A. Guerrero-Ruiz, C. Ramirez-Barria, I. Rodriguez-Ramos, J.A. Anderson, Selective hydrogenation of mixed alkyne/alkene streams at elevated pressure over a palladium sulfide catalyst, J. Catal. 355 (2017) 40–52.
[45] M. Kuhn, M. Lucas, P. Claus, Precise recognition of catalyst deactivation during acetylene hydrogenation studied with the advanced TEMKIN reactor, Catal. Commun. 72 (2015) 170–173.
[46] M. Gonzalez-Miquel, J. Palomar, F. Rodriguez, Selection of ionic liquids for enhancing the gas solubility of volatile organic compounds, J. Phys. Chem. B 117 (1) (2013) 296–306.
[47] W. Li, Z. Zhang, B. Han, S. Hu, Y. Xie, G. Yang, Effect of Water and Organic Solvents on the Ionic Dissociation of Ionic Liquids, The Journal of Physical Chemistry B 111 (23) (2007) 6452–6456.
[48] NIST, Ionic Liquids Database - (ILThermo). 2013.
[49] P. Pässler, W. Hefner, K. Buckl, H. Meinass, A. Meiswinkel, H.-J. Wernicke, G. Ebersberg, R. Müller, J. Bässler, H. Behringer, D. Mayer, Acetylene, in: Ullmann's Encyclopedia of Industrial Chemistry. 2000, Wiley-VCH Verlag GmbH & Co. KGaA.

Supplementary Material

Acetylene absorption by ionic liquids: A multiscale analysis based on molecular and process simulation

R. Santiago, J. Bedia, D. Moreno, C. Moya, J. de Riva, M. Larriba, J. Palomar*

Sección de Ingeniería Química. Universidad Autónoma de Madrid. 28049 Madrid. Spain.

*Corresponding author. E-mail: pepe.palomar@uam.es

Index

Table S1. List of Ionic Liquids.

Table S2: Henry's Law constants (K_H) for acetylene in ionic liquids at T=298.15 K computed by COSMO-RS.

Table S3: Diffusion Coefficients (D) $x10^{12}$ for acetylene in ionic liquids at T=313 K computed by COSMO-RS.

Table S4: Experimental and Aspen Plus simulated values of isotherms for acetylene-ILs systems at T=313 K using the three different COSMOSAC models

Figure S1: experimental (points) vs calculated (lines) P-x diagrams of 5 ILs involved in the work

Figure S2: Experimental vs calculated viscosity by COSMO-RS at 313 K

Figure S3: Experimental vs COSMO-RS Henry's law constants of solutes in ILs using experimental vapour pressure of the different solutes for CA model

Figure S4: Experimental vs COSMO-RS Henry's law constants of solutes in ILs using COSMO predicted vapor pressure of the different solutes for CA model (A) and C+A model (B)

Table S1. List of Ionic Liquids

CATIONS		
Abbreviation	Name	Formula
choline	(2-hydroxyethyl)-trimethyl ammonium	C5H14NO
Opyr	1-octylpyrrolidinium	C12H22N
Hxpyr	1-hexylpyrrolidinium	C10H18N
Bpyr	1-butylpyrrolidinium	C8H14N
EtOHmim	1-(2-hydroxyethyl)-3-methylimidazolium	C6H11N2O
emim	1-ethyl-3-methylimidazolium	C6H11N2
epy	1-ethylpyridinium	C7H10N
mmim	1,3-Dimethylimidazolium	C5H9N2
bmim	1-butyl-3-methylimidazolium	C8H15N2
dcmim	1-decyl-3-methylimidazolium	C14H27N2
omim	1-octyl-3-methylimidazolium	C12H23N2
hxpy	1-hexylpyridinium	C11H18N
1e3mpy	1-ethyl-3-methylpyridinium	C8H12N
N_{4444}	tetrabutylammonium	C16H36N
P_{4444}	tetrabutylphosphonium	C16H36P
N_{2222}	tetraethylammonium	C8H20N
P_{2222}	tetraethylphosphonium	C8H20P

ANIONS		
Abbreviation	Name	Formula
Cl	chloride	Cl
MeCOO	acetate	C2H3O2
$MeSO_3$	methanesulfonate	CH3SO3
$(Et)_2PO_4$	diethylphosphate	C4H10PO4
$(Me)_2PO_4$	dimethylphosphate	C2H6PO4
$tolSO_3$	toluenesulfonate	C7H7O3S
$MeSO_4$	methylsulfate	CH3SO4
$EtSO_4$	ethylsulfate	C2H5SO4
SCN	thiocyanate	CNS
TFA	trifluoroacetate	C2F3O2
BF4	tetrafluoroborate	BF4
DCN	dicyanamide	C2N3
TfO	trifluoromethanesulfonate	CF3O3S
$B(CN)_4$	tetracyanoborate	C4BN4
NTf_2	bis(trifluoromethylsulfonyl)imide	C2F6NO4S2
PF_6	hexafluorophosphate	PF6

Table S2: Henry's Law constants (K_H) for acetylene in ionic liquids at T=298.15 K computed by COSMO-RS.

	[Cl]	[MeCOO]	[$MeSO_3$]	[$(Et)_2PO_4$]	[$(Me)_2PO_4$]	[$tolSO_3$]	[$MeSO_4$]	[$EtSO_4$]	[SCN]	[TFA]	[DCN]	[BF_4]	[TfO]	[$B(CN)_4$]	[NTf_2]	[PF_6]	[$FeCl_4$]	[FEP]
[N_{4HHH}]	36.56	48.70	28.27	20.94	25.11	20.61	37.43	30.10	78.92	73.55	55.45	70.83	56.93	32.99	42.40	54.14	30.85	29.98
[N_{2HHH}]	34.63	77.09	48.89	27.07	36.09	27.57	75.26	50.09	305.08	128.42	120.10	285.47	94.98	41.30	49.63	36.55	25.52	31.44
[choline]	0.81	3.21	4.49	7.55	6.13	9.38	9.36	11.26	11.94	19.27	17.68	16.77	29.40	26.50	29.97	69.55	42.86	29.05
[opyr]	5.11	5.87	6.53	6.05	6.12	7.45	9.59	9.27	15.43	12.99	13.53	14.72	15.56	16.92	20.92	21.16	22.94	23.90
[hxpyr]	4.91	5.90	6.57	6.09	6.15	7.53	9.85	9.48	16.47	13.60	14.36	15.89	16.38	17.55	21.41	23.07	23.71	23.97
[bpyr]	4.38	5.90	6.61	6.25	6.25	7.78	10.32	9.93	18.33	14.87	16.06	18.17	18.11	19.03	22.51	27.31	25.36	24.33
[EtOHmim]	1.51	3.63	4.47	5.90	5.19	7.50	8.12	8.77	12.98	14.02	14.88	14.60	19.00	21.47	23.14	34.64	31.27	24.84
[emim]	0.86	1.65	2.56	3.26	2.79	4.65	4.92	5.40	7.43	7.47	8.21	8.67	11.65	15.09	18.49	21.00	24.98	22.78
[epy]	0.85	1.77	2.62	3.44	2.93	4.82	4.97	5.48	7.59	7.70	8.74	8.69	11.82	16.03	18.25	21.61	24.81	22.11
[mmim]	0.53	1.45	2.27	3.53	2.83	5.02	4.73	5.56	6.66	8.29	8.78	8.16	13.52	18.01	20.28	26.89	28.48	23.14
[bmim]	1.58	2.12	3.26	3.37	3.13	4.77	5.69	5.82	8.75	7.46	8.38	9.80	11.03	13.42	17.47	18.17	22.11	22.69
[dcmim]	2.74	2.72	4.17	3.73	3.68	5.22	6.61	6.53	9.54	7.68	8.57	10.40	10.92	12.94	17.22	16.41	20.70	23.16
[omim]	2.49	2.59	3.97	3.62	3.54	5.08	6.40	6.35	9.42	7.58	8.50	10.29	10.85	12.88	17.11	16.60	20.75	22.90
[hxpy]	2.23	2.58	3.75	3.61	3.46	4.99	6.10	6.11	9.35	7.52	8.69	10.00	10.67	13.12	16.67	16.75	20.52	22.04
[1e3mpy]	0.81	1.27	2.10	2.52	2.18	3.74	4.00	4.33	5.89	5.57	6.24	6.91	9.03	12.55	16.21	15.87	21.76	21.90
[N_{4444}]	1.17	0.85	2.20	1.75	1.70	3.07	4.17	4.17	4.98	3.91	4.37	7.73	7.82	9.64	16.21	14.62	21.64	26.12
[P_{4444}]	1.35	1.02	2.43	1.95	1.92	3.32	4.48	4.46	5.40	4.31	4.76	8.09	8.21	9.98	16.41	14.89	21.65	26.01
[N_{2222}]	0.54	0.70	1.55	1.77	1.50	2.87	3.17	3.50	4.02	3.86	4.10	5.80	7.56	9.85	15.98	14.48	22.85	24.00
[P_{2222}]	0.57	0.62	1.48	1.55	1.35	2.61	3.02	3.25	3.81	3.41	3.72	5.62	6.84	9.06	14.98	13.16	20.92	23.60

Table S3: Diffusion Coefficients (D) x10^{12} for acetylene in ionic liquids at T=313 K computed by COSMO-RS.

	[B(CN)$_4$]	**[FEP]**	**[DCN]**	**[SCN]**	**[NTf$_2$]**	**[TfO]**	**[TFA]**	**[FeCl$_4$]**	**[MeSO$_4$]**	**[Cl]**	**[BF$_4$]**	**[EtSO$_4$]**	**[PF$_6$]**	**[MeSO$_3$]**	**[MeCOO]**	**[(Et)$_2$PO$_4$]**	**[(Me)$_2$PO$_4$]**	**[tolSO$_3$]**
[emim]	250.20	1508.66	170.49	11459.00	199.54	223.84	145.99	53.63	37.38	42.42	26.85	24.00	21.97	22.33	20.57	6.79	11.52	6.39
[epy]	257.51	2584.72	176.03	141.79	220.83	260.83	164.54	56.62	39.43	45.69	28.27	25.07	22.97	23.38	21.56	7.01	11.94	6.59
[mmim]	275.58	252.96	190.87	154.41	294.05	450.94	244.91	65.38	45.65	57.72	32.68	28.07	25.88	26.46	24.56	7.56	13.08	7.08
[1e3mpy]	255.42	2150.74	172.13	1994.84	208.02	219.42	142.57	54.34	37.47	40.79	26.66	24.27	22.03	22.39	20.55	6.94	11.68	6.54
[N$_{2222}$]	220.19	563.03	2892.13	248.16	138.85	127.80	90.39	42.48	29.23	29.27	20.85	19.70	17.80	17.93	16.30	5.93	9.75	5.61
[P$_{2222}$]	209.72	421.19	519.65	167.58	120.28	105.43	76.32	38.63	26.56	25.64	18.93	18.22	16.36	16.48	14.95	5.62	9.14	5.32
[bmim]	308.14	124.35	95.12	59.90	56.33	48.43	37.78	22.39	15.87	15.05	11.62	11.31	10.21	10.26	9.34	3.69	5.90	3.50
[EtOHmim]	428.62	118.65	120.62	72.64	56.56	52.90	41.61	23.09	16.78	17.51	12.61	11.67	10.79	10.84	9.99	3.67	6.02	3.47
[hxpy]	308.14	124.35	95.12	59.90	56.33	48.43	37.78	22.39	15.87	15.05	11.62	11.31	10.21	10.26	9.34	3.69	5.90	3.50
[choline]	307.70	102.25	103.51	64.04	50.36	47.38	37.40	20.99	15.24	15.94	11.50	10.61	9.89	9.86	9.05	3.34	5.48	3.16
[N$_{4444}$]	116.95	84.72	50.44	34.87	40.15	31.81	25.09	16.50	11.52	9.85	8.26	8.54	7.51	7.54	6.79	2.96	4.57	2.83
[P$_{4444}$]	117.02	85.25	50.63	35.05	40.42	31.98	25.25	16.63	11.62	9.92	8.33	8.62	7.57	7.62	6.86	3.00	4.62	2.86
[bpyr]	152.68	79.90	66.58	44.75	40.45	36.30	28.91	17.29	12.50	12.43	9.38	8.88	8.20	8.17	7.47	2.89	4.66	2.73
[omim]	106.71	72.94	49.15	34.29	36.29	30.21	24.06	15.40	10.96	9.96	8.03	8.01	7.18	7.20	6.54	2.72	4.27	2.59
[N$_{2HHH}$]	138.66	57.80	67.80	43.07	32.54	33.31	26.30	14.83	10.60	10.29	8.18	7.26	7.32	6.79	5.73	2.24	3.73	2.12
[hxpyr]	69.08	50.32	36.15	26.09	26.71	22.96	18.52	11.90	8.58	8.11	6.41	6.26	5.71	5.69	5.19	2.12	3.35	2.01
[dcmim]	64.69	51.50	33.02	23.88	26.67	21.82	17.54	11.68	8.31	7.36	6.08	6.17	5.49	5.51	5.00	2.15	3.33	2.05
[opyr]	42.76	35.33	23.77	17.64	19.21	16.11	13.08	8.74	6.30	5.75	4.68	4.66	4.21	4.21	3.82	1.62	2.52	1.54
[N$_{4HHH}$]	29.35	25.69	16.06	11.74	14.47	12.47	9.77	6.73	4.55	3.51	3.38	3.33	3.28	2.96	2.41	1.13	1.78	1.08

Table S4: Experimental and Aspen Plus simulated values of isotherms for acetylene-ILs systems at T=313 K using the three different COSMOSAC models

Cation	Anion	Experimental			Simulated CA model			Simulated C+A model		
		Pressure (kPa)	Mole fraction (%)	Ref	x (%) Model 1	x (%) Model 2	x (%) Model 3	x (%) Model 1	x (%) Model 2	x (%) Model 3
bmim	MeCOO	9.1	1.58	[1]	10.81	1.71	1.86	10.05	1.47	1.96
		21.72	3.61		18.46	4.03	4.34	18.95	3.40	4.50
		38.2	6.13		27.88	6.69	7.13	26.47	5.80	7.53
		56.74	8.66		33.88	9.54	10.10	32.21	8.32	10.62
MRD (%)		-	-	-	396.90	9.68	17.69	391.27	5.54	23.51
bmim	TFA	12.89	0.92	[1]	2.25	0.86	0.72	3.16	0.91	0.96
		26.27	1.87		3.76	1.69	1.43	6.13	1.83	1.93
		41.99	2.96		5.89	2.69	2.28	9.31	2.90	3.05
		59.57	4.15		8.53	3.82	3.29	12.49	4.07	4.27
MRD (%)		-	-	-	112.39	8.25	22.69	221.73	1.32	3.30
bmim	$MeSO_4$	10.76	1.04	[1]	3.49	1.08	0.98	4.36	0.95	1.07
		23.92	2.25		8.59	2.32	2.12	9.04	2.08	2.35
		37.51	3.48		12.99	3.62	3.31	13.27	3.22	3.63
		56.05	5.1		18.00	5.24	4.79	18.24	4.73	5.32
MRD (%)		-	-	-	260.19	3.44	5.66	289.99	7.88	4.07
bmim	BF_4	13.24	0.77	[1]	1.18	0.59	0.56	1.17	0.53	0.61
		26.75	1.54		2.41	1.21	1.15	2.34	1.07	1.23
		42.54	2.44		3.61	1.92	1.82	3.66	1.69	1.94
		60.6	3.43		4.78	2.71	2.57	5.13	2.39	2.74
MRD (%)		-	-	-	48.74	21.79	25.79	50.79	30.53	20.53
bmim	NTf_2	13.03	0.63	[1]	0.83	0.62	0.51	1.03	0.70	0.65
		29.51	1.36		1.71	1.38	1.13	2.32	1.58	1.46
		46.54	2.13		2.86	2.18	1.78	3.61	2.48	2.28
		70.88	3.22		3.99	3.33	2.74	5.39	3.74	3.45
MRD (%)		-	-	-	27.76	1.82	16.79	67.83	15.06	6.06
Average MRD (%)		-	-	-	169.19	8.99	17.72	204.32	12.07	11.50

Where x is molar fraction of acetylene in the ILs

Calculated viscosity correction

It is important to remark that COSMOtherm computes the pure compounds viscosity from a QSPR, whose descriptors do not predict this property with the same accuracy than thermodynamic properties determined by the chemical potential of mixture components. For this reason, a correction obtained from linear regression between experimental (by using the available data in literature [2]) and COSMO-RS viscosity data [$\mu_{corrected} = 1.991\mu_{COSMO\text{-}RS} - 23.198$] was used to correct COSMO-RS predictions.

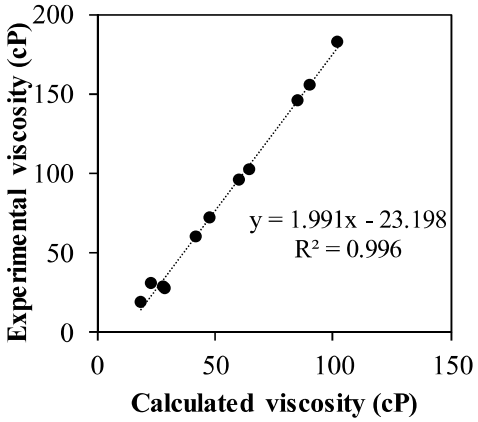

Figure S1: Experimental vs calculated viscosity by COSMO-RS at 313 K

Henry's law constant validation

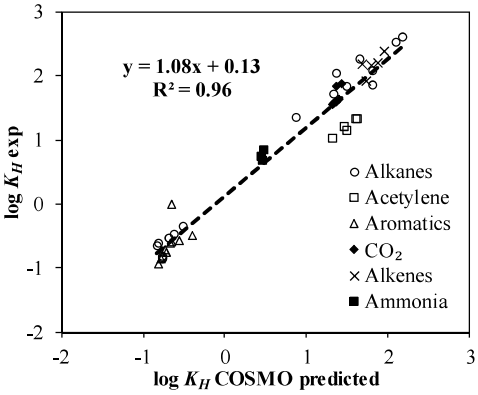

Figure S2: Experimental vs COSMO-RS Henry's law constants of solutes in ILs using experimental vapour pressure of the different solutes for CA model

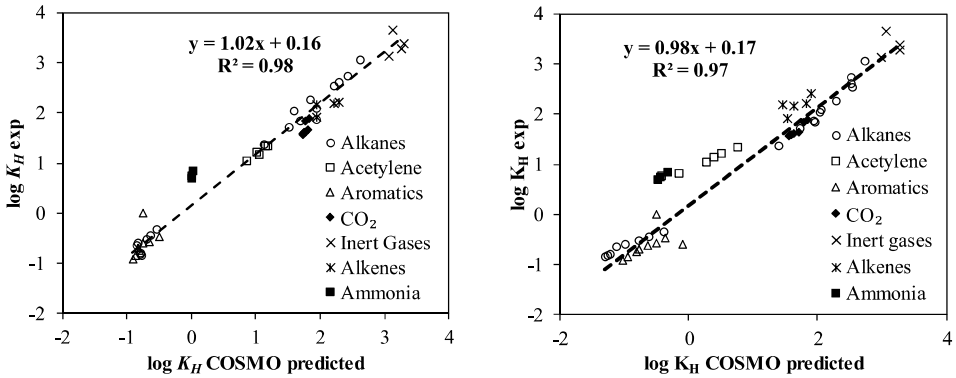

Figure S3: Experimental vs COSMO-RS Henry's law constants of solutes in ILs using COSMO predicted vapor pressure of the different solutes for CA model (A) and C+A model (B)

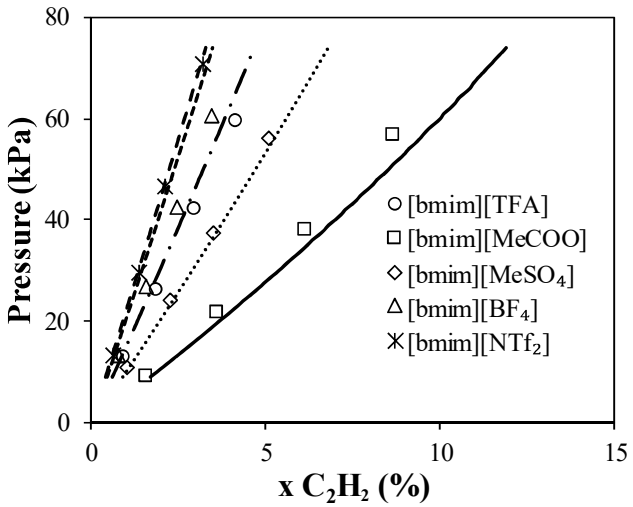

Figure S4: experimental (points) vs calculated (lines) P-x diagrams of 5 ILs involved in the work

References

1. Palgunadi, J., et al., *Ionic liquids for acetylene and ethylene separation: Material selection and solubility investigation.* Chemical Engineering and Processing: Process Intensification, 2010. **49**(2): p. 192-198.
2. de Riva, J., et al., *Statistical Refinement and Fitting of Experimental Viscosity-to-Temperature Data in Ionic Liquids.* Industrial & Engineering Chemistry Research, 2014. **53**(25): p. 10475-10484.

5.2 Assessment of ionic liquids as H_2S physical absorbents by thermodynamic and kinetic analysis based on process simulation

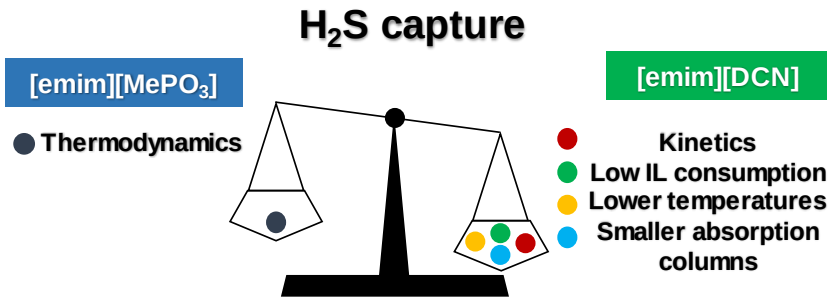

Assessment of Ionic Liquids as H_2S Physical Absorbents by Thermodynamic and Kinetic Analysis based on Process Simulation

Rubén Santiago, Jesús Lemus*, Ana Xiao Outomuro, Jorge Bedia and José Palomar

Chemical Engineering Department. Universidad Autónoma de Madrid. 28049 Madrid. Spain.

*Corresponding author. E-mail: jesus.lemus@uam.es

Keywords: H_2S; Absorption; COSMO-RS; Ionic Liquids; Aspen Plus

Abstract

A comprehensive evaluation of ionic liquids (ILs) as potential H_2S absorbents was performed using both molecular and process simulation. First, the Conductor-like-Screening MOdel for Real Solvents (COSMO-RS method) was applied to select promising ILs absorbents and understand the H_2S gas solubility from a molecular point of view. The ILs screening among more than 700 ionic combinations determines that H_2S physical absorption is mainly controlled by the hydrogen-bond acceptor capacity of the anion, due to the easily hydrogen bond formation when mixed with the acidic solute. Based on molecular simulation analysis, 6 ILs of different nature were evaluated in a typical industrial packed absorption column using COSMO-based/Aspen Plus methodology. Equilibrium based simulations demonstrated higher H_2S separation efficiency *(i.e.* lower solvent expenses and smaller equipment sizes) when increasing H_2S absorption capacity of the IL solvent. In contrast, rigorous process simulation analysis (including kinetic equations) reveals a strong mass transfer kinetic control in the H_2S absorption in commercial packed column, which severely limits the maximum H_2S absorption given by thermodynamics. As a result, ILs that present the best performance in the thermodynamic aspect, become worse for the operation. In fact, it was found that H_2S recovery at given operating conditions increases when decreasing the viscosity of IL, being 1-ethyl-3-methylimidazolium dicyanamide, the one that presents the best absorbent performance, requiring the lowest operating temperatures and liquid volume flows. Lastly, the absorption operation was designed to achieve fixed H_2S recovery using different liquid/gas feed ratios, resulting in column heights and diameters inside the

typical range marked by heuristic rules for usual industrial packed columns. In sum, current prospective study based on COSMO-RS and Aspen Plus have been proved as a useful tool to analyze the potential industrial application of ILs in the H_2S capture and to select the most adequate ILs, before starting with experimental tests, highly demanding in cost and time.

Introduction

In recent years, natural gas has become one of the most promising alternatives to the traditional and pollutant energy sources due to its cleanliness [1]. The active component in natural gas is methane (CH_4), but it usually contains undesired impurities such as carbon dioxide (CO_2) and hydrogen sulfide (H_2S) [2]. H_2S is an extremely toxic and corrosive gas that can cause several diseases and even the potential dead in enough concentrations [3]. H_2S is one of the responsible compounds of the well-known "acid rain" when it is oxidized to SO_2, causing extremely negative effects to the different ecosystems [4]. For all these reasons, the complete removal of H_2S from natural gas is required not only for a safety transport, but also for its correct utilization. Furthermore, the removal of this acid gas increases the calorific value of the natural gas [5].

Some technologies are available for H_2S treatment. Starting with the adsorption operation, some adsorbents such as silica gel, active carbon and zeolites are traditionally used. Specially, high specific surface zeolites demonstrated a great efficiency with high H_2S selectivity, and great stability until high temperatures [6]. However, the main disadvantage of this technology is the high energy demanding in the regeneration operation that hinders the application of this technology [7]. The technology most widely studied is H_2S absorption. In fact, a huge number of solvent-based processes were analyzed to remove this acid gas [8]. The separation has been accomplished by using chemical and/or physical absorption processes. Starting with the former, the most typical absorbents used are the aqueous organic amine solutions [9, 10]. They present high absorption capacities at low partial pressures, but they become less effective when the absorbent is reaching the saturation [8]. These absorbents show some disadvantages in their use, such as the high energy consumption due to the heat requirements to release the H_2S from the solvent and their high losses because of their high volatility [11]. In addition, the presence of CO_2 in the streams, results in competitive absorption, being the H_2S separation capacity reduced [11]. In the case of physical absorption, it presents some

advantages when compared with the chemical one, such as the easy regeneration at lower temperatures. Some physical absorbents are methanol, dimethylether, and morpholine derivatives, which are employed in commercial processes: Rectisol®, Selexol® and Morphysorb®, respectively [12]. However, Rectisol® presents a high volatility and low H_2S selectivity when CO_2 is present on the stream to treat. Selexol® presents lower vapor pressure than traditional solvents usually employed, but it presents high viscosity, which will result in low mass transfer kinetics. Morphysorb® presents high volatility, which will make more difficult the regeneration stage. [13]. These advantageous properties are the high and tunable solvent capacity, negligible volatility, non-flammability, low corrosivity and relatively high chemical and thermal stability [13, 14]. Furthermore, the possibility of customizing the cation and/or the anion for specific tasks made them considered as "designer solvents" [15]. The introduction of the ILs to physically absorb H_2S has attracted a great scientific community interest in recent years. Several works studying the H_2S solubility in different ILs physical absorbents were reported [16-20]. In that way, a pioneer work by Pomelli *et al*. [21] reported an experimental and theoretical study on solubility using different nature based ILs, concluding the importance of hydrogen bond interactions between the anion and the acid gas showing less importance the cation selection. This finding was confirmed later by Aparicio *et al.* [22] and Sakhaeinia *et al.* [23]. In parallel, several studies using COSMO-RS method performed computational screenings to select ILs with high H_2S gas solubility, in order to minimize the high cost and time demanding experimental tests [24-26].

In recent years, we have followed a multiscale research strategy, that integrates molecular and process simulations, to design new gas separation process based on ILs [27-29], successfully applied to the capture of CO_2 [30-33], NH_3 [34], toluene [35], acetylene [27] and other volatiles organic compounds [36-38]. This computational methodology can be applied to preliminary evaluate the technical viability of novel gas absorption process using ILs prior to experimental tests. For this purpose, the free ILUAM database [28] was recently developed to include 100 common ILs as compounds in Aspen Plus/Hysys software, in order to easily model individual operation units and complete separation processes based on ILs. This COSMO-based/Aspen Plus approach allows considering, simultaneously, thermodynamic, kinetic, technical, energetic and economic criteria in the selection of the most adequate IL absorbent. In addition, operating conditions, equipment

design and process configuration can be optimized in order to promote the technical and economic viability of the new separation process based on ILs [30, 31, 39, 40].

The main aim of this work is to evaluate and select adequate ILs for the H_2S absorption by means of the COSMO-based/Aspen Plus methodology. First, molecular simulation was used to select ILs with favorable thermodynamic properties for H_2S capture. For this purpose, a COSMO–RS screening of Henry's law constants of H_2S in more than 700 ILs was carried out to determine the more favorable cation-combination for H_2S absorption, selecting a sample of ILs with favorable H_2S absorbent properties. Then, the excess enthalpies of H_2S-IL binary mixtures were analyzed in terms of the solute-solvent intermolecular interactions, in order to obtain deeper insight of H_2S physical absorption phenomena in IL. Finally, process simulation with Aspen Plus process simulator was accomplished to describe the H_2S capture by IL in packing column at industrial scale. An equilibrium-based model was preliminary applied to analyze the role of thermodynamics in H_2S absorption operation, including the influence of the operating pressure, gas/liquid ratio (L/G) and number of column stages (N) on the H_2S recovery. Then, the potential kinetic control on the H_2S absorption process at different operating temperatures was analyzed by using rigorous rate-based column model. Finally, the sizing of the absorption column was performed for the best IL in order to achieve 95% H_2S recovery at different L/G ratios, obtaining in each case the required height and diameter of the packed column and comparing the results with the heuristic industrial parameters.

Methodology

COSMO-RS calculations

The first stage in COSMO-RS calculations is to create the *.cosmo files of the ILs for their use in COSMOtherm software. For this, the optimization of the compounds was performed at BP86/TZVP computational level by using Turbomole 7.0 software. ILs are defined using the molecular model of independent counter ions ($C + A$) in which the cation and the anion are optimized separately. These optimizations were carried out taking the compounds to the structure of minimum energy, with the solvent effect through the COSMO continuum solvation method. Once the optimization was finished, the polarized charge distribution of the compounds is obtained by a COSMO single point calculation, saving it into *.cosmo files. Then, the COSMO-RS calculations were performed using the COSMOtherm program package (version C30_1704) and its parametrization

BP_TZVP_C30_1701. The charge distributions of both H_2S, as pure solute, and ILs, as absorbents, can be easily visualized in σ-profile and σ-potential. In addition, vapor pressure calculation of H_2S at different temperatures was performed. In the case of the solute-solvent mixtures, Henry's law constants of H_2S in ILs and detailed contributions to excess enthalpies in equimolar mixtures were calculated as well. First, Henry's law constants (K_H) are calculated as follows:

$$K_H = \gamma_i^{\infty} \cdot p_0^{vap} \quad [1]$$

where K_H is calculated as the product of γ_i^{∞}, which is the activity coefficient of the solute at infinite dilution in the IL (calculated by COSMOtherm) and p_0^{vap}, which is the vapor pressure of the pure gas, estimated by Antoine equation (experimental data from reference [41]).

Second, the excess enthalpy of an equimolar mixture (H^E) is calculated by COSMOtherm following the next expression:

$$H^E = H^E(MF) + H^E(HB) + H^E(vdW) \quad [2]$$

Where $H^E(MF)$ is the energy contribution associated to Misfit forces; $H^E(MF)$ is that attributed to the hydrogen bonding and $H^E(vdW)$ is the one ascribed to Van der Waals forces.

Process simulation details

ILs were directly used from ILUAM database [28], which includes information and parameters of 100 commercial ILs for its application in Aspen Process simulators. COSMOSAC property package was selected for the thermodynamic calculations. In the case of the conventional gaseous compounds used in this work, which are N_2, CH_4, H_2S, and CO_2, they were loaded from Aspen Plus Database including two parameters for the complete definition of COSMOSAC property package. In this sense, the σ-profile and COSMO volume of the gaseous compounds were first calculated by using COSMOtherm software and then introduced to Aspen Plus process simulator. The use of COSMOSAC property package lets the user select the model that better fits to the system. Therefore, the user can select between: (i) the original COSMO-SAC model proposed by Lin and Sandler [42] (denoted as COSMOSAC 1); (ii) the original COSMO-RS model developed by Klamt [43] (COSMOSAC 2); and (iii) a modification of the Lin and Sandler model performed by P. Mathias *et. al* [44] (COSMOSAC 3). In the present work, the three

models were used for selecting the one that best fits to the experimental data. Mean relative error were calculated by eq. 3 using the experimental and calculated gas-liquid equilibria (GLE) data 30%. COSMOSAC 1 property model shows the best fit to the experimental data, with errors lower than 16%, which can be considered an admissible error on initial stages of conceptual engineering [39]. Therefore, COSMOSAC 1 is selected as the property model for next stages of the work.

$$Mean\ relative\ error\ (\%) = \frac{1}{N_{point}} \sum \frac{|x_{calculated} - x_{experimental}|}{x_{calculated}} \cdot 100 \quad [3]$$

The RADFRAC model implemented as default in Aspen Plus v9.0 was used to model the H_2S absorption column. To accomplish this, two operation modes of RADFRAC model were used: *Equilibrium* mode, in which only the thermodynamic equilibrium is considered, and *Rate-Based* mode, in which also the mass transfer kinetics is taken into account. For *Rate-Based* calculations, a fractional capacity of 65% was fixed to ensure a similar fluid dynamic behavior. A packing type *Raschig Rings* with a diameter of 76.2 mm was selected following the heuristic rules for maintaining a *D/d* ratio around 20 [45].

The inlet gas feed presents the composition summarized in Table 1, accordingly to Faramawy *et. al*. work, for typical acid gas natural streams of industrial plants [2].

Table 1. Inlet gas feed general characteristics.

Stream characteristics		**Value**	
P, atm		0.98	
T, ºC		25	
Total Molar Flow, kmol/h		1301	
Total Mass Flow, ton/h		22.5	
Component	***MW*, kg/kmol**	**y_i**	**Flow, kmol/h**
CH_4	16	0.940	1222.9
CO_2	44	0.025	32.5
N_2	14	0.015	19.5
H_2S	34	0.020	26.1

Different simulation cases were performed for studying both the thermodynamics and the kinetics of the H_2S absorption operation using ILs: *Case 1):* The *Equilibrium* mode of RADFRAC column was used for studying the influence of the *L/G* ratio at two given

pressures in the H_2S recovery in different ILs. *Case 2):* Once again using the equilibrium column, the number of stages was varied for obtaining 99% of recovery at a fixed *L/G* ratio. *Case 3):* The H_2S recoveries as a function of the temperature are estimated for the selected ILs using *Equilibrium* and *Rate-Based* mode in RADFRAC column (1 m of height). *Case 4):* Comparison of *L/G* ratio for reaching a 95% H_2S recovery at different temperatures between *Equilibrium* and *Rate-Based* mode of different ILs. All the used conditions for each case are summarized in Table 2. Last, the column design (height and diameter) was accomplished for the best case taking into account heuristic rules. In this sense, the enough height for reaching a 95% H_2S recovery, and the diameter needed for a fractional approach to maximum capacity of 65% as a function of the *L/G* ratio.

Table 2. Conditions of the different cases of study.

Case	**1**	**2**	**3**	**4**
Mode	EQ	EQ	EQ/RB	EQ/RB
Pressure, atm	3-30	30	30	30
***T*, ºC**	25	25	0-200	0-100
***L/G*, kg/kg**	0-200	-	30	-
H_2S recov, %	-	99	-	95
Number of Stages	2	2-10	5	5

Results

Molecular simulation

COSMO-RS methodology allows predicting the thermodynamic properties of solute-IL systems and analyzing the intermolecular interactions governing the mixture behavior. This is due to the quantification of the interaction energy between the surfaces by means of the polarized charge distribution (σ). This charge distribution can be summarized in a histogram named σ-profile that permits a simple analysis of the chemical nature of the compounds involved. Next, COSMO-RS introduces an additional tool called σ-potential in which the charge density concept is introduced. This is defined as the chemical potential of a surface unit with a polarized charge distribution in a solvent, and allows

analyzing the intermolecular interactions between the compound and its environment [46]. In this sense, Figure 1 shows the σ-profile and σ-potential results of the solute studied (H_2S). It is important to remark the three different regions in which the histograms are divided. The first one that includes the range of polarities $\sigma < -0.0082$ e/Å^2 is referred to the hydrogen bond donor groups, the second one ($-0.0082 < \sigma > +0.0082$ e/Å^2) includes the non-polar region and the last one $\sigma > +0.0082$ e/Å^2 associated to hydrogen bond acceptor groups. The σ-profile of H_2S presents a peak at the negative region (hydrogen bond donor group), in agreement with the weak H_2S acidity. On the other hand, attending to the σ-potential (Figure 1B), it is observed that H_2S presents attractive interactions with non-polar compounds and polar compounds presenting hydrogen bond acceptor groups.

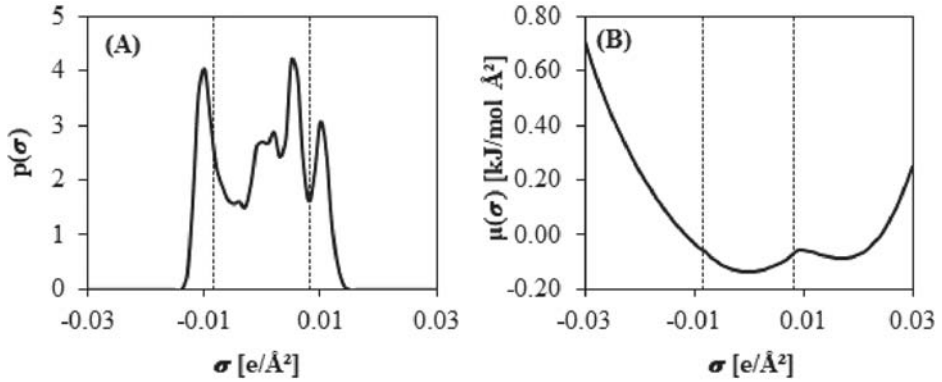

Figure 1: **(A)** σ-profile and **(B)** σ-potential of pure H_2S

The next stage of molecular simulation is to select ILs among a huge database. A widely used key parameter for the selection of ILs as absorbent -attending to thermodynamic criteria- is the Henry's law constant of the gas solute in the IL. Following the equation (1), COSMO-RS method calculates K_H by means of the activity coefficient of the solute at infinite dilution in the mixture and the vapor pressure of the pure solute. In current COSMO-RS calculations, the experimental vapor pressure was included in the software by means of Andrade equation parameters (A= 4.52887; B= 958.587 and C= -0.539 units of bar). For validation purposes, Figure 2 shows the experimental K_H *vs* the calculated K_H

for several different solutes in ILs, using the [*C*+*A*] model to describe the IL component in COSMO-RS simulations, following the methodology of previous works [27, 32, 36]. It is important to remark that the experimental K_H values were collected from Gonzalez-Miquel *et. al.* work [36] (more information in Table S1 of Supporting Information). As can be seen, the statistical parameters (slope = 0.99 and square correlation coefficient R^2 = 0.98) show the good predictability of COSMO-RS approach used in this work, including the available data for H_2S-IL systems (Table S1 of Supporting Information collects all the data and references presented in Figure 2).

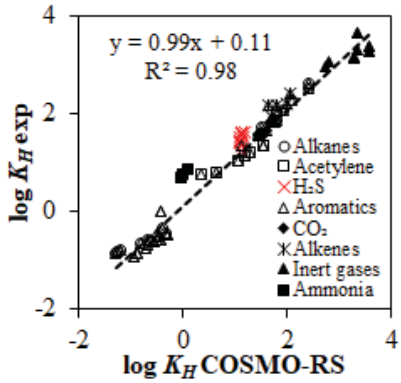

Figure 2: Henry's law constant prediction validation using [*C*+*A*] model and experimental vapor pressure of solutes using COSMO-RS calculations

Then, a complete Henry's law constant screening among more than 20 combinations cation-anion (>700 ILs) was performed for selecting ILs with potential properties for H_2S absorption. Remarkably different nature cations and anions were used for the screening (see Table S2 in the Supplementary Material for the nomenclature of the ILs used). Figure 3 presents the results of predicted K_H of H_2S in the different cation-anion combinations. It is important to remark that, following the equation (1), low K_H values are traduced into high solubility values in molar terms. Therefore, we search combinations cation-anion that present the lowest K_H values. Analyzing the Figure 3, it is observed that the K_H values for several ILs are lower than 2 bar, indicating a higher H_2S solubility than that of CO_2 in ILs [33] and in the order of that of similar to NH_3 in ILs [47]; *i.e*, we found favorable cation-anion combinations for the H_2S absorption in comparison to other solutes [36]. Attending to COSMO-RS predictions depicted in Figure 3, the selection of both anion and cation has significant influence on the H_2S

absorption capacity of the IL [40], obtaining higher values with those ILs composed by anion with basic character ($[MePO_3]^-$, $[(Me)_2PO_4]^-$, $[MeSO_3]^-$ …) and aprotic cations with

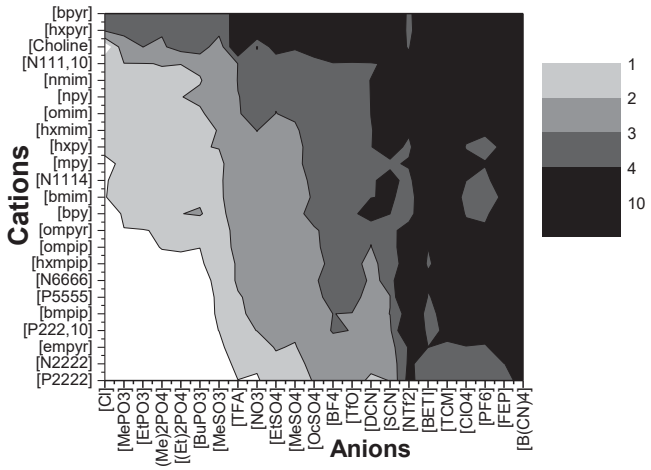

non-polar character (phosphonium, ammonium …).

Figure 3: Henry's law constants screening (bar) of H_2S in 529 ILs at 25 ºC

To analyze the possible relationship between the H_2S solubility in ILs and the excess enthalpy of H_2S-IL mixtures, COSMO-RS method was applied to calculate the H^E values of the H_2S-IL mixtures at H_2S concentrations corresponding to the solubility data in ILs. Figure 4 relates the predicted K_H values of H_2S in IL to the excess enthalpy of the equimolar solute-solvent mixtures at 25 ºC and 1 atm. As can be seen, the gas solubility increases (lower K_H) in more exothermic mixtures, indicating that the favorable intermolecular interactions between H_2S and IL determine the absorption process, in good agreement with the previously observed for CO_2, NH_3, VOCs, etc. capture [27, 30, 32, 34, 36, 40, 47]. As can be seen, from molecular simulations, we can select ILs that present higher exothermic mixtures and lower K_H values than common ILs widely used in bibliography [16-18, 48, 49].

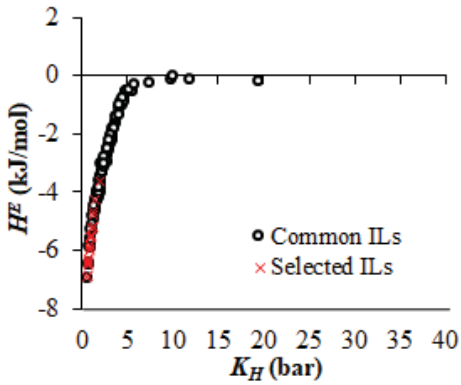

Figure 4: Molar Excess Enthalpies (H^E) *vs* Henry's law constants (K_H) of equimolar H_2S-ILs mixtures at 25 ºC

In order to obtain more insights in the intermolecular contributions to the H_2S absorption, different COSMO-RS analysis can be performed. In this sense, we first analyze the effect of the anion nature on H_2S-IL mixture behavior. It is going to be analyzed different chemical nature effects of ILs. First, Figure 5 presents the calculated H^E and K_H for ILs series of common $[emim]^+$ cation and different anions. As can be seen, remarkably enhanced H_2S gas solubility can be obtained by the proper selection of the anion. Thus, ILs with strong hydrogen-bond acceptor groups promote favorable solute-solvent intermolecular interactions that increase the gas solubility. On the contrary, anion with delocalized charge, such as $[PF_6]^-$, is not able to form local HB interactions with the solute, and as result, low solubility of H_2S in the ILs formed by this anion is expected. It was demonstrated that the anion contributes majority to the H_2S physical absorption and the importance of selecting anions that present basic character.

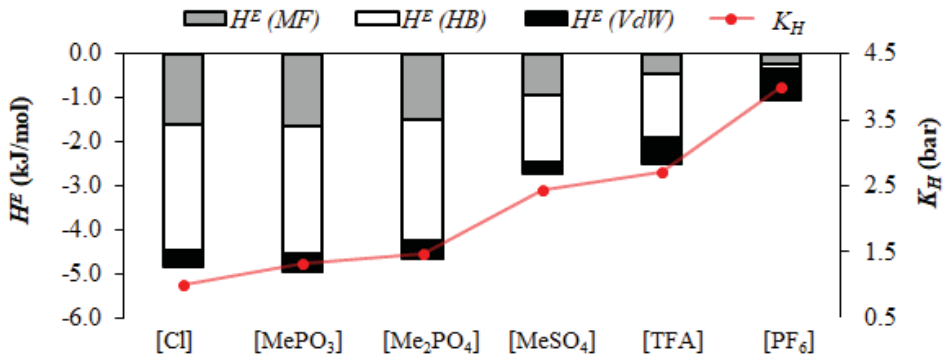

Figure 5: Excess Enthalpies (H^E) contributions (MF, HB and vdW) and Henry's law constants (K_H) of H_2S with different anions nature with the same cation $[emim]^+$

It is also analyzed the effect of different alkyl chains with the same anion ($[(Me)_2PO_4]^-$). Figure 6 presents the contributions to excess enthalpy and K_H as a function of the alkyl chain of the methylimidazolium based cation. As can be seen, the cation nature also affects the H_2S solubility in the IL, but with less influence than that of the anion. In all studied cases, the hydrogen bonding interactions present the higher contribution, being almost 68% of the total. The exothermic behavior of mixture is related to favorable solute-solvent interactions. ILs formed by methylimidazolium based cations with short alkyl chains present slightly better performance in the H_2S absorption, since the attractive electrostatic interactions are more effective when using shorter alkyl chains.

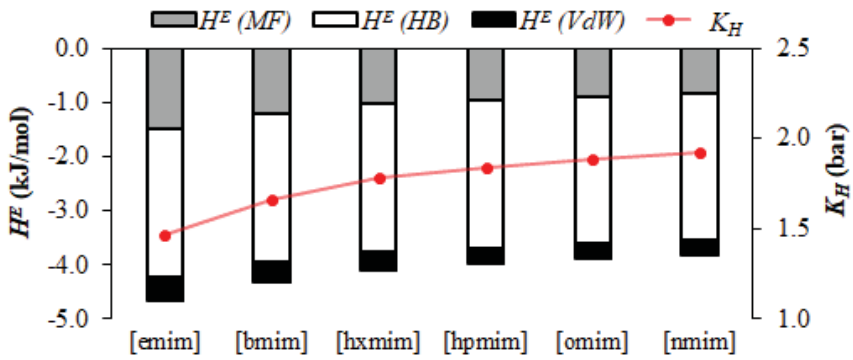

Figure 6: Excess Enthalpies (H^E) contributions (MF, HB and vdW) and Henry's law constants (K_H) of H_2S in different imidazolium based cations with the same anion $[(Me)_2PO_4]^-$

The last effect is shown in Figure 7 presenting the results of all the contributions to excess enthalpies and K_H of H_2S in different ILs presenting the same anion $[MePO_3]^-$, but varying the head group of the cation. As in previous analysis, the main contribution to the H_2S-IL mixing behavior is the hydrogen bond interactions (HB), representing a 70% of the total excess enthalpy value. ILs with cations presenting hydrogen-bond donor groups (as imidazolium or pyrrolidinium) present lower H_2S gas solubility, due to the competition between hydrogen-bond interactions of cation and anion and H_2S–anion interactions, as it was observed with other solutes [36, 40, 50]. In sum, current COSMO-RS results reveal that both anion and cation present great influence in the behavior of H_2S-IL mixtures. For the following process simulation analysis in this work, we selected 3 ILs that present favorable thermodynamic properties ([emim][$MePO_3$], [bmim][TFA] and [emim][$OcSO_4$]) from COSMO-RS analysis. In addition, we selected three ILs

([emim][DCN], [emim][SCN] and [emim][NTf_2]) that present worse thermodynamic behavior but lower viscosities and thus better expected transport properties [33].

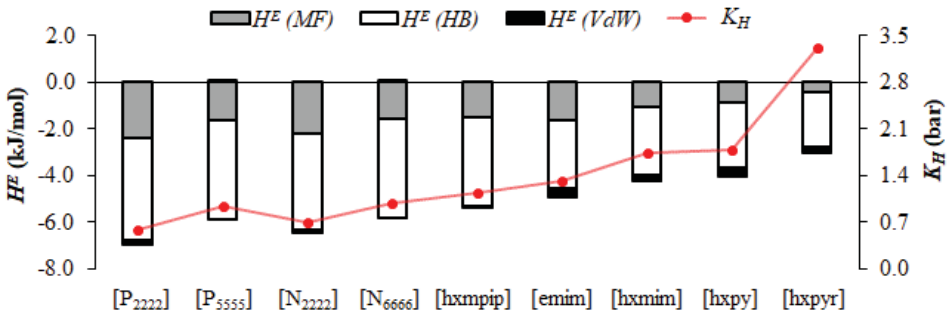

Figure 7: Excess Enthalpies *(H^E)* contributions (MF, HB and vdW) and Henry's law constants *(K_H)* of H_2S with different cations nature with the same anion $[MePO_3]^-$

Process Simulation Analysis

As first stage, COSMO-based/Aspen methodology was validated for the prediction gas-liquid equilibria data of H_2S-IL mixtures by comparing to available experimental data. Table 3 collects the mean relative errors of the gas-liquid equilibria (eq. 3) of four different ILs using the three COSMOSAC models commented in the methodology section. The experimental and calculated gas-liquid equilibria (GLE) data used to calculate these errors are collected in Figure S1 of the Supplementary Material. All the models describe reasonably well the GLE behavior of the mixture, presenting relative error < 30%. COSMOSAC 1 property model shows the best fit to the experimental data, with errors lower than 16%. This low dispersion can be considered an admissible error on initial stages of conceptual engineering of new processes based on ILs [28]. Therefore, COSMOSAC 1 is selected as the property model for next stages of the work.

Table 3: Mean relative errors of calculated solubilities using the different COSMOSAC property models, at temperatures between 30-80 ºC

IL	**[omim][PF_6]**	**[emim][NTf_2]**	**[hxmim][NTf_2]**	**[omim][NTf_2]**
Reference	[51]	[49]	[48]	[48]
P range (MPa)	0.12-1.92	0.16-1.61	0.11-2.02	0.13-1.69
COSMOSAC model	**Relative Error (%)**			
1	15.3	16.0	14.3	8.5
2	22.5	27.2	27.7	15.3
3	16.1	18.7	16.4	9.1

Once COSMO-based/Aspen approach was validated, different process simulations were carried out to systematically evaluate the performance of the selected ILs in H_2S absorption from a typical acid gas natural stream (Table 1), attending to the four cases detailed in Table 2.

Case 1: The performance of the selected ILs was first evaluated by modeling the absorption column in *Equilibrium* mode at a given number of stages and operating temperature. Figure 8 presents the achieved H_2S recovery when using the 6 different ILs with increasing liquid mass flow at two operating pressures (3 and 30 atm).

It is clear shown the advantage of using [emim][$MePO_3$] from the thermodynamic point of view, due to the lower *L/G* ratios required to reach high H_2S recoveries when compared to the other ILs. Comparing the two operation pressures (3 to 30 atm), it can be seen that a higher operating pressure allows using lower *L/G* ratios to reach the same H_2S recovery. [emim][$MePO_3$] presents the best thermodynamic behavior at both pressures. The overall process analysis suggests that H_2S absorption by ILs is not impeded from the thermodynamic point of view, reaching at 30 atm high solute recoveries with *L/G* ratios in the industrial range [52].

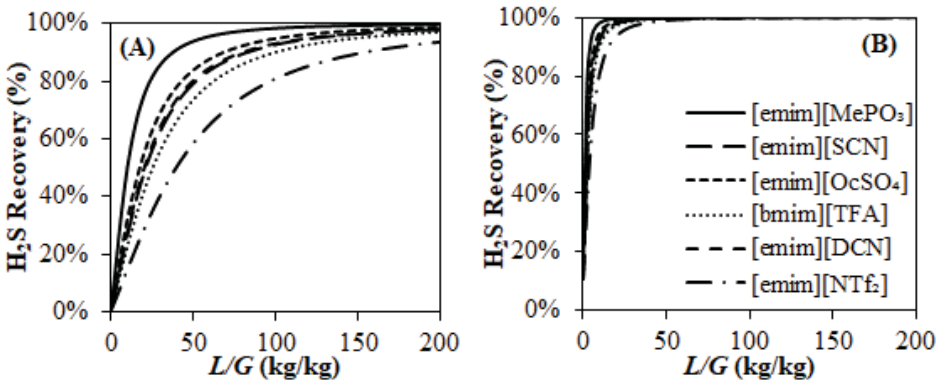

Figure 8: H_2S recoveries as a function of the *L/G* ratio at **(A)** 3 atm and **(B)** 30 atm (*Case 1* in Table 2)

Case 2: The aim of this study is to analyze the effect of the number of equilibrium stages of the absorption column in H_2S separation. Figure 9 presents the calculated number of stages required for reaching a H_2S recovery of 99% when using different *L/G* ratio for the selected ILs. As can be seen, from equilibrium-based simulations, it is possible to obtain high H_2S recoveries in a wide range of *L/G* and N_{stages} design variables. As expected, increasing the number of stages in the absorption column decreases the IL mass flow

required to achieve 99% of recovery. However, when increasing more than 5 stages, the required *L/G* ratio decreases in less proportion, converging into the same value. The shaded zone of the graph is referred to the work range (3 – 5 stages) more usually employed. This range was selected taking into account the heuristic value of 1 – 1.5 of *L/G* minimum for the separation [53]. For next stages, it was decided to work with an absorption column of 5 stages.

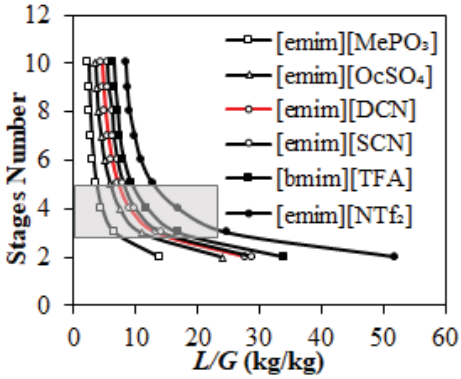

Figure 9: Stages number vs *L/G* ratio needed to reach a 99% H_2S recovery, using different ILs at 30 atm of pressure (*Case 2* in Table 2)

Case 3: This case of study introduces the mass transfer kinetics in the description of the absorption operation by using RADFRAC column in Rate-based mode. Thus, a more realistic scenario is studied, considering the transport properties of the mixture to estimate the H_2S separation efficiency by ILs in commercial packed columns. Figure 10 compares the H_2S recovery as a function of the absorption temperature using RADFRAC column in *Equilibrium* and *Rate-Based* modes with [emim][$MePO_3$] and [emim][DCN] ILs as absorbers. Simulations based on equilibrium show curves that follow the expected trends from exclusively thermodynamic consideration, *i.e.* the H_2S recovery increases when temperature decreases for both ILs, due to the higher gas solubility. In contrast, when absorption rate is considered in calculations, very low H_2S separation recovery was obtained for [emim][$MePO_3$] at near room temperature, as it was already observed when analyzing CO_2 capture by physical absorption with ILs [31, 33]. The results observed in Figure 10A reveal a strong kinetic control in the H_2S absorption phenomena in [emim][$MePO_3$] when using a commercial packed column at relatively low temperatures, assignable to the high viscosity of IL [31, 33]. Then, when increasing the operating temperature, the diffusivity of H_2S in IL is progressively enhanced, as consequence of the decreased IL viscosity [54], obtaining a maximum of H_2S recovery curve at 120 ºC, then

thermodynamics start to control the absorption process. Similar results are obtained for [emim][DCN] (Figure 10B), but with less remarkable differences between *Equilibrium* and *Rate-Based* mode due to the much lower viscosity of [emim][DCN] (16.83 cP @ 25 ºC [55]) when compared to [emim][$MePO_3$] (149.12 cP @ 25 ºC [56]).

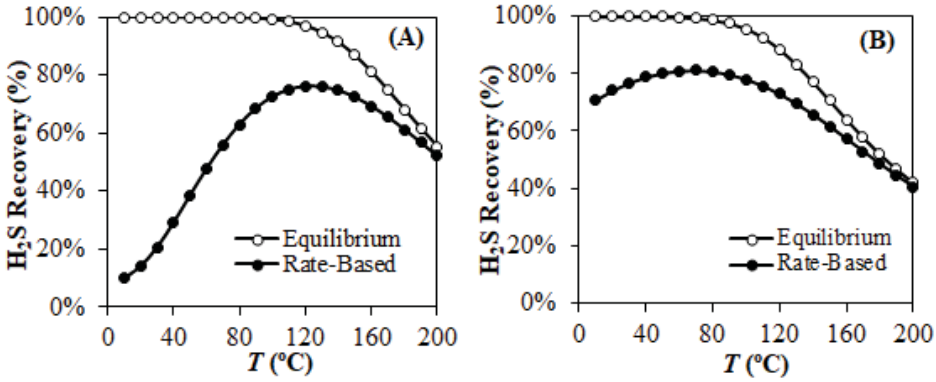

Figure 10: Comparative of the different H_2S recoveries as a function of the absorption temperature in both *Equilibrium* and *Rate-Based* modes of **(A)** [emim][$MePO_3$] and **(B)** [emim][DCN] (*Case 3* in Table 2)

Figure 11 completes current analysis, presenting the obtained H_2S recovery for all selected ILs when rigorous *Rate-based* absorption column model was used in simulations at different operating temperatures (25-200 ºC). The curves pass through a maximum in all cases, but at different temperature depending on the IL. Thus, [emim][DCN], [emim][SCN] and [emim][NTf_2] allow obtaining the maximum H_2S recovery at lower operating temperatures than those of [emim][$MePO_3$], [emim][$OcSO_4$] and [emim][TFA]. This may be explained by the lower viscosities of the first IL group compared to those of the second one [54]. In fact, at near room temperatures, the H_2S absorbent performance follows the trend of the IL viscosity values, which confirms that the mass transfer rate is controlling the H_2S absorption process in the column. On the contrary, at higher operating temperatures (than that corresponding to curve maximum) the absorption separation is determined by the thermodynamics of the H_2S-IL mixture (as in Figure 8). Based on current results, it is concluded that the IL [emim][DCN] operating at an absorption temperature of 50 ºC presents the best performance as H_2S absorbent.

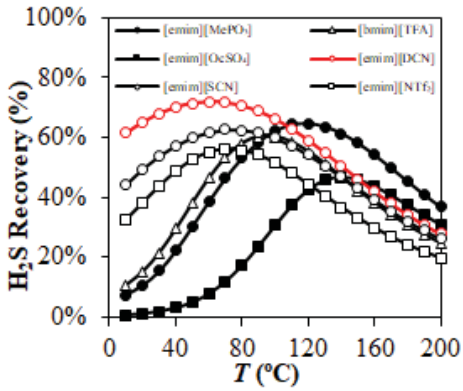

Figure 11: H_2S recoveries of the different ILs as a function of the absorption temperature (*Case 3* in Table 2)

Case 4. Finally, simulations to estimate the solvent consumption required to reach 95% of H_2S recovery at fixed operating conditions (see Table 2) were carried out for the selected ILs. Figure 12 presents the calculated *L/G* ratios needed to achieve this separation at different temperatures by using *Equilibrium* (only thermodynamic equilibrium is considered) and *Rate-Based* mode (mass transfer kinetic is also taken into account).

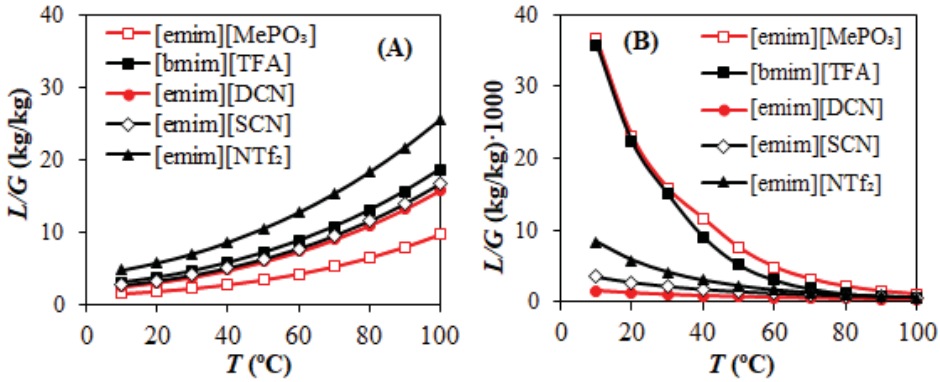

Figure 12: *L/G* mass ratio needed to reach a 95% of H_2S recovery at different temperatures for each IL using the RADFRAC model in **(A)** *Equilibrium* and **(B)** *Rate-Based* mode *(*Case 4 *in Table 2)*

As can be seen, huge differences are obtained when using the two different simulation approaches (*Equilibrium* or *Rate-Based* mode). Attending to Figure 12A, all the ILs present the same trend with absorption temperature, increasing IL mass flows by increasing temperatures, due to the lower H_2S gas solubility. In this case, the IL that presents the most favorable thermodynamic behavior is [emim][$MePO_3$]. In contrast, Figure 12B shows opposite trends of required *L/G* when increasing the operating

absorption temperature. In this case, the IL solvent expenses are higher at low temperatures due to the increasing IL viscosities [33]. In fact, the curves in Figure 12B follow an exponential decrease in good agreement with the dependence of viscosity values with temperature [54]. Again, it is observed that the IL [emim][DCN] presents the less viscous solvent. It is also important to remark the much higher *L/G* ratio needed (1000 time higher) when the mass transfer kinetics is taken into account in separation simulations at near room temperatures.

Absorption column design

Based on above results, the last purpose of the analysis is to design an H_2S absorption operation using [emim][DCN] at 50 ºC and 30 atm, to obtain a H_2S recovery of 95%. Figure 13 presents the required height (*H*) and diameter (*D*) of the packed column as a function of the *L/G* ratio. As can be seen, the use of a higher *L/G* ratio entails smaller column heights. On the other hand, an increase in the liquid mass flow demands larger column diameters for maintaining the fixed fractional capacity of 65%. The grey region corresponds to the design zone in which all the heuristic parameters are satisfied. In this sense, the height/diameter ratio in industrial absorption columns is between 3-15 [45] so different absorption columns with [emim][DCN] are possible. Thus, this study confirms the viability of [emim][DCN] IL to be used as absorbent of H_2S in gas streams in real applications. Future works with detailed cost estimations will be needed in order to optimize the design variables of H_2S absorption process based on ILs and compare their behavior with that of conventional absorbents.

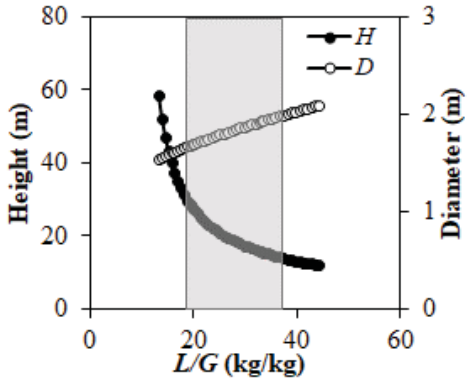

Figure 13: Absorption column design using [emim][DCN] as absorbent

Conclusions

In the present work, the modeling of H_2S absorption operation using ILs was accomplished. For this, a COSMO-based/Aspen Plus multiscale methodology was used. This methodology allows the *a priori* evaluation of the thermodynamic properties of a huge number of H_2S-IL mixtures. First, COSMOtherm molecular simulator was successfully applied to select different ILs among more than 700 attending to thermodynamic criteria (Henry's law constants). The results showed that it is expected a high H_2S solubility in some ILs due to the low K_H obtained. In addition, it was clear that the selection of the anion would have a great influence in the solubility, being favored with ions of hydrogen-bond acceptor character. The intermolecular interactions analysis remarks the high contribution on hydrogen bonding between H_2S solute and IL anion, traducing this into more exothermic mixtures. Second, Aspen Plus process simulator was used to test the H_2S solvent performance of selected ILs in absorption column. Despite the fact that no thermodynamic restrictions to H_2S separation were found (equilibrium-based recoveries of more than 99%), the strong kinetic control of the operation was determinant for the selection of both the operation conditions and the IL used. In this sense, the IL that shows the best thermodynamic behavior presents severe limited transport properties, implying very low H_2S recovery at near room temperatures. The IL that presents the best performance as H_2S absorbent is [emim][DCN], mainly due to its low viscosity, and thus improved transport properties. The operation temperature is the key parameter of the column design; being 50 ºC the one selected in which the recovery curve reaches the maximum absorption capacity. Lastly, the column design was accomplished with different design proposals, confirming the technical viability of the operation. Therefore, integrated molecular (COSMO-RS) and process (Aspen Plus) simulations analysis have been proved as a useful tool to achieve a prospective analysis of the potential application of ILs in the H_2S capture, providing a key comprehension on the IL selection and its application in a commercial absorption column before required experimental tests.

Acknowledgments

The authors thank Comunidad Autónoma de Madrid (Project P2018/EMT4348) and Ministerio de Economía y Competitividad (MINECO) of Spain (Project CTQ2017-

89441-R) for financial support. We are very grateful to Centro de Computación Científica de la Universidad Autónoma de Madrid for computational facilities.

References

1. British Petroleum, *Statistical review of world energy*. 2018.
2. Faramawy, S., T. Zaki, and A.A.E. Sakr, *Natural gas origin, composition, and processing: A review.* Journal of Natural Gas Science and Engineering, 2016. **34**: p. 34-54.
3. Astaria, G., D.W. Savage, and A. Bisio, *Gas treating with chemical solvents*. 1983: J. Wiley and Sons,New York, NY; None. Medium: X; Size: Pages: 493.
4. Ozekmekci, M., G. Salkic, and M.F. Fellah, *Use of zeolites for the removal of H_2S: A mini-review.* Fuel Processing Technology, 2015. **139**: p. 49-60.
5. Peters, L., et al., *CO_2 removal from natural gas by employing amine absorption and membrane technology—A technical and economical analysis.* Chemical Engineering Journal, 2011. **172**(2): p. 952-960.
6. Sigot, L., G. Ducom, and P. Germain, *Adsorption of hydrogen sulfide (H_2S) on zeolite (Z): Retention mechanism.* Chemical Engineering Journal, 2016. **287**: p. 47-53.
7. Zhou, L., et al., *Feasibility study on pressure swing sorption for removing H_2S from natural gas*. Vol. 59. 2004. 2401-2406.
8. Kidnay, A.J. and W.R. Parrish, *Fundamentals of Natural Gas Processing*. 2006: CRC Press.
9. Mandal, B.P., A.K. Biswas, and S.S. Bandyopadhyay, *Selective absorption of H_2S from gas streams containing H_2S and CO_2 into aqueous solutions of N-methyldiethanolamine and 2-amino-2-methyl-1-propanol.* Separation and Purification Technology, 2004. **35**(3): p. 191-202.
10. Lu, J.-G., Y.-F. Zheng, and D.-L. He, *Selective absorption of H_2S from gas mixtures into aqueous solutions of blended amines of methyldiethanolamine and 2-tertiarybutylamino-2-ethoxyethanol in a packed column.* Separation and Purification Technology, 2006. **52**(2): p. 209-217.
11. Bara, J.E., *Potential for Hydrogen Sulfide Removal Using Ionic Liquid Solvents*, in *Green Solvents II: Properties and Applications of Ionic Liquids*, A. Mohammad and D. Inamuddin, Editors. 2012, Springer Netherlands: Dordrecht. p. 155-167.
12. Burr, B. and L. Lyddon, *A Comparison of Physical Solvents for Acid Gas Removal*. Vol. 1. 2008.
13. Wilkes, J.S., P. Wasserscheid, and T. Welton, *Ionic Liquids in Synthesis*. 2008: Wiley-VCH Verlag GmbH & Co. KGaA. 1-6.
14. Welton, T., *Ionic liquids: a brief history.* Biophysical Reviews, 2018. **10**(3): p. 691-706.
15. Shang, D., et al., *Ionic liquids in gas separation processing.* Current Opinion in Green and Sustainable Chemistry, 2017. **5**: p. 74-81.
16. Jou, F.-Y. and A.E. Mather, *Solubility of Hydrogen Sulfide in [bmim][PF_6]*. International Journal of Thermophysics, 2007. **28**(2): p. 490.
17. Jalili, A.H., et al., *Solubility of H_2S in Ionic Liquids [bmim][PF_6], [bmim][BF_4], and [bmim][Tf_2N]*. Journal of Chemical & Engineering Data, 2009. **54**(6): p. 1844-1849.

18. Jalili, A.H., et al., *Solubility and diffusion of CO_2 and H_2S in the ionic liquid 1-ethyl-3-methylimidazolium ethylsulfate.* The Journal of Chemical Thermodynamics, 2010. **42**(10): p. 1298-1303.
19. Shiflett, M.B., A.M.S. Niehaus, and A. Yokozeki, *Separation of CO_2 and H_2S Using Room-Temperature Ionic Liquid [bmim][$MeSO_4$]*. Journal of Chemical & Engineering Data, 2010. **55**(11): p. 4785-4793.
20. Zhao, Y., et al., *Hydrogen Sulfide Solubility in Ionic Liquids (ILs): An Extensive Database and a New ELM Model Mainly Established by Imidazolium-Based ILs.* Journal of Chemical & Engineering Data, 2016. **61**(12): p. 3970-3978.
21. Pomelli, C.S., et al., *Influence of the Interaction between Hydrogen Sulfide and Ionic Liquids on Solubility: Experimental and Theoretical Investigation.* The Journal of Physical Chemistry B, 2007. **111**(45): p. 13014-13019.
22. Aparicio, S. and M. Atilhan, *Computational Study of Hexamethylguanidinium Lactate Ionic Liquid: A Candidate for Natural Gas Sweetening.* Energy & Fuels, 2010. **24**(9): p. 4989-5001.
23. Sakhaeinia, H., et al., *Solubility of H_2S in 1-(2-hydroxyethyl)-3-methylimidazolium ionic liquids with different anions.* Fluid Phase Equilibria, 2010. **298**(2): p. 303-309.
24. Zhao, Y., et al., *Predicting H_2S solubility in ionic liquids by the quantitative structure-property relationship method using S sigma-profile molecular descriptors.* Rsc Advances, 2016. **6**(74): p. 70405-70413.
25. Kamgar, A. and F. Esmaeilzadeh, *Prediction of H_2S solubility in hmim Pf(6) , hmim Bf(4) and hmim Tf_2N using UNIQUAC, NRTL and COSMO-RS.* Journal of Molecular Liquids, 2016. **220**: p. 631-634.
26. Mortazavi-Manesh, S., M.A. Satyro, and R.A. Marriott, *Screening ionic liquids as candidates for separation of acid gases: Solubility of hydrogen sulfide, methane, and ethane.* Aiche Journal, 2013. **59**(8): p. 2993-3005.
27. Santiago, R., et al., *Acetylene absorption by ionic liquids: A multiscale analysis based on molecular and process simulation.* Separation and Purification Technology, 2018. **204**: p. 38-48.
28. Ferro, V.R., et al., *Enterprise Ionic Liquids Database (ILUAM) for Use in Aspen ONE Programs Suite with COSMO-Based Property Methods.* Industrial & Engineering Chemistry Research, 2018. **57**(3): p. 980-989.
29. Ferro, V.R., et al., *Introducing process simulation in ionic liquids design/selection for separation processes based on operational and economic criteria through the example of their regeneration.* Separation and Purification Technology, 2012. **97**: p. 195-204.
30. De Riva, J., et al., *Aspen Plus supported analysis of the post-combustion CO2 capture by chemical absorption using the [P_{2228}][CNPyr] and [P_{66614}][CNPyr] AHA Ionic Liquids.* International Journal of Greenhouse Gas Control, 2018. **78**: p. 94-102.
31. de Riva, J., et al., *Ionic liquids for post-combustion CO_2 capture by physical absorption: Thermodynamic, kinetic and process analysis.* International Journal of Greenhouse Gas Control, 2017. **61**: p. 61-70.
32. Palomar, J., et al., *Understanding the Physical Absorption of CO_2 in Ionic Liquids Using the COSMO-RS Method.* Industrial & Engineering Chemistry Research, 2011. **50**(6): p. 3452-3463.
33. Palomar, J., et al., *Demonstrating the key role of kinetics over thermodynamics in the selection of ionic liquids for CO_2 physical absorption.* Separation and Purification Technology, 2019. **213**: p. 578-586.

34. Palomar, J., et al., *Task-specific ionic liquids for efficient ammonia absorption.* Separation and Purification Technology, 2011. **82**: p. 43-52.
35. Bedia, J., et al., *Optimized ionic liquids for toluene absorption.* Aiche Journal, 2013. **59**(5): p. 1648-1656.
36. Gonzalez-Miquel, M., J. Palomar, and F. Rodriguez, *Selection of Ionic Liquids for Enhancing the Gas Solubility of Volatile Organic Compounds.* The Journal of Physical Chemistry B, 2013. **117**(1): p. 296-306.
37. Fallanza, M., et al., *Screening of RTILs for propane/propylene separation using COSMO-RS methodology.* Chemical Engineering Journal, 2013. **220**: p. 284-293.
38. Liu, X., et al., *High Solubilities for Methane, Ethane, Ethylene, and Propane in Trimethyloctylphosphonium Bis(2,4,4-trimethylpentyl) Phosphinate ([P_{8111}][TMPP]).* Industrial & Engineering Chemistry Research, 2014. **53**(1): p. 363-368.
39. de Riva, J., et al., *Aspen Plus supported conceptual design of the aromatic–aliphatic separation from low aromatic content naphtha using 4-methyl-N-butylpyridinium tetrafluoroborate ionic liquid.* Fuel Processing Technology, 2016. **146**: p. 29-38.
40. Moreno, D., et al., *Absorption refrigeration cycles based on ionic liquids: Refrigerant/absorbent selection by thermodynamic and process analysis.* Applied Energy, 2018. **213**: p. 179-194.
41. Stull, D.R., *Vapor Pressure of Pure Substances. Organic and Inorganic Compounds.* Industrial & Engineering Chemistry, 1947. **39**(4): p. 517-540.
42. Lin, S.-T. and S.I. Sandler, *A Priori Phase Equilibrium Prediction from a Segment Contribution Solvation Model.* Industrial & Engineering Chemistry Research, 2002. **41**(5): p. 899-913.
43. Klamt, A., *Conductor-like Screening Model for Real Solvents: A New Approach to the Quantitative Calculation of Solvation Phenomena.* The Journal of Physical Chemistry, 1995. **99**(7): p. 2224-2235.
44. S.-T. Lin, P.M.M., Y. Song, C.-C. Chen, and S. I. Sandler, *Improvements of Phase-Equilibrium Predictions for Hydrogen-Bonding Systems from a New Expression for COSMO Solvation Models*, in *AIChE Annual Meeting*. 2002: Indianapolis.
45. Ulrich, G.D., *Chemical Engineering Process Design and Economics: A Practical Guide*. 2004: Process Publishing.
46. Klamt, A., F. Eckert, and W. Arlt, *COSMO-RS: An Alternative to Simulation for Calculating Thermodynamic Properties of Liquid Mixtures.* Annual Review of Chemical and Biomolecular Engineering, 2010. **1**(1): p. 101-122.
47. Ruiz, E., et al., *Evaluation of ionic liquids as absorbents for ammonia absorption refrigeration cycles using COSMO-based process simulations.* Applied Energy, 2014. **123**: p. 281-291.
48. Jalili, A.H., et al., *Solubility of CO_2, H_2S, and Their Mixture in the Ionic Liquid 1-Octyl-3-methylimidazolium Bis(trifluoromethyl)sulfonylimide.* The Journal of Physical Chemistry B, 2012. **116**(9): p. 2758-2774.
49. Sakhaeinia, H., et al., *Solubility of H_2S in Ionic Liquids 1-Ethyl-3-methylimidazolium Hexafluorophosphate ([emim][PF_6]) and 1-Ethyl-3-methylimidazolium Bis(trifluoromethyl)sulfonylimide ([emim][Tf_2N]).* Journal of Chemical & Engineering Data, 2010. **55**(12): p. 5839-5845.
50. Ruiz, E., et al., *Interactions of Ionic Liquids and Acetone: Thermodynamic Properties, Quantum-Chemical Calculations, and NMR Analysis.* The Journal of Physical Chemistry B, 2013. **117**(24): p. 7388-7398.

51. Safavi, M., et al., *Study of the solubility of CO_2, H_2S and their mixture in the ionic liquid 1-octyl-3-methylimidazolium hexafluorophosphate: Experimental and modelling.* The Journal of Chemical Thermodynamics, 2013. **65**: p. 220-232.
52. Azizi, M., et al., *Simulation of hydrogen sulphide absorption in alkaline solution using a packed column.* Vol. 35. 2014. 3105-3115.
53. Sinnott, R.K., *Chapter 11 - Separation Columns (Distillation and Absorption)*, in *Coulson and Richardson's Chemical Engineering (Second Edition)*, R.K. Sinnott, Editor. 1993, Pergamon: Amsterdam. p. 439-564.
54. de Riva, J., et al., *Statistical Refinement and Fitting of Experimental Viscosity-to-Temperature Data in Ionic Liquids.* Industrial & Engineering Chemistry Research, 2014. **53**(25): p. 10475-10484.
55. Neves, C.M.S.S., et al., *Systematic Study of the Thermophysical Properties of Imidazolium-Based Ionic Liquids with Cyano-Functionalized Anions.* The Journal of Physical Chemistry B, 2013. **117**(35): p. 10271-10283.
56. Hiraga, Y., et al., *Densities at Pressures up to 200 MPa and Atmospheric Pressure Viscosities of Ionic Liquids 1-Ethyl-3-methylimidazolium Methylphosphate, 1-Ethyl-3-methylimidazolium Diethylphosphate, 1-Butyl-3-methylimidazolium Acetate, and 1-Butyl-3-methylimidazolium Bis(trifluoromethylsulfonyl)imide.* Journal of Chemical & Engineering Data, 2015. **60**(3): p. 876-885.

Assessment of Ionic Liquids as H_2S Physical Absorbents by Thermodynamic and Kinetic Analysis based on Process Simulation

Rubén Santiago, Jesús Lemus*, Ana Xiao Outomuro, Jorge Bedia and José Palomar

Chemical Engineering Department. Universidad Autónoma de Madrid. 28049 Madrid. Spain.

*Corresponding author. E-mail: jesus.lemus@uam.es

Supporting Information

Table S1. Experimental and COSMO-RS Henry's law constants of solutes in ILs at near-ambient temperature and atmospheric pressure using experimental vapor pressures of pure compounds..... 2
Table S2: List of cations and anions..... 4

Figure S1: Experimental and calculated solubility values with the three COSMO-SAC models of (A) [omim][PF_6], (B) [emim][NTf_2], (C) [hxmim][NTf_2] and (D) [omim][NTf_2]. 5

Table S1. Experimental and COSMO-RS Henry's law constants of solutes in ILs at near-ambient temperature and atmospheric pressure using experimental vapor pressures of pure compounds

Solute	IL	log (K_H exp) (bar)	log (K_H COSMO-RS) (bar)	Reference
Acetone	[emim][BF_4]	-0.34	-0.39	[1]
Acetone	[bmim][BF_4]	-0.46	-0.32	[1]
Acetone	[hxmim][BF_4]	-0.52	-0.47	[1]
Acetone	[bmim][PF_6]	-0.60	-0.67	[1]
Acetone	[hxmim][PF_6]	-0.66	-0.81	[1]
Acetone	[emim][NTf_2]	-0.80	-1.21	[1]
Acetone	[bmim][NTf_2]	-0.83	-1.26	[1]
Acetone	[hxmim][NTf_2]	-0.85	-1.29	[1]
Benzene	[bmim][BF_4]	0.00	-0.43	[1]
Benzene	[emim][BF_4]	-0.48	-0.28	[1]
Benzene	[bmim][BF_4]	-0.57	-0.43	[1]
Benzene	[hxmim][BF_4]	-0.61	-0.56	[1]
Benzene	[bmim][PF_6]	-0.60	-0.50	[1]
Benzene	[hxmim][PF_6]	-0.70	-0.69	[1]
Benzene	[emim][NTf_2]	-0.76	-0.73	[1]
Benzene	[bmim][NTf_2]	-0.85	-0.86	[1]
Benzene	[hxmim][NTf_2]	-0.93	-0.95	[1]
C_2H_4	[bmim][NTf_2]	1.92	1.70	[2]
C_2H_4	[emim][NTf_2]	2.17	1.81	[2]
C_2H_4	[hxmim][NTf_2]	2.18	1.63	[2]
C_2H_4	[bmim][PF_6]	2.20	2.01	[2]
C_2H_4	[bmim][BF_4]	2.40	2.07	[2]
C_2H_6	[hxmim][NTf_2]	1.86	1.80	[3]
C_2H_6	[bmim][NTf_2]	2.08	1.93	[4]
C_2H_6	[bmim][PF_6]	2.53	2.40	[4]
C_2H_6	[bmim][BF_4]	2.61	2.40	[5]
C_3H_8	[emim][NTf_2]	1.84	1.76	[2]
C_3H_8	[bmim][PF_6]	2.27	2.08	[2]
C_4H_{10}	[bmim][NTf_2]	1.36	1.13	[2]
C_4H_{10}	[bmim][BF_4]	2.04	1.79	[2]
C_2H_2	[bmim][BF_4]	1.22	1.29	[6]
C_2H_2	[bmim][MeCOO]	0.81	0.63	[6]

Solute	IL	log (K_H exp) (bar)	log (K_H COSMO-RS) (bar)	Reference
C_2H_2	[bmim][TFA]	1.15	1.17	[6]
C_2H_2	[bmim][NTf_2]	1.34	1.54	[6]
C_2H_2	[bmpyr][NTf_2]	1.33	1.54	[6]
C_2H_2	[bmim][$MeSO_4$]	1.04	1.06	[6]
C_2H_2	[bmpyr][MeCOO]	0.77	0.36	[6]
CO_2	[dcmim][NTf_2]	1.56	1.43	[3]
CO_2	[omim][NTf_2]	1.59	1.45	[7]
CO_2	[hxmim][NTf_2]	1.60	1.48	[4]
CO_2	[bmim][NTf_2]	1.61	1.52	[4]
CO_2	[emim][NTf_2]	1.65	1.59	[4]
CO_2	[bmim][PF_6]	1.84	1.67	[4]
CO_2	[bmim][BF_4]	1.88	1.74	[4]
H_2	[hxmim][NTf_2]	3.12	3.29	[8]
H_2	[bmim][PF_6]	3.27	3.57	[5]
H_2	[bmim][BF_4]	3.38	3.58	[5]
H_2	[bmim][NTf_2]	3.65	3.36	[5]
N_2	[bmim][NTf_2]	2.98	2.74	[9]
N_2	[emim][NTf_2]	3.06	2.79	[9]
N_2	[bmim][PF_6]	3.17	3.27	[9]
N_2	[bmim][BF_4]	3.30	3.35	[9]
NH_3	[emim][BF_4]	0.85	0.09	[10]
NH_3	[hxmim][BF_4]	0.70	-0.05	[10]
NH_3	[bmim][BF_4]	0.74	-0.01	[10]
H_2S	[hxmim][BF_4]	1.10	1.08	[11]
H_2S	[hxmim][NTf_2]	1.24	1.11	[12]
H_2S	[hxmim][PF_6]	1.25	1.13	[11]
H_2S	[omim][PF_6]	1.09	1.13	[11]
H_2S	[omim][NTf_2]	1.00	1.12	[12]
H_2S	[bmim][BF_4]	1.19	1.08	[11]
H2S	[emim][NTf2]	1.17	1.10	[13]
H_2S	[bmim][NTf_2]	1.14	1.10	[13]
H_2S	[bmim][PF_6]	1.27	1.14	[11]
H_2S	[emim][BF_4]	0.55	0.70	[14]
H_2S	[bmim][TfO]	0.49	0.71	[15]

Table S2: List of cations and anions

CATION	
Abb.	**Complete Name**
emim	1-ethyl-3-methylimidazolium
bmim	1-buthyl-3-methylimidazolium
hxmim	1-hexyl-3-methylimidazolium
hpmim	1-heptyl-3-methylimidazolium
omim	1-octyl-3-methylimidazolium
nmim	1-nonyl-3-methylimidazolium
bpy	1-butylpyridinium
mpy	1-methylpyridinium
hxpy	1-hexylpyridinium
npy	1-nonylpyridinium
empyr	1-ethyl-3-methylpyrrolidinium
bpyr	1-butylpyrrolidinium
hxpyr	1-hexylpyrrolidinium
ompyr	1-octyl-3-methylpyrrolidinium
bmpip	1-butyl-3-methylpiperidinium
hxmpip	1-hexyl-3-methylpiperidinium
ompip	1-octyl-3-methylpiperidinium
N1114	trimethylbuthylammonium
N2222	tetraethylammonium
N6666	tetrahexylammonium
N111,10	trimethyldecylammonium
Choline	(2-hydroxiethyl)-trimethyl ammonium
P2222	tetraethylphosphonium
P5555	tetrapentylphosphonium
P222,10	triethyldecylphosphonium

ANION	
Abb.	**Complete Name**
Cl	chloride
$MePO_3$	methylphosphonate
$EtPO_3$	ethylphosphonate
$(Me)_2PO_4$	dimethylphosphate
$(Et)_2PO_4$	diethylphosphate
$BuPO_3$	butylphosphonate
$MeSO_3$	methanesulfonate
TFA	trifluoroacetate
NO_3	nitrate
$EtSO_4$	ethylsulfate
$MeSO_4$	methylsulfate
$OcSO_4$	octylsulfate
BF_4	tetrafluoroborate
TfO	trifluoromethanesulfanate
DCN	dicyanamide
SCN	tiocyanate
NTf_2	bis(trifluoromethylsulfonil)imide
BETI	bis(perfluoroethanesulfonil)imide
TCM	tricyanomethanide
ClO_4	perclorate
PF_6	hexafluorophosphate
FEP	tri(pentafluoroethyl)trifluorophosphate
$B(CN)_4$	tetracyanoborate

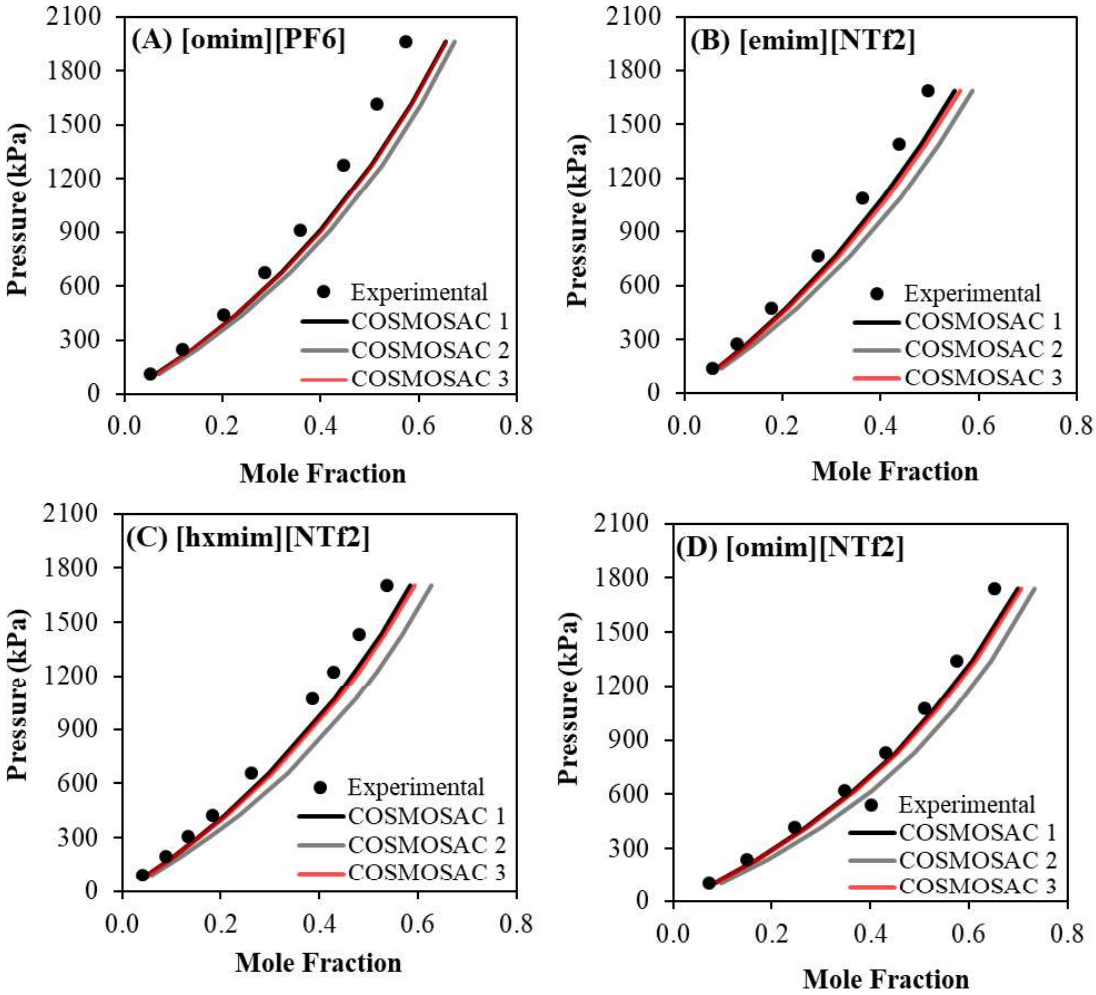

Figure S1: Experimental and calculated solubility values with the three COSMO-SAC models of (A) [omim][PF_6], (B) [emim][NTf_2], (C) [hxmim][NTf_2] and (D) [omim][NTf_2].

References:

1. Li, C.-H., K.-X. Gao, Y.-N. Meng, X.-K. Wu, F. Zhang, and Z.-X. Wang, *Solution Thermodynamics of Imidazolium-Based Ionic Liquids and Volatile Organic Compounds: Benzene and Acetone.* Journal of Chemical & Engineering Data, **2015**. 60(6): p. 1600-1607.

2. Camper, D., C. Becker, C. Koval, and R. Noble, *Low Pressure Hydrocarbon Solubility in Room Temperature Ionic Liquids Containing Imidazolium Rings Interpreted Using Regular Solution Theory.* Industrial & Engineering Chemistry Research, **2005**. 44(6): p. 1928-1933.

3. Kilaru, P.K. and P. Scovazzo, *Correlations of Low-Pressure Carbon Dioxide and Hydrocarbon Solubilities in Imidazolium-, Phosphonium-, and Ammonium-Based Room-Temperature Ionic Liquids. Part 2. Using Activation Energy of Viscosity.* Industrial & Engineering Chemistry Research, **2008**. 47(3): p. 910-919.

4. Anderson, J.L., J.K. Dixon, and J.F. Brennecke, *Solubility of CO2, CH4, C2H6, C2H4, O2, and N2 in 1-Hexyl-3-methylpyridinium Bis(trifluoromethylsulfonyl)imide: Comparison to Other Ionic Liquids.* Accounts of Chemical Research, **2007**. 40(11): p. 1208-1216.

5. Jacquemin, J., M.F. Costa Gomes, P. Husson, and V. Majer, *Solubility of carbon dioxide, ethane, methane, oxygen, nitrogen, hydrogen, argon, and carbon monoxide in 1-butyl-3-methylimidazolium tetrafluoroborate between temperatures 283K and 343K and at pressures close to atmospheric.* The Journal of Chemical Thermodynamics, **2006**. 38(4): p. 490-502.

6. Palgunadi, J., H.S. Kim, J.M. Lee, and S. Jung, *Ionic liquids for acetylene and ethylene separation: Material selection and solubility investigation.* Chemical Engineering and Processing: Process Intensification, **2010**. 49(2): p. 192-198.

7. Almantariotis, D., T. Gefflaut, A.A.H. Pádua, J.Y. Coxam, and M.F. Costa Gomes, *Effect of Fluorination and Size of the Alkyl Side-Chain on the Solubility of Carbon Dioxide in 1-Alkyl-3-methylimidazolium Bis(trifluoromethylsulfonyl)amide Ionic Liquids.* The Journal of Physical Chemistry B, **2010**. 114(10): p. 3608-3617.

8. Costa Gomes, M.F., *Low-Pressure Solubility and Thermodynamics of Solvation of Carbon Dioxide, Ethane, and Hydrogen in 1-Hexyl-3-methylimidazolium Bis(trifluoromethylsulfonyl)amide between Temperatures of 283 K and 343 K.* Journal of Chemical & Engineering Data, **2007**. 52(2): p. 472-475.

9. Camper, D., J. Bara, C. Koval, and R. Noble, *Bulk-Fluid Solubility and Membrane Feasibility of Rmim-Based Room-Temperature Ionic Liquids.* Industrial & Engineering Chemistry Research, **2006**. 45(18): p. 6279-6283.

10. Palomar, J., M. Gonzalez-Miquel, J. Bedia, F. Rodriguez, and J.J. Rodriguez, *Task-specific ionic liquids for efficient ammonia absorption.* Separation and Purification Technology, **2011**. 82: p. 43-52.

11. Safavi, M., C. Ghotbi, V. Taghikhani, A.H. Jalili, and A. Mehdizadeh, *Study of the solubility of CO2, H2S and their mixture in the ionic liquid 1-octyl-3-methylimidazolium hexafluorophosphate: Experimental and modelling.* The Journal of Chemical Thermodynamics, **2013**. 65: p. 220-232.

12. Jalili, A.H., M. Safavi, C. Ghotbi, A. Mehdizadeh, M. Hosseini-Jenab, and V. Taghikhani, *Solubility of CO2, H2S, and Their Mixture in the Ionic Liquid 1-Octyl-3-methylimidazolium Bis(trifluoromethyl)sulfonylimide.* The Journal of Physical Chemistry B, 2012. 116(9): p. 2758-2774.

13. Sakhaeinia, H., A.H. Jalili, V. Taghikhani, and A.A. Safekordi, Solubility of H2S in Ionic Liquids 1-Ethyl-3-methylimidazolium Hexafluorophosphate ([emim][PF6]) and 1-Ethyl-3-methylimidazolium Bis(trifluoromethyl)sulfonylimide ([emim][Tf2N]). Journal of Chemical & Engineering Data, 2010. 55(12): p. 5839-5845.

14. Jalili, A.H., M. Shokouhi, G. Maurer, A.T. Zoghi, J.S. Ahari, and K. Forsat, Measuring and modelling the absorption and volumetric properties of CO2 and H2S in the ionic liquid 1-ethyl-3-methylimidazolium tetrafluoroborate. Journal of Chemical Thermodynamics, 2019. 131: p. 544-556.

15. Jalili, A.H., M. Mehrabi, A.T. Zoghi, M. Shokouhi, and S.A. Taheri, Solubility of carbon dioxide and hydrogen sulfide in the ionic liquid 1-butyl-3-methylimidazolium trifluoromethanesulfonate. Fluid Phase Equilibria, 2017. 453: p. 1-12.

5.3 From kinetics to equilibrium control in CO_2 capture columns using Encapsulated Ionic Liquids (ENILs)

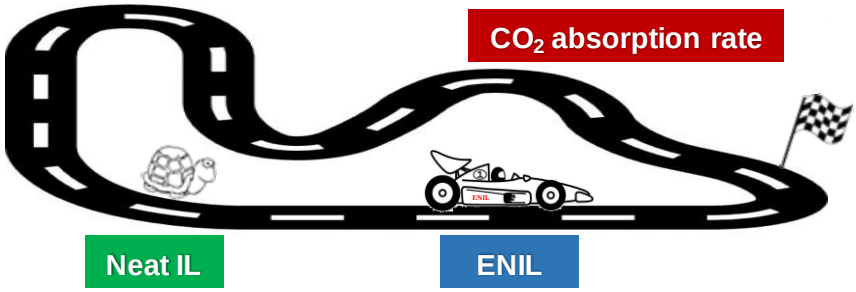

Chemical Engineering Journal 348 (2018) 661–668

Contents lists available at ScienceDirect

Chemical Engineering Journal

journal homepage: www.elsevier.com/locate/cej

From kinetics to equilibrium control in CO_2 capture columns using Encapsulated Ionic Liquids (ENILs)

R. Santiago, J. Lemus, D. Moreno, C. Moya, M. Larriba, N. Alonso-Morales, M.A. Gilarranz, J.J. Rodríguez, J. Palomar*

Sección de Ingeniería Química, Universidad Autónoma de Madrid, 28049 Madrid, Spain

HIGHLIGHTS

- ILs with high viscosity values gets worse absorbent performance and CO_2 recovery.
- ENIL materials overcome the mass transfer constrains in CO_2 absorption by ILs.
- ENIL morphology increases the contact area of the neat IL.
- ENIL tests in fixed bed demonstrate the equilibrium control in CO_2 capture.

ARTICLE INFO

Keywords:
CO_2 capture
Ionic liquids
ENIL
Physical absorption
ILUAM
Aspen

ABSTRACT

A novel approach based on Encapsulated Ionic Liquids (ENILs) is proposed for overcoming the mass transfer constraints in CO_2 physical absorption by ILs. Absorption process simulation using COSMO-based/Aspen Plus methodology -an a priori approach- was carried to select four ILs with high and similar CO_2 absorption capacity but markedly different transport properties: EmimTCM, BmimTCM, BmimDCN, and BmimOcSO$_4$. Simulations using equilibrium- and rate-based column models for these ILs showed that CO_2 recovery and the absorbent performance are severely reduced when the viscosity of the IL increases. Experimental gravimetric analyses with the selected ILs confirmed the large differences in solubility and absorption rate, this last also dependent on viscosity. ENILs were prepared by encapsulation of ILs in hollow carbon sub-microcapsules with a porous shell. The experimental gravimetric analysis evidenced that the ILs maintain their CO_2 absorption capacity after encapsulation, whereas the absorption rate is ca. 50 times higher for ENILs than neat ILs. ENIL tests in fixed bed operation at different operating conditions yielded bed utilization values dependent on the CO_2 solubility in the ENIL, while equivalent mass transfer zone lengths were obtained for all the materials. The results demonstrate the fast CO_2 mass transfer rates in ENILs -related to the high contact area provided- allows overcoming the mass transfer limitations controlling the CO_2 rate of physical absorption by ILs.

1. Introduction

The greenhouse effect and global warming caused by CO_2 have become serious environmental concerns and have awakened the population attention [1]. One of the most promising methodologies for limiting the global warming effects caused by greenhouse gases consists on the direct physical or chemical absorption of CO_2 from post-combustion streams due to their efficiency and lower cost [2,3]. Regarding physical absorption, solvents such as Purisol [4], Rectisol [5] and Selexol [6], among others, are used to capture CO_2 working at high pressure. However, they present problems such as corrosive nature, toxicity and high volatility resulting in high solvent losses [3]. On the other hand, amines [7] are widely used in chemical absorption processes [8], but they present degradation and corrosivity, resulting in high solvent losses, environmental impact and substantial maintenance costs [9].

Therefore, there is a demand for innovative and cost-effective technologies capable of efficiently capturing CO_2, overcoming these problems of commercially available systems. In this sense, ILs are presented as promising novel solvents, which have attracted growing interests as shown by the number of studies on CO_2 capture [10]. The advantages of using ILs as absorbents are their high and tailorable absorption capacity, low vapor pressure and high thermal stability. However, they present some disadvantages such as: high price,

* Corresponding author.
E-mail address: pepe.palomar@uam.es (J. Palomar).

https://doi.org/10.1016/j.cej.2018.05.029
Received 7 March 2018; Received in revised form 4 May 2018; Accepted 5 May 2018
Available online 07 May 2018
1385-8947/

environmental-concerns and limitations in their transport properties. The high viscosity of ILs is probably the main technical limitation for their practical application [11], which can even increase in some cases due to the dissolution of CO_2 [12]. In fact, recent process simulation analyses have demonstrated that the efficiency of CO_2 capture by physical absorption in packed columns is severely reduced by the strong kinetic control of the operation, obtaining CO_2 recoveries significantly lower than those expected from the high absorption capacities of ILs [13]. Therefore, modifications of neat ILs may be necessary before they can be widely accepted for CO_2 separation [14].

The Encapsulated Ionic Liquid (ENIL) concept has been proposed as a promising alternative to overcome the mass transfer rate limitations of separation process based on ILs [15]. ENILs consist of hollow carbonaceous sub-microcapsules (C_{cap}) filled with ILs [16]. The synthesis of ENILs is favored by the high affinity between ILs and porous carbons [17]. The ENILs can be prepared with a high proportion of IL (75–85% in weight) and small capsule size (500–700 nm). Therefore, the ENIL material involves a change from continuous to discrete IL phase with submicrometric drop size. Due to ENIL morphology, the specific contact area is drastically increased with respect to the neat IL, enhancing the rate of mass transfer phenomena but maintaining the properties of the ILs as solvents [15]. This novel approach, based on ENIL materials has been successfully applied to NH_3 separation [18] and CO_2 capture based on chemical absorbents as acetate-based ILs [19]. Recently, ENIL systems were also efficiently applied in CO_2 capture by physical absorption with ILs [20]. From an economical point of view, ENIL materials would not only improved the mass transport properties, but also enhance the regeneration step and take advantage from the amount of IL used, becoming a more effective material than neat ILs.

On the other hand, the evaluation of IL performance in practical applications at industrial scale is a key issue in the development of new separation processes based on ILs [21]. In the last years, our group has developed the COSMO-based/Aspen Plus multiscale methodology – based on integrating molecular and process simulation tools- of great utility in the preliminary: i) selection of ILs attending to thermodynamic, kinetic, technical or economical criteria; and ii) viability analysis of the proposed IL-based process and comparison to available technologies [22]. COSMO-based/Aspen methodology has been tested in the study of IL regeneration by distillation [23] and in toluene [24] and acetylene [25] absorption. In addition, it was applied to aromatic-aliphatic separation by liquid-liquid extraction [26] or by extractive distillation [27], CO_2 capture by physical absorption [13] and absorption refrigeration cycles based on ILs [28]. Since COSMO-based/Aspen methodology is an *a priori* approach, which does not require experimentation, process simulations can also be an alternative or a previous step to the experimentation, with the aim of reducing and focusing the number of ILs studied and, thereby, minimizing the consumption of resources in experimental work.

The objective of this work is to evaluate the potential application of ENIL materials in the capture of CO_2 by physical absorption with ILs. For this purpose, unfavorable conditions from the kinetic point of view were selected, i.e. postcombustion processes (10–13% CO_2 concentrations). Firstly, process simulations using COSMO-based/Aspen Plus methodology are carried out to evaluate the behavior of a large set of ILs in the physical absorption of CO_2 in commercial packed columns. From this theoretical analysis, a selection of 4 ILs with similar absorption capacities (provided by equilibrium-based column model) and markedly different kinetic behavior (provided by the Rated-Based column model) is made. The reason to select ILs providing different absorption rates is to analyze if the encapsulation in ENILs maintain the CO_2 absorption capacity of ILs and also improves the kinetics of the CO_2 uptake. The ILs selected were characterized using a high-pressure microbalance to obtain CO_2 absorption capacities and CO_2 diffusion values at three temperatures and pressures (301–333 K and 1–6 bar). The next step is the synthesis and characterization of ENIL materials using the previously selected ILs. The ENIL were tested in gravimetric essays to analyze their CO_2 sorption capacity and rate. Finally, fixed-bed sorption experiments were carried out at temperatures from 303 to 333 K and 0.1 bar CO_2, in order to evaluate if the application of the proposed approach based on ENIL systems allows overcoming the mass transfer rate limitations of the CO_2 physical absorption by the free ILs.

2. Experimental section

2.1. Materials

The ILs 1-butyl-3-methylimidazolium dicyanamide (95%) BmimDCN, 1-butyl-3-methylimidazolium tricyanomethanide (95%) BmimTCM and 1-ethyl-3-methylimidazolium tricyanomethanide (95%) EmimTCM were purchased from Iolitec and 1-butyl-3-methylimidazolium octylsulfate (95%) $BmimOcSO_4$ from Sigma-Aldrich. The synthesis of the hollow sub-microcapsules was carried out using phenol (99%), paraformaldehyde (95–100%), aluminum trichloride (95–100%), ammonia (34%) and absolute ethanol supplied by Panreac. Tetraethylorthosilicate (98%) (TEOS), hexadecyltrimethoxysilane (90%) (C16TMS) and hydrofluoric acid (48%) were supplied by Sigma-Aldrich. Carbon dioxide, nitrogen, and helium were supplied by Praxair, Inc., with a minimum purity of 99.999%. Furthermore, a mixture containing 10,000 ppmv of carbon dioxide in nitrogen was supplied by Praxair, Inc and used in fixed bed capture experiments.

Before the absorption experiments, all the ILs and ENIL materials used were dried and degassed at 333 K under vacuum (10^{-3} mbar) during 24 h to ensure a water content lower than 200 ppm.

2.2. ENIL preparation and characterization

The hollow sub-microcapsules (C_{Cap}) synthesized for their use as ENIL support were prepared following the methodology reported by our group in previous works [16,18,19] and based on the procedure described by Büchel et al. [29]. In summary, C_{Cap} were prepared by a templating method using an aluminosilicate template formed by a solid core and a mesoporous shell. A phenolic resin was infiltrated into the template to serve as a carbon precursor. Then, the infiltrated template was subjected to pyrolysis at 700 °C during 5 h and the template was removed using HF.

The ENIL materials were prepared by incipient wetness impregnation of 100 mg of C_{Cap} with 1 mL of an IL-acetone solution. The solution was added dropwise onto the support. After impregnation acetone was removed by evaporation at 333 K during 24 h. In the current work, the four ENIL tested were prepared with an IL nominal load of 80%w/w. The amount of IL incorporated was checked by elemental analysis. This methodology was successfully applied in our previous publications allowing a homogeneous distribution of the IL inside the C_{Cap} [18,19].

The CHN content of the hollow sub-microcapsules and ENIL materials were characterized by elemental analysis in a LECO CHNS-932 apparatus. The IL amount loaded into the spheres could be calculated by this characterization essay. Then, the porous texture of the carbon material was characterized by 77 K N_2 adsorption/desorption in a TriStar II 3020 (Micromeritics) system after 12 h of degassing at 0.1 mbar and 393 K. The surface area was calculated by using the BET equation. The microstructure and morphology of C_{Cap} and ENILs were studied by scanning electron microscopy (SEM) and transmission electron microscopy (TEM). SEM analyses were performed with a Hitachi S-3000N apparatus and TEM images were obtained in Philips 420, JEM-2000 FX and JEM-4000 EX microscopes.

2.3. Gravimetric CO_2 absorption measurements

The measurements of CO_2 solubility (mg CO_2/g IL) in ILs and ENILs were performed in a gravimetric high-pressure sorption analyzer (ISOSORP GAS LP-flow, Rubotherm) equipped with a magnetic suspension balance (MSB). The balance covers a weight range up to 10 g,

with a precision of 10^{-5} g. In addition, it can operate in a wide range of temperatures (from room temperature to 150 °C) and pressures (from 10^{-3} mbar to 30 bar). A full description of the thermogravimetric experimental methodology is available in previous works [30].

The CO_2 absorption isotherms for the four selected ILs and their corresponding ENILs were obtained at three different temperatures (301.5, 316.5 and 331.5 K) and three different pressures (1, 3 and 6 bar). In a standard run a 100 mL/min flow of pure CO_2 at 1 bar is passed through the sorbent sample (100–150 mg for neat IL and ENIL materials) and the increase in the mass is recorded over the time at fixed temperature. Once the sample is saturated, i.e. weight change < 0.02 mg/h, the pressure is increased. The buoyancy effect is corrected and the amount of CO_2 absorbed is quantified in terms of ~~as~~ mg of CO_2 per g of IL and molar ratio (z_{CO2}):

$$z_{CO_2} = \frac{m_{CO_2}/M_{CO_2}}{m_{IL}/M_{IL}} \tag{1}$$

where m_{CO2} is the absorbed CO_2 mass, m_{IL} is the IL mass after degasification and M_{CO2} and M_{IL} are the molecular weights of CO_2 and IL, respectively.

The CO_2 diffusion coefficients in the different ILs were estimated from gravimetric analysis by using a mass diffusion model reported by Shifflet and Yokozeki [31] and later used by other authors [30] for CO_2-IL systems. The proposed model assumes linear diffusion of the CO_2 over a quiescent mass of IL placed in the bottom of a sample container [31]. In these conditions the CO_2 diffusion can be expressed as follows:

$$\frac{\partial C}{\partial t} = D\cdot\frac{\partial^2 C}{\partial t^2} \tag{2}$$

where C is the concentration of CO_2 in the IL at a given time (t) and D is the diffusion coefficient of CO_2 in the IL. Initial conditions consider that $C = C_0$ when $t = 0$ and $0 < z < L$, and boundary conditions are: i) $C = C_s$ when $t > 0$ and $z = 0$; ii) $\partial C/\partial z = 0$ at $z = L$, where z is a vertical location and L is the depth of IL in the container, which is calculated by using the volume of the sample and the inner diameter of the container (1.5 cm). The integration of Eq. (2) leads to:

$$\overline{C} = C_s\cdot\left[1-2\cdot\left(1-\frac{C_0}{C_s}\right)\cdot\sum_{n=0}^{\infty}\frac{\exp(-\lambda_n^2\cdot D\cdot t)}{L^2\cdot\lambda_n^2}\right] \tag{3}$$

where C_0 and C_s are respectively the CO_2 initial and saturation concentration at each temperature and pressure, C is the CO_2 concentration at each time, D is the diffusivity, t is the time, L is the height of the sample (calculated from the sample density and mass and almost 2.2 mm in all cases) and λ_n a parameter calculated from Eq. (4):

$$\lambda_n = \left(n+\frac{1}{2}\right)\cdot\frac{\pi}{L} \tag{4}$$

Finally, the time-dependent data obtained from the gravimetric measurements were fitted to Eq. (3) to obtain the diffusion coefficient. Although Eq. (3) shows a sum of infinite terms, only the first ten terms are enough for the calculation in practical applications.

2.4. Fixed-bed CO_2 sorption experiments

The fixed-bed experiments were carried out in a Microactivity unit (PID Eng&Tech, Spain) provided with a stainless-steel tube of 9.5 mm of internal diameter and 15 cm of length and a distributor of sintered stainless-steel. The tube is placed into a furnace which allows controlling the temperature from almost ambient to 573 K. The pressure inside the fixed bed can be controlled from atmospheric to 20 bar. The outlet gas flow was analyzed by an Agilent 7820A gas chromatograph equipped with a 20 m column (Agilent PoraPlot U) and a TCD detector, which allows calculating the CO_2 concentration. For each experiment, the fixed bed was loaded with 4 g of fresh ENIL, i.e. a bed height (H) of ~15 cm. The inlet gas is continuously fed through the fixed bed composed of an N_2-CO_2 mixture (10% v/v of CO_2) with a flow of 3.3 NmL/min. For each ENIL, breakthrough curves at three different temperatures (303, 318 and 333 K) at 1 bar of total pressure were obtained. Once the ENIL material was saturated, the furnace temperature was increased to 333 K for regenerating it. We did not appreciate any capacity difference before and after the regeneration step which allows us using the ENIL material in different sorption-desorption cycles. A blank experiment was performed with the fixed bed loaded with inert material with the same bed height as ENILs. In that way, the calculations were done by subtracting the blank measurement curve at each temperature to the breakthrough curve of each ENIL material at that temperature. The sorption capacity (q_e, *mg/g*) was calculated from the breakthrough curves using the following equation:

$$q_e = \frac{Q}{m}\cdot\int_0^{t_s}(C_o - C)dt \tag{5}$$

where Q is the gas flow rate (L/min)), m is the ENIL mass (g) in the fixed bed, C and C_0 are respectively the outlet and the inlet concentration (g/L), and t_s is the saturation time (min). The breakthrough curves were fitted to the equation described by Yoon and Nelson [32]:

$$t = t_{0.5} + \frac{1}{k}\cdot\ln\left(\frac{C}{C_0 - C}\right) \tag{6}$$

where t is the operation time (min), $t_{0.5}$ is the time at which the outlet concentration is half of the inlet one (min), and k is the Yoon and Nelson constant (min^{-1}), which is used in our study as kinetic key parameter for comparing the ENILs tested. This model has been successfully applied in sorption operations using fixed beds [32,33]. The length of the mass transfer zone (H_{MTZ}) was calculated from each breakthrough curve as an additional parameter to evaluate the kinetics of the process using the equation:

$$H_{MTZ} = H\cdot\frac{(t_{0.95} - t_{0.05})}{t_{0.95}} \tag{7}$$

where H is the height of the bed, and $t_{0.05}$ and $t_{0.95}$ are the time at which the outlet CO_2 concentration reaches 5% and 95% of the inlet one, respectively. The bed utilization fraction (f) was estimated from H_{MTZ}, considering an antisymmetric breakthrough curve:

$$f = 1 - \frac{0.5H_{MTZ}}{H} \tag{8}$$

2.5. Process simulation details

COSMO-based/Aspen Plus methodology was applied to model the CO_2 physical absorption by ILs in a column with a commercial packing using *Equilibrium*- and *Rate-based* models [13]. ILUAM database [22] was used to incorporate 44 ILs as pseudo-components in Aspen Plus v9.0 (they are not available as conventional compounds in the extensive Aspen Properties database) to perform process simulation using COSMOSAC property package which only need theoretical information obtained from COSMO-RS software to define the ILs (molecular weight, density at 60 °F, boiling point, σ-profile and COSMO volume) and also includes experimental viscosity and its dependence with the temperature. For more details on this methodology, see the work developed by Ferro et al. [22]. The selection of 44 ILs for this study was done based on different commercial cations/anions combinations widely studied in the literature for CO_2 physical absorption. The CO_2 absorption operation using ILs was modeled using the *RADFRAC* column model implemented as default in Aspen Plus v9.0. The operating conditions were selected based on a CO_2 capture operation at pilot plant scale studied in previous works [13]. The gas feed was defined as a 1000 kmol/h (30 ton/h) stream with 13%v of CO_2 and 87%v of N_2 at 303 K and 1 atm of total pressure. The IL stream was defined as a pure IL stream with a flow rate of 400 ton/h (L/G = 13, weight). The *RADFRAC* column was

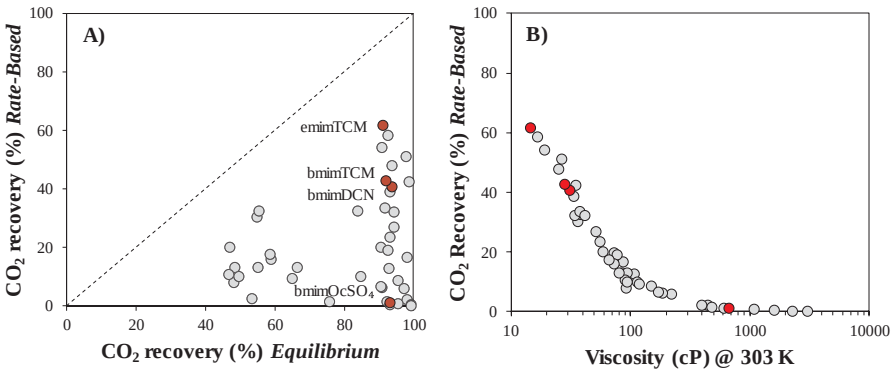

Fig. 1. (A) CO_2 recoveries for 44 ILs calculated by Aspen Plus process simulator using *Rate-based* and *Equilibrium* modes of RADFRAC column; (B) CO_2 recoveries for 44 ILs calculated using Rate-based mode vs viscosity of ILs at 303 K. Red circles: ILs selected for the experimental study.

specified as an absorption column without condenser or reboiler with 10 equilibrium stages. First, the equilibrium model, in which mass transfer kinetic is not taken into account, was used. Once the calculation in equilibrium mode was converged, the rate-based calculation was specified. In this stage, the definition of the type of internal packing used in the column is needed. As in previous works [13,24], 0.625-in FLEXIRING KOCH Metal packing was used in this study. Column diameters were calculated to ensure a column capacity of 62 ± 5%, and based on these results a column height of 20 m was chosen for assuring a height/diameter ratio of almost 10. The recovery of CO_2 was calculated as the ratio between the CO_2 absorbed by the IL and the CO_2 in the gas feed.

3. Results

3.1. Process simulation

Fig. 1A compares the CO_2 recoveries achieved for 44 commercial ILs in a packed column at fixed operating conditions using *RADFRAC Equilibrium* mode (only thermodynamics is considered) and *Rate-based* mode (mass transfer kinetic is also taken into account) simulations. As can be seen, there is a wide range of recoveries for the studied ILs. When *Equilibrium* mode is analyzed, the ILs considered provide recoveries of CO_2 ranging from 46% to 98% at fixed operating conditions (see "Process simulation details" section). In contrast, when the absorption kinetics is taken into account in the calculations by using the *Rate-based* mode, drastic reductions in the CO_2 recovery are obtained at identical operating conditions, with values from 0.3 to 62% for the more viscous ILs. From these results, it can be inferred that despite the very high CO_2 recoveries in *Equilibrium* mode obtained for the majority of the ILs, when the mass transfer kinetics is considered they can present very different behaviors. From these results, we have selected four ILs (EmimTCM, BmimTCM, BmimDCN and $BmimOcSO_4$, red circles in Fig. 1) that show similar absorption efficiency attending to the thermodynamics (almost 91% CO_2 recovery in *Equilibrium* mode), but show different recovery values in the range of kinetic behavior (from 1% to 62% of CO_2 recovery in *Rate-based* mode. These ILs were selected for the experimental study and the encapsulatation in ENIL systems in next stages of this work. Fig. 1B shows the CO_2 recoveries obtained using *Rate-based* simulations as a function of the viscosity of ILs at 303 K. As can be seen, the recovery of CO_2 decreases markedly when the viscosity of the IL increases, regardless of their CO_2 absorption capacity. Negligible CO_2 recovery is obtained when IL viscosity is higher than 200 cP.

3.2. Gravimetric CO_2 absorption by ILs

Thermodynamic and kinetic analyses of CO_2 physical absorption by the selected ILs (EmimTCM, BmimTCM, BmimDCN, and $BmimOcSO_4$) were carried out by gravimetric measurements in the MSB equipment at three different pressures (1, 3 and 6 bar) and temperatures (301, 316 and 331 K). Table 1 shows the physical properties of the ILs selected. From the recorded increase of mass of the IL sample over the time, the CO_2 absorption capacity and CO_2 diffusion coefficient (D) for each IL were estimated at the different operating conditions (Table 2). As can be seen, the four selected ILs present nearly the same CO_2 solubility values (from 3.1 to 3.8 $mg \cdot g^{-1}$ at 1 bar and 301.5 K), *i.e.* they show similar solvent performance from a thermodynamic point of view. These results are in agreement with the conclusion achieved from the process analysis above, where the four ILs presented almost the same CO_2 recovery using equilibrium-based simulations. In contrast, the CO_2 diffusion coefficients (D) for each IL are remarkably different (Table 2), following the order EmimTCM > BmimTCM > BmimDCN > $BmimOcSO_4$, and confirming the different absorption kinetic behavior revealed by process simulations (Fig. 1). As can be seen, $BmimOcSO_4$ presents a particularly low CO_2 diffusion coefficient ($D = 1.8 \cdot 10^{-10}\ m^2 \cdot s^{-1}$ at 301 K and 1 bar) compared to the other ILs ($D = 8–9 \cdot 10^{-10}\ m^2 \cdot s^{-1}$ at 301 K and 1 bar). For the long saturation times, we made the decision of only studying this IL at 301.5 K. Thus, the sequence of D values in Table 2 follows the same trend as the IL viscosity values (Table 1). Current experimental results are in agreement with the conclusions extracted in the previous section from process simulation, indicating that the efficiency of CO_2 capture by physical absorption can be severely limited in the case of ILs showing unfavorable transport properties, basically viscosity, even though they have a high CO_2 absorption capacity at equilibrium.

3.3. ENIL preparation and characterization

In order to evaluate the role of IL encapsulation on the CO_2 capture by physical absorption with ILs, four ENILs were prepared and characterized using the ILs selected in the previous sections. Table 3

Table 1
Physical properties of selected ILs at 298.15 K.

ILs	MW ($g \cdot mol^{-1}$)	ρ ($g \cdot cm^{-3}$)	μ (cP)
EmimTCM	201.23	1.08 [34]	14.6 [35]
BmimTCM	229.28	1.05 [34]	28.5 [36]
BmimDCN	205.26	1.06 [35]	31.1 [36]
$BmimOcSO_4$	348.50	1.06 [37]	669.4 [38]

Table 2
Experimental solubility and diffusion coefficients of selected ILs at different temperatures and pressures.

T (K)	ILs	Solubility			z_{CO2}			D ($\cdot 10^{-11}$)		
		($mg \cdot g^{-1}$)			($mol \cdot mol^{-1}$)			($m^2 \cdot s^{-1}$)		
		1 bar	3 bar	6 bar	1 bar	3 bar	6 bar	1 bar	3 bar	6 bar
301.5	EmimTCM	3.8	11.1	22.2	0.017	0.048	0.092	90	125	150
	BmimTCM	3.7	10.5	21.4	0.019	0.052	0.100	85	110	130
	BmimDCN	3.1	8.9	18.0	0.014	0.040	0.077	80	100	110
	$BmimOcSO_4$	3.1	8.1	15.1	0.007	0.032	0.059	18	20	26
316.5	EmimTCM	3.1	7.9	16.0	0.014	0.035	0.068	130	170	200
	BmimTCM	2.9	7.9	16.0	0.015	0.040	0.077	120	150	170
	BmimDCN	2.4	6.7	13.5	0.011	0.030	0.059	110	140	155
331.5	EmimTCM	2.3	6.1	11.5	0.010	0.027	0.050	160	205	250
	BmimTCM	2.3	6.1	12.3	0.012	0.031	0.060	150	190	220
	BmimDCN	1.9	5.2	10.4	0.009	0.024	0.046	145	175	180

Uncertainties: $u(P) = 0.01$ bar; $u(solubility) = 0.01\ mg \cdot g^{-1}$; $u(z) = 0.0001\ mol \cdot mol^{-1}$ $u(D) = 25\ m^2 \cdot s^{-1}$; $u(T) = 0.1$ K

Table 3
ENIL and C_{cap} characterization.

		C_{cap}	EmimTCM	BmimTCM	BmimDCN	$BmimOcSO_4$
A_{BET} ($m^2 \cdot g^{-1}$)		1304	< 5	< 5	< 5	< 5
EA (%, w)	C	93.0	60.8	67.8	62.5	62.1
	H	1.1	4.9	5.6	6.4	7.5
	N	0.1	27.8	24.9	27.3	6.3
IL content (%, w)		–	79.7	81.5	80.0	77.7

summarizes the characterization results of carbon capsules (C_{cap}) and ENILs by means of elemental analysis and 77 K N_2 adsorption/desorption isotherms. As can be seen, the synthesized C_{cap} presents a high BET surface area (1304 $m^2 \cdot g^{-1}$) and 93% C content. Some amount of silica template may be remaining in the C_{cap}, but not affecting the porous texture, morphology and functional properties. SEM and TEM images of C_{cap} in Fig. 2 show a homogenous material composed of spheres with an external diameter around 750 nm and a shell thickness around 100 nm. Once the IL is incorporated, the accessible porosity of the C_{cap} is filled by the IL, as can be observed from the low values of BET surface area (5 $m^2 \cdot g^{-1}$, accuracy of the equipment). As a result of it, the carbonaceous surface in direct contact with the gas phase is almost negligible and the uptake of CO_2 can be attributed essentially to absorption. In addition, the IL fills the hollow carbon spheres. Thus, the IL content of all prepared ENILs, calculated by elemental analysis following the nitrogen content [21], is near 80% (Table 3).

3.4. CO_2 sorption by ENIL materials

Fig. 3 compares the kinetic curves of CO_2 uptake by ILs and ENIL materials obtained by gravimetric analysis at 301.5 K and 1 bar of CO_2 partial pressure. As can be seen, the uptake of CO_2 by neat ILs is much slower than for ENILs, and the neat ILs selected show very different saturation times, being EmimTCM the fastest (ca. 300 min) and $BmimOcSO_4$ the slowest (> 600 min). The different behavior of the ILs selected is in agreement with the results from *Rate-based* process simulations and the experimental CO_2 diffusion values in ILs discussed above. Noticeably, the saturation time is greatly reduced and nearly the same (~10 min) for all prepared ENILs, regardless of the IL used. These results indicate that the CO_2 uptake rate is governed by the high contact area conferred to the IL by the morphology and small size of C_{Cap}, rather than by the mass transfer kinetics in the IL solvent. In good agreement with previous studies [15,18,19], the encapsulation of the ILs into the hollow microcapsules maintains the CO_2 solubility in the IL (almost 3 $mg \cdot g^{-1}$ in all cases) but drastically boosts the kinetics of the sorption process. Fig. 4 presents the breakthrough curves of CO_2 capture tests in fixed bed using ENIL as sorbents at three temperatures (303, 318 and 333 K) and 0.1 bar of CO_2 partial pressure. Table 4 collects the characteristic thermodynamic and kinetic parameters obtained from the breakthrough curves. It should be remarked that the CO_2 sorption capacities calculated for ENILs from the breakthrough curves nearly match the capacity values of neat ILs from the CO_2 absorption isotherms obtained by gravimetry at different temperatures (see Fig. 5A). Regarding kinetic aspects, Yoon and Nelson model can be considered to describe adequately the breakthrough curve slopes ($R^2 > 0.98$). The estimated kinetic constants (k parameter in Table 4) fall within a narrow range, between 6 and 10 min^{-1} for all the ILs and temperatures tested, in contrast with the variability of D_{CO2} values from the absorption tests summarized in Table 2, where changes by a factor of 160 depending on the IL and temperature can be observed. The height of the mass transfer zone (H_{MTZ} in Table 4) is an additional parameter of interest to evaluate the performance of CO_2 capture by ENILs. The breakthrough curves depicted in Fig. 5 show a remarkable steep-shape for all the ENILs. Therefore, H_{MTZ} values are in a narrow range from 4 to 6 cm, slightly higher than those obtained with ENILs prepared with ILs that provide CO_2 capture by chemical absorption

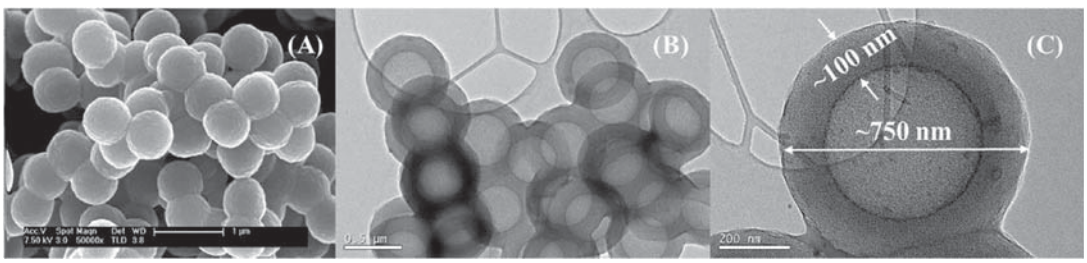

Fig. 2. (A) SEM and TEM images (B, C) of C_{cap} used as support for ENIL preparation.

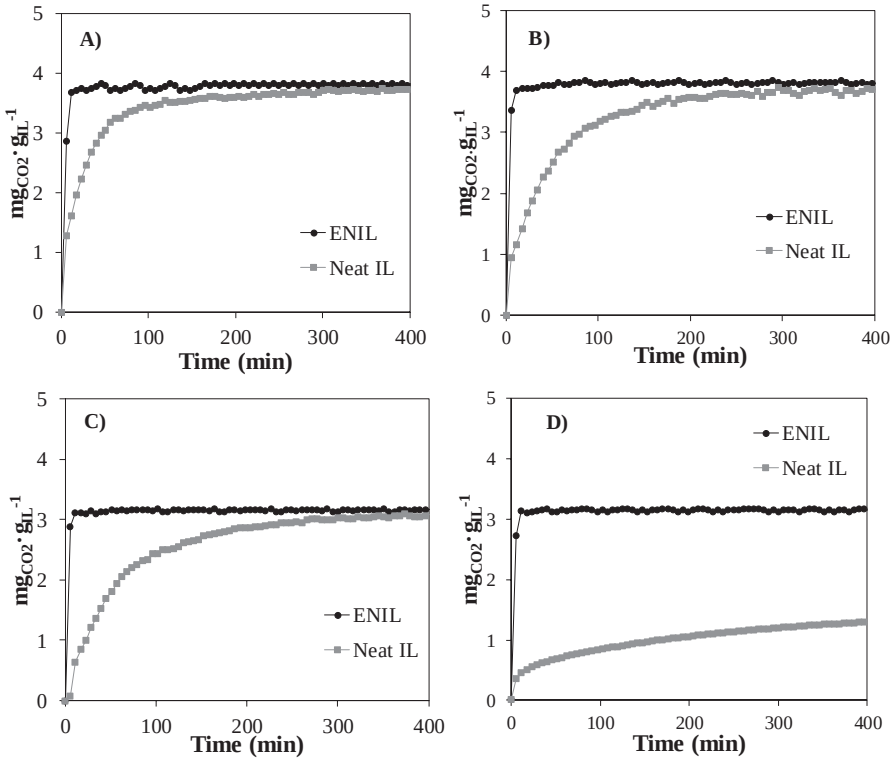

Fig. 3. Kinetic curves of CO_2 uptake in ENIL and neat IL at 301.5 K and p_{CO2} = 1 bar for A) EmimTCM, B) BmimTCM, C) BmimDCN and D) $BmimOcSO_4$.

[19] and in the order of H_{MTZ} values obtained in CO_2 fixed bed capture using solid sorbents [39]. Consequently, using ENILs prepared with IL physical absorbent provides high bed utilization (f > 88% for all ILs and temperatures) (Table 4). These results reveal fast and favorable CO_2 physical sorption into ENILs in fixed-bed operation, ascribable to the large contact area and the small particle size, thus minimizing and overcoming the influence of mass transfer rate.

The experimental values of the representative thermodynamic and kinetic parameters collected in Table 4 can be used to perform a process analysis similar to the one shown in Fig. 1. Thus, simulations of fixed bed operation with the four ENILs tested at fixed operating conditions were conducted to estimate CO_2 recovery, using an ideal equilibrium model where mass transfer limitations are not considered (equivalent to *Equilibrium* mode) and the Yoon and Nelson model (equivalent to *Rate-based* mode). For this purpose, the breakthrough curves for the four ENILs were simulated considering a bed with 1 kg of sorbent and an inlet flow of 100 Nml/min of a stream with a CO_2 concentration of 10% at 303 K, maintaining constant the space velocity in the simulation of scaled-up bed. For the equilibrium recovery, a kinetic constant of infinite value is considered, which results in a breakthrough curve with infinite slope value placed at $t_{0.5}$. The results of this analysis are collected in Fig. 5B.

The differences in CO_2 recoveries obtained with the ideal equilibrium model and Yoon and Nelson model simulations in a fixed bed with the different ENILs are in the range of 2–4%. This implies that in a conventional fixed bed operation the ENIL sorbent can be almost fully saturated and that the separation efficiency, i.e. the amount of CO_2 captured per mass of IL used, can be increased by using ILs where CO_2 is more soluble, even if they do not have good mass transfer-related properties. Fig. 5B can be analyzed in terms of CO_2 recovery at a fixed breakthrough time; for instance, the time at which the CO_2 concentration at the outlet reaches 10% of the inlet value when using EmimTCM-ENIL. At such time, CO_2 recoveries (EmimTCM: 99%, BmimTCM: 99%, bmimDCN: 81%, $bmimOcSO_4$: 54%) are clearly related to experimental absorption capacity (Table 2) but not to the diffusion coefficient of CO_2 in neat ILs (Table 2). In sum, these results indicate that the encapsulation of the ILs in ENILs makes possible to use them in fixed bed operation overcoming the mass transfer limitations of the CO_2 capture process by physical absorption, being the solubility of CO_2 in the IL the main parameter to be considered for the design.

4. Conclusions

Encapsulated ionic liquids (ENILs) are proposed for overcoming the mass transfer limitations that neat ILs present in the physical absorption of CO_2. *RADFRAC* absorption columns on *Equilibrium* and *Rate-based* modes of Aspen Plus software were simulated for 44 ILs from ILUAM database showing a wide range of recoveries in both modes. EmimTCM, BmimTCM, BmimDCN, and $BmimOcSO_4$ were selected for the experimental determination of CO_2 solubilities and diffusivities by gravimetric analysis The results are in agreement with those from process simulation, yielding almost the same CO_2 solubility values (3 $mg{\cdot}g^{-1}$ at 301 K) for the four ILs tested and markedly different CO_2 diffusivity values. In order to solve these mass transfer limitations, ENILs were prepared with the selected ILs and tested in an MSB equipment, showing that the solubility of the IL loaded is maintained while the mass transfer rate is enhanced and the saturation time is reduced by two orders of magnitude. Finally, the ENILs were tested in CO_2 capture using fixed beds, showing no significant differences in absorption rate and a bed utilization determined mainly by the solubility of CO_2 in the

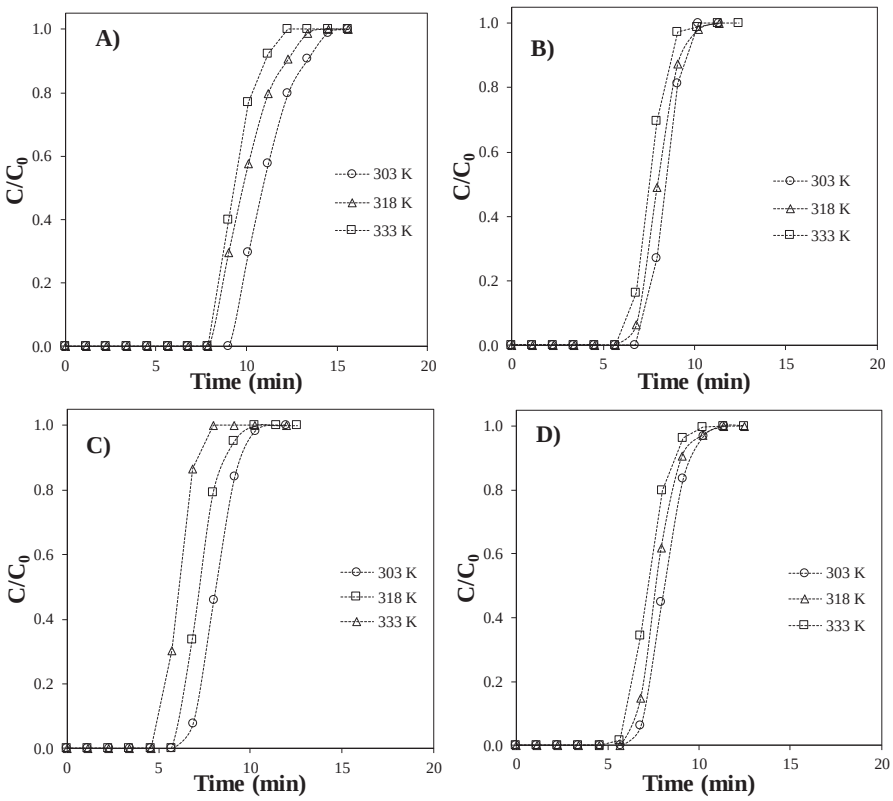

Fig. 4. Breakthrough curves at different temperatures and 0.1 bar CO_2 partial pressure for ENILs prepared with A) EmimTCM, B) BmimTCM, C) BmimDCN and D) $BmimOcSO_4$.

ILs. Therefore, these results demonstrate the fast CO_2 mass transfer rates in ENILs-related to the high contact area provided-allows overcoming the mass transfer limitations that typically control the rate of physical absorption of CO_2 in neat ILs.

Acknowledgments

The authors are grateful to Comunidad de Madrid (project *S2013-MAE-2800*) and Ministerio de Economía y Competitividad of Spain (project *CTQ2017-89441-R*) for financial support and Centro de Computación Científica de la Universidad Autónoma de Madrid for computational facilities. Marcos Larriba also thanks MINECO for awarding him a Juan de la Cierva-Formación Contract (Reference FJCI-2015-25343).

Appendix A. Supplementary data

Supplementary data associated with this article can be found, in the online version, at http://dx.doi.org/10.1016/j.cej.2018.05.029.

Table 4
Operating conditions and results of the fixed bed CO_2 sorption experiments with the ENILs tested.

ENIL	Fixed bed mass (g)	T (K)	q_e (mg·g$_{IL}^{-1}$)	k (min^{-1})	R^2	H_{MTZ} (cm)	f
EmimTCM	3.36	303.1	0.43	8.5	0.996	4.5	0.85
		318.1	0.32	9.2	0.998	4.9	0.84
		333.1	0.26	9.9	0.996	5.9	0.80
BmimTCM	3.58	303.1	0.42	8.1	0.988	4.1	0.86
		318.1	0.31	9.0	0.994	4.8	0.84
		333.1	0.25	9.8	0.990	5.2	0.83
BmimDCN	4.15	303.1	0.33	7.6	0.998	4.8	0.84
		318.1	0.27	8.7	0.996	5.7	0.81
		333.1	0.20	9.5	0.996	6.1	0.80
$BmimOcSO_4$	4.36	303.1	0.22	6.1	0.994	5.1	0.83
		318.1	0.19	7.5	0.984	5.9	0.81
		333.1	0.17	8.8	0.980	5.9	0.80

Uncertainties: u *(bed mass)* = 0.01 g; u *(T)* = 0.1 K; u *(*q_e*)* = 0.05 mg·g^{-1}; u *(k)* = 0.1 min^{-1}; u *(*H_{MTZ}*)* = 0.1 cm; u *(f)* = 0.01.

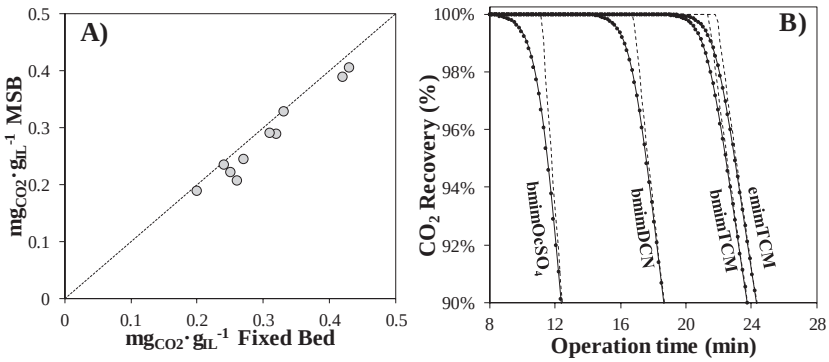

Fig. 5. A) CO_2 solubility in ENIL materials (IL basis) measured in MSB and fixed bed reactor at p_{CO2} = 0.1 bar and three different temperatures (303, 318 and 333 K). B) CO_2 recovery in fixed bed operation over time with ENILs, calculated using the Yoon and Nelson model (symbols) and the ideal equilibrium model (dash-line).

References

[1] (a) M.K. Mondal, H.K. Balsora, P. Varshney, Energy 46 (2012) 431–441;
(b) M. Wang, A. Lawal, P. Stephenson, J. Sidders, C. Ramshaw, Chem. Eng. Res. Des. 89 (2011) 1609–1624.
[2] J.D. Figueroa, T. Fout, S. Plasynski, H. McIlvried, R.D. Srivastava, Int. J. Greenhouse Gas Control 2 (2008) 9–20.
[3] C.-H. Yu, Aerosol Air Qual. Res. (2012).
[4] P.D. Vaidya, V.V. Mahajani, Ind. Eng. Chem. Res. 44 (2005) 1868–1873.
[5] C.J. Chang, C.Y. Day, C.M. Ko, K.L. Chiu, Fluid Phase Equilib. 131 (1997) 243–258.
[6] A.-L. Revelli, F. Mutelet, J.-N. Jaubert, J. Phys. Chem. B 114 (2010) 12908–12913.
[7] (a) G. Ferrara, A. Lanzini, P. Leone, M.T. Ho, D.E. Wiley, Energy 130 (2017) 113–128;
(b) G.T. Rochelle, Science 325 (2009) 1652–1654.
[8] J. Kothandaraman, A. Goeppert, M. Czaun, G.A. Olah, G.K.S. Prakash, Green Chem. 18 (2016) 5831–5838.
[9] S. Tang, G.A. Baker, H. Zhao, Chem. Soc. Rev. 41 (2012) 4030–4066.
[10] a) K. Anderson, M.P. Atkins, J. Estager, Y. Kuah, S. Ng, A.A. Oliferenko, N.V. Plechkova, A.V. Puga, K.R. Seddon, D.F. Wassell, Green Chem. 17 (2015) 4340–4354;
b) C. Wang, H. Luo, X. Luo, H. Li, S. Dai, Green Chem. 12 (2010) 2019–2023;
c) E.I. Izgorodina, J.L. Hodgson, D.C. Weis, S.J. Pas, D.R. MacFarlane, J. Phys. Chem. B 119 (2015) 11748–11759;
d) S. Sarmad, J.P. Mikkola, X. Ji, ChemSusChem 10 (2017) 324–352;
e) S. Zeng, X. Zhang, L. Bai, X. Zhang, H. Wang, J. Wang, D. Bao, M. Li, X. Liu, S. Zhang, Chem. Rev. 117 (2017) 9625–9673.
[11] M. Bui, C.S. Adjiman, A. Bardow, E.J. Anthony, A. Boston, S. Brown, P.S. Fennell, S. Fuss, A. Galindo, L.A. Hackett, J.P. Hallett, H.J. Herzog, G. Jackson, J. Kemper, S. Krevor, G.C. Maitland, M. Matuszewski, I.S. Metcalfe, C. Petit, G. Puxty, J. Reimer, D.M. Reiner, E.S. Rubin, S.A. Scott, N. Shah, B. Smit, J.P.M. Trusler, P. Webley, J. Wilcox, N. Mac Dowell, Energy Environ. Sci. (2018).
[12] (a) C. Wu, T.P. Senftle, W.F. Schneider, Phys. Chem. Chem. Phys. 14 (2012) 13163–13170;
(b) J. Huang, T. Ruether, Aust. J. Chem. 62 (2009) 298–308.
[13] J. de Riva, J. Suarez-Reyes, D. Moreno, I. Díaz, V. Ferro, J. Palomar, Int. J. Greenhouse Gas Control 61 (2017) 61–70.
[14] J.E. Brennecke, B.E. Gurkan, J. Phys. Chem. Lett. 1 (2010) 3459–3464.
[15] J. Palomar, J. Lemus, N. Alonso-Morales, J. Bedia, M.A. Gilarranz, J.J. Rodriguez, Chem. Commun. (Camb.) 48 (2012) 10046–10048.
[16] N. Alonso-Morales, M.A. Gilarranz, J. Palomar, J. Lemus, F. Heras, J.J. Rodriguez, Carbon 59 (2013) 430–438.
[17] a) J. Lemus, J. Palomar, M.A. Gilarranz, J.J. Rodriguez, Adsorption 17 (2011) 561–571;
b) J. Lemus, C. Neves, C.F.C. Marques, M.G. Freire, J.A.P. Coutinho, J. Palomar, Environ. Sci. Process. Impacts 15 (2013) 1752–1759.
[18] J. Lemus, J. Bedia, C. Moya, N. Alonso-Morales, M.A. Gilarranz, J. Palomar, J.J. Rodriguez, RSC Adv. 6 (2016) 61650–61660.
[19] C. Moya, N. Alonso-Morales, M.A. Gilarranz, J.J. Rodriguez, J. Palomar, ChemPhysChem 17 (2016) 3891–3899.
[20] J. Lemus, F.A. Da Silva, F.J. Palomar, P.J. Carvalho, J.A.P. Coutinho, Separ. Purif. Technol. (2017).
[21] K. Dong, X. Liu, H. Dong, X. Zhang, S. Zhang, Chem. Rev. 117 (2017) 6636–6695.
[22] V.R. Ferro, C. Moya, D. Moreno, R. Santiago, J. de Riva, G. Pedrosa, M. Larriba, I. Diaz, J. Palomar, Ind. Eng. Chem. Res. 57 (2018) 980–989.
[23] V.R. Ferro, E. Ruiz, J. de Riva, J. Palomar, Sep. Purif. Technol. 97 (2012) 195–204.
[24] J. Bedia, E. Ruiz, J. de Riva, V.R. Ferro, J. Palomar, J.J. Rodriguez, AIChE J. 59 (2013) 1648–1656.
[25] R. Santiago, J. Bedia, D. Moreno, C. Moya, J. de Riva, M. Larriba, J. Palomar, Sep. Purif. Technol. 204 (2018) 38–48.
[26] (a) J. de Riva, V.R. Ferro, D. Moreno, I. Diaz, J. Palomar, Fuel Process. Technol. 146 (2016) 29–38;
(b) M. Larriba, J. de Riva, P. Navarro, D. Moreno, N. Delgado-Mellado, J. Garcia, V.R. Ferro, F. Rodriguez, J. Palomar, Sep. Purif. Technol. 190 (2018) 211–227.
[27] I. Diaz, J. Palomar, M. Rodriguez, J. de Riva, V. Ferro, E.J. Gonzalez, Chem. Eng. Res. Des. 115 (2016) 382–393.
[28] a) E. Ruiz, V.R. Ferro, J. de Riva, D. Moreno, J. Palomar, Appl. Energy 123 (2014) 281–291;
b) D. Moreno, V.R. Ferro, J. de Riva, R. Santiago, C. Moya, M. Larriba, J. Palomar, Appl. Energy 213 (2018) 179–194.
[29] G. Büchel, K.K. Unger, A. Matsumoto, K. Tsutsumi, Adv. Mater. 10 (1998) 1036–1038.
[30] C. Moya, J. Palomar, M. Gonzalez-Miquel, J. Bedia, F. Rodriguez, Ind. Eng. Chem. Res. 53 (2014) 13782–13789.
[31] M.B. Shiflett, A. Yokozeki, Ind. Eng. Chem. Res. 44 (2005) 4453–4464.
[32] Y.H. Yoon, J.H. Nelson, Am. Ind. Hyg. Assoc. J. 53 (1992) 303–316.
[33] (a) J. Lemus, M. Martin-Martinez, J. Palomar, L. Gomez-Sainero, M.A. Gilarranz, J.J. Rodriguez, Chem. Eng. J. 211–212 (2012) 246–254;
(b) Y.H. Yoon, J.H. Nelson, Am. Ind. Hyg. Assoc. J. 45 (1984) 517–524.
[34] M. Součková, J. Klomfar, J. Pátek, Fluid Phase Equilib. 406 (2015) 181–193.
[35] C.M.S.S. Neves, K.A. Kurnia, J.A.P. Coutinho, I.M. Marrucho, J.N.C. Lopes, M.G. Freire, L.P.N. Rebelo, J. Phys. Chem. B 117 (2013) 10271–10283.
[36] P.J. Carvalho, T. Regueira, L.M.N.B.F. Santos, J. Fernandez, J.A.P. Coutinho, J. Chem. Eng. Data 55 (2010) 645–652.
[37] M.J. Davila, S. Aparicio, R. Alcalde, B. Garcia, J.M. Leal, Green Chem. 9 (2007) 221–232.
[38] J. Jacquemin, P. Husson, V. Majer, A.A.H. Padua, M.F.C. Gomes, Green Chem. 10 (2008) 944–950.
[39] A.M. Mastral, T. García, R. Murillo, M.S. Callén, J.M. López, M.V. Navarro, Ind. Eng. Chem. Res. 42 (2003) 5280–5286.

Supplementary Material

From Kinetics to Equilibrium Control in CO_2 capture columns using Encapsulated Ionic Liquids (ENILs)

R. Santiago, J. Lemus, D. Moreno, C. Moya, M. Larriba, N. Alonso-Morales, M.A. Gilarranz, J.J. Rodríguez and J. Palomar*

Sección de Ingeniería Química. Universidad Autónoma de Madrid. 28049 Madrid. Spain.

*Corresponding author. E-mail: pepe.palomar@uam.es

Index

Table S1. List of Ionic Liquids.

Figure S1: Blank measurements: breakthrough curves at different temperatures and 0.1 bar CO_2 partial pressure of glass balls inert material

Table S1. List of Ionic Liquids

CATIONS		
Abbreviation	Name	Formula
mmim	1-3-dimethylimidazolium	C5H9N2
emim	1-ethyl-3-methylimidazolium	C6H11N2
bmim	1-butyl-3-methylimidazolium	C8H15N2
hxmim	1-hexyl-3-methylimidazolium	C10H19N2
omim	1-octyl-3-methylimidazolium	C12H23N2
dcmim	1-decyl-3-methylimidazolium	C14H27N2
(EtOH)mim	1-(2-hydroxyethyl)-3-methylimidazolium	C6H11N2O
3mbpy	N-butyl-3-methylpyridinium	C10H16N
bmpyr	N-butyl-N-methylpyrrolidinium	C9H20N
Choline	(2-hydroxyethyl)-trimethyl ammonium	C5H14NO
$P_{666,14}$	trihexyl-tetradecylphosphonium	C32H68P
P_{8888}	tetraoctylphosphonium	C32H68P

ANIONS		
Abbreviation	Name	Formula
Cl	chloride	Cl
Br	bromide	Br
BF_4	tetrafluoroborate	BF4
PF_6	hexafluorophosphate	PF6
NTf2	bis(trifluoromethylsulfonyl)imide	C2F6NO4S2
FEP	tris(pentafluoroethyl)trifluorophosphate	C6F18P
MeCOO	acetate	C2H3O2
BzCOO	benzoate	BzCOO
SCN	thiocyanate	CNS
DCN	dicyanamide	C2N3
TCM	tricyanomethanide	C4N3
$B(CN)_4$	tetracyanoborate	BC4N4
$(Me)_2PO_4$	dimethylphosphate	C2H6PO4
$MePO_3$	Methylphosphite	C1H4PO3
$MeSO_4$	methylsulfate	CH3SO4
$EtSO_4$	ethylsulfate	C2H5SO4
$OcSO_4$	octylsulfate	C8H17SO4

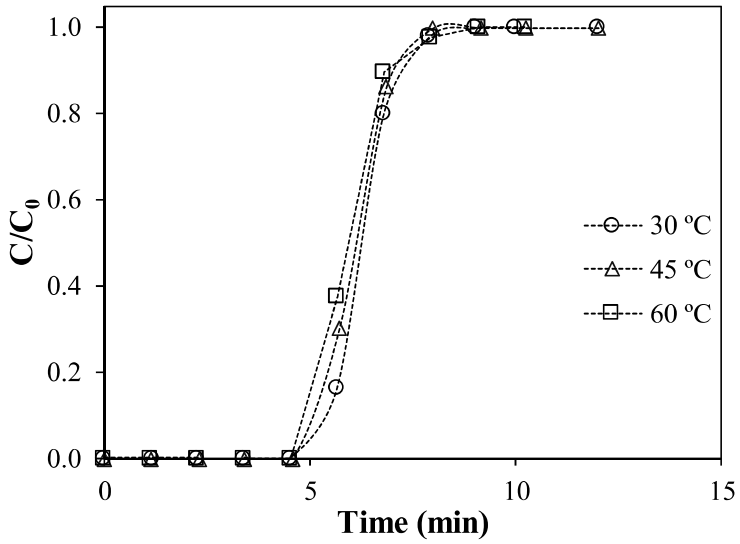

Figure S1: Blank measurements: breakthrough curves at different temperatures and 0.1 bar CO_2 partial pressure of glass balls inert material

5.4 Encapsulated Ionic Liquids to enable the practical application of amino acid-based ionic liquids in CO_2 capture

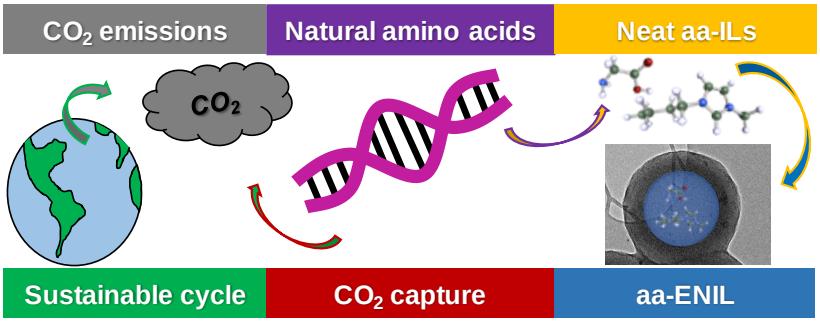

ACS Sustainable Chemistry & Engineering

Research Article

Cite This: ACS Sustainable Chem. Eng. 2018, 6, 14178−14187

pubs.acs.org/journal/ascecg

Encapsulated Ionic Liquids to Enable the Practical Application of Amino Acid-Based Ionic Liquids in CO_2 Capture

Rubén Santiago, Jesús Lemus, Cristian Moya, Daniel Moreno, Noelia Alonso-Morales, and José Palomar*

Departamento de Ingeniería Química, c/Francisco Tomás y Valiente 7, Facultad de Ciencias, Universidad Autónoma de Madrid, 28049 Madrid, Spain

Supporting Information

ABSTRACT: The performance of three amino-acid-based ionic liquids (aa-ILs) has been evaluated in CO_2 capture by means of gravimetric measurements. The tested aa-ILs were 1-butyl-3-methylimidazolium prolinate, [Bmim][PRO]; 1-butyl-3-methylimidazolium methioninate, [Bmim][MET]; and 1-butyl-3-methylimidazolium glycinate, [Bmim][GLY]. First, the CO_2 chemical absorption process was analyzed by *in situ* Fourier transform infrared spectroscopy−attenuated total reflection (FTIR-ATR), following the characteristic vibrational signals of the reactants and products, and comparing them with theoretical measurements obtained by quantum chemical calculations. This study let us confirm a mechanism of CO_2 chemical absorption on amino-acid-based ILs. Then, gravimetric experiments were carried out to characterize the CO_2 capture by aa-ILs. It was found that CO_2 absorption quantification of these ILs was rather slow, because of their high viscosities, so alternative methodologies had to be employed to use them as absorbents in CO_2 capture. In this sense, aa-ILs were encapsulated in porous carbon capsules (aa-ENIL), since it has been previously reported as material that defeats the kinetic limitations and preserves the favorable CO_2 capture capacity of the neat ILs, promoting efficient chemical absorption. These aa-ENIL materials permit evaluation of CO_2 capture at equilibrium and experimentally characterize the thermodynamics absorption phenomena, in terms of reaction enthalpy and the contribution of physical (H) and chemical (K_{eq}) CO_2 absorption for each IL. ENIL materials allow a fast CO_2 capture with high sorption capacity and easy regeneration due to the favorable thermodynamics and kinetics of the process.

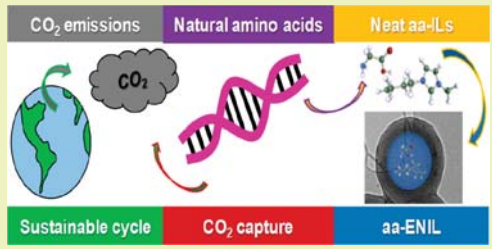

KEYWORDS: *Chemical CO_2 capture, Amino-acid-based, Ionic liquids, aa-ENIL*

INTRODUCTION

Emissions of greenhouse gases, mainly carbon dioxide (CO_2), have caused a serious problem—global warming—which has resulted in great concern from the international community.[1,2] Recently, a great amount of research effort has been dedicated toward CO_2 capture.[3] Among them, chemical absorption with amines, e.g., monoethanolamine (MEA), is commonly employed for acid gas removal, as H_2S or CO_2, from flue gas in industries.[4,5] Some of the disadvantages of this amine scrubbing process are the high corrosivity of the amines, the solvent loss during regeneration, the high energy requirement for regeneration, and consequently high operational costs.[6,7] Especially for large-scale applications such as power plants, depending on the nature of combustion (precombustion or postcombustion technology) and the concentration of CO_2 in the flue gas stream, it is important to develop new and efficient solvents for CO_2 capture.[8−10]

In this sense, during the past few decades, ionic liquids (ILs) have awakened great attention due to their unique properties such as very low vapor pressure, good thermal and chemical stability, and high polarity.[11] In CO_2 capture, ILs can be applied to absorb CO_2 by either physical or chemical absorption.[12,13] For physical absorption, the factors influencing CO_2 solubility in IL include free volume and the nature of cation and anion.[14] For the use of ILs in chemical absorption, a structure of IL with an active site that can react with CO_2 is required. This functionalization can be based on amino-based ILs, azolate-based ILs, phenolated-based ILs, or pyridine-containing ILs among others.[13] These kinds of ILs are synthesized with the desired properties, and it has been found that absorption capacity of CO_2 is many times higher than ILs in physical absorption.[12,15−17]

This work is focused on amino-acid-based ILs (aa-ILs), where safe amino acids were utilized in functionalizing the imidazolium-based IL.[17,18] These aa-ILs are particularly promising because of their low cost, abundant availability, and nontoxic biodegradability.[19−21] Several papers have reported the high chemical absorption capacity of these aa-ILs[22−26] and the limited mass transfer CO_2 rate.[27,28] However, CO_2 absorption in aa-ILs presents the kinetic limitations of the CO_2 absorption in aa-ILs due to their high viscosity, especially after reaction with CO_2, as

Received: June 13, 2018
Revised: August 22, 2018
Published: September 21, 2018

DOI: 10.1021/acssuschemeng.8b02797
ACS Sustainable Chem. Eng. 2018, 6, 14178−14187

a result of the CO_2-complexed aa-ILs forming a salt bridge hydrogen-bonded network, reported by Goodrich et al.[28] Therefore, in order to reduce the limitations caused by unfavorable transport properties, two main, different alternatives have been proposed, IL dilution with cosolvents of lower viscosity to overcome the mass transfer limitations of the fluid and the use of a solid phase to immobilize the IL.[20,29] Attending to the immobilization of IL, the first approach was SILP materials (supported ionic liquid phase).[30] SILP consists of spreading the IL on a solid support to increase the mass transfer rate of the CO_2 absorption in ILs, giving high gas−liquid interfacial area and allowing an improvement in the mass transport rates of CO_2 capture in IL, but limited by the maximum amount of IL load in the support.[31,32] A more recent alternative is encapsulated ionic liquids (ENILs), materials with a high content of IL inside them due to the central hollow of the porous capsule.[33−44] In recent years, the microencapsulation technique was applied using different polymers[37,40,41] and carbonaceous capsules,[33,38,39,42−44] these being sorbent materials evaluated in CO_2 capture by physical[41,42,44] and chemical absorption[37,39,40,43] in ILs. Recently, we developed ENIL materials formed by hollow carbon submicrospheres (C_{Cap}) with a diameter between 400 and 700 nm filled by a large amount of IL (up to 80% in weight).[33] This novel material, with solid appearance, allows discretizing the IL fluid in microdrops, increasing drastically the gas−liquid contact surface.[38] It has been reported that ENIL maintains the absorbent capacity of the IL and drastically enhances the CO_2 sorption rate for both physical[42] and chemical[39,43] absorption phenomena. In particular, ENIL has been proved to be useful to adequately characterize the thermodynamics of a CO_2−IL mixture when the absorption phenomenon is mainly controlled by the kinetics.[39,42] Therefore, it is achieved to defeat the limited mass transfer rate due to the high viscosity of ILs, especially those ILs promoting CO_2 chemical absorption.[39,43]

This work aims to evaluate the applicability of aa-ILs as separating agents for the purification of gas streams contaminated with CO_2. Taking the advantage of the use of ENIL in gas application[39,43,44] and due to the very low mass transfer rate of the CO_2 absorption on neat aa-ILs,[27,28] the ENIL materials were used for testing CO_2 capture by aa-ILs. Therefore, the aa-ENIL materials have been designed to provide high CO_2 sorption capacities and high mass transfer rates. Three aa-ILs were selected attending to their high CO_2 absorption capacities,[26,45] which are 1-butyl-3-methylimidazolium prolinate, [Bmim][PRO]; 1-butyl-3-methylimidazolium methioninate, [Bmim][MET]; and 1-butyl-3-methylimidazolium glycinate, [Bmim][GLY]. Hollow carbon submicrocapsules with a thick porous wall were synthesized by using the "templating" method,[46,47] and then, the aa-ENIL materials were prepared filling high loads (55−60% w/w) of the selected aa-IL—that present great CO_2 sorption capacity[26,45]—in the microcapsules. The carbon submicrocapsules and aa-ENIL materials were characterized by several techniques, including scanning and transmission electron microscopy (SEM and TEM), elemental analysis (EA), N_2 adsorption−desorption at 77 K, thermogravimetric analysis (TGA), and differential scanning calorimetry (DSC). Before the quantification of the CO_2 sorption capacity of these materials, chemical reaction of CO_2 and aa-ILs was checked by using the attenuated total refection (ATR) technique in conjunction with Fourier transform infrared spectroscopy (FTIR) in a gas−liquid Golden Gate reactor at 298 K and 5 bar of CO_2 partial pressure. Spectroscopic results were compared to theoretical vibrations obtained with DFT calculations in order to assign the characteristic signals of reactants and products involved in the proposed chemical reaction mechanism. Finally, sorption gravimetric experiments were carried out using aa-ILs and aa-ENILs at 303, 318, and 333 K, for CO_2 partial pressure in the range of 0.3−20 bar. The influence of the encapsulation and chemical nature of the aa-ILs was analyzed under different operating conditions. A thermodynamic model was used to obtain physical and chemical CO_2 absorption contributions by means of reaction equilibrium constant (K_{eq}) and Henry's law constant (H) in order to affirm the presence of reactants and products involved in the proposed reaction mechanism of the CO_2 capture on aa-ENIL materials, allowing to characterize the thermodynamics of the chemical absorption phenomena (reaction enthalpy) involved.

EXPERIMENTAL SECTION

Materials. The aa-ILs used in this study were synthesized by Iolitec at 95% purity. These aa-ILs are 1-butyl-3-methylimidazolium prolinate, [Bmim][PRO]; 1-butyl-3-methylimidazolium methioninate, [Bmim][MET]; and 1-butyl-3-methylimidazolium glycinate, [Bmim][Gly].

The synthesis of the hollow submicrocapsules was carried out using phenol (99%), paraformaldehyde (95−100%), aluminum trichloride (95−100%), ammonia (34%), and absolute ethanol supplied by Panreac. Tetraethylorthosilicate (98%; TEOS), octadecyltrimethoxysilane (90%; C18TMS), and hydrofluoric acid (48%) were supplied by Sigma-Aldrich.

Carbon dioxide (CO_2) and nitrogen (N_2) were supplied by Praxair, with a minimum purity of 99.999%.

Synthesis of aa-ENIL. The hollow microcapsules (C_{Cap}) synthesized for their use as aa-ENIL support were prepared following the methodology reported by our group in previous works[38,39,46] and based on the procedure described by Büchel et al.[48] A solid core and mesoporous shell aluminosilicate (SCMS) were used as the template. The solid core was achieved following the Störbe synthesis,[49] where a volume of 15 mL of tetraethoxysilane (TEOS) was added to a reaction medium formed by 12.6 mL of ammonia aqueous solution (20%, v), 185 mL of ethanol, and 20.3 mL of deionized water. The mixture was maintained at 303 K with vigorous stirring over 1 h to achieve a colloidal solution of silica spheres. A mixture containing 12.5 mL of TEOS and 5 mL of octadecyltrimethoxysilane (C18TMS) was added to the colloidal solution to form the mesoporous shell around them. This addition was repeated twice to get a double wall (12.5 + 5 mL). After 1 h of reaction, the spheres formed were isolated by filtration and calcined at 823 K for 6 h under an air atmosphere. The silica spheres were impregnated by a solution consisting on 0.27 g of $AlCl_3{\cdot}6H_2O$ in 0.3 mL of deionized water. The resulting powder was dried in air at 353 K and calcined at 823 K for 5 h in air to form SCMS aluminosilicate. A phenol-formaldehyde resin has been used as a carbon precursor to obtain the carbon submicrocapsules. A mixture of 0.374 g of phenol per gram of template was heated at 373 K for 14 h under 150 mm of Hg static vacuum (rotavapor equipment). Then, 0.238 g of paraformaldehyde per gram of SCMS was added and maintained for 24 h under a static vacuum at 403 K to obtain a phenol-formaldehyde resin in the SCMS template. This material was heated to 433 K with a rate of 1 K·min^{-1} and held at that temperature for 5 h under a nitrogen flow of 200 N mL·min^{-1} in a vertical furnace (i.d., 26 mm; length, 12 cm). Then, the temperature was raised up to 1123 K with a heat rate of 5 K·min^{-1} and held at that temperature for 7 h. The resulting carbon aluminosilicate was washed with HF (48%, (v) to generate the carbon capsules (C_{Cap}).

Then, the aa-ENIL materials were prepared by incipient wetness impregnation of 100 mg of C_{Cap} with 1 mL of an IL-acetone solution. The solution was added dropwise onto the support. After impregnation, acetone was removed by evaporation at 333 K over 24 h. In the current work, the three aa-ENILs tested were prepared with an IL nominal load of 60% w/w. The amount of IL incorporated was checked by elemental analysis. This methodology was successfully applied in our previous publications allowing a homogeneous distribution of the IL inside the C_{Cap}.[38,39]

DOI: 10.1021/acssuschemeng.8b02797
ACS Sustainable Chem. Eng. 2018, 6, 14178−14187

Table 1. Properties of the Three aa-ILs Tested in This Work

Name	Abreviature	Chemical structure		M_{weight} ($g \cdot mol^{-1}$)	Density ($g \cdot mL^{-1}$)	$V_{molecular}$[a] ($Å^3$)
		Cation	*Anion*			
1-Butyl-3-methylimidazolium glycinate	[Bmim][GLY]	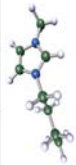		213	1.00 [26]	376
1-Butyl-3-methylimidazolium methioninate	[Bmim][MET]		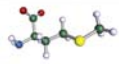	287	1.00 [26]	440
1-Butyl-3-methylimidazolium prolinate	[Bmim][PRO]			253	1.13 [26]	410

Samples Characterization. The hollow carbon capsules (C_{Cap}) and the aa-ENIL materials were characterized by elemental analysis in a LECO CHNS-932 apparatus. Then, the porous texture of the carbon material was characterized by 77 K N_2 adsorption/desorption in a TriStar II 3020 (Micromeritics) system after 12 h of degassing at 0.1 mbar and 393 K. The surface area was calculated by using the BET equation. The microstructure and morphology of C_{Cap} and aa-ENIL materials were studied by scanning electron microscopy (SEM) and transmission electron microscopy (TEM). SEM analyses were performed with a Hitachi S-3000N apparatus, and TEM images were obtained in JEOL JEM 2100 HT microscope. The thermal stability of the samples was evaluated by thermal gravimetric analysis (TGA) and differential scanning calorimetry (DSC) under a N_2 atmosphere within the range of 283−800 K with a heat rate of 10 $K \cdot min^{-1}$, using a DSC/DTA/TGA module from TA Instrument. This serves to check some possible interaction of the IL with the support that may reduce the stability.

ATR-FTIR Experiments. Measurements were carried out in an Agilent Cary 660 FTIR spectrometer, equipped with a Reaction Cell Golden Gate ATR from Specac. This accessory is a stainless steel pressure vessel equipped with heating capacity (up to 573 ± 1 K) that seals over a diamond in a tungsten carbide disc. The cell has an approximate volume of 30 mL and can be pressurized up to 200 ± 0.1 bar. It is equipped with inlet and outlet pipes that allow circulating a gas flow through the reaction chamber.

For CO_2 absorption experiments on aa-ILs, a small amount of IL (50 mg) is placed into the reaction chamber at almost room temperature (298 K). Then, a CO_2 flow of 50 mL/min is introduced into the reactor until the total pressure of the system is 5 bar. The IR spectra between 700 and 4000 cm^{-1} are recorded at time 0 (degassed IL without any gas flow throw it) and up to 24 h later, when the intensity of the vibrational signals remains constant, at which time the system is considered to have attained equilibrium. Note that the liquid is quiescent, not being stirred or agitated in any way.

Gravimetric CO_2 Capture. The measurements of CO_2 solubility in aa-ILs and aa-ENILs were performed in a gravimetric high pressure sorption analyzer (ISOSORP GAS LP-flow, Rubotherm) equipped with a magnetic suspension balance (MSB). The balance covers a weight range up to 10 g, with a precision of 10^{-5} g. In addition, it can operate in a wide range of temperatures (from room temperature to 150 °C) and pressures (from 10^{-3} mbar to 30 bar). A full description of the termogravimetric experimental methodology is available in previous works.[50,51]

The CO_2 absorption isotherms for the aa-ENIL materials were obtained at three different temperatures (303, 318, and 333 K) and CO_2 partial pressure in the range of 0.3−20 bar (in order to reach 0.3 and 0.5 bar CO_2 partial pressure, a mixture of CO_2/N_2 was done). In a standard run, an initial outgassed step at 333 K under 10^{-3} bar of vacuum until constant weight is reached (<0.02 mg/h) was carried out to ensure the water free conditions (<200 ppm) of aa-ILs and aa-ENIL materials. Then, a 100 mL/min flow of pure CO_2 is passed through the sorbent sample (150 mg of aa-ENIL materials), and the increase in the mass is recorded over time at a fixed temperature. Once the sample is saturated, i.e., weight change <0.02 mg/h, the pressure is increased. The buoyancy effect is corrected, and the amount of CO_2 absorbed is quantified in terms of grams of CO_2 per gram of IL and as molar ratio (z_{CO_2}):

$$z_{CO_2} = \frac{m_{CO_2}/M_{CO_2}}{m_{IL}/M_{IL}} \quad (1)$$

where m_{CO_2} is the absorbed CO_2 mass, m_{IL} is the IL mass after degasification, and M_{CO_2} and M_{IL} are the molecular weights of CO_2 and IL, respectively.

Computational Details. The chemical structure of the aa-ILs was calculated using TURBOMOLE v7.2 (with TmoleX v4.2.1 graphic interface) software. The molecular structures of aa-ILs were described by the ion-pair model [CA] in which the cation and the anion are optimized as a whole. Then, the CO_2-aa-ILs complexes were also optimized for predicting the IR spectrum of both stages (before and after CO_2 reaction). In fact, this calculation was carried out by a frequency calculation, which allows predicting the IR spectrum. In addition, the ideal screening charges of the molecular surface for each aa-IL were calculated by the continuum solvation COSMO model using the BP/TZVP level of theory, giving as a result the *.cosmo file used as input in COSMO-RS calculations in COSMOtherm.[52]

The molecular volumes of the aa-ILs, collected in Table 1, were calculated by COSMO-RS at 298 K using COSMOtherm software. The computational approach was described elsewhere[53] and describes the aa-IL compound with an ion-pair structure. According to the chosen quantum method, the functional, and the basis set, we used the corresponding parametrization (BP_TZVP_ C30_1201).[54]

RESULTS

aa-IL and aa-ENIL Material Characterization. The three selected aa-ILs in this work present similar density values, close to 1 $g \cdot mL^{-1}$,[26] and slightly different molecular weight and molecular volumes, as shown in Table 1. The characteristic ^1H NMR spectra of the three aa-ILs are provided in the Supporting Information, where the purity of these compounds is shown.

The carbon capsules (C_{Cap}) with a micro/mesoporous shell structure and hollow core, like those developed by Yoon et al., were selected to prepare the aa-ENIL materials.[55] Thus, spherical capsules were obtained containing high carbon content (94% w/w), homogeneous morphology (∼700 nm of diameter and ∼150 nm of shell thickness), high pore volume (>3.5 $cm^3 \cdot g^{-1}$), and BET surface area (1644 $m^2 \cdot g^{-1}$). Scanning electron microscopy (SEM), transmission electron microscopy (TEM) images, and size distribution of synthesized C_{Cap} are depicted in Figure 1, resulting in hollow carbon capsules with a narrow size distribution around 700 nm. The results of the characterization of

DOI: 10.1021/acssuschemeng.8b02797
ACS Sustainable Chem. Eng. 2018, 6, 14178−14187

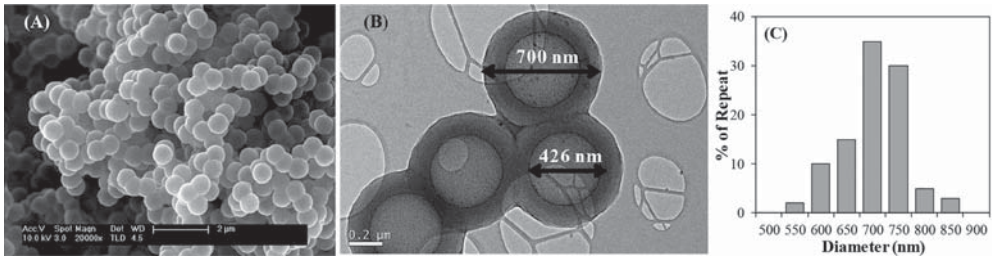

Figure 1. (A) SEM and (B) TEM images of the carbon capsules to obtain the aa-ENIL material and (C) size distribution of synthesized C_{Cap}.

Table 2. Characterization of Carbon Capsules, aa-ILs, and aa-ENIL Materials

			aa-IL			aa-ENIL		
		C_{Cap}	[Bmim] [GLY]	[Bmim] [PRO]	[Bmim] [MET]	[Bmim] [GLY]	[Bmim] [PRO]	[Bmim] [MET]
A_{BET}	($m^2 \cdot g^{-1}$)	1644				<5	<5	<5
EA	%C	94.0	52.9	59.5	52.6	58.7	59.2	59.1
	%H	1.0	8.6	8.6	8.4	6.6	6.9	6.6
	%N	2.0	18.3	16	13.9	9.9	10.6	9.4
%IL	EA					50.2	63.6	63.9
	TGA					46.6	56.1	55.9
T_{DTGA}	(K)	stable until 823 K	516	523	502	520	513	500

the carbon capsules by means of elemental analysis (EA), 77 K N_2 adsorption−desorption isotherm, and thermogravimetric analysis are summarized in Table 2. The technique of direct impregnation, employed in our previous work to prepare SILP systems,[56] was used to introduce the aa-ILs into the C_{Cap}, with an IL mass load of 50−60% of IL. In previous works,[33,38,39] it was demonstrated by TEM that the IL in ENIL materials is located in the great central hollow and filling the double shell pores of the C_{Cap}. The characteristic of the different aa-ENIL materials is shown in Table 2. Elemental analysis allowed quantifying the incorporation of aa-IL into ENIL materials, by measuring the percentage of N in the final material, which can be related to the uptake of imidazolium cations and amino acid anions. The EA results of Table 2 confirm the adequate incorporation of aa-IL (50−65% in mass) into ENIL material. On the other hand, TGA experiments can also be used to obtain reasonable estimations of the aa-IL amount contained in ENIL,[39,56] as the difference between the percentage of aa-ENIL material after total decomposition of aa-IL (800 K) and the percentage after water loss (373 K) removed in the degasification stage in the MSB equipment. The amount of aa-IL in the ENIL material is estimated by TGA in the range of 45−55% in weight, in reasonable agreement with the results obtained by EA.

The thermal stability of aa-ENIL materials is of special interest for gas phase applications, concretely in the regeneration step where high temperatures may be required. Although the decomposition temperature of neat IL is generally above the process temperature, the interaction when it is encapsulated may lead to a reduction in the thermal stability. As a first approach, the thermal stability of neat and encapsulated aa-ILs was examined by TGA and DSC in the range of 298 to 800 K. The TGA curves of Figure 2 show several pieces of evidence. First, aa-ENIL materials present some water absorbed (~6% in weight) which needs to be removed in the degasification stage prior to CO_2 capture experiments. The high hygroscopic character of these aa-ILs was previously reported.[57] The thermal stabilities of these three aa-ILs are quite similar, starting to decompose at about 450 K, and at 560 K less than 2% of the residual weight is remaining. These values can be compared with those of typical ILs designed for CO_2 chemical absorption. Starting with carboxylate family ILs, [bmim][acetate] presents a decomposition temperature of almost 473 K,[39] clearly lower than the aa-ILs one. If we now compare an IL specifically designed for the CO_2 chemical capture such as $[P_{666,14}][2CNPyr]$, the decomposition temperature is 573 K,[43] which is close to those of aa-ILs presented in this work. Finally, the pattern decomposition between neat and encapsulated IL is quite similar. Moreover, considering the very low decomposition of the C_{Cap} support in this temperature range (stable until 800 K), the mass loss of aa-ENIL in TGA curves is mainly attributed to IL degradation. Thus, the aa-ENIL is confirmed as thermally stable under the CO_2 capture and regeneration conditions used in this study.

Figure 2 also reports the DSC results of the three aa-ILs showing endothermic peaks (red line), assigned to water (<373 K), subsequently the amino-acid-based anion (~450 K), and finally the $[Bmim]^+$ cation (~510 K). This result is endorsed for the three aa-ILs used, and it is consistent with previous TGA observations and the difference in molar mass of the counterions.

FTIR Analysis of CO_2 Absorption on Neat aa-IL. ATR-FTIR experiments were carried out in a Golden Gate gas−liquid reactor to analyze the CO_2 absorption in neat aa-IL ([Bmim][MET]) at 298 K and a CO_2 partial pressure of 5 bar. The exact mechanism of CO_2 absorption in aa-ILs is still under discussion, but in summary a zwitterion mechanism similar to alkanolamines can be expected.[45] Scheme 1 shows the global reaction proposed for [Bmim][MET], where the CO_2 molecule is incorporated next to the amine group of the anion to form a carbamate and a protonated amine, giving as a result a 2:1 stoichiometry. Figure 3 compares the experimental and calculated infrared spectra of the neat and after-CO_2-exposure spectra of [Bmim][MET] aa-IL ([Bmim][GLY] and [Bmim][PRO] spectra are shown in Figure S1 and Figure S2 of Supporting Information). The characteristic bands of aa-ILs are depicted in

DOI: 10.1021/acssuschemeng.8b02797
ACS Sustainable Chem. Eng. 2018, 6, 14178−14187

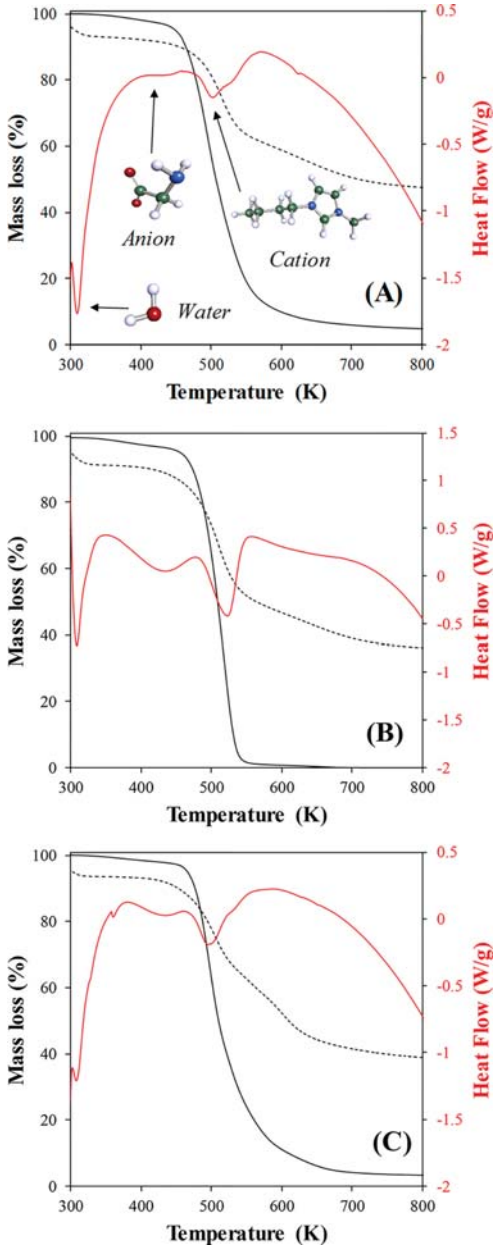

Figure 2. TGA of neat aa-IL and aa-ENIL (black solid and dash lines) and DSC (red solid line) curves of (A) [Bmim][GLY], (B) [Bmim][PRO], and (C) [Bmim][MET] under a nitrogen atmosphere with a heating rate of 10 K/min.

the spectra (black line of Figure 3), obtaining peaks at[29,58,59] (i) 3400 cm^{-1} corresponding to both N−H stretching in the amino acid [MET] of the anion and O−H stretching of water present in the sample (peak 1), since this analysis was carried out without a prior outgassed step due to the aa-IL solid formation; (ii) a 3200−3000 cm^{-1} band ascribed to the stretching vibration of saturated C−H groups belonging to the cation and anion of the aa-IL (peak 1); (iii) a 1750−1600 cm^{-1} band assigned to the C═O stretching vibration carboxylate group and N−H bending in amine (peak 2); (iv) a 1300 cm^{-1} band corresponding to the alkyl chain of the anion (peak 3); and (v) 700 cm^{-1} assigned to protons of the cation ring (peak 4).

Scheme 1. Structure of the Chemical Species Involved in the Chemical Absorption of CO_2 in [Bmim][MET]

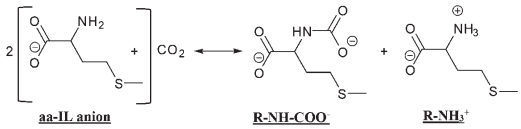

These signals are in good agreement with those calculated by the DFT method. Figure 3B shows the theoretical spectra of neat [Bmim][MET] and the complex with CO_2, with the appearance of new peaks after CO_2 exposure (marked peaks 1 to 4). The main theoretical peak is the 1800 cm^{-1} assigned to the carboxylate group incorporated in the anion, which experimentally is translated into the widening of the band around 1800−1600 cm^{-1}. Moreover, a decrease in the peak assigned to $-NH_2$ (3400 cm^{-1}) is also observed when CO_2 is incorporated due to a shielding of this amine group. Therefore, it can be concluded that both FTIR measurements and DFT calculations support the proposed mechanism.

Gravimetric Analysis of CO_2 Capture by aa-ENIL Materials. Regarding the sorption behavior of the neat and encapsulated aa-IL, Figure 4 shows the CO_2 kinetic sorption curves recorded for the neat and encapsulated [Bmim][MET] at 301.5 K and 1 bar of CO_2 partial pressure, using a similar sorbent sample mass (∼150 mg). The CO_2 sorption rate is drastically enhanced using the amino-acid-derived ENIL material, since these ILs turned solid when the CO_2 was absorbed. Under these experimental conditions (where no stirring is present, unlike previous experimental studies,[25,26] where the experiments were carried out under continuous stirring which allows quantifying the CO_2 absorption on the neat aa-ILs), the initial CO_2 absorption leads to the formation of a crust in the IL surface that makes unfeasible the saturation of the sample. This methodology of IL encapsulation not only enhances the mass transport properties of the neat IL but also lets us use ILs that would not reach the thermodynamic equilibrium under reasonable conditions due to the kinetic impediments. This huge improvement is due to the large increase of the contact surface between the gas phase and the aa-IL, upon dispersion of the absorbent in submicro-drops using aa-ENIL system.

The thermodynamics of the CO_2 capture in the three aa-ENIL materials was characterized by gravimetry. Figure 5 compares the CO_2 sorption isotherm of these encapsulated aa-ILs at 303, 318, and 333 K and CO_2 partial pressures from 0.3 to 20 bar, defining the sorption capacity as moles of CO_2 per mole of neat IL (z_{CO_2}). The shape of the nine curves shows the characteristic behavior of chemical sorption. At CO_2 partial pressures below 1 bar, the observed high initial slope is due to the chemisorption of CO_2 in aa-ENIL material (almost no physical sorption at low pressures), whereas at higher pressures, the CO_2 uptake is governed by the less thermodynamically favored physical sorption phenomena. Similar behavior was reported for other CO_2−IL systems that present chemical reaction.[39,43] The

DOI: 10.1021/acssuschemeng.8b02797
ACS Sustainable Chem. Eng. 2018, 6, 14178−14187

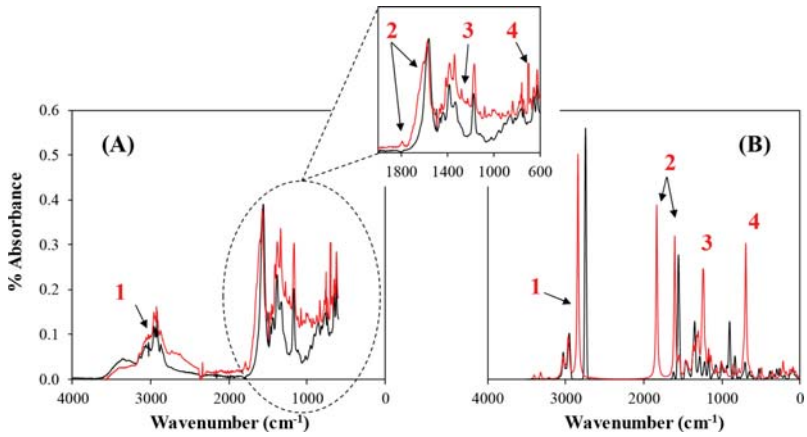

Figure 3. (A) Infrared spectra (FTIR) of [Bmim][MET] before (black line) and after (red line) CO_2 absorption at 298 K and 5 bar of CO_2 partial pressure and (B) theoretical spectra obtained with DFT calculations using the neat IL (black line) and a complex with CO_2.

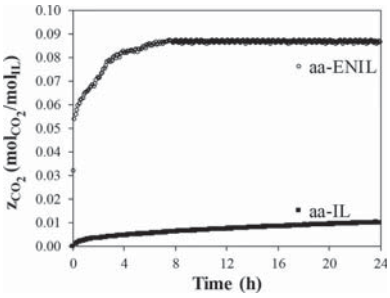

Figure 4. Kinetic curves of CO_2 uptake in neat aa-ILs and aa-ENIL based material at 301.5 K and p_{CO_2} = 0.3 bar, using [Bmim][MET].

obtained CO_2 isotherms determined by gravimetric techniques confirmed that the CO_2 solubility increases when decreasing the temperature and increasing the pressure for all the aa-ENIL materials studied. Regarding the structure of the anion, results show that the solubility of the CO_2 in the aa-ENIL containing $[Bmim]^+$ as a common cation follows the subsequent trend $[GLY]^- > [PRO]^- > [MET]^-$, being possible to achieve a maximum molar fraction of uptake CO_2 corresponding to stoichiometric, 0.53, 0.52, and 0.50, respectively at 303 K and 20 bar. The comparison of the measured uptake with the previously reported values for CO_2 in aa-ILs[26] shows that our data are in the range of the available published data by Sistla et al. where z_{CO_2} values between 0.42 and 0.62 for these aa-ILs at 10 bar are slightly lower since the temperature used was 298 K.

Thermodynamic Analysis of CO_2 Capture by aa-ENIL Materials. In order to analyze the physical and chemical absorption contributions to CO_2 capture by aa-ILs, a chemical equilibrium constant (K_{eq}) through eq 2, considering the 2:1 stoichiometry of the proposed reaction (Scheme 1), can be defined:

$$K_{eq} = \frac{X_{R-NH-COO^-} \cdot X_{R-NH_3^+}}{X_{aa-IL}^2 \cdot X_{CO_2}} \quad (2)$$

where $X_{R-NH-COO^-}$ and $X_{R-NH_3^+}$ are the molar fractions of the chemical absorbed CO_2 and the protonated amine, X_{aa-IL} is the molar fraction of aa-IL, and X_{CO_2} is the amount of CO_2 physically dissolved, which can be calculated through Henry's law constant (H) of eq 3:

$$X_{CO_2} = \frac{P_{CO_2}}{H} \quad (3)$$

From eq 2 and eq 3, the total amount of CO_2 captured corresponds to the sum of the chemical and physical contributions ($X_{R-NH-COO^-}$ and X_{CO_2}). Isotherms in Figure 5 have been adjusted to these equations (red lines) to obtain values of K_{eq} and H, collected in Table 3.

Attending to results from Table 3, it can be observed that the chemical reaction constant (K_{eq}), which informs us about the chemical contribution in the absorption of CO_2, is controlling the operation and follows the same order as the CO_2 uptake ($[GLY]^- > [PRO]^- > [MET]^-$). On the other hand, the high values of the Henry constant (H) inform about the low physical control of these aa-ILs. Comparing these two equilibrium constants, the physical contribution (determined by H) is smaller than the chemical one (determined by K_{eq}), never reaching more than 10% of the total uptake. Attending to the quantitative results shown in Table 3, the H values are in the range of 112 to 139 (bar) at 303 K, [Bmim][MET] being the most favored. However, [Bmim][MET] has the lowest experimental CO_2 uptake, due to the chemical contribution (K_{eq}) of 2.40 being the lowest, compared to 7.65 and 9.25 for [Bmim][PRO] and [Bmim][GLY], respectively. Both values (K_{eq} and H) are close to those reported for ILs with an aprotic heterocyclic anion (AHA-ILs),[43] which have specifically been proposed for CO_2 capture because they present efficient CO_2 absorption but are less energy demanding in the regeneration stage.

Experimentally, the results at 1 bar showed a decrease of z_{CO_2} from 0.13 to 0.07 at 303 and 333 K, respectively, for [Bmim][MET]. Therefore, an increase in the temperature implies an unfavorable effect on the thermodynamics of CO_2 capture by aa-ENILs.

Figure 6 shows the temperature effect on the K_{eq} and H in the CO_2 and aa-IL encapsulated systems. An increase in the operating temperature displaces the chemical equilibrium toward the reactant (aa-IL), reducing the amount of CO_2 chemically

DOI: 10.1021/acssuschemeng.8b02797
ACS Sustainable Chem. Eng. 2018, 6, 14178−14187

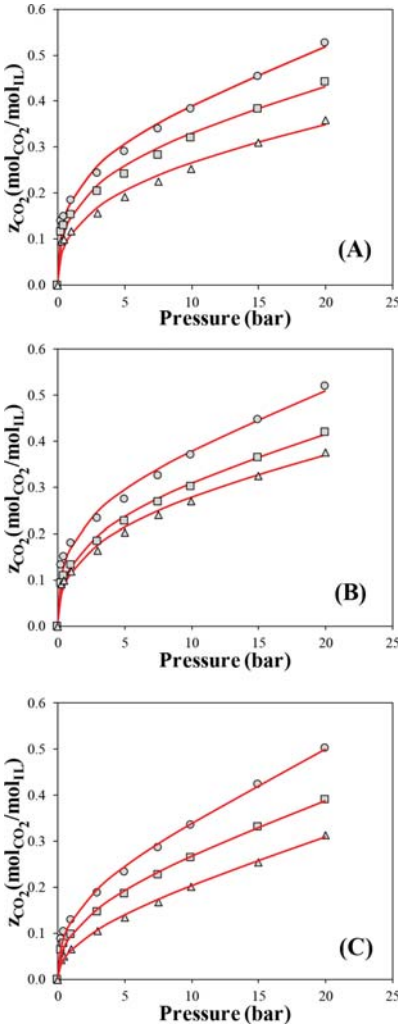

Figure 5. CO_2 isotherms of aa-ENIL based on (A) [Bmim][GLY], (B) [Bmim][PRO], and (C) [Bmim][MET] at (●) 303, (■) 318, and (▲) 333 K. The red line corresponds to the proposed chemical capture model.

bonded. Eq 2 reproduces the temperature effect adequately, since increasing the temperature makes the CO_2 capture lower, i.e., the K_{eq} of [Bmim][GLY] moves from 9.25 at 303 K to 4.82 at 333 K in good agreement with typical exothermic reactions reported in CO_2 capture with ILs.[43] On the other hand, analyzing the physical contribution (H values), an increase of the operating temperature decreases the amount of dissolved CO_2 (higher H at higher T), as expected for the physical absorption of a gas by an IL.

Reaction enthalpies can be determined from the temperature-dependence of the reaction equilibrium constants through a Van't Hoff relationship. The close linearity of Figure 6 indicates a good thermodynamic consistency of the model, proving correct the initial 2:1 stoichiometry guess. The isotherm-derived values of reaction enthalpies −16.3, −19.2, and −34.4 kJ·mol^{-1} of CO_2 are similar or even slightly lower than those reported for AHA-ILs (−20 to −60 kJ·mol^{-1}), solvents specifically designed to obtain less exothermic CO_2+IL reaction, with the aim of decreasing the energy consumed in the regeneration stage.[43,60] In sum, aa-ILs present relatively high CO_2 absorption capacities and low energy-demanding solvent regeneration, added to their advantages of low cost, abundant availability, thermal stability, and nontoxic biodegradability, making them promising alternatives to carboxylate-based ILs in CO_2 capture.

CONCLUSIONS

Encapsulated amino acid ionic liquids (aa-ENIL) are proposed as promising materials in CO_2 capture for solving the problems that the neat aa-ILs present (very viscous and solid formation when reacting with CO_2). Characterization of aa-ENIL by various techniques shows that this material is composed of spherical microparticles with high aa-IL content (60% in weight) and high thermal stability (more than 400 K). ATR-FTIR analysis results provided good support for the proposed CO_2 absorption mechanism with the aa-ILs used, showing apparent chemical stoichiometry of absorbed CO_2. Gravimetric experiments of CO_2 capture by neat aa-ILs show the inconvenience of long CO_2 saturation times (even not saturation) due to the formation of crusts when reacting with CO_2. When the aa-ENILs were used, they revealed a dramatic increase in the CO_2 absorption rates when encapsulated aa-IL was used compared to neat fluid, maintaining the high absorption capacity of the aa-IL as a chemical absorbent. The anions $[GLY]^-$ and $[MET]^-$ showed similar and the highest CO_2 sorption capacity (almost 0.035 g/g$_{IL}$ at 1 bar of CO_2 partial pressure), whereas the $[PRO]^-$ anion presented a lower one (0.020 g/g$_{IL}$ at 1 bar of CO_2 partial pressure). The estimated reaction enthalpies between CO_2 and aa-ILs are remarkably low (from −16 to

Table 3. Physical and Chemical Equilibrium Constants (H and K_{eq}), Reaction Enthalpy (ΔH_r), and Solubility Results for CO_2 Capture on the Different aa-ENIL Materials

ILs	T (K)	K_{eq}	H (bar)	R^2	ΔH_r (kJ/mol)	z_{CO_2}[a] (mol$_{CO2}$/mol$_{IL}$)	g$_{CO_2}$/g$_{IL}$[a]	q_e[a] (mmol/g$_{IL}$)
[Bmim][GLY]	303	9.25	139	0.994	−19.16	0.19	0.038	0.864
	318	7.28	195	0.989		0.15	0.032	0.727
	333	4.82	277	0.984		0.12	0.024	0.545
[Bmim][PRO]	303	7.65	137	0.991	−16.30	0.18	0.031	0.705
	318	4.70	186	0.995		0.13	0.023	0.523
	333	4.50	236	0.992		0.12	0.021	0.477
[Bmim][MET]	303	2.40	112	0.997	−34.37	0.13	0.020	0.455
	318	1.69	148	0.998		0.10	0.015	0.341
	333	0.69	156	0.998		0.07	0.010	0.227

[a]Calculated at p_{CO_2} = 1 bar.

DOI: 10.1021/acssuschemeng.8b02797
ACS Sustainable Chem. Eng. 2018, 6, 14178−14187

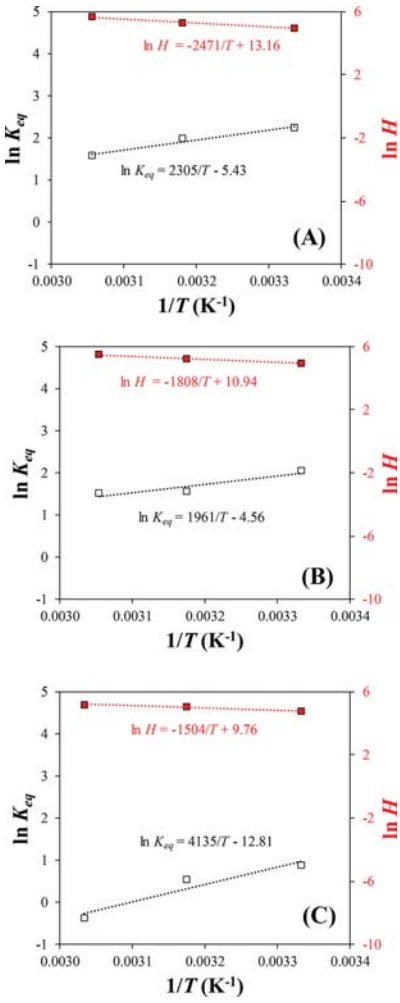

Figure 6. Henry constant (■, H) and chemical equilibrium constant (□, K_{eq}) of CO_2 capture on aa-ENIL based on (A) [Bmim][GLY], (B) [Bmim][PRO], and (C) [Bmim][MET].

−35 kJ·mol^{-1}), favoring the reaction reversibility and the sorbent regeneration under mild operating conditions. Therefore, aa-ENILs are found to be promising materials to be used in CO_2 capture technologies, presenting high CO_2 sorption capacities and rates, low-energy demanding regeneration, and high stability, allowing us to use ILs derived from natural amino acids, which present low cost, abundant availability, and nontoxic biodegradability.

■ ASSOCIATED CONTENT

Supporting Information

The Supporting Information is available free of charge on the ACS Publications website at DOI: 10.1021/acssuschemeng.8b02797.

Tabulated data for the NMR analysis: 500 MHz ^{1}H NMR in D_2O [δ/ppm (multiplicity, number of protons and assignment)] of the three aa-ILs; infrared spectra of two aa-ILs before and after CO_2 absorption (PDF)

■ AUTHOR INFORMATION

Corresponding Author

*E-mail: pepe.palomar@uam.es.

ORCID

Rubén Santiago: 0000-0002-6877-9001
Daniel Moreno: 0000-0001-9197-9936
Noelia Alonso-Morales: 0000-0001-5855-7336
José Palomar: 0000-0003-4304-0515

Notes

The authors declare no competing financial interest.

■ ACKNOWLEDGMENTS

The authors are grateful to Comunidad de Madrid (project S2013-MAE-2800) and Ministerio de Economía y Competitividad of Spain (project CTQ2017-89441-R) for financial support and Centro de Computación Científica de la Universidad Autónoma de Madrid for computational facilities.

■ REFERENCES

(1) Mondal, M. K.; Balsora, H. K.; Varshney, P. Progress and trends in CO_2 capture/separation technologies: A review. *Energy* **2012**, *46* (1), 431−441.

(2) D'Alessandro, D. M.; Smit, B.; Long, J. R. Carbon Dioxide Capture: Prospects for New Materials. *Angew. Chem., Int. Ed.* **2010**, *49* (35), 6058−6082.

(3) Yu, C.-H.; Huang, C.-H.; Tan, C.-S. A Review of CO_2 Capture by Absorption and Adsorption. *Aerosol Air Qual. Res.* **2012**, *12* (5), 745−769.

(4) Rochelle, G. T. Conventional amine scrubbing for CO_2 capture. In *Absorption-Based Post-Combustion Capture of Carbon Dioxide*, Feron, P. H. M., Ed.; Woodhead Publishing, 2016; pp 35−67, DOI: 10.1016/B978-0-08-100514-9.00003-2.

(5) Ferrara, G.; Lanzini, A.; Leone, P.; Ho, M. T.; Wiley, D. E. Exergetic and exergoeconomic analysis of post-combustion CO_2 capture using MEA-solvent chemical absorption. *Energy* **2017**, *130*, 113−128.

(6) Jones, C. W.; Prausnitz, J. M. CO_2 Capture from Dilute Gases as a Component of Modern Global Carbon Management. *Annu. Rev. Chem. Biomol. Eng.* **2011**, *2*, 31−52.

(7) Papatryfon, X. L.; Heliopoulos, N. S.; Molchan, I. S.; Zubeir, L. F.; Bezemer, N. D.; Arfanis, M. K.; Kontos, A. G.; Likodimos, V.; Iliev, B.; Romanos, G. E.; Falaras, P.; Stamatakis, K.; Beltsios, K. G.; Kroon, M. C.; Thompson, G. E.; Kloeckner, J.; Schubert, T. J. S. CO_2 Capture Efficiency, Corrosion Properties, and Ecotoxicity Evaluation of Amine Solutions Involving Newly Synthesized Ionic Liquids. *Ind. Eng. Chem. Res.* **2014**, *53* (30), 12083−12102.

(8) Wang, M.; Lawal, A.; Stephenson, P.; Sidders, J.; Ramshaw, C. Post-combustion CO_2 capture with chemical absorption: A state-of-the-art review. *Chem. Eng. Res. Des.* **2011**, *89* (9), 1609−1624.

(9) Attalla, M. I. *Recent Advances in Post-Combustion CO_2 Capture Chemistry*; American Chemical Society, 2012; Vol. *1097*, DOI: 10.1021/bk-2012-1097.

(10) Liu, H.; Huang, J.; Pendleton, P. Tailoring Ionic Liquids for Post-Combustion CO_2 Capture. *Recent Advances in Post-Combustion CO_2 Capture Chemistry*; American Chemical Society, 2012; Vol. *1097*, pp 153−175, DOI: 10.1021/bk-2012-1097.ch008.

(11) Amde, M.; Liu, J.-F.; Pang, L. Environmental Application, Fate, Effects, and Concerns of Ionic Liquids: A Review. *Environ. Sci. Technol.* **2015**, *49* (21), 12611−12627.

(12) Wu, C.; Senftle, T. P.; Schneider, W. F. First-principles-guided design of ionic liquids for CO_2 capture. *Phys. Chem. Chem. Phys.* **2012**, *14* (38), 13163−13170.

(13) Cui, G.; Wang, J.; Zhang, S. Active chemisorption sites in functionalized ionic liquids for carbon capture. *Chem. Soc. Rev.* **2016**, *45* (15), 4307−4339.
(14) Carvalho, P. J.; Kurnia, K. A.; Coutinho, J. A. P. Dispelling some myths about the CO_2 solubility in ionic liquids. *Phys. Chem. Chem. Phys.* **2016**, *18* (22), 14757−14771.
(15) Mjalli, F. S. Novel amino acids based ionic liquids analogues: Acidic and basic amino acids. *J. Taiwan Inst. Chem. Eng.* **2016**, *61*, 64−74.
(16) Guzman, J.; Ortega-Guevara, C.; Garcia de Leon, R.; Martinez-Palou, R. Absorption of CO_2 with Amino Acid-Based Ionic Liquids and Corresponding Amino Acid Precursors. *Chem. Eng. Technol.* **2017**, *40* (12), 2339−2345.
(17) Ohno, H.; Fukumoto, K. Amino Acid Ionic Liquids. *Acc. Chem. Res.* **2007**, *40* (11), 1122−1129.
(18) Kagimoto, J.; Fukumoto, K.; Ohno, H. Effect of tetrabutylphosphonium cation on the physico-chemical properties of amino-acid ionic liquids. *Chem. Commun.* **2006**, *21*, 2254−2256.
(19) Kirchhecker, S.; Esposito, D. Amino acid based ionic liquids: A green and sustainable perspective. *Curr. Opin. Green Sustain. Chem.* **2016**, *2*, 28−33.
(20) Chen, F.-F.; Huang, K.; Fan, J.-P.; Tao, D.-J. Chemical solvent in chemical solvent: A class of hybrid materials for effective capture of CO_2. *AIChE J.* **2018**, *64* (2), 632−639.
(21) Chen, F.-F.; Huang, K.; Zhou, Y.; Tian, Z.-Q.; Zhu, X.; Tao, D.-J.; Jiang, D.; Dai, S. Multi-Molar Absorption of CO_2 by the Activation of Carboxylate Groups in Amino Acid Ionic Liquids. *Angew. Chem., Int. Ed.* **2016**, *55* (25), 7166−7170.
(22) Sharma, P.; Park, S. D.; Park, K. T.; Nam, S. C.; Jeong, S. K.; Yoon, Y. I.; Baek, I. H. Solubility of carbon dioxide in amine-functionalized ionic liquids: Role of the anions. *Chem. Eng. J.* **2012**, *193*−*194*, 267−275.
(23) Vijayraghavan, R.; Pas, S. J.; Izgorodina, E. I.; MacFarlane, D. R. Diamino protic ionic liquids for CO_2 capture. *Phys. Chem. Chem. Phys.* **2013**, *15* (46), 19994−19999.
(24) Saravanamurugan, S.; Kunov-Kruse, A. J.; Fehrmann, R.; Riisager, A. Amine-functionalized amino acid-based ionic liquids as efficient and high-capacity absorbents for CO_2. *ChemSusChem* **2014**, *7* (3), 897−902.
(25) Sistla, Y. S.; Khanna, A. Carbon dioxide absorption studies using amine-functionalized ionic liquids. *J. Ind. Eng. Chem.* **2014**, *20* (4), 2497−2509.
(26) Sistla, Y. S.; Khanna, A. CO_2 absorption studies in amino acid-anion based ionic liquids. *Chem. Eng. J.* **2015**, *273*, 268−276.
(27) Galán Sánchez, L. M.; Meindersma, G. W.; de Haan, A. B. Kinetics of absorption of CO_2 in amino-functionalized ionic liquids. *Chem. Eng. J.* **2011**, *166* (3), 1104−1115.
(28) Goodrich, B. F.; de la Fuente, J. C.; Gurkan, B. E.; Lopez, Z. K.; Price, E. A.; Huang, Y.; Brennecke, J. F. Effect of Water and Temperature on Absorption of CO_2 by Amine-Functionalized Anion-Tethered Ionic Liquids. *J. Phys. Chem. B* **2011**, *115* (29), 9140−9150.
(29) Hiremath, V.; Jadhav, A. H.; Lee, H.; Kwon, S.; Seo, J. G. Highly reversible CO_2 capture using amino acid functionalized ionic liquids immobilized on mesoporous silica. *Chem. Eng. J.* **2016**, *287*, 602−617.
(30) Mehnert, C. P.; Cook, R. A.; Dispenziere, N. C.; Afeworki, M. Supported Ionic Liquid Catalysis − A New Concept for Homogeneous Hydroformylation Catalysis. *J. Am. Chem. Soc.* **2002**, *124* (44), 12932−12933.
(31) Romanos, G. E.; Schulz, P. S.; Bahlmann, M.; Wasserscheid, P.; Sapalidis, A.; Katsaros, F. K.; Athanasekou, C. P.; Beltsios, K.; Kanellopoulos, N. K. CO_2 Capture by Novel Supported Ionic Liquid Phase Systems Consisting of Silica Nanoparticles Encapsulating Amine-Functionalized Ionic Liquids. *J. Phys. Chem. C* **2014**, *118* (42), 24437−24451.
(32) Zhang, S.; Zhang, J.; Zhang, Y.; Deng, Y. Nanoconfined Ionic Liquids. *Chem. Rev.* **2017**, *117* (10), 6755−6833.
(33) Palomar, J.; Lemus, J.; Alonso-Morales, N.; Bedia, J.; Gilarranz, M. A.; Rodriguez, J. J. Encapsulated ionic liquids (ENILs): from continuous to discrete liquid phase. *Chem. Commun.* **2012**, *48* (80), 10046−10048.
(34) Minami, H.; Fukaumi, H.; Okubo, M.; Suzuki, T. Preparation of ionic liquid-encapsulated polymer particles. *Colloid Polym. Sci.* **2013**, *291* (1), 45−51.
(35) Chen, D.-x.; OuYang, X.-k.; Wang, Y.-g.; Yang, L.-y.; Wu, K.-j.; He, C.-h. Adsorption of caprolactam from aqueous solution by novel polysulfone microcapsules containing [Bmim][PF_6]. *Colloids Surf., A* **2014**, *441*, 72−76.
(36) Du, Q.; Ma, T.; Fu, C.; Liu, T.; Huang, Z.; Ren, J.; Shao, H.; Xu, K.; Tang, F.; Meng, X. Encapsulating Ionic Liquid and Fe_3O_4 Nanoparticles in Gelatin Microcapsules as Microwave Susceptible Agent for MR Imaging-guided Tumor Thermotherapy. *ACS Appl. Mater. Interfaces* **2015**, *7* (24), 13612−13619.
(37) Stolaroff, J. K.; Ye, C.; Oakdale, J. S.; Baker, S. E.; Smith, W. L.; Nguyen, D. T.; Spadaccini, C. M.; Aines, R. D. Microencapsulation of advanced solvents for carbon capture. *Faraday Discuss.* **2016**, *192* (0), 271−281.
(38) Lemus, J.; Bedia, J.; Moya, C.; Alonso-Morales, N.; Gilarranz, M. A.; Palomar, J.; Rodriguez, J. J. Ammonia capture from the gas phase by encapsulated ionic liquids (ENILs). *RSC Adv.* **2016**, *6* (66), 61650−61660.
(39) Moya, C.; Alonso-Morales, N.; Gilarranz, M. A.; Rodriguez, J. J.; Palomar, J. Encapsulated Ionic Liquids for CO_2 Capture: Using 1-Butyl-methylimidazolium Acetate for Quick and Reversible CO_2 Chemical Absorption. *ChemPhysChem* **2016**, *17* (23), 3891−3899.
(40) Stolaroff, J. K.; Ye, C.; Nguyen, D. T.; Oakdale, J.; Knipe, J. M.; Baker, S. E. CO_2 Absorption Kinetics of Micro-encapsulated Ionic Liquids. *Energy Procedia* **2017**, *114*, 860−865.
(41) Kaviani, S.; Kolahchyan, S.; Hickenbottom, K. L.; Lopez, A. M.; Nejati, S. Enhanced solubility of carbon dioxide for encapsulated ionic liquids in polymeric materials. *Chem. Eng. J.* **2018**, *354*, 753−757.
(42) Lemus, J.; Da Silva, F. A. F.; Palomar, J.; Carvalho, P. J.; Coutinho, J. A. P. Solubility of carbon dioxide in encapsulated ionic liquids. *Sep. Purif. Technol.* **2018**, *196*, 41−46.
(43) Moya, C.; Alonso-Morales, N.; de Riva, J.; Morales-Collazo, O.; Brennecke, J. F.; Palomar, J. Encapsulation of Ionic Liquids with an Aprotic Heterocyclic Anion (AHA-IL) for CO_2 Capture: Preserving the Favorable Thermodynamics and Enhancing the Kinetics of Absorption. *J. Phys. Chem. B* **2018**, *122* (9), 2616−2626.
(44) Santiago, R.; Lemus, J.; Moreno, D.; Moya, C.; Larriba, M.; Alonso-Morales, N.; Gilarranz, M. A.; Rodríguez, J. J.; Palomar, J. From kinetics to equilibrium control in CO_2 capture columns using Encapsulated Ionic Liquids (ENILs). *Chem. Eng. J.* **2018**, *348*, 661−668.
(45) Yang, Q. W.; Wang, Z. P.; Bao, Z. B.; Zhang, Z. G.; Yang, Y. W.; Ren, Q. L.; Xing, H. B.; Dai, S. New Insights into CO_2 Absorption Mechanisms with Amino-Acid Ionic Liquids. *ChemSusChem* **2016**, *9* (8), 806−812.
(46) Alonso-Morales, N.; Gilarranz, M. A.; Palomar, J.; Lemus, J.; Heras, F.; Rodriguez, J. J. Preparation of hollow submicrocapsules with a mesoporous carbon shell. *Carbon* **2013**, *59*, 430−438.
(47) Alonso-Morales, N.; Ruiz-Garcia, C.; Palomar, J.; Heras, F.; Calvo, L.; Rodriguez, J. J.; Gilarranz, M. A. Hollow Nitrogen- or Boron-Doped Carbon Submicrospheres with a Porous Shell: Preparation and Application as Supports for Hydrodechlorination Catalysts. *Ind. Eng. Chem. Res.* **2017**, *56* (27), 7665−7674.
(48) Buchel, G.; Unger, K. K.; Matsumoto, A.; Tsutsumi, K. A novel pathway for synthesis of submicrometer-size solid core/mesoporous shell silica spheres. *Adv. Mater.* **1998**, *10* (13), 1036−1038.
(49) Stöber, W.; Fink, A.; Bohn, E. Controlled growth of monodisperse silica spheres in the micron size range. *J. Colloid Interface Sci.* **1968**, *26* (1), 62−69.
(50) Gonzalez-Miquel, M.; Bedia, J.; Palomar, J.; Rodriguez, F. Solubility and Diffusivity of CO_2 in [hxmim][NTf_2], [omim][NTf_2], and [dcmim][NTf_2] at T = (298.15, 308.15, and 323.15) K and Pressures up to 20 bar. *J. Chem. Eng. Data* **2014**, *59* (2), 212−217.

DOI: 10.1021/acssuschemeng.8b02797
ACS Sustainable Chem. Eng. 2018, 6, 14178−14187

(51) Moya, C.; Palomar, J.; Gonzalez-Miquel, M.; Bedia, J.; Rodriguez, F. Diffusion Coefficients of CO_2 in Ionic Liquids Estimated by Gravimetry. *Ind. Eng. Chem. Res.* **2014**, *53* (35), 13782−13789.
(52) Klamt, A. COnductor-like Screening MOdel for real solvents - A new approach to the quantitative calculation of solvation phenomena. *J. Phys. Chem.* **1995**, *99* (7), 2224−2235.
(53) Moreno, D.; Ferro, V. R.; de Riva, J.; Santiago, R.; Moya, C.; Larriba, M.; Palomar, J. Absorption refrigeration cycles based on ionic liquids: Refrigerant/absorbent selection by thermodynamic and process analysis. *Appl. Energy* **2018**, *213*, 179−194.
(54) Klamt, A.; Eckert, F.; Arlt, W. COSMO-RS: An Alternative to Simulation for Calculating Thermodynamic Properties of Liquid Mixtures. *Annu. Rev. Chem. Biomol. Eng.* **2010**, *1*, 101−122.
(55) Lee, B. S.; Lin, S. T. A priori prediction of the octanol-water partition coefficient (K-ow) of ionic liquids. *Fluid Phase Equilib.* **2014**, *363*, 233−238.
(56) Lemus, J.; Palomar, J.; Gilarranz, M. A.; Rodriguez, J. J. Characterization of Supported Ionic Liquid Phase (SILP) materials prepared from different supports. *Adsorption* **2011**, *17* (3), 561−571.
(57) Shaikh, A. R.; Karkhanechi, H.; Kamio, E.; Yoshioka, T.; Matsuyama, H. Quantum Mechanical and Molecular Dynamics Simulations of Dual-Amino-Acid Ionic Liquids for CO_2 Capture. *J. Phys. Chem. C* **2016**, *120* (49), 27734−27745.
(58) Balsamo, M.; Erto, A.; Lancia, A.; Totarella, G.; Montagnaro, F.; Turco, R. Post-combustion CO_2 capture: On the potentiality of amino acid ionic liquid as modifying agent of mesoporous solids. *Fuel* **2018**, *218*, 155−161.
(59) Danon, A.; Stair, P. C.; Weitz, E. FTIR Study of CO_2 Adsorption on Amine-Grafted SBA-15: Elucidation of Adsorbed Species. *J. Phys. Chem. C* **2011**, *115* (23), 11540−11549.
(60) Seo, S.; Quiroz-Guzman, M.; DeSilva, M. A.; Lee, T. B.; Huang, Y.; Goodrich, B. F.; Schneider, W. F.; Brennecke, J. F. Chemically Tunable Ionic Liquids with Aprotic Heterocyclic Anion (AHA) for CO_2 Capture. *J. Phys. Chem. B* **2014**, *118* (21), 5740−5751.

DOI: 10.1021/acssuschemeng.8b02797
ACS Sustainable Chem. Eng. 2018, 6, 14178−14187

Supporting information

Encapsulated Ionic Liquids to enable the practical application of amino acid-based Ionic Liquids in CO_2 capture

Rubén Santiago, Jesús Lemus, Cristian Moya, Daniel Moreno, Noelia Alonso-Morales and José Palomar*

Sección de Ingeniería Química. c/ Francisco Tomás y Valiente 7, Facultad de Ciencias. Universidad Autónoma de Madrid. 28049 Madrid. Spain.

*Corresponding author. E-mail: pepe.palomar@uam.es

Table of Contents

Table S1a……page S2

Table S1b……page S3

Table S1c……page S4

Figures S1 and S2……page S5

Number of pages: 5

Number of figures: 2

Number of tables: 3

Table S1a. 1-Butyl-3-methylimidazolium Prolinate [bmim][PRO]

500 MHz ^{1}H-NMR in D_2O [δ/ppm, (multiplicity, number of protons and assignment)]:

Cation [Bmim]$^{+}$:

1. Not appear in D_2O (s, 1H, ring N-**CH**-N),
2. 7.40 (d, 2H, ring N-**CH**-**CH**-N),
3. 4.14 (t, 2H, -**CH$_2$**-Nring),
4. 3.81 (s, 3H, **CH$_3$**-Nring),
5. 1.79 (m, 2H, -**CH$_2$**),
6. 1.36 (m, 2H, -**CH$_2$**),
7. 0.85 (t, 3H, -**CH$_3$**).

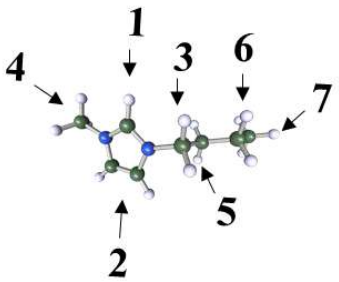

Anion [PRO]$^{-}$:

1. Not appear in D_2O (s, H, **NH**-CH- [PRO]),
2. 4.78 (m, 1H, -COO-**CH**-CH_2 [PRO]),
3. 3.68 (m, 2H, -NH-**CH$_2$**-CH_2 [PRO]),
4. 3.13 (m, 2H, -CH-**CH$_2$**-CH_2 [PRO]),
5. 2.92 (m, 2H, -CH_2-**CH$_2$**-CH_2 [PRO]),

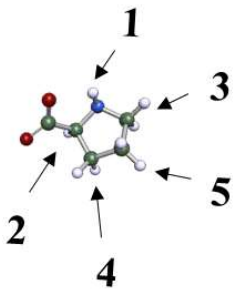

Table S1b. 1-Butyl-3-methylimidazolium Methioninate [bmim][MET]

500 MHz ^{1}H-NMR in D_2O [δ/ppm, (multiplicity, number of protons and assignment)]:

Cation [Bmim]$^{+}$:

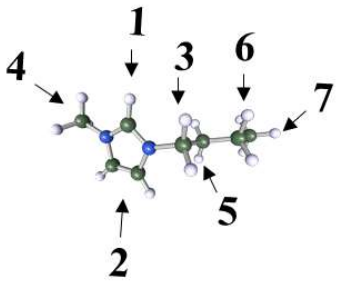

1. Not appear in D_2O (s, 1H, ring N-**CH**-N),
2. 7.40 (d, 2H, N-**CH**-**CH**-N),
3. 4.12 (t, 2H, -**CH$_2$**-Nring),
4. 3.82 (s, 3H, **CH$_3$**-Nring),
5. 1.79 (m, 2H, -**CH$_2$**),
6. 1.25 (m, 2H, -**CH$_2$**),
7. 0.86 (t, 3H, -**CH$_3$**).

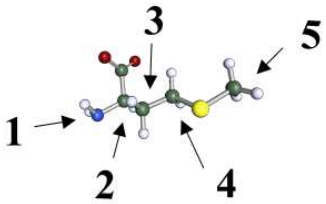

Anion [MET]$^{-}$:

1. Not appear in D_2O (s, 2H, **NH$_2$**-CH- [MET]),
2. 2.51 (t, 2H, -S-**CH$_2$**-CH_2 [MET]),
3. 2.16 (m, 2H, -S-CH_2-**CH$_2$** [MET]),
4. 2.05 (s, 3H, **CH$_3$**-S [MET]),
5. 1.90 (m, H, -CH_2-**CH**-NH_2 [MET]),

Table S1c. 1-Butyl-3-methylimidazolium Glycinate [bmim][GLY]

500 MHz ^{1}H-NMR in D_2O [δ/ppm, (multiplicity, number of protons and assignment)]:

Cation [Bmim]$^{+}$:

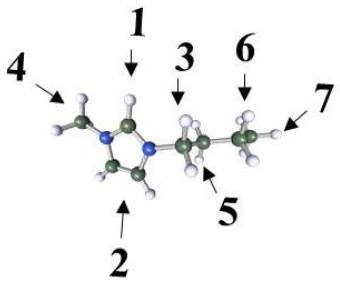

1. Not appear in D_2O (s, 1H, ring N-**CH**-N),
2. 7.40 (d, 2H, ring N-**CH**-**CH**-N),
3. 4.13 (t, 2H, -**CH$_2$**-Nring),
4. 3.81 (s, 3H, **CH$_3$**-Nring),
5. 1.78 (m, 2H, -**CH$_2$**),
6. 1.23 (m, 2H, -**CH$_2$**),
7. 0.83 (t, 3H, -**CH$_3$**).

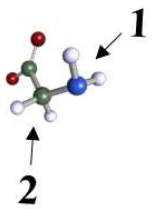

Anion [GLY]$^{-}$:

1. Not appear in D_2O (s, 2H, **NH$_2$**-CH$_2$- [GLY]),
2. 3.10 (s, 2H, NH$_2$-**CH$_2$**- [GLY]).

500 MHz ^{1}H-NMR experiments of neat aa-ILs were recorded on a Varian Unity 500 spectrometer, using a solution of the aa-IL and D_2O over 10 mmol.

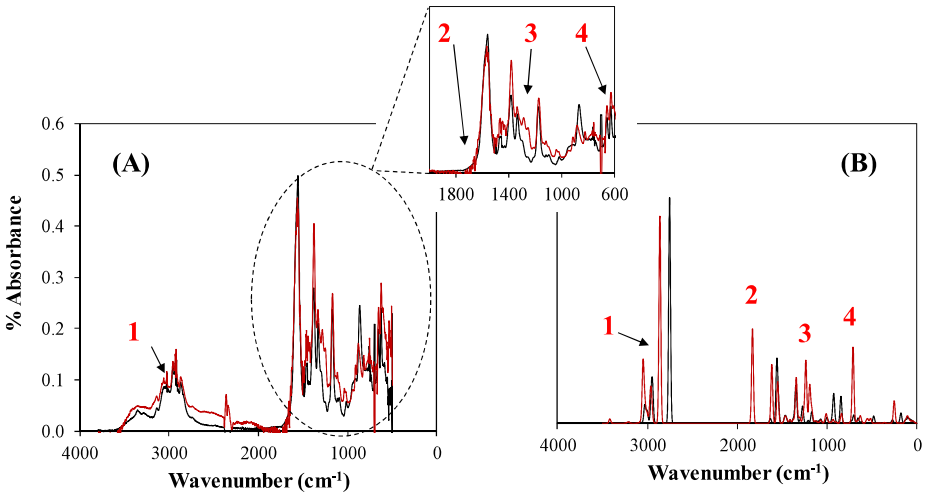

Figure S1. Infrared spectra (FTIR) of [Bmim][GLY] before (black line) and after (red line) CO_2 absorption a 298 K and 5 bar of partial pressure (**A**) and theoretical spectra obtained with Turbomole using the neat IL (black line) and a complex with CO_2 (**B**).

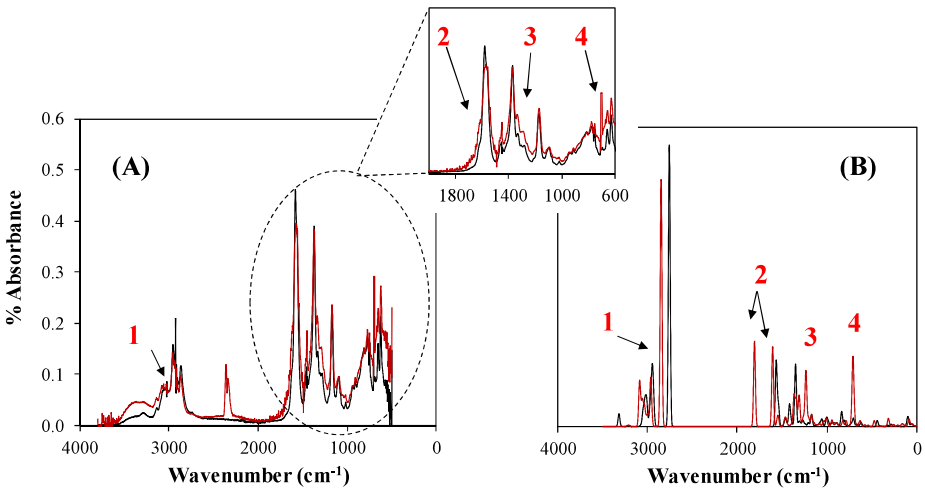

Figure S2. Infrared spectra (FTIR) of [Bmim][PRO] before (black line) and after (red line) CO_2 absorption a 298 K and 5 bar of partial pressure (**A**) and theoretical spectra obtained with Turbomole using the neat IL (black line) and a complex with CO_2 (**B**).

5.5 CO_2 capture by Supported Ionic Liquid Phase (SILP): Highlighting the role of the particle size

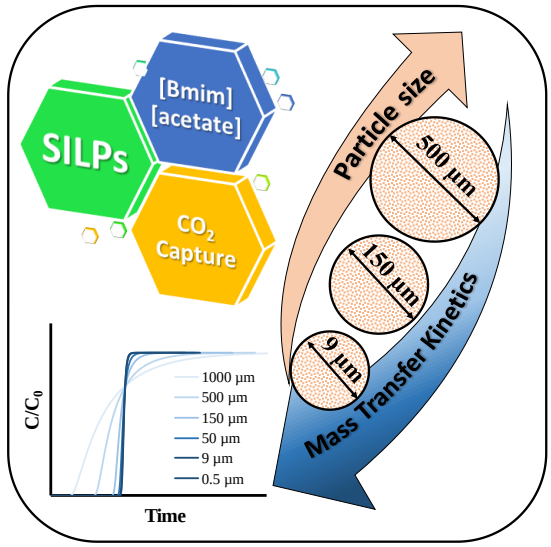

ACS Sustainable Chemistry & Engineering

Cite This: ACS Sustainable Chem. Eng. 2019, 7, 13089−13097

Research Article

pubs.acs.org/journal/ascecg

CO_2 Capture by Supported Ionic Liquid Phase: Highlighting the Role of the Particle Size

Ruben Santiago, Jesus Lemus, Daniel Hospital-Benito, Cristian Moya, Jorge Bedia, Noelia Alonso-Morales, Juan J. Rodriguez, and Jose Palomar*

Chemical Engineering Department, C/Francisco Tomás y Valiente 7, Universidad Autónoma de Madrid, 28049 Madrid, Spain

Supporting Information

ABSTRACT: CO_2 capture by fixed-bed sorption has been evaluated using Supported Ionic Liquid Phase (SILP) based on the ionic liquid 1-butyl-3-methylimidazolium acetate ([bmim][acetate]). The SILP sorbent was prepared with three remarkably different mean particle sizes and characterized by porous texture, morphology, thermal stability, and elemental composition. The thermodynamics and kinetics of the CO_2 capture process has been studied, testing the effects of SILP particle size, sorption temperature, gas flow rate, and CO_2 partial pressure. The CO_2 sorption isotherms at different temperatures were obtained by gravimetric measurements, revealing that the equilibrium sorption capacity is only due to the IL incorporated on the silica support of SILP. The experimental isotherms were successfully fitted to the Langmuir−Freundlich model. Fixed-bed experiments of CO_2 capture were carried out to evaluate the performance of the SILP sorbents at different operating conditions. All the breakthrough curves were well described by a linear driving force model. The obtained kinetic coefficients revealed that the CO_2 sorption rate in fixed-bed linearly increases when decreasing the SILP particle size and increasing the operating temperature. Higher CO_2 partial pressure in the inlet gas stream led to a faster mass transfer rate, affecting both the mass transfer driving force and kinetic coefficient. Aspen Adsorption simulator was successfully applied to model the fixed-bed operation, highlighting the role of the particle size on separation efficiency. Simulations results indicate that at very low CO_2 partial pressure chemical absorption is the controlling step, while increasing that partial pressure shifts the regime toward diffusion into the SILP. This methodology will allow designing CO_2 sorption systems based on SILPs that fulfill the separation requirements at given conditions (CO_2 partial pressure and temperature), minimizing the SILP needs by optimizing the particle size and type of IL.

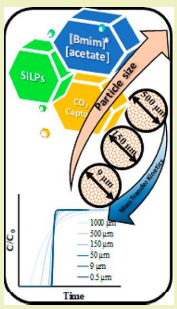

KEYWORDS: *CO_2 capture, Ionic liquids, SILP, Fixed-bed, Particle size, Kinetics*

INTRODUCTION

Concerns for climate change owing to anthropogenic emissions of carbon dioxide (CO_2) are now well recognized and have resulted in a number of initiatives to reduce CO_2 emissions.[1,2] In this sense, carbon capture and storage (CCS) technologies are considered a main strategy, due to their efficiency and relatively low cost.[3−5] Regarding physical absorption, high operating pressures are required, and solvents such as glyme mixtures (comprising Selexol solvent) are widely used.[6,7] However, these solvents present problems, such as high toxicity, corrosive nature, and high volatility resulting in high solvent losses and negative environmental impact.[8,9] On the other hand, in chemical absorption processes, amines are commonly used, but they are corrosive and suffer degradation, also resulting in high solvent losses, environmental impact, and considerable maintenance and operating costs.[10,11] In order to overcome these disadvantages, ionic liquids (ILs) have gained increased attention due to their unique properties, such as very low vapor pressure, good thermal and chemical stability, and high solvent capacity.[12−14] In CO_2 capture, ILs can be applied to uptake CO_2 by either physical[15] or chemical absorption.[16] It is widely reported that CO_2 possesses relatively high solubility in ILs.[17] More recently, it has been suggested that CO_2 capture by chemical absorption seems to be the most convenient strategy for the CO_2 retention with ILs, being acetate-based ILs[18] or Aprotic Heterocyclic Anions-based ILs (AHA)[19] widely used. Nevertheless, they still present some drawbacks mainly due to their limited transport properties. This technical limitation for the practical application of ILs in CO_2 capture is a consequence of their high viscosity (compared with other solvents as amine solutions),[20] which can even increases in some cases upon reaction with CO_2.[21] In fact, some recent works demonstrate that mass transfer controls the rate of CO_2 capture based on ILs.[20,22,23]

Therefore, novel strategies using ILs are needed in order to overcome those limitations. In this scenario, Supported Ionic Liquid Phase (SILP), consisting of the immobilization of ILs on a solid support, has been proposed as a potential solution.[24] SILP materials are commonly prepared by spreading a film of IL onto the surface of a solid support, mostly consisting of materials with high specific surface area, like activated carbon, zeolite, or silica.[25] It has been demonstrated that the IL immobilization on a porous support drastically increases the gas/liquid contact area, leading to much faster sorption than

Received: April 24, 2019
Revised: June 24, 2019
Published: June 27, 2019

DOI: 10.1021/acssuschemeng.9b02277
ACS Sustainable Chem. Eng. 2019, 7, 13089−13097

with the bulk ionic liquid.[26,27] In addition, the negligible vapor pressure, large liquid range, and thermal stability of ILs ensure that the solvent is retained on the support in its fluid state even at elevated temperatures; this makes SILP highly suitable for gas separation continuous processes.[28] Recently, our group developed the Encapsulated Ionic Liquids (ENILs), which consist of uploading a large amount of IL inside carbonaceous submicrocapsules,[29] being tested in the capture of different gases (NH_3 or CO_2).[30−34] It was demonstrated that it is possible to overcome the mass transfer limitations (that typically control the absorption rates) in neat ILs by increasing the gas−liquid contact area using ENIL or SILP materials.[30−34] Consequently, in the last years, huge efforts have been addressed to develop novel sorbents based on ILs, which could be used to mitigate the world's CO_2 emissions.

On the other hand, the development of CO_2 capture processes by fixed-bed adsorption has also attracted the attention of the scientific community, with a wide variety of proposed adsorbents (active carbon, silica, or zeolites, among others).[35−38] In such studies, the particle size of the adsorbent has been a key issue, determining the sorption rate and, consequently, the adsorbent need and the separation efficiency.[39−42] However, to the best of our knowledge, no systematic studies dealing with the CO_2 capture with SILPs of different support particle sizes have been published. In addition, the modeling of the thermodynamics and kinetics of CO_2 sorption in SILPs has still not been explored. This modeling would allow designing the operation by process simulation, which is a key framework for the development of new separation processes based on ILs.[20,32] In this context, Aspen Adsorption (implemented in the Aspen ONE suite package) has been successfully used to model experimental breakthrough curves of different adsorbents and, consequently, to perform process analysis to estimate adsorbent loads, column dimensions, operating time, used bed fraction, etc.[43−45]

In this work, the experimental sorption isotherms and breakthrough curves of CO_2 in SILP material were obtained at different operating conditions. Three SILP sorbents have been tested, all based on the IL 1-butyl-3-methylimidazolium acetate supported on silica but with remarkably different particle sizes (difference of 3 orders of magnitude). They contained almost the same IL loading (~40%w/w) and were characterized by N_2 adsorption/desorption at 77 K, SEM microscopy, thermal stability, and elemental analysis. The aim of the study is to evaluate and describe the influence of the particle size in both the thermodynamics and kinetics of the process at different operating conditions. The corresponding equilibrium isotherms were obtained by a gravimetric procedure using a magnetic suspension balance at different sorption temperatures (299−333 K) within a CO_2 partial pressures range of 0.3 to 20 bar. The isotherms were well described by the Langmuir−Freundlich model. Then, fixed-bed CO_2 capture experiments using the SILP sorbents−with the three different particle sizes−were carried out at different temperatures, gas flow rates, and CO_2 partial pressures. The experimental breakthrough curves were successfully described by a linear driving force model (LDF) with a lumped resistance, which allows estimating the overall kinetic coefficient (k_{MTC}). A relationship of k_{MTC} with the particle radius, sorption temperature, and CO_2 partial pressure was found to describe the SILP performance in fixed-bed CO_2 capture. Finally, the resulting thermodynamic and kinetic models were used in Aspen Adsorption to simulate the CO_2 capture operation based on SILP material, allowing for evaluation of the remarkable effect of the particle size on the breakthrough curves, depending on the CO_2 partial pressure in the feed stream.

EXPERIMENTAL SECTION

Materials. The silica gel particles of different size ranges (250−500 μm, 63−210 μm, and <37 μm), the IL 1-butyl-3-methylimidazolium acetate [bmim][acetate] (>95% purity), and acetone (>99.5% purity) were purchased from Sigma-Aldrich. Carbon dioxide, nitrogen, and helium were supplied by Praxair, Inc., with a minimum purity of 99.999%. In addition, a mixture containing 10,000 ppmv of carbon dioxide in nitrogen was supplied by Praxair, Inc., which was used in the fixed-bed runs.

SILP Preparation and Characterization. The silica particles used as support in the SILP material were used without any treatment, directly from the commercial supplier. The SILPs synthesis was carried out by incipient wetness impregnation.[28] In all cases, 1 g of SiO_2 and its corresponding amount of IL for a nominal load of 40% w/w (maximum load that can be introduced in the SiO_2 by the incipient wetness impregnation method) were mixed with acetone. Prior to the synthesis, the IL was dried and degassed at 333 K under vacuum (10^{-3} mbar) for at least 24 h to ensure a water content below 200 ppm. Then, the solution was added dropwise onto the SiO_2 support and remained 1 h at room temperature. After the impregnation, the resulting SILP was dried at 333 K for 24 h. Then, the amount of IL incorporated to the support was checked by elemental analysis. This methodology has been successfully applied in a previous work of our group[28] showing the homogeneous distribution of the IL inside the pores of different supports.

The thermal stability of the SILPs was studied by thermogravimetry, using a TA Instruments SDT 650 model. The tests were performed under inert atmosphere (50 N mL/min of N_2) with a heating rate of 10 °C/min up to 600 °C. The porous texture of both the SiO_2 particles and SILP material was characterized by N_2 adsorption/desorption at 77 K in a TriStar II 3020 (Micromeritics) system after 15 h of previous degassing at 0.1 mbar and 363 K. The surface area was calculated using the BET equation. The CHN content of the samples was checked by elemental analysis in a LECO CHNS-932. The microstructure and morphology of the empty SiO_2 particles were studied by scanning electron microscopy (SEM) allowing the calculation of the particle size distribution of each sample. SEM analyses were performed with a Hitachi S-3000N apparatus.

Gravimetric CO_2 Sorption Measurements. The CO_2 sorption capacity in SILP material (mol_{CO_2}/kg_{SILP}) was obtained using a gravimetric high-pressure sorption analyzer (ISOSORP GAS LP-flow, Rubotherm) equipped with a magnetic suspension balance (MSB). The apparatus allows controlling the inlet mass flow (up to 500 N mL/min) with two mass flow meters (N_2 and CO_2), the sorption temperature (from room to 150 °C), and the total pressure (from 10^{-6} to 30 bar). The microbalance is able to measure weights up to 10 g, with a precision of 10^{-5} g. A full description of the procedure used in the high-pressure sorption tests can be found elsewhere.[15,31] In this work, the CO_2 sorption isotherms for the different SILPs were obtained at three different temperatures (299, 314, and 329 K). A typical sorption test used 100−150 mg of SILP material. First, before each CO_2 sorption test, degasification was accomplished by heating the sample up to 333 K at 10^{-3} mbar residual pressure during 24 h. Then, for gravimetric experiments at 0.3 and 0.5 bar of CO_2 partial pressure, a mixture of CO_2−N_2 (total flow of 100 N mL/min) was used. For gravimetric experiments between 1 and 20 bar of CO_2 partial pressure, pure CO_2 was passed through the sample. The mass increase with time was recorded until the SILP was completely saturated (weight change <0.02 mg/h) at constant temperature and CO_2 partial pressure. Afterward, the total pressure was increased progressively up to a maximum value of 20.0 bar of pure CO_2. Lastly, in order to have reliable sorption values, the buoyancy effect caused by the MSB must be corrected. To accomplish this, an inert gas was

DOI: 10.1021/acssuschemeng.9b02277
ACS Sustainable Chem. Eng. 2019, 7, 13089−13097

flowed through the sample prior to the sorption test at different pressures and the testing temperature. The uncertainties of the MSB are $u(P)$ = 0.01 bar, $u(T)$ = 0.1 K, and $u(q_e)$ = 0.0001 mol/kg.

Fixed-Bed CO_2 Sorption Experiments. The quartz tube of 6 mm of internal diameter and 15 cm of length containing the fixed-bed (SILP length of 10 cm) was placed in a Microactivity unit (PID Eng&Tech, Spain). The tube is placed inside an oven that allows working at temperatures from room to 773 K. Two mass flow meters (N_2 and mixture of CO_2-N_2) fed the reactor in a down-flow direction. The setup consists of a pressure gauge at the gas inlet connected to a pressure valve at the exit of the fixed-bed. In current fixed-bed experiments, the pressure at the gas inlet is fixed at 1 bar. The gas outlet is connected to a gas chromatograph (GC Agilent 7820A) equipped with a 20 m column (PoraPlot U) and a TCD detector. In a typical fixed-bed experiment, the quartz tube was filled with 1.5−2.5 g of fresh SILP (corresponding approximately to 9 cm of bed height depending on the material). A mixture of N_2−CO_2 (10% v/v of CO_2) was passed through the bed at 1 atm of total pressure, until the sorbent was completely saturated. For each sorbent, three different temperatures (303, 318, and 333 K), flow rates (10, 20, and 50 N mL/min), and CO_2 inlet concentrations (2.5, 5 and 10% v/v) were tested, at 1 atm total pressure in all cases. Once the bed was saturated, the furnace temperature was raised up to 333 K, and inert gas passed during 2 h to allow complete regeneration of the sorbent. The uncertainties of the fixed-bed are $u(P)$ = 0.1 bar and $u(T)$ = 1 K.

Computational Details: Aspen Adsorption. *Isotherms Modeling.* Experimental CO_2 isotherms were modeled by using the available estimation module implemented in Aspen Adsorption v10.0 software. First, three different equilibrium models (see Figure S1 in the Supporting Information) were checked to fit the experimental CO_2 isotherms. The Langmuir−Freundlich equation (L−F eq 1) is shown below, and the two others can be found in the Supporting Information. The gases used (CO_2 and N_2) were selected from the Aspen Properties database, choosing as property package Peng−Robinson. It was confirmed that N_2 presents a negligible sorption in our materials[46]

$$w_{CO_2}\left[\frac{\text{mol}}{\text{kg}}\right] = \frac{IP_1 \cdot IP_2 \cdot p_{CO_2}^{IP_3} \cdot e^{IP_4/T}}{1 + IP_5 \cdot p_{CO_2}^{IP_3} \cdot e^{IP_6/T}} \quad (1)$$

where w_{CO_2} is the equilibrium CO_2 sorption capacity at each partial pressure; p_{CO_2} is the CO_2 partial pressure (bar); T is the temperature (K); and IP_1, IP_2, IP_3, IP_4, IP_5, and IP_6 are the fitting parameters of the equation.

Breakthrough Curves Modeling. The pseudo-first-order LDF kinetic model has been used to describe mass transfer between the gas and the sorbent. In Aspen Adsorption software, this kinetic model is known as lumped resistance linear (LR eq 2).

$$\frac{\partial w_{CO_2}}{\partial t} = K_{MTC} \cdot (w_{CO_2}{}^{*} - w_{CO_2}) \quad (2)$$

It considers all resistances to mass transfer lumped as a single overall factor or one mass transfer controlling resistance. The driving force is a function of CO_2 adsorbent capacity. The values of the effective kinetic coefficient (k_{MTC}) were calculated by the Aspen Adsorption's estimation module fitting the experimental breakthrough curves using eq 2 (named Lumped-Resistance model in the software). To accomplish this, some bed parameters and the operating conditions must be fed to the simulator as input information. That information includes bed size, particle radius, bed and particle porosity, bulk sorbent density, and operating conditions (pressure, temperature, inlet molar flow, and inlet CO_2 partial pressure) as well as the isotherms parameters (IP) obtained after the equilibrium model validation. The following assumptions were made: pressure and gas velocity are constant, bed porosity is uniform, plug flow pattern without effect of axial and radial dispersion, and constant temperature.

Modeling CO_2 Capture Operation. Once the thermodynamic and kinetic models were conveniently defined, Aspen Adsorption was used to scale up the CO_2 capture process in fixed-bed under different conditions to optimize the SILP needs in each case. Since it was possible to describe the k_{MTC} as a function of temperature, particle radius, and CO_2 partial pressure, the breakthrough curves were modeled using predicted k_{MTC} values for different SILP particle sizes using the dynamic mode. Table 1 shows the operating conditions employed in these Aspen Adsorption simulations. For more input simulation details, see Table S2 of the Supporting Information.

Table 1. Fixed Bed Operating Conditions Used in Aspen Adsorption

bed characteristics	
height of sorbent bed (m)	2
internal diameter of column (m)	0.3
operating conditions	
inlet molar flow rate ($mol_{CO_2+N_2}$/min)	1.12
CO_2 mole fraction	0.005−0.5
temperature (K)	303−333
pressure (bar)	1

RESULTS

SILP Characterization. Silica particles within three different size ranges were used as supports of SILP material as received from the supplier. Figure 1 shows SEM micrographs of representative samples. In all cases, it is clearly observed a fairly irregular morphology with a narrow size distribution. The highest size sample presents a mean size of about 500 μm, the medium one around 150 μm and the smallest near 9 μm (Figure 2). These significant differences allow checking the behavior in SILPs CO_2 sorption depending on the size of the support.

Table 2 shows the characterization of both the SiO_2 support and SILP material in terms of porous texture, elemental analysis, and thermal stability. The 77 K N_2 adsorption−desorption isotherms are given in Figure S1 of the Supporting Information. The starting supports present similar values of BET surface area in the vicinity of 550 m^2/g. The SILP sorbents synthesized upon incorporation of the IL yielded values below 50 m^2/g, which means that the IL fills most of the support pores. The CHN analysis serves to assess the amount of IL on the support from the %N (only present in the imidazolium cation), as demonstrated in previous works.[28,29] As expected, the CHN content of the empty SiO_2 particles is close to zero (Table 2), and once the IL was incorporated, the elemental analysis reflects that inclusion. In all cases, IL loading onto SILP material was varied between 37 and 39%, which allows comparing their performance with nearly the same composition but significantly different particle size. Lastly, the thermal stability of these materials was proved by TGA. The corresponding profiles are given in Figure S2 of the Supporting Information. The SiO_2 particles show no weight loss until at least 600 °C, while for the SILPs, the mass decay can be attributed to the IL component. The amount of IL on the SILPs from TGA measurements was between 37 and 39%, in agreement with the results obtained from the elemental analysis.

CO_2 Sorption by Gravimetric Measurements. The thermodynamic (equilibrium) behavior of each SILP in CO_2 capture was first tested by gravimetric measurements. Figure 3 shows the CO_2 sorption isotherms at three different temperatures. Figures S3 and S4 of the Supporting Information compare the CO_2 sorption by the SILPs, the neat IL

DOI: 10.1021/acssuschemeng.9b02277
ACS Sustainable Chem. Eng. 2019, 7, 13089−13097

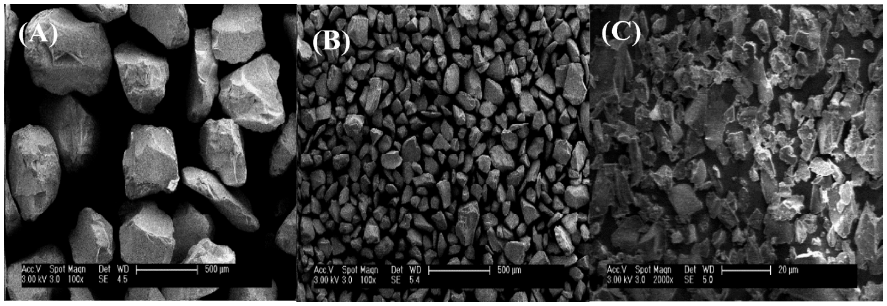

Figure 1. Representative SEM images of the SiO_2 supports of different sizes. Particle size: (A) 500 μm, (B) 150 μm, and (C) 9 μm.

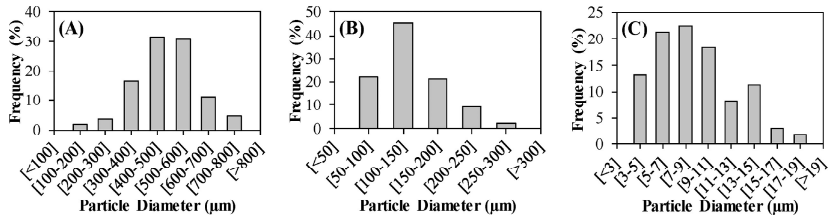

Figure 2. Size distribution of the SiO_2 supports. Mean particle size: (A) 500 μm, (B) 150 μm, and (C) 9 μm.

Table 2. Characterization of SiO_2 Supports and SILP Material of Different Particle Size

		SiO_2			SILP		
		9 μm	150 μm	500 μm	9 μm	150 μm	500 μm
A_{BET}	(m^2/g)	555.5	541.9	588.0	28	28	53
EA	%C	0.01	0.01	0.01	23.1	22.6	21.8
	%H	0.98	1.00	0.99	4.3	4.2	4.0
	%N	0.01	0.01	0.01	5.4	5.2	5.1
%IL	EA				37.9	36.7	36.6
	TGA				40.6	38.4	37.4
T_{DTGA}	(K)		stable until 873 K		510.1	510.1	510.1

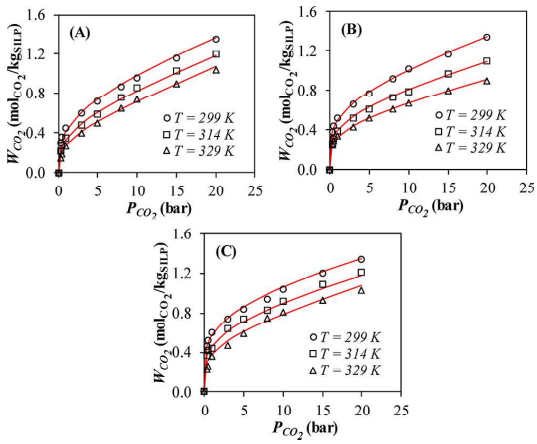

Figure 3. CO_2 isotherms of the three SILP sorbents with different mean particle sizes: (A) 500 μm, (B) 150 μm, and (C) 9 μm.

[bmim][acetate], and the empty SiO_2. It was defined the CO_2 sorption capacity per mass of IL, confirming that the only contribution to CO_2 uptake is due to the IL, in good agreement with previously tested SILP or ENIL materials.[29−34] In fact, the CO_2 uptake at the same temperature is quite similar for the three SILP sorbents, independently of the particle size of the support, since the IL load is also fairly similar (37−39%). This result is consistent with the dramatic decrease of BET surface area, which confirms the almost complete filling of the SiO_2 pores by the IL.[28,29] Therefore, it can be concluded that the CO_2 capture by the SILPs is determined by the CO_2 absorption in the IL. The shape of the curves is indicative of dominant chemical absorption, as described in a previous work for the CO_2-[bmim][acetate] system.[31] This fact has been reported in previous works with this and other ILs that chemically retain CO_2.[30,31,33] Given the great performance of the SILP at low CO_2 partial pressures, we worked within that range in the fixed-bed experiments. As can be seen, the equilibrium data (experimental points) fit very well the Langmuir−Freundlich model (red lines), with $R^2 > 0.99$ in all cases. This model describes the CO_2−SILP equilibrium better than the Langmuir and Freundlich equations, confirming the occurrence of chemical and physical absorption of CO_2 in the IL within the range of CO_2 partial pressure tested, and both of them are considered in the L−F model. The values of the fitting parameters are collected in Table 3.

DOI: 10.1021/acssuschemeng.9b02277
ACS Sustainable Chem. Eng. 2019, 7, 13089−13097

Table 3. Fitting Parameters of the Langmuir–Freundlich Model for Each Temperature and SILP Material

model	parameter	SILP - 500 μm			SILP - 150 μm			SILP - 9 μm		
Langmuir–Freundlich	T (K)	299	314	329	299	314	329	299	314	329
	IP_1		1.23×10^{-3}			1.18×10^{-3}			4.91×10^{-4}	
	IP_2		1.23×10^{-3}			1.26×10^{-3}			1.65×10^{-3}	
	IP_3		0.2326			0.1254			0.1272	
	IP_4		1587.73			1529.43			1778.91	
	IP_5		−1.73			−0.6701			−1.89	
	IP_6		−551.44			−85.12			−428.27	
	R^2[a]	0.999	0.999	0.997	0.999	0.998	0.999	0.998	0.998	0.992
	SD[a]	0.015	0.014	0.021	0.013	0.013	0.010	0.020	0.018	0.033

[a]Statistic parameters calculated comparing experimental and calculated equilibrium data: R^2: square regression coefficient; SD: standard deviation.

Fixed-Bed Experiments. Potential full-scale application of SILP sorbents requires learning on its performance in fixed-bed, where the effects of different variables, such as SILP particle size, temperature, gas flow rate, and CO_2 partial pressure need to be evaluated.

The three SILP sorbents with different particle sizes were first tested at 0.05 bar of CO_2 inlet partial pressure, sorption temperatures of 303, 318, and 333 K, and 10 N mL/min of total gas flow. The results are depicted in Figure 4, showing

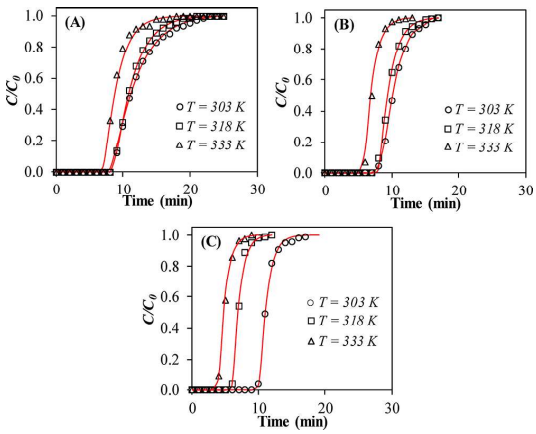

Figure 4. Breakthrough curves at different temperatures and 0.05 bar CO_2 partial pressure for SILPs with different particle sizes: (A) 500 μm, (B) 150 μm, and (C) 9 μm. The red lines correspond to the LDF model implemented in Aspen Adsorption (named the Lumped-Resistance model).

that the LDF model fits very well the experimental data (R^2 > 0.99) in all cases. The breakthrough time increases at decreasing temperature, consistently with the higher sorption capacity according to the equilibrium curves of Figure 3.

Figure 5A shows the values of the kinetic coefficient (k_{MTC} of eq 2) at different temperatures for the three SILPs tested. As can be seen, these values increase while decreasing the SILP particle size, consistently with the higher gas-IL contact area. The k_{MTC} values also increase with temperature. The dependence with temperature is more pronounced at higher particle size. In fact, the breakthrough curves for the least size SILP (d_p = 9 μm) are the steepest, close to ideal, and nearly independent of the temperature; i.e., the kinetics is so fast that the temperature hardly affects the process within the 30 °C range tested. In this work, we present the behavior of a SILP

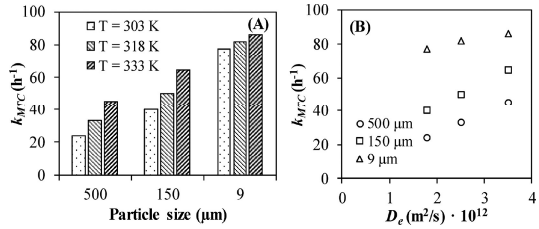

Figure 5. Values of the kinetic coefficient (k_{MTC}) for the tested SILPs at different temperatures (A) and vs the CO_2 diffusivity (D_e) in the neat IL (B).

based on [bmim][acetate] IL, but looking at these results, it is expected that the viscosity of the IL is a key issue regarding the design of fixed-bed operations with SILPs, especially at particle sizes above 100 μm. Figure 5B represents the values of the kinetic coefficient vs the CO_2 diffusivity (D_e) in the neat IL at each temperature, obtained in previous works[15,20,31,32] by the Shifflet and Yokozeki method.[47] A nearly linear relationship can be observed, suggesting that the CO_2 sorption rate in SILP is governed by the absorption phenomena in IL film, favored at lower IL viscosity (higher temperatures). The values of the kinetic coefficient at different temperatures fitted well the Arrhenius equation. Table 4 summarizes the corresponding

Table 4. Values of the Apparent Activation Energy and Pre-Exponential Factor

	SILP - 500 μm	SILP - 150 μm	SILP - 9 μm
E_a (kJ/mol)	17.7	13.5	3.0
k_0 (s^{-1})	7.62	2.35	0.07
R^2	0.993	0.990	0.999

vales of apparent activation energy and the pre-exponential factor, which will be used in later Aspen Adsorption simulations of the breakthrough curves of CO_2 capture in SILP sorbents.

Figure 6 shows the breakthrough curves obtained at 303 K and 0.05 bar of CO_2 partial pressure in the inlet stream using different gas flow rates. Again, the LDF kinetic model (red lines) fits well the experimental data (R^2 > 0.99 in all cases). Figure 7 collects the k_{MTC} values at different gas flow rates. Consistently with the previous conclusions, the kinetic coefficient increases when decreasing the SILP particle size, independently on the gas flow rate. This last barely affects the k_{MTC}, indicating the absence of mass-transfer limitations in the gas-phase.

DOI: 10.1021/acssuschemeng.9b02277
ACS Sustainable Chem. Eng. 2019, 7, 13089–13097

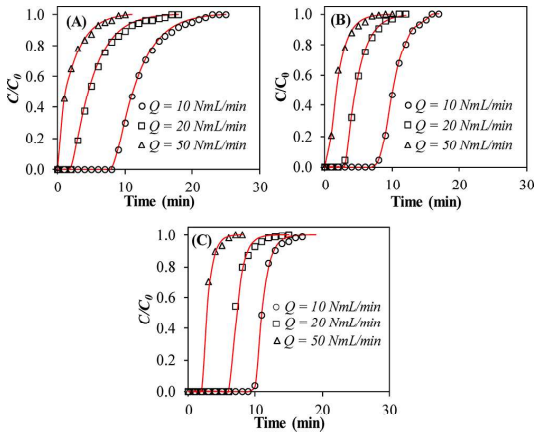

Figure 6. Breakthrough curves at different gas flow rates for SILPs of different particle sizes: (A) 500 μm, (B) 150 μm, and (C) 9 μm [T = 303 K, p_{CO_2} = 0.10 bar].

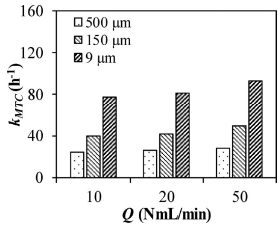

Figure 7. k_{MTC} values for SILPs at different particle sizes and gas flow rates from the breakthrough curves of Figure 6 [T = 303 K, p_{CO_2} = 0.10 bar, P = 1 bar].

Fixed-bed experiments at three different CO_2 inlet partial pressures (0.025, 0.05, and 0.10 bar) were carried out at 303 K, 1 atm of total pressure, and 10 N mL/min gas flow rate. The results are shown in Figure 8. It is important to remark that in all cases the IL load remained unchanged after all the CO_2 sorption tests, as confirmed by elemental analysis. The LDF kinetic model again describes well the experimental breakthrough curves (R^2 > 0.99 in all cases). It is clearly seen that a higher CO_2 partial pressure implies a faster sorption, consistently with the higher driving force. Figure 9 shows the values of the kinetic coefficient (k_{MTC}) at the three CO_2 partial pressures tested in the feed gas stream. It is concluded that the inlet gas CO_2 partial pressure not only determines the mass transfer driving force but significantly affects the value of the kinetic coefficient (k_{MTC}).

Modeling CO_2 Chemical Sorption in Fixed-Bed Using SILP Material. To learn more on the phenomenological aspects of the sorption process investigated, the overall resistance ($1/k_{MTC}$) was separated in two terms, according to eq 3, which was found to fit well the experimental results.

$$\frac{1}{k_{MTC}} = A + B\cdot\frac{r_p}{D_e} \tag{3}$$

In that expression, r_p corresponds to the equivalent mean particle radius of the SILP, and D_e was already defined as the diffusivity of CO_2 in the neat IL. Its dependence with

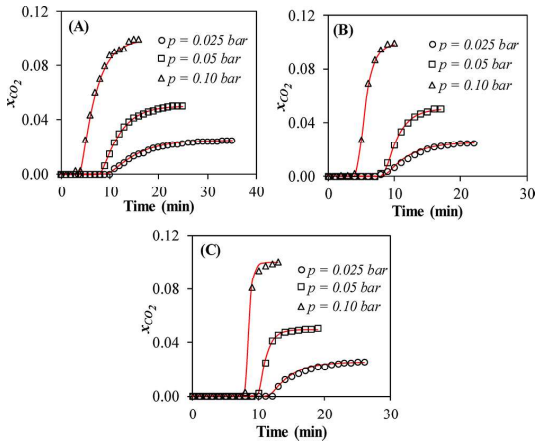

Figure 8. Breakthrough curves at different CO_2 partial pressures for the SILPs of different particle sizes: (A) 500 μm, (B) 150 μm, and (C) 9 μm [T = 303 K; P = 1 atm; gas flow rate = 10 N mL/min].

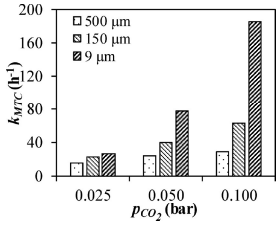

Figure 9. k_{MTC} values for SILPs of different particle sizes at three CO_2 partial pressures (see Figure 8 for operating conditions).

temperature can be expressed by eq 4 from previous experiments:[31]

$$D_e\left[\frac{m^2}{s}\right] = 3\cdot10^{-9}\cdot e^{-2561.55/T} \tag{4}$$

As can be seen in Figure 10, the slope of the linear relationship given by eq 3 is independent of the CO_2 partial pressure, while

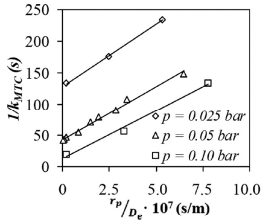

Figure 10. Fitting of eq 3 at different CO_2 partial pressures and SILP particle sizes. At p_{CO_2} = 0.05 bar, values at different temperatures are also included (T affects D_e).

the intercept value strongly depends on it. Thus, eq 3 was modified into

$$\frac{1}{k_{MTC}} = \frac{1}{1.85\cdot p_{CO_2}^{1.5}} + 2.65\cdot10^{-7}\cdot\frac{r_p}{3\cdot10^{-9}\cdot e^{(-2561.55/T)}} \tag{5}$$

DOI: 10.1021/acssuschemeng.9b02277
ACS Sustainable Chem. Eng. 2019, 7, 13089−13097

The k_{MTC} values calculated by this expression fit fairly well the experimental ones, as can be seen in Figure 11. Equation 5

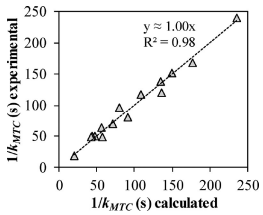

Figure 11. Validation of eq 3. All the experimental data of the work is taken into account.

considers two resistances in series. The first one, dependent on p_{CO_2}, is related to the chemical absorption by the IL, while the second one corresponds to CO_2 diffusion in the ionic liquid phase of the SILP.

The breakthrough curves of CO_2 sorption with the SILPs tested were simulated using Aspen Adsorption in dynamic mode within SILP particle size and CO_2 inlet partial pressure ranges wider than those tested in the experiments described so far. Figure 12 shows the resulting curves at 303 K.

The curves become steeper at increasing CO_2 partial pressure. Regarding the effect of SILP particle size, it strongly depends on the inlet CO_2 partial pressure. At very low CO_2 partial pressure, the SILP particle size does not affect the kinetics of the process, having almost the same curve shape in all cases. At higher p_{CO_2} values, the length of the mass-transfer zone becomes shorter as the SILP particle size decreases, being the effect more pronounced at increasing p_{CO_2}. These results indicate the existence of different rate control regimes depending on the operating range of these two variables. At very low CO_2 partial pressure, the rate of the process is governed by the chemical reaction determining CO_2 sorption; while as p_{CO_2} increases so does the reaction rate, and the CO_2 diffusion in the IL turns out to be the controlling step.

CO_2 capture would commonly be carried out from gas streams with a relative concentration of this component well above the limit when mass-transfer control already occurs, and therefore, the SILP particle size is an important issue to be considered for a cost-effective use of this type of sorbent. A balance between the effective bed sorption capacity at the established breaking point and the gas pressure loss, depending on the particle size of the sorbent material, must be optimized. In principle, looking at the breakthrough curves at high and intermediate p_{CO_2}, a SILP particle size somewhere in the range of 0.15 to 0.5 mm seems to be the most reasonable. Further research is addressed toward this main question regarding potential application of these SILPs for CO_2 capture upon fixed bed sorption.

CONCLUSIONS

SILP material with remarkably different particle sizes, based on the IL 1-butyl-3-methylimidazolium acetate, was evaluated in detail as CO_2 sorbents. The prepared SILP material was characterized by SEM, porous texture, thermal stability, and elemental composition. The gravimetric measurements at three different temperatures show that the CO_2 sorption capacity is only attributed to the IL. The CO_2 sorption isotherms were successfully fitted to the Langmuir−Freundlich model implemented in Aspen Adsorption. The effect of the SILP particle size, temperature, gas flow rate, and CO_2 partial pressure was evaluated in fixed-bed experiments. The different breakthrough curves were successfully fitted using Aspen Adsorption to a linear driving force model, allowing to obtain the effective overall kinetic coefficient k_{MTC}. The k_{MTC} values revealed that the CO_2 sorption rate increases when decreasing the SILP particle size and increasing the temperature. The gas flow rate does not have any noticeable effect on the mass transfer rate in the range investigated. The increase in the p_{CO_2} presents a remarkable effect on the sorption rate. The results suggest that at very low p_{CO_2} the chemical absorption is the controlling step, while as that partial pressure increases, CO_2 diffusion in the IL phase of SILP turns to be the governing stage. Aspen Adsorption simulator was used to evaluate the SILP behavior within particle size and CO_2 inlet partial pressure covering wider ranges than those tested in the experimental runs. Depending on inlet CO_2 partial pressure, it was found a remarkably different effect of particle size on SILP sorbent performance, because of the shift of control regime from chemical absorption to CO_2 diffusion in the IL. This methodology allows the optimization of the operation at given conditions of temperature and p_{CO_2}, by selecting the type of IL and SILP particle size.

ASSOCIATED CONTENT

Supporting Information

The Supporting Information is available free of charge on the ACS Publications website at DOI: 10.1021/acssuschemeng.9b02277.

Detailed information on isotherm models used and additional Aspen Adsorption input required to simulate in dynamic mode not described in paper, N_2 adsorption/desorption isotherms @ 77 K of empty silica particles of

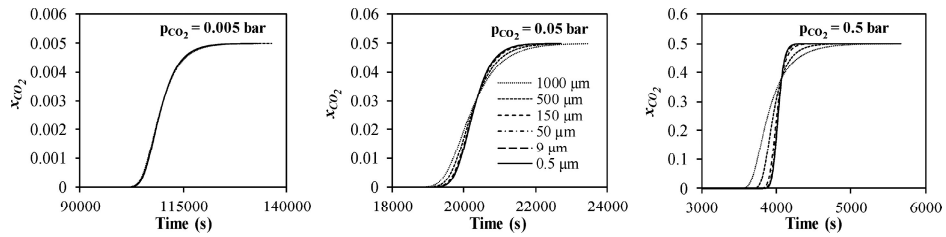

Figure 12. Breakthrough curves of CO_2 sorption in fixed-bed calculated by Aspen Adsorption in dynamic mode for different SILP particle sizes and CO_2 partial pressures (T = 303 K).

DOI: 10.1021/acssuschemeng.9b02277
ACS Sustainable Chem. Eng. 2019, 7, 13089−13097

three different sizes, TGA analysis of empty silica and prepared SILP materials, comparison of CO_2 sorption capacity of pure IL and SILP materials, and CO_2 adsorption blank experiment with empty SiO_2 (PDF)

AUTHOR INFORMATION

Corresponding Author

*E-mail: pepe.palomar@uam.es.

ORCID

Ruben Santiago: 0000-0002-6877-9001

Noelia Alonso-Morales: 0000-0001-5855-7336

Jose Palomar: 0000-0003-4304-0515

Notes

The authors declare no competing financial interest.

ACKNOWLEDGMENTS

The authors are very grateful to Ministerio de Economía y Competitividad (MINECO) of Spain (project CTQ2017-89441-R) and Comunidad de Madrid (P2018/EMT4348) for financial support and Centro de Computación Científica de la Universidad Autónoma de Madrid for computational facilities.

REFERENCES

(1) Plasseraud, L. *Carbon Dioxide as Chemical Feedstock*; Aresta, M., Ed.; 2010; Vol. 3, pp 631−632, DOI: 10.1002/cssc.201000097.

(2) Hatzigeorgiou, E.; Polatidis, H.; Haralambopoulos, D. Energy CO_2 Emissions for 1990−2020: A Decomposition Analysis for EU-25 and Greece. *Energy Sources, Part A* **2010**, *32* (20), 1908−1917.

(3) Baena-Moreno, F. M.; Rodríguez-Galán, M.; Vega, F.; Alonso-Fariñas, B.; Vilches Arenas, L. F.; Navarrete, B. Carbon capture and utilization technologies: a literature review and recent advances. *Energy Sources, Part A* **2019**, *41* (12), 1403−1433.

(4) Bui, M.; Adjiman, C. S.; Bardow, A.; Anthony, E. J.; Boston, A.; Brown, S.; Fennell, P. S.; Fuss, S.; Galindo, A.; Hackett, L. A.; Hallett, J. P.; Herzog, H. J.; Jackson, G.; Kemper, J.; Krevor, S.; Maitland, G. C.; Matuszewski, M.; Metcalfe, I. S.; Petit, C.; Puxty, G.; Reimer, J.; Reiner, D. M.; Rubin, E. S.; Scott, S. A.; Shah, N.; Smit, B.; Trusler, J. P. M.; Webley, P.; Wilcox, J.; Mac Dowell, N. Carbon capture and storage (CCS): the way forward. *Energy Environ. Sci.* **2018**, *11* (5), 1062−1176.

(5) Gaurina-Medimurec, N.; Novak-Mavar, K.; Majic, M. Carbon Capture and Storage (CCS): Technology, Projects and Monitoring Review. *Rud.-Geol.-Naftni Zb.* **2018**, *33* (2), 1−15.

(6) Amaral, M.; Crespo, E. A.; Dariva, C.; Vega, L. F.; Carvalho, P. J.; Coutinho, J. A. P. High-pressure solubility of CO_2 in glymes. *Fuel* **2018**, *219*, 120−125.

(7) Jaramillo, P.; Griffin, W. M.; McCoy, S. T. Life Cycle Inventory of CO_2 in an Enhanced Oil Recovery System. *Environ. Sci. Technol.* **2009**, *43* (21), 8027−8032.

(8) Xu, Y.; Schutte, R. P.; Hepler, L. G. Solubilities of Carbon Dioxide, Hydrogen Sulfide and Sulfur Dioxide in Physical Solvents. *Can. J. Chem. Eng.* **1992**, *70*, 569−573.

(9) Fillion, J. J.; Bennett, J. E.; Brennecke, J. F. The Viscosity and Density of Ionic Liquid + Tetraglyme Mixtures and the Effect of Tetraglyme on CO_2 Solubility. *J. Chem. Eng. Data* **2017**, *62* (2), 608−622.

(10) Jones, C. W. CO_2 Capture from Dilute Gases as a Component of Modern Global Carbon Management. *Annu. Rev. Chem. Biomol. Eng.* **2011**, *2* (1), 31−52.

(11) Papatryfon, X. L.; Heliopoulos, N. S.; Molchan, I. S.; Zubeir, L. F.; Bezemer, N. D.; Arfanis, M. K.; Kontos, A. G.; Likodimos, V.; Iliev, B.; Romanos, G. E.; Falaras, P.; Stamatakis, K.; Beltsios, K. G.; Kroon, M. C.; Thompson, G. E.; Klöckner, J.; Schubert, T. J. S. CO_2 Capture Efficiency, Corrosion Properties, and Ecotoxicity Evaluation of Amine Solutions Involving Newly Synthesized Ionic Liquids. *Ind. Eng. Chem. Res.* **2014**, *53* (30), 12083−12102.

(12) Rogers, R. D.; Seddon, K. R. Ionic Liquids–Solvents of the Future? *Science* **2003**, *302* (5646), 792−793.

(13) Earle, M.; Seddon, K. Ionic liquids. Green solvents for the future. In *Clean Solvents*; ACS Symposium Series, 2002; Vol. *819*, pp 10−25, DOI: 10.1021/bk-2002-0819.ch002.

(14) Welton, T. Ionic liquids: a brief history. *Biophys. Rev.* **2018**, *10* (3), 691−706.

(15) Moya, C.; Palomar, J.; Gonzalez-Miquel, M.; Bedia, J.; Rodriguez, F. Diffusion Coefficients of CO_2 in Ionic Liquids Estimated by Gravimetry. *Ind. Eng. Chem. Res.* **2014**, *53* (35), 13782−13789.

(16) Saravanamurugan, S.; Kunov-Kruse, A. J.; Fehrmann, R.; Riisager, A. Amine-Functionalized Amino Acid- based Ionic Liquids as Efficient and High- Capacity Absorbents for CO_2. *ChemSusChem* **2014**, *7* (3), 897−902.

(17) Aghaie, M.; Rezaei, N.; Zendehboudi, S. A systematic review on CO_2 capture with ionic liquids: Current status and future prospects. *Renewable Sustainable Energy Rev.* **2018**, *96*, 502−525.

(18) Carvalho, P. J.; Kurnia, K. A.; Coutinho, J. A. P. Dispelling some myths about the CO_2 solubility in ionic liquids. *Phys. Chem. Chem. Phys.* **2016**, *18* (22), 14757−14771.

(19) Seo, S.; Quiroz-Guzman, M.; DeSilva, M. A.; Lee, T. B.; Huang, Y.; Goodrich, B. F.; Schneider, W. F.; Brennecke, J. F. Chemically Tunable Ionic Liquids with Aprotic Heterocyclic Anion (AHA) for CO_2 Capture. *J. Phys. Chem. B* **2014**, *118* (21), 5740−5751.

(20) Palomar, J.; Larriba, M.; Lemus, J.; Moreno, D.; Santiago, R.; Moya, C.; de Riva, J.; Pedrosa, G. Demonstrating the key role of kinetics over thermodynamics in the selection of ionic liquids for CO_2 physical absorption. *Sep. Purif. Technol.* **2019**, *213*, 578−586.

(21) Goodrich, B. F.; de la Fuente, J. C.; Gurkan, B. E.; Lopez, Z. K.; Price, E. A.; Huang, Y.; Brennecke, J. F. Effect of Water and Temperature on Absorption of CO_2 by Amine-Functionalized Anion-Tethered Ionic Liquids. *J. Phys. Chem. B* **2011**, *115* (29), 9140−9150.

(22) Mota-Martinez, M. T.; Brandl, P.; Hallett, J. P.; Mac Dowell, N. Challenges and opportunities for the utilisation of ionic liquids as solvents for CO_2 capture. *Mol. Syst. Des. Eng.* **2018**, *3* (3), 560−571.

(23) Leclaire, J.; Heldebrant, D. J. A call to (green) arms: a rallying cry for green chemistry and engineering for CO_2 capture, utilisation and storage. *Green Chem.* **2018**, *20* (22), 5058−5081.

(24) Kolding, H.; Fehrmann, R.; Riisager, A. CO_2 Capture technologies: Current status and new directions using supported ionic liquid phase (SILP) absorbers. *Sci. China: Chem.* **2012**, *55* (8), 1648−1656.

(25) Riisager, A.; Flicker, S.; Haumann, M.; Wasserscheid, P.; Fehrmann, R. Supported Ionic Liquid-Phase (Silp) Catalysts in Continuous Flow Processes. *Proc. − Electrochem. Soc.*; 2004; Vol. *2004-24*, pp 630−638, DOI: 10.1149/200424.0630PV.

(26) Romanos, G. E.; Schulz, P. S.; Bahlmann, M.; Wasserscheid, P.; Sapalidis, A.; Katsaros, F. K.; Athanasekou, C. P.; Beltsios, K.; Kanellopoulos, N. K. CO_2 Capture by Novel Supported Ionic Liquid Phase Systems Consisting of Silica Nanoparticles Encapsulating Amine-Functionalized Ionic Liquids. *J. Phys. Chem. C* **2014**, *118* (42), 24437−24451.

(27) Balsamo, M.; Erto, A.; Lancia, A.; Totarella, G.; Montagnaro, F.; Turco, R. Post-combustion CO_2 capture: On the potentiality of amino acid ionic liquid as modifying agent of mesoporous solids. *Fuel* **2018**, *218*, 155−161.

(28) Lemus, J.; Palomar, J.; Gilarranz, M.; J. Rodriguez, J. Characterization of Supported Ionic Liquid Phase (SILP) materials prepared from different supports. *Adsorption* **2011**, *17*, 561−571.

(29) Palomar, J.; Lemus, J.; Alonso-Morales, N.; Bedia, J.; Gilarranz, M. A.; Rodriguez, J. J. Encapsulated ionic liquids (ENILs): from continuous to discrete liquid phase. *Chem. Commun.* **2012**, *48* (80), 10046−10048.

(30) Moya, C.; Alonso-Morales, N.; de Riva, J.; Morales-Collazo, O.; Brennecke, J. F.; Palomar, J. Encapsulation of Ionic Liquids with an Aprotic Heterocyclic Anion (AHA-IL) for CO_2 Capture: Preserving

the Favorable Thermodynamics and Enhancing the Kinetics of Absorption. *J. Phys. Chem. B* **2018**, *122* (9), 2616−2626.
(31) Moya, C.; Alonso-Morales, N.; Gilarranz, M. A.; Rodriguez, J. J.; Palomar, J. Encapsulated Ionic Liquids for CO_2 Capture: Using 1-Butyl-methylimidazolium Acetate for Quick and Reversible CO_2 Chemical Absorption. *ChemPhysChem* **2016**, *17* (23), 3891−3899.
(32) Santiago, R.; Lemus, J.; Moreno, D.; Moya, C.; Larriba, M.; Alonso-Morales, N.; Gilarranz, M. A.; Rodríguez, J. J.; Palomar, J. From kinetics to equilibrium control in CO_2 capture columns using Encapsulated Ionic Liquids (ENILs). *Chem. Eng. J.* **2018**, *348*, 661−668.
(33) Santiago, R.; Lemus, J.; Moya, C.; Moreno, D.; Alonso-Morales, N.; Palomar, J. Encapsulated Ionic Liquids to Enable the Practical Application of Amino Acid-Based Ionic Liquids in CO_2 Capture. *ACS Sustainable Chem. Eng.* **2018**, *6* (11), 14178−14187.
(34) Lemus, J.; Bedia, J.; Moya, C.; Alonso-Morales, N.; Gilarranz, M.; Palomar, J.; Rodriguez, J. Ammonia Capture from Gas Phase by Encapsulated Ionic Liquids (ENILs). *RSC Adv.* **2016**, DOI: 10.1039/C6RA11685J.
(35) Mota-Martinez, M. T.; Brandl, P.; Hallett, J. P.; Mac Dowell, N. Challenges and for the utilisation of ionic liquids as solvents for CO_2 capture. *Mol. Syst. Des. Eng.* **2018**, *3* (3), 560−571.
(36) Ben-Mansour, R.; Habib, M. A.; Bamidele, O. E.; Basha, M.; Qasem, N. A. A.; Peedikakkal, A.; Laoui, T.; Ali, M. Carbon capture by physical adsorption: Materials, experimental investigations and numerical modeling and simulations - A review. *Appl. Energy* **2016**, *161*, 225−255.
(37) Rashidi, N. A.; Yusup, S. An overview of activated carbons utilization for the post-combustion carbon dioxide capture. *J. CO_2 Util.* **2016**, *13*, 1−16.
(38) Wang, J. Y.; Huang, L.; Yang, R. Y.; Zhang, Z.; Wu, J. W.; Gao, Y. S.; Wang, Q.; O'Hare, D.; Zhong, Z. Y. Recent advances in solid sorbents for CO_2 capture and new development trends. *Energy Environ. Sci.* **2014**, *7* (11), 3478−3518.
(39) Balsamo, M.; Rodríguez-Reinoso, F.; Montagnaro, F.; Lancia, A.; Erto, A. Highlighting the Role of Activated Carbon Particle Size on CO_2 Capture from Model Flue Gas. *Ind. Eng. Chem. Res.* **2013**, *52* (34), 12183−12191.
(40) Dadwhal, M.; Kim, T. W.; Sahimi, M.; Tsotsis, T. T. Study of CO_2 Diffusion and Adsorption on Calcined Layered Double Hydroxides: The Effect of Particle Size. *Ind. Eng. Chem. Res.* **2008**, *47* (16), 6150−6157.
(41) Gatti, G.; Vittoni, C.; Costenaro, D.; Paul, G.; Mangano, E.; Brandani, S.; Marchese, L.; Bisio, C. The influence of particle size of amino-functionalized MCM-41 silicas on CO_2 adsorption. *Phys. Chem. Chem. Phys.* **2017**, *19* (43), 29449−29460.
(42) Mastalerz, M.; Hampton, L.; Drobniak, A.; Loope, H. Significance of analytical particle size in low-pressure N_2 and CO_2 adsorption of coal and shale. *Int. J. Coal Geol.* **2017**, *178*, 122−131.
(43) Bhatt, T. S.; Sliepcevich, A.; Storti, G.; Rota, R. Experimental and Modeling Analysis of Dual-Reflux Pressure Swing Adsorption Process. *Ind. Eng. Chem. Res.* **2014**, *53* (34), 13448−13458.
(44) Bhatt, T. S.; Storti, G.; Rota, R. Detailed simulation of dual-reflux pressure swing adsorption process. *Chem. Eng. Sci.* **2015**, *122*, 34−52.
(45) Santos, M. G. R. S.; Correia, L. M. S.; de Medeiros, J. L.; Araujo, O. d. Q. F. Natural gas dehydration by molecular sieve in offshore plants: Impact of increasing carbon dioxide content. *Energy Convers. Manage.* **2017**, *149*, 760−773.
(46) Lei, Z.; Dai, C.; Chen, B. Gas Solubility in Ionic Liquids. *Chem. Rev.* **2014**, *114* (2), 1289−1326.
(47) Shiflett, M. B.; Yokozeki, A. Solubilities and Diffusivities of Carbon Dioxide in Ionic Liquids: [bmim][PF_6] and [bmim][BF_4]. *Ind. Eng. Chem. Res.* **2005**, *44* (12), 4453−4464.

DOI: 10.1021/acssuschemeng.9b02277
ACS Sustainable Chem. Eng. 2019, 7, 13089−13097

Supplementary Material

CO_2 capture by Supported Ionic Liquid Phase (SILP): Highlighting the role of the particle size

Ruben Santiago, Jesus Lemus, Daniel Hospital-Benito, Cristian Moya, Jorge Bedia, Noelia Alonso-Morales, Juan J. Rodriguez and Jose Palomar*

Chemical Engineering Department. Universidad Autónoma de Madrid. 28049 Madrid. Spain

Number of Pages: 6

Number of Figures: 4

Number of Tables: 2

List of Tables and Figures:

Table S 1: Isotherm models employed in the work 2

Table S 2: Additional Aspen Adsorption input required to simulate in dynamic mode. 7

Figure S1: 77K N_2 adsorption/desorption isotherms of empty SiO_2 of three different sizes used in this work 3

Figure S2: TGA analysis of empty silica (SiO_2) and SILP [bmim][acetate] of three different particle sizes (SILP 500 – 9 μm). Analysis carried out with a temperature increase of 10 ºC·min^{-1} under 50 mL·min^{-1} of N_2. 4

Figure S3: Comparison of CO_2 sorption isotherms on SILP of different particle sizes and on neat IL at 299 K. 5

Figure S 4: CO_2 adsorption isotherm of empty SiO_2-500 μm. 6

Table S 1: Isotherm models employed in the work

Isotherm Model	Equation	R^2 coefficient
Langmuir	$w_{CO_2} = \frac{IP_1 \cdot p_{CO_2}}{1 + IP_2 \cdot p_{CO_2}}$	0.86-0.87
Freundlich	$w_{CO_2} = IP_1 \cdot p_{CO_2}^{IP_2}$	0.95-0.97
Langmuir-Freundlich	$w_{CO_2} = \frac{IP_1 \cdot IP_2 \cdot p_{CO_2}^{IP_3} \cdot e^{IP_4/T}}{1 + IP_5 \cdot p_{CO_2}^{IP_3} \cdot e^{IP_6/T}}$	> 0.99

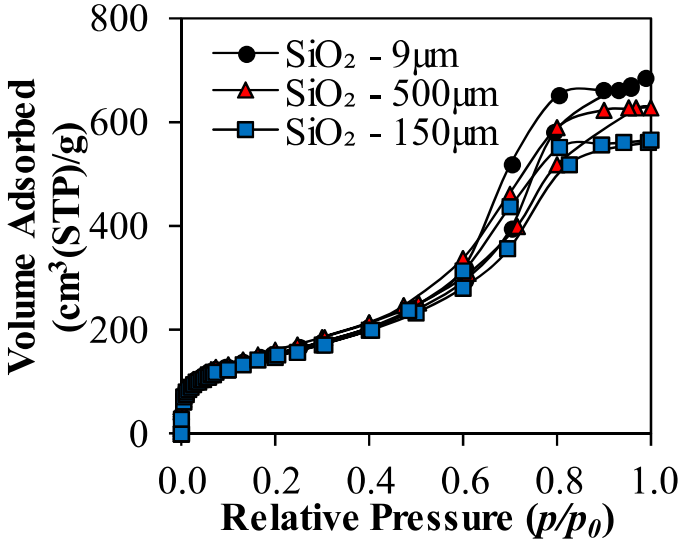

Figure S1: 77K N_2 adsorption/desorption isotherms of empty SiO_2 of three different sizes used in this work

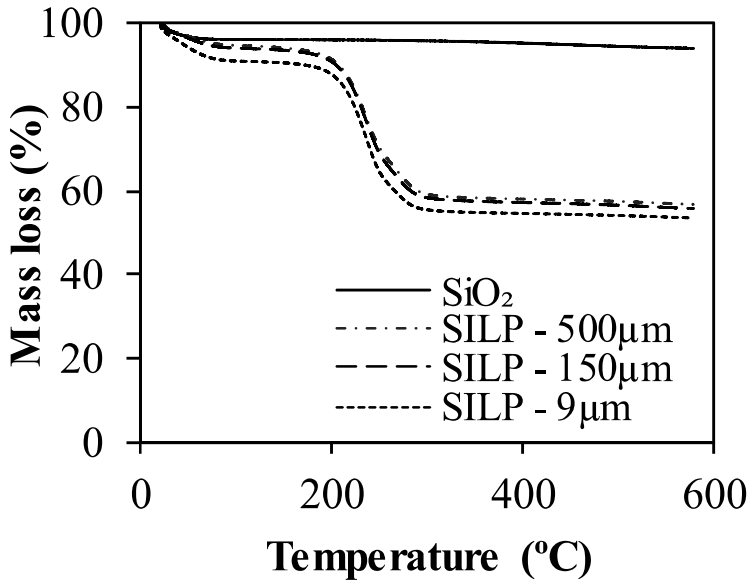

Figure S2: TGA analysis of empty silica (SiO_2) and SILP [bmim][acetate] of three different particle sizes (SILP 500 – 9 µm). Analysis carried out with a temperature increase of 10 ºC·min^{-1} under 50 mL·min^{-1} of N_2.

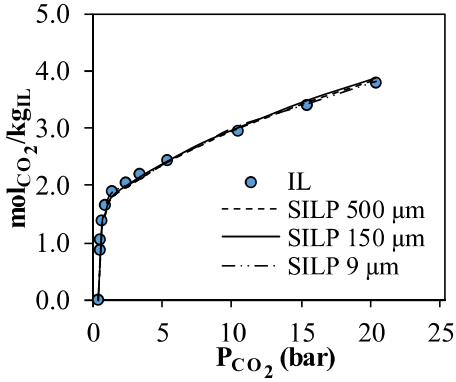

Figure S3: Comparison of CO_2 sorption isotherms on SILP of different particle sizes and on neat IL at 299 K.

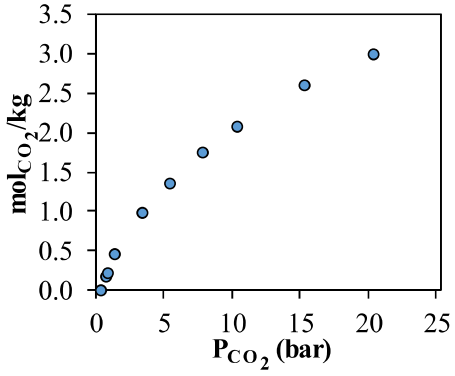

Figure S 4: CO_2 adsorption isotherm of empty SiO_2-500 µm.

Table S 2: Additional Aspen Adsorption input required to simulate in dynamic mode.

Bed characteristics	
Inter-particle porosity (m^3 void/m^3 bed)	0.5
Sorbent properties	
Intra-particle porosity (m^3 void/m^3 bed)	$1 \cdot 10^{-10}$
Sorbent solid bulk density (kg/m^3)	810
Sorbent particle radius (mm)	$2.5 \cdot 10^{-7}$-$1.0 \cdot 10^{-1}$

The inter-particle porosity was 0.5 in all cases due to the typical ranges in conventional adsorbents, such as zeolites or active carbons [1-3]. Moreover, the expected maximum inter-particle porosity considering spherical adsorbents is 0.6, so a value of 0.5 seems to be reasonably good for the estimations. The intra-particle porosity was $1 \cdot 10^{-10}$ because the pores of the SiO_2 particles are completely filled of IL (as demonstrated with the textural analysis by means of 77 K N_2 adsorption/desorption isotherms). In Aspen Adsorption, the solid bulk density is referred to the bed apparent density [1], which was experimentally calculated from the experimental fixed-bed tested. The sorbent particle radius was varied from 0.5 – 1000 μm.

References

1. Bhatt, T.S., et al., *Experimental and Modeling Analysis of Dual-Reflux Pressure Swing Adsorption Process.* Industrial & Engineering Chemistry Research, 2014. **53**(34): p. 13448-13458.
2. Webley, P.A., et al., *A New Multi-bed Vacuum Swing Adsorption Cycle for CO2 Capture from Flue Gas Streams.* Energy Procedia, 2017. **114**: p. 2467-2480.
3. Hauchhum, S., P. Mahanta, and J. De Wilde, *Capture of CO2 from Flue Gas onto Coconut Fibre-Based Activated Carbon and Zeolites in a Fixed Bed*. Vol. 110. 2015.

5.6 Methanol promoted oxidation of nitrogen oxide (NOx) by Encapsulated Ionic Liquids (ENILs)

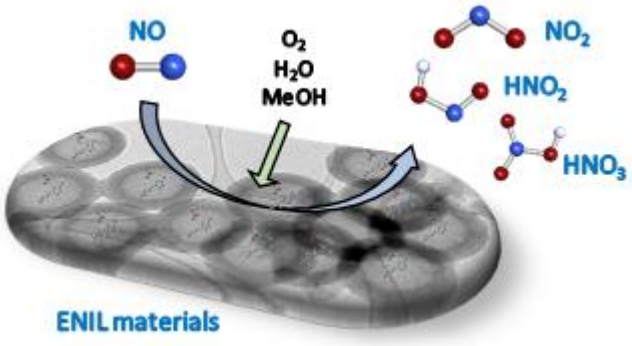

Methanol Promoted Oxidation of Nitrogen Oxide (NO_x) by Encapsulated Ionic Liquids (ENILs)

Rubén Santiago[1*], Susanne Mossin[2], Jorge Bedia[1], Rasmus Fehrmann[2], and José Palomar[1]

[1]*Chemical Engineering Department. Universidad Autónoma de Madrid. 28049 Madrid. Spain*

[2]*Centre for Catalysis and Sustainable Chemistry, Department of Chemistry, Technical University of Denmark, DK-2800 Kgs. Lyngby (Denmark).*

Corresponding author: ruben.santiago@uam.es

Keywords: NO oxidation; NO_x removal; Ionic Liquids; ENIL; Flue gas

Abstract

The removal of nitrogen oxides (NO_x) has been extensively studied due to their harmful effects to health and environment. In this work, Encapsulated Ionic Liquids (ENILs) are used as catalysts for the NO oxidation at humid conditions and low temperatures. Hollow carbon capsules (C_{Cap}) were first synthetized to contain different amounts of 1-butyl-3-methylimidazolium nitrate IL ([bmim][NO_3]), responsible for the catalytic oxidation. Then, the materials were characterized using different techniques, by analyzing microstructure, porosity, elemental composition and thermal stability. The catalytic performance of ENIL materials was tested for NO conversion at different conditions. Thus, NO concentration was fixed at 2,000 ppm at dry and humid conditions. Then, the methanol promotion of the reaction was demonstrated, increasing the NO conversion values in all cases, and the alcohol/water ratio was optimized. The temperature effect was studied as well, using the optimal conditions based on the previous measurements. The results reflect that humid conditions do not have a negative effect in terms of NO conversion when using ENILs, opposite behavior as the observed for C_{Cap} and traditional catalysts studied before. Low amount of IL inside the material (40% in mass) was found to be the optimum for the task, reaching conversions of almost 45% in near industrial conditions of temperature and O_2 and H_2O concentrations in the flue gas with a GHSV = 10,000 h^{-1}.

Introduction

Nitrogen oxides (NO_x) are one of the major air pollutants from traditional electrical production as fossil fuel combustion, leading to well-known harmful effects [1, 2]. These negative effects comprise not only to the human health, causing important respiratory problems [3], but also atmospheric pollution by acid rain, photochemical smog and ozone layer depletion [4, 5]. The major constituents of NO_x are nitrogen dioxide (NO_2) and nitric oxide (NO), which is an intermediate of the nitric acid synthesis in the chemical industry. Due to the low solubility of this gas in traditional solvents [6], it is attractive to develop systems to remove or convert this compound into value-added or not harmful products. The most important technologies of the chemical industry to remove NO_x present in the flue gas are the well stablished SCR (selective catalytic reduction) and SNCR (selective non-catalytic reduction) of NO_x [7, 8]. However, these methods are not able to remove NO_x completely because of some disadvantages during their use at high operating temperatures [9], which also means high costs of the process. The catalysts typically used in SCR, mainly based on V_2O_5, work at temperatures above 300 ºC [10], taking advantage of the high temperatures of the power plants systems but placed in high dust position, promoting catalyst deactivation. However, other industrial units like waste incineration plants and ships demand also low temperature –end-of-pipe- de-NO_x technologies. Therefore, research efforts have been centered on the development of new catalysts able to eliminate NO at lower temperatures. In this sense, not only the reduction process was taken into account, but others such as catalytic oxidation that was proved to work at lower temperature.

Several works were published in this field using zeolites [11] or carbonaceous materials [12] in presence of water at low temperature, giving as conclusion that the reaction occurs in the micropores of the material. Recently, an interesting work published by Ghafari *et al.* reports conversions up to 35 % of NO to NO_2 in presence of water by using a polymer based catalyst at near room temperatures [13]. However, the presence of water decreased the polymer based catalysts performance. For this reason, it is important to develop catalysts are less affected in presence of water, or even with water as promoter to convert NO to value-added products.

Other alternatives to remove NO were also investigated, such as absorption [14, 15]. In this case, the absorption capacity of NO in aqueous solutions is reported to be low [15]. For these reasons, big efforts has been tried to enhancing this absorption capacity by means

of using additives [16]. Furthermore, it was detected the easy combination of NO with transition metals, so different metals were specifically designed for NO capture [17]. All these absorbents were aqueous solutions, limited by the low NO solubility in water [18].

In last years, ionic liquids (ILs) are proposed as new chemical solvents, attracting a huge number of studies in e.g. gas capture applications [19], due to their characteristic properties such as high absorption capacity, low vapor pressure and high thermal and chemical stability [20], among others. Therefore, ILs have been extensively evaluated in gas capture, for instance of CO_2 [21], SO_2 [22], H_2S [23], NH_3 [24], and volatile organic compounds [25]. It is remarkable that, however, few works on NO capture by ILs have been reported so far. Chen *et al.* [26] reported the first functional IL to capture NO, with the disadvantage of the high difficulty in the synthesis stage. Then, Sun *et al.* [27] synthetized a metallic functional ionic liquid able to chemically absorb NO. Recently, Kunov-Kruse *et al.* [28] reported that the IL 1-butyl-3-methylimidazolium nitrate ([bmim][NO_3]) is a successful catalyst for NO oxidation into nitric acid in presence of water. However, it is well stated that the practical application of ILs are limited by their unfavorable transport properties [29, 30]. In fact, several efforts have been centered on developing systems and materials able to reduce the kinetic control in the absorption operations based on ILs [31-33]. Thus, Supported Ionic Liquid Phase (SILP) concept was invented [34-36]. It consists of IL deposition in the pores of a solid support (silica, carbon, among others). In the case of gas capture application, these materials increase the mass transport rates compared with pure ILs due to the increase in the gas-liquid interfaces [37]. In the case of catalysis, it can be used like a solid heterogeneous catalyst for continuous fixed bed reactor systems [35, 38]. A first approach to the NO separation using SILP materials (using silica as support) was successfully applied by Fehrmann's group [33]. However, the IL loading can limit the practical application of gas capture [32]. A more recent alternative has emerged: the Encapsulated Ionic Liquids (ENILs) concept, in which a high amount of IL (up to 80%) is contained inside hollow carbon capsules (internal diameter of 400-700 nm) with high specific surface area [31]. The performance of ENIL materials was tested by different gas capture applications such as ammonia [31, 39] and CO_2 in both physical [30, 40] and chemical [41-43] absorption. These works concluded that the encapsulation of the IL does not decrease absorption capacities and increase very significantly the absorption rates, due to the strong increase of contact surface after IL encapsulation. Furthermore, the nature of the IL does not significantly matter to the gas capture kinetics when using ENIL materials, since it is

controlled by carbon capsule morphology [48]. Therefore, ENIL materials are able to solve the kinetic restrictions that pure ILs present in gas capture applications.

At this point, it emerged the idea of taking advantage of the improved mass transfer kinetics of ENIL materials for its application in NO oxidation by ionic liquid catalysis. Therefore, we propose 1-butyl-3-methylimidazolium nitrate ([bmim][NO_3]) for its encapsulation into ENIL materials with different loadings. The IL selection was decided based on the previous work in which it was demonstrated that could be NO oxidized. The aim of this work is to evaluate the performance of a new support (based on hollow carbon capsules) in which the IL is encapsulated forming the ENIL materials in NO catalytic oxidation into NO_2, HNO_2 and HNO_3 in presence of water at low temperatures.

Experimental section

Materials

The IL 1-butyl-3-methylimidazolium nitrate (98 %) was purchased from Iolitec. The reagents used for hollow carbon capsules synthesis: phenol (99 %), paraformaldehyde (95-100 %), aluminum trichloride (95-100 %), ammonia (34 %) and absolute ethanol were supplied by Panreac. In addition, tetraethylorthosilicate (98 %) (TEOS), hexadecyltrimethoxysilane (90 %) (C16TMS) and hydrofluoric acid (48 %) were supplied by Sigma-Aldrich. Nitrogen, air and the mixture containing 10,000 ppmv of NO in nitrogen were supplied by AGA. The methanol (99.8 %) used for the promoted NO oxidation was supplied by Sigma-Aldrich.

ENIL synthesis

The hollow carbon capsules (C_{Cap}) were synthetized as ENIL materials following the procedure reported by Büchel *et al.* [44]. This methodology has been successfully applied by our group in the last years [41, 43, 45, 46] to obtain the C_{Cap} and then the ENIL materials for their use in gas capture applications. The full description of the procedure can be found in the referred works. In summary, C_{Cap} were synthetized following a "templating" method in which the solid core and the mesoporous shell aluminosilicate (SCMS) were used as template. The colloidal solution was maintained at 30 ºC with vigorous stirring to achieve homogenous diameters of the spheres. Then, the shell was grown around the silica core by adding TEOS and C16TMS (to give porosity to the double shell). After being filtrated and calcined at 550 ºC, the SCMS was impregnated by a phenolic resin (generated in situ) that will serve as carbon precursor (prior pyrolysis

stage). To accomplish this, aluminum trichloride was impregnated in the SCMS as catalyst of the phenolic resin generation. Then, a mixture of paraformaldehyde and phenol was added to completely impregnate the material generating the phenol-paraformaldehyde resin. The resulting material could be heated until 160 ºC that is the curing temperature of the resin, during 5 hours and then increased until 850 ºC under a nitrogen atmosphere to accomplish the pyrolysis of the material. The resulting carbon was washed with HF in order to remove the remaining silica present, being able to obtain the final hollow carbon capsules (C_{Cap}).

From C_{Cap}, the ENIL materials were prepared using incipient wetness impregnation. 400 mg of C_{Cap} were used and 1 mL of methanol-IL solution was added drop by drop onto the carbon support. Then, the resulting ENIL materials were heated until 85 ºC to completely remove the remaining methanol. In this work, four different ILs loadings were tested (20, 40, 60, and 80 % w/w). The methodology used was applied in several works of our group demonstrating the homogenous distribution of the IL inside the C_{Cap} [30, 39, 41-43].

ENIL characterization

The C_{Cap} samples were characterized by means of elemental analysis in a LECO CHNS-932 apparatus. The porous structure of the hollow spheres was also characterized by 77 K N_2 adsorption/desorption using a TriStar II 3020 (Micromeritics) equipment after 10 h of degassing at 0.1 mbar and 393 K. The microstructure and morphology of C_{Cap} were studied by transmission electron microscopy (TEM) using a JEOL JEM 2100 HT microscope. Then, the ENIL materials prepared were characterized by means of thermal gravimetric analysis (TGA) and elemental composition to check the amount of IL inside the material before and after reaction using a Mettler Toledo TGA/DSC 1 STARe system. This was carried out under a N_2 flow of 50 mL/min from room temperature until 600 ºC with a heating rate of 10 ºC/min.

NO oxidation measurements

The prepared ENIL materials and hollow carbon spheres (C_{Cap}) were tested as NO catalysts using a fixed-bed reactor with ENILs masses between 0.4-1.0 g depending on the load of IL used (volume 1.2 cm^3). Most experiments were carried out at room temperature (near 24 ºC). However, in the experiments in which the temperature was changed, the reactor was placed inside an oven able to control the temperature (regeneration experiments as well). A flue gas was passed through the reactor with a NO

concentration of 2,000 ppm. The O_2 content was varied from 6.2 to 16.8 % and balanced with N_2. Three mass flow controllers were used: i) connected to a 1% NO-N_2 bottle; ii) connected to an air bottle; iii) connected to a N_2 bottle. The total gas flow for each experiment was set at 200 mL/min. All the reactions were conducted at atmospheric pressure. Furthermore, the top of the reactor was fitted with a three-way valve that allows introducing the gases and the liquid inside the fixed-bed reactor. The flow of the liquid was controlled by a NE-300 Syringe Pump. In this sense, the relative humidity (RH) of the flue gas was changed and studied from 10 to 75 % utilizing a syringe filled of deionized water. The addition of the methanol to promote the oxidation reaction was accomplished by adding a water/methanol solution to the system by the Syringe Pump. The methanol concentration (varied from 100 to 1600 ppm) and the flow rate needed were calculated in each experiment in order to maintain the desired conditions. The bottom of the reactor was conducted into a gas cuvette inside a Thermo Scientific Evolution 220 UV-Visible Spectrophotometer. Each measurement collects the whole spectrum from 200 to 600 nm. NO have absorption bands in the ultra-violet (UV) region at 204 nm, 215 nm and 226 nm. This last peak was used to quantify the NO in the exit of the reactor and calculate the conversion. Peakfit.m matlab script was used for deconvolution of the three peaks, using last one at 226 nm to calculate conversions as a function of the peak area using a standard curve performed with different NO concentrations mixed with an inert gas (N_2). Other peaks that could be identified in the spectra are due to NO_2 having a broad peak around 405 nm and HNO_2 that presents four different peaks from 340 to 390 nm; and the HNO_3 exhibiting a broad peak in the NO region (from 200 to 250 nm). These peaks can indicate which species are being formed depending on the operation conditions tested. In all cases, the conversion was calculated at steady state, i.e. identical spectra obtained during at least 2 hours. Before changing the relative humidity of the inlet gas, the desorption experiment was carried out after heating the sample up to 130 ºC using 100 mL/min of N_2 in presence of water (ratio 1:1) to totally remove the water, methanol and nitric acid present in the sample.

Results

C_{Cap} and ENILs characterization

The hollow carbon capsules (C_{Cap}) and the four prepared ENIL materials were characterized by means of microscopy, pore structure, elemental analysis and thermal stability. Thus, Figure 1A shows TEM microscopy image of the C_{cap} while Figure 1C

shows the size distribution of the analyzed sample by several TEM images. Figure 1B presents the N_2 adsorption-desorption isotherm of the C_{Cap} before the incorporation of [bmim][NO_3] IL.

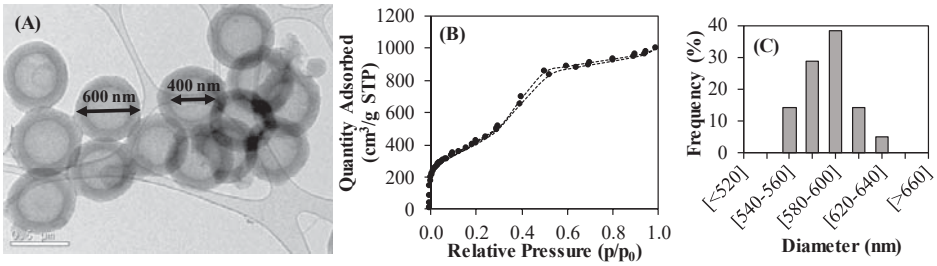

Figure 1: **(A)** TEM image of the hollow carbon capsules (C_{Cap}) to prepare ENIL materials; **(B)** N_2 adsorption/desorption isotherms @ 77 K of C_{Cap} and **(C)** size distribution of C_{Cap}

Figure 1A shows the homogenous size distribution of the material with spherical shape and an external diameter of almost 600 nm with a shell thickness of 200 nm and a large central hole. The N_2 adsorption-desorption isotherm (Figure 1B) is typical of a mesoporous material with a significant microporosity contribution (both as a consequence of the porosity of the shell). Table 1 reflects the elemental analysis and the summarized information extracted from the N_2 adsorption-desorption isotherms.

Table 1: Carbon capsules (C_{Cap}) characterization by means of elemental analysis and N_2 adsorption-desorption @ 77 K.

Characterization technique			
Elemental Analysis		N_2 adsorption-desorption	
% C (w)	91.40	S_{BET} (m^2/g)	1,494
% H (w)	1.80	$V_{micropore}$ (cm^3/g)	0.55
% N (w)	0.10	$V_{mesopore}$ (cm^3/g)	0.68
		Pore size (Å)	41.35

The elemental analysis extracted from Table 1 confirm the carbonaceous nature of the material (more than 90% of carbon). The incorporation of the different amounts of IL in the support is possible due to the high porosity. The material possesses both mesoporosity and microporosity mainly based on the porous shell grown around the central hollow core. Thus, the average pore size is almost 40 Å, which reflects the mesoporosity of the material. In that way, the different amounts of IL can be incorporated

in the support filling the double shell first (until 40% of IL) and the large central hole afterwards [31]. Once the C_{Cap} were synthetized and characterized, the ENIL materials can be prepared with different amounts of IL. In order to check the amount of IL incorporated in each sample, Figure *2* shows the TGA analysis of each one.

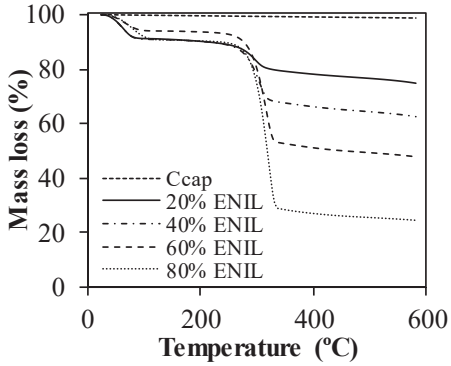

Figure 2: TGA analysis of the materials used in this work: hollow carbon capsules (C_{cap}) and ENIL materials with four different IL loading (20, 40, 60 and 80 % of [bmim][NO_3]). Analysis carried out with a temperature increase of 10 ºC·min^{-1} under 50 mL·min^{-1} of N_2.

Starting with the TGA analysis of C_{Cap}, as can be seen in Figure *2*, our support is stable at least until 600 ºC under nitrogen. Therefore, using this curve as reference, it is possible to estimate the amount of IL present in each sample taking into account the remaining mass at 600 ºC (attributed to the carbon support). In all cases, after a little decay prior to 100 ºC (possible sorbed water) the final value corresponds perfectly to the nominal amount of each material. The elemental composition results of each material (see Table S1 of Supplementary Information) confirm the conclusions of TGA analysis.

NO oxidation in dry conditions

The different prepared catalysts were first tested in absence of moisture. Prior to test the ENIL materials performance in NO catalytic oxidation, it is important to understand the behavior of the support (C_{Cap}) under different oxidation conditions. Figure *3* shows the NO conversion in the hollow carbon capsules using different O_2 contents.

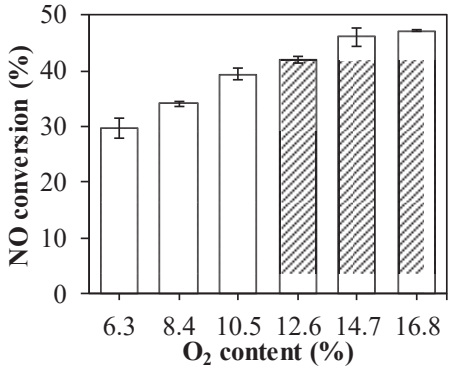

Figure 3: NO conversion of hollow carbon capsules (C_{cap}) in dry conditions at different oxygen contents. Gas composition: 2,000 ppm NO, 6.3-16.8% O_2, balance N_2, Flow: 200 mL·min^{-1}, GHSV=10,000 h^{-1}. Experiments conducted at room temperature.

As can be seen, the trend clearly shows higher catalytic activity by increasing the amount of O_2 in the system, reaching almost 48 % of conversion at 16.8% of O_2. This means that the presence of more O_2 in the system leads to the formation of more NO_2, resulting in higher conversion values (see Figure S1 in Supporting Information). Compared to those previously reported in the literature, we used 10.5% O_2 (almost 40 % NO conversion) which corresponds to those applied at industrial conditions to treat almost 2,000 ppm of NO [47]. Zeolite based catalysts exhibit NO conversions from 5 to 45 % [11] depending on the modifications carried out, concluding that those with higher micropore volume show the greatest performance. Zhang *et al.* [12] reported NO conversions up to 57 % using microporous activated carbons. Sousa *et al.* [48] used doped carbons reaching conversions up to 75 % in the best case. In view of all these results, our C_{Cap} material, later used as support for ENIL materials, presents NO conversion in dry O_2 conditions in the range of the zeolite catalysts and slightly lower when compared with activated carbons prior to their modification at almost same conditions. These differences may be attributed to the different porous structure of the materials. It is believed and proved that a high microporous structure leads to higher conversions. In the case of our material, it is basically a mesoporous material but presenting high micropore volume (see Table 1). The C_{Cap} performance can be compared with the ENIL catalysts at 10.5% of O_2. In Figure 4, the NO conversion reached by each material (including the previous discussed C_{Cap}) are compared.

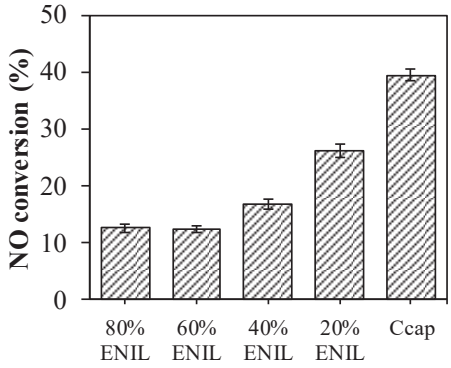

Figure 4: NO conversion of the different materials of the work in dry conditions. Gas composition: 2,000 ppm NO, 10.5% O_2, balance N_2, Flow: 200 mL·min^{-1}, GHSV=10,000 h^{-1}. Experiments conducted at room temperature.

As can be seen, NO conversion decreases by increasing the amount of IL in the catalyst until the conversion remains constant (from 60% IL loading). This could be explained due to filling of the pores of the C_{Cap} material. In the case of 20% and 40% ENIL material, the higher conversion may be attributed to partly filled pores exhibiting more efficient IL distribution on the pore surface. From the previous reported data with [bmim][NO_3] IL [28], it seems that the presence of water is key leading to the formation of more [NO_3]$^-$ anions (anion part of the IL) that may improve the NO removal.

NO oxidation in wet gas

In order to simulate near industrial conditions the catalytic performance of our materials was investigated in gas streams that contain around 10% O_2 and water.

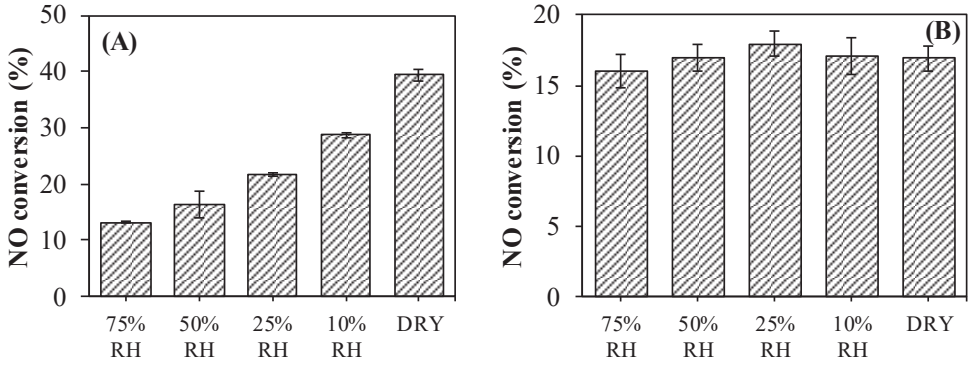

Figure 5: NO conversion of **(A)** the hollow carbon capsules (C_{cap}) and **(B)** the 40 % [bmim][NO_3] ENIL material in different dry and wet conditions (from 10 to 75% Relative Humidity). Gas composition: 2,000 ppm NO, 10.5% O_2, balance N_2, Flow: 200 mL·min^{-1}, GHSV=10,000 h^{-1}. Experiments conducted at room temperature.

Figure 5A clearly shows the catalytic inhibition when water was added into the system employing C_{Cap} as catalyst. NO conversion reaches only a value of 13% at 75% RH. This may be explained by the decrease of the NO adsorption mainly caused by the competitive water adsorption. Some works reported that water affects negatively the NO oxidation using activated carbons (AC) or zeolites. They reached the same conclusion: the NO oxidation inhibition in presence of water is caused by adsorption competition. Thus, Mochida *et al.* [49] showed a huge decrease in conversion by increasing RH in AC catalysts. Another work by Mochida *et al.* [50] showed the limitation of RH > 60% to the NO oxidation using AC catalysts. Guo *et al.* [51] reported the complete stop in NO oxidation when RH is higher than 20% using AC catalysts. The moisture influence was also studied in zeolite based catalysts [52] reaching conversions of only 10% when 8% of H_2O is present in the flue gas stream, showing a dramatic inhibiting effect in that kind of catalysts. The most recent study at wet conditions concerns a new polymer based catalyst [13] in which the inhibition was also demonstrated when 50% RH was employed. In addition, we believe that the inhibition may also be caused by means of *capillary condensation*, described by the Kelvin equation [53]. At the pore diameter of C_{Cap} (about 41 Å, see Table 1), *capillary condensation* at room temperature is expected to occur at a RH around 50-60% [54] and may thus cause the observed deactivation in Figure 5A for RH > 50%. This phenomenon definitely does not occur when the IL is completely filling the pores of the support. As can be seen, the presence of water does not inhibit the NO oxidation when using ENIL material. This may be explained by the different NO oxidation mechanism by the [bmim][NO_3] catalyst in presence of water that leads to conversion to HNO_3 instead of NO_2 in the dry gas as concluded in the previous work [28]. A slight increase in the HNO_3 and decrease in the NO_2 regions of the UV-Vis spectrum (see Figure S2 in Supporting Information) was thus found by adding water to the system compared to the C_{Cap} catalyst. Therefore, this IL catalyst the first reported NO oxidation catalyst that is not negatively affected by presence of water.

Figure 6 shows the NO conversion of the studied materials at two different gas humidity levels.

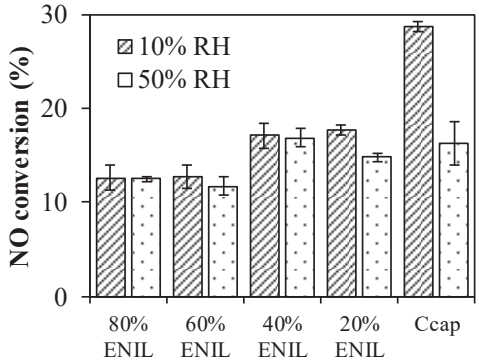

Figure 6: NO conversion of the different materials at two different wet conditions (10 and 50% Relative Humidity). Gas composition: 2,000 ppm NO, 10.5% O_2, balance N_2, Flow: 200 mL·min^{-1}, GHSV=10,000 h^{-1}. Experiments conducted at room temperature.

For 10% RH, it can be seen that the C_{Cap} material exhibits the highest conversion compared to the ENILs. It seems therefore the water levels are not enough for the ENIL materials to exhibit a decreased performance. The conversion follows almost the same trend as observed for the dry experiments, i.e. the NO conversion decreases while increasing the amount of IL in the material until 60% loading above, which it remains constant. However, a closer look reveals that the presence of water in the gas for the 20% ENIL catalyst seems to be partially inhibited compared to dry conditions, as in the case for the C_{Cap}. This may mean that there are still some pores not completely filled with the IL.

Analyzing the 50% RH exposure, the presence of available pores for NO oxidation in the case of 20% ENIL material seems obvious due to the observed reduction in the NO conversion (but to a lesser extent than for C_{Cap}) when compared with 10% RH exposure. This behavior was also concluded in terms of available pores while increasing the amount of ILs in the support by Lemus *et al.* [31, 32]. The rest of the materials exhibit unaltered behavior, since their activities are not affected by the addition of more water. If we now compare the performance of the materials at 50% RH, it can be seen that the 40% ENIL exhibits slightly higher NO conversion than C_{Cap}, probably due to the difference in mechanism, while the 20% ENIL material shows almost the same behavior as C_{Cap}, followed closely by the other two ENILs. Thus, it can be concluded that flue gas streams that contain high amount of water does not affect the ENIL materials performance (in terms of NO conversion), in contrast to the typical carbon materials (C_{Cap}), in which the reaction is strongly inhibited.

Methanol promoted NO oxidation in wet gas

In the 1990's, methanol promoted NO oxidation at high temperatures (from 700 ºC up to 1,000 ºC) was investigated [55, 56]. An increase in terms of NO conversion was reported when methanol was added to the system. Zamansky *et al.* proposed [56] the addition of a MeOH/H_2O_2 mixture to further increase the catalytic performance. No more work related to the methanol promoted NO oxidation has been published as far as we know. Then, research efforts moved to methanol oxidation in presence of NO. Thus, some papers [57-59] showed an increase in the MeOH conversion in presence of NO (temperatures from 600 up to 1,200 ºC). Furthermore, they proposed a possible mechanism of the oxidation reaction, concluding that radical formation in presence of NO was occurring. Since methanol promotes the NO oxidation, we screened different methanol concentrations to examine our catalysts performance. As far as we know, this is the first work in which this methodology is applied at room temperature using IL-based catalysts. Thus, Figure 7 shows the NO conversion as a function of the RH and the methanol concentration for the 40% ENIL material.

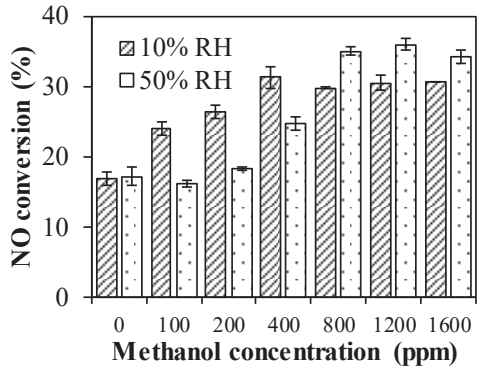

Figure 7: NO conversion in 40% [bmim][NO_3] ENIL material with relative humidity of 10 and 50% and different concentrations of MeOH in the gas phase. Gas composition: 2,000 ppm NO, 10.5% O_2, balance N_2, Flow: 200 mL·min^{-1}, GHSV=10,000 h^{-1}. Experiments conducted at room temperature.

From Figure 7, it can be seen how the NO conversion increases by increasing the methanol concentration until reaching a maximum. That maximum depends on the RH studied but it is located at a MeOH/NO ratio between 0.2-0.4 depending on the RH. Starting with 10% RH, it is clearly seen that NO conversion increases while increasing the amount of methanol until 400 ppm of MeOH whereafter it remains constant up to 1,600 ppm of MeOH. For 50% RH, the same trend is observed but the maximum is reached at 800 ppm of MeOH. It seems that for 50% RH, the NO conversion is higher

than at 10% RH at methanol concentrations above 800 ppm. This interesting difference in the trends might be explained by increased HNO_3 formation when more water is present in the system (see figure S3 of the Supporting Information). An interesting work by Xiao *et al.* [60] studying the mechanism of the methanol oxidation in presence of NO (room temperature performed as well) indicated that NO_2 may play a role in the methanol oxidation. They proposed a series of intermediate reactions involved in the MeOH oxidation when NO_2 is present. In this context, we believe that two of the proposed reactions may be occurring in our system:

$$CH_3OH + \cdot NO_2 \rightarrow \cdot CH_2OH + HONO \quad (1)$$

$$CH_3OH + \cdot NO_2 \rightarrow CH_3O\cdot + HONO \quad (2)$$

Reactions (1) and (2) may be occurring in our system due to the observed nitrous acid (HONO) and the absence of NO_2 in the UV-Vis spectrum (see Figure S3 in Supporting Information), not only while adding the first droplets but also at the steady state (especially when high conversions were found). This was immediately found when methanol was added to the system. Furthermore, huge amounts of HNO_3 were detected while adding MeOH to the system (see Figure S3 in Supporting Information), this may be explained by the proposed mechanism by Kunov-Kruse *et al.* [28] when using [bmim][NO_3] as catalyst in which HNO_3 was formed in the catalytic reaction in presence of water. In addition, the presence of HONO may lead to fast formation of HNO_3 (due to nitrous acids well-known instability). Therefore, promoted oxidation of NO in presence of MeOH may be explained by radical formation in both the liquid and the gas phase.

Based on the optimized MeOH addition, two different concentrations for each RH (200 and 400 ppm for 10% RH and 400 and 800 ppm for 50% RH) respectively were selected for testing the different materials.

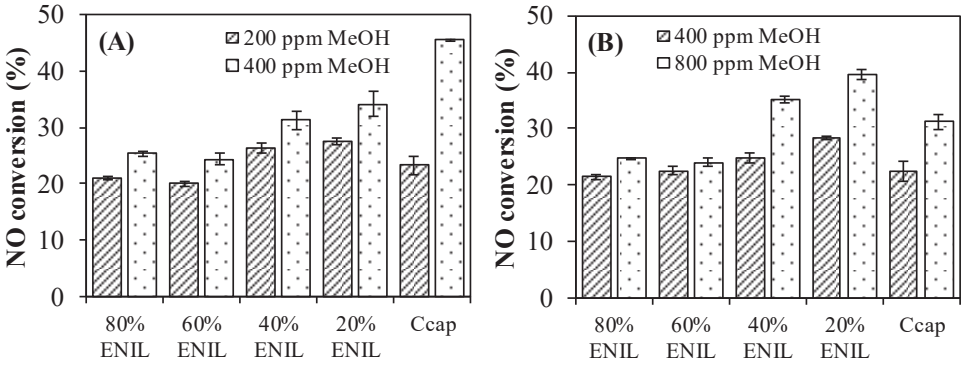

Figure 8: NO conversion of the different materials at relative humidity of **(A)** 10% RH and **(B)** 50% RH and two different concentrations of MeOH in the gas phase. Gas composition: 2,000 ppm NO, 10.5% O_2, balance N_2, Flow: 200 mL·min^{-1}, GHSV=10,000 h^{-1}. Experiments conducted at room temperature.

In Figure 8A, the methanol promoted NO conversions of the different materials at 10% RH can be analyzed. In general terms, all the materials exhibit greater conversions with the addition of MeOH when compared to the same moisture conditions without MeOH. For 200 ppm methanol, it can be seen that the 20% ENIL material presents the highest NO conversions while it seems that the amount of MeOH added is not enough for overcoming the inhibition in C_{Cap} material pores. However, when increasing to 400 ppm of MeOH, the hollow carbon capsules exhibit the highest activity. The measurements show in general that the addition of methanol promotes the reaction at wet conditions independent of the catalyst used.

Figure 8B shows that the 20% and 40% ENIL materials present the highest conversion at 50% RH, even higher than hollow carbon capsules. This suggests that at high concentrations of water, the presence of MeOH is not compensating for the inhibition of the NO reaction in the C_{Cap} material probably due to pore condensation of water. The results confirm that for wet conditions with addition of methanol, the ENIL materials exhibit a positive effect regarding the NO removal (increase of more than 50% in NO conversion when compared to the same moisture conditions without methanol - Figure 6).

It is important to remark that after testing the performance of each material, TGA analysis was performed to check the amount of IL that remains in the support (see Figure S4 in Supporting Information) after adding water and methanol to the system. In all cases,

it was obtained that the same initial amount of IL remained inside the support compared to before the catalytic tests.

Temperature effect on NO conversion

Previous studies reported an increased NO conversion when decreasing the temperature (a negative apparent activation energy) [61, 62], in good agreement with homogenous phase oxidation [61]. Figure 9 shows the NO conversion as a function of the temperature for the C_{Cap} material and the ENIL materials at 50% RH and 800 ppm of MeOH.

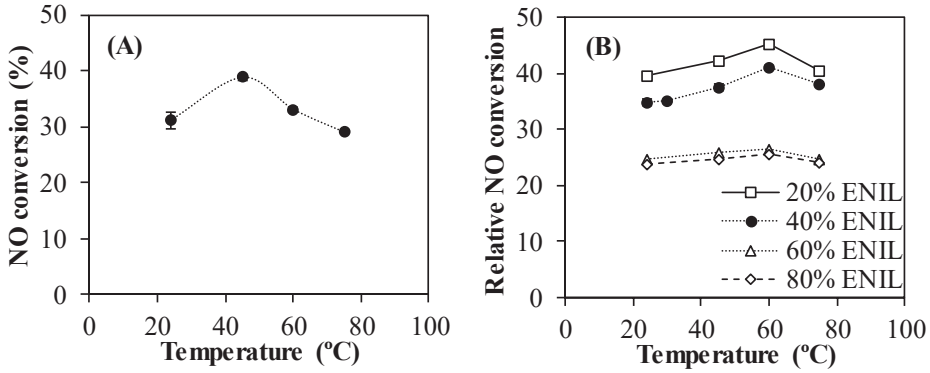

Figure 9: NO conversions in **(A)** hollow carbon capsules (C_{cap}) and **(B)** ENIL materials as a function of the temperature using 50% Relative Humidity and 800 ppm of MeOH in the gas phase. Gas composition: 2,000 ppm NO, 10.5% O_2, balance N_2, Flow: 200 $mL \cdot min^{-1}$, GHSV=10,000 h^{-1}.

As shown in Figure 9A, the C_{Cap} material optimum was found at 45 ºC while in the case of the ENIL material (Figure 9B), the maximum is located at 60 ºC. In the case of the ENIL material, the maximum at 60 ºC may be attributed to the competing limitations (radical formation) at low temperature and the lower gas solubility in the IL at higher temperatures. These conclusions concern the 20 and 40% ENIL materials in which most of the IL seems to be accessible to the gas, contrary to the 60 and 80% ENILs, where the temperature does not affect the NO conversion. However in general, the impact of the temperature on the NO conversion is not very important, reaching about 25% at maximum.

It can be concluded that the oxidation at higher temperatures (approaching flue gas stack temperatures) results in a slight increment of NO conversion, i.e. at temperatures close to 60 ºC, the NO conversion is in the range of 45%, in presence of water in the gas phase.

Encapsulated Ionic Liquids (ENILs) were successfully applied as catalysts for NO oxidation at low temperatures. ENILs with different loads of the IL [bmim][NO_3] were synthetized and then characterized by means of elemental analysis, thermal stability, porous structure and microscopy. Experiments in dry gas show higher NO conversion of the hollow carbon capsules compared to ENILs, where the conversion increased with decreasing the IL loading. Experiments conducted at different relative humidities showed positive effect on NO conversion for the ENIL materials. On the contrary, the results of empty carbon material showed inhibition of the NO oxidation by increasing humidity in the system. The reaction was promoted (in presence of water) by addition of methanol to the system. The amount of methanol added to the system was optimized (at different RH), showing an optimal MeOH/NO ratio between 0.2-0.4. In this case, ENILs composed of 20 and 40% of IL exhibited the greatest performance (including hollow carbon capsules) reaching conversions near 45%. The temperature effect on the reaction revealed an optimum temperature of 60 ºC when using ENILs, accomplishing relative NO conversions 20% higher than at room temperature ones. These results demonstrate potential application of ENILs as catalysts at near industrial flue gas conditions to create "fast SCR" for a down-stream traditional SCR catalyst.

Acknowledgments

The authors thank the Ministerio de Economía y Competitividad (MINECO) of Spain (project CTQ2017-89441-R) and Comunidad de Madrid (P2018/EMT4348) for financial support. Rubén Santiago also thanks David Nielsen for his great support at DTU.

References

1. Chang, S. G.; Liu, D. K., Removal of nitrogen and sulphur oxides from waste gas using a phosphorus/alkali emulsion. *Nature* **1990,** *343*, 151.
2. Pham, E. K.; Chang, S.-G., Removal of NO from flue gases by absorption to an iron(ii) thiochelate complex and subsequent reduction to ammonia. *Nature* **1994,** *369*, 139.
3. Kanchongkittiphon, W.; Mendell, M. J.; Gaffin, J. M.; Wang, G.; Phipatanakul, W., Indoor Environmental Exposures and Exacerbation of Asthma: An Update to the 2000 Review by the Institute of Medicine. *Environmental Health Perspectives* **2015,** *123* (1), 6-20.
4. Solomon, S., Stratospheric ozone depletion: A review of concepts and history. *Reviews of Geophysics* **1999,** *37* (3), 275-316.
5. Volz, A.; Kley, D., Evaluation of the Montsouris series of ozone measurements made in the nineteenth century. *Nature* **1988,** *332*, 240.
6. Liu, N.; Lu, B.-H.; Zhang, S.-H.; Jiang, J.-L.; Cai, L.-L.; Li, W.; He, Y., Evaluation of Nitric Oxide Removal from Simulated Flue Gas by Fe(II)EDTA/Fe(II)citrate Mixed Absorbents. *Energy & Fuels* **2012,** *26* (8), 4910-4916.

7. Jirat, J.; Stepanek, F.; Marek, M.; Kubicek, M., Comparison of design and operation strategies for temperature control during selective catalytic reduction of NOx. *Chemical Engineering & Technology* **2001,** *24* (1), 35-40.
8. Maisuls, S. E.; Seshan, K.; Feast, S.; Lercher, J. A., Selective catalytic reduction of NOx to nitrogen over Co-Pt/ZSM-5: Part A. Characterization and kinetic studies. *Applied Catalysis B: Environmental* **2001,** *29* (1), 69-81.
9. Gao, Y.; Luan, T.; LÜ, T.; Cheng, K.; Xu, H., Performance of V2O5-WO3-MoO3/TiO2 Catalyst for Selective Catalytic Reduction of NOx by NH3. *Chinese Journal of Chemical Engineering* **2013,** *21* (1), 1-7.
10. Busca, G.; Lietti, L.; Ramis, G.; Berti, F., Chemical and mechanistic aspects of the selective catalytic reduction of NOx by ammonia over oxide catalysts: A review. *Applied Catalysis B: Environmental* **1998,** *18* (1), 1-36.
11. Zhang, Z.; Atkinson, J. D.; Jiang, B.; Rood, M. J.; Yan, Z., NO oxidation by microporous zeolites: Isolating the impact of pore structure to predict NO conversion. *Applied Catalysis B: Environmental* **2015,** *163*, 573-583.
12. Zhang, Z.; Atkinson, J. D.; Jiang, B.; Rood, M. J.; Yan, Z., Nitric oxide oxidation catalyzed by microporous activated carbon fiber cloth: An updated reaction mechanism. *Applied Catalysis B: Environmental* **2014,** *148-149*, 573-581.
13. Ghafari, M.; Atkinson, J. D., Catalytic NO Oxidation in the Presence of Moisture Using Porous Polymers and Activated Carbon. *Environ Sci Technol* **2016,** *50* (10), 5189-5196.
14. Long, X. L.; Xin, Z. L.; Chen, M. B.; Xiao, W. D.; Yuan, W. K., Nitric oxide absorption into cobalt ethylenediamine solution. *Separation and Purification Technology* **2007,** *55* (2), 226-231.
15. Khan, N. E.; Adewuyi, Y. G., Absorption and Oxidation of Nitric Oxide (NO) by Aqueous Solutions of Sodium Persulfate in a Bubble Column Reactor. *Industrial & Engineering Chemistry Research* **2010,** *49* (18), 8749-8760.
16. Demmink, J. F.; van Gils, I. C. F.; Beenackers, A. A. C. M., Absorption of Nitric Oxide into Aqueous Solutions of Ferrous Chelates Accompanied by Instantaneous Reaction. *Industrial & Engineering Chemistry Research* **1997,** *36* (11), 4914-4927.
17. Chien, T. W.; Hsueh, H. T.; Chu, B. Y.; Chu, H., Absorption kinetics of NO from simulated flue gas using Fe(II)EDTA solutions. *Process Safety and Environmental Protection* **2009,** *87* (5), 300-306.
18. Zhu, H.-S.; Mao, Y.-P.; Chen, Y.; Long, X.-L.; Yuan, W.-K., Removal of nitric oxide and sulfur dioxide from flue gases using a FeII-ethylenediamineteraacetate solution. *Korean Journal of Chemical Engineering* **2013,** *30* (6), 1241-1247.
19. Welton, T., Ionic liquids: a brief history. *Biophys Rev* **2018,** *10*, 691-706.
20. Kosmulski, M.; Gustafsson, J.; Rosenholm, J. B., Thermal stability of low temperature ionic liquids revisited. *Thermochimica Acta* **2004,** *412* (1), 47-53.
21. Aghaie, M.; Rezaei, N.; Zendehboudi, S., A systematic review on CO2 capture with ionic liquids: Current status and future prospects. *Renewable & Sustainable Energy Reviews* **2018,** *96*, 502-525.
22. Lin, H.; Bai, P.; Guo, X. H., Ionic Liquids for SO2 Capture: Development and Progress. *Asian J. Chem.* **2014,** *26* (9), 2501-2506.
23. Wang, L. Y.; Xu, Y. L.; Li, Z. D.; Wei, Y. N.; Wei, J. P., CO2/CH4 and H2S/CO2 Selectivity by Ionic Liquids in Natural Gas Sweetening. *Energy & Fuels* **2018,** *32* (1), 10-23.
24. Bedia, J.; Palomar, J.; Gonzalez-Miquel, M.; Rodriguez, F.; Rodriguez, J. J., Screening ionic liquids as suitable ammonia absorbents on the basis of thermodynamic and kinetic analysis. *Separation and Purification Technology* **2012,** *95*, 188-195.

25. Bedia, J.; Ruiz, E.; de Riva, J.; Ferro, V. R.; Palomar, J.; Jose Rodriguez, J., Optimized Ionic Liquids for Toluene Absorption. *AlChE J.* **2013,** *59* (5), 1648-1656.
26. Chen, K. H.; Shi, G. L.; Zhou, X. Y.; Li, H. R.; Wang, C. M., Highly Efficient Nitric Oxide Capture by Azole-Based Ionic Liquids through Multiple-Site Absorption. *Angewandte Chemie-International Edition* **2016,** *55* (46), 14362-14366.
27. Sun, Y.; Ren, S.; Hou, Y.; Zhang, K.; Wu, W., Absorption of nitric oxide in simulated flue gas by a metallic functional ionic liquid. *Fuel Processing Technology* **2018,** *178*, 7-12.
28. Kunov-Kruse, A. J.; Thomassen, P. L.; Riisager, A.; Mossin, S.; Fehrmann, R., Absorption and Oxidation of Nitrogen Oxide in Ionic Liquids. *Chemistry-a European Journal* **2016,** *22* (33), 11745-11755.
29. Hu, Z. H.; Margulis, C. J., Room-temperature ionic liquids: Slow dynamics, viscosity, and the red edge effect. *Accounts Chem. Res.* **2007,** *40* (11), 1097-1105.
30. Santiago, R.; Lemus, J.; Moreno, D.; Moya, C.; Larriba, M.; Alonso-Morales, N.; Gilarranz, M. A.; Rodríguez, J. J.; Palomar, J., From kinetics to equilibrium control in CO2 capture columns using Encapsulated Ionic Liquids (ENILs). *Chemical Engineering Journal* **2018,** *348*, 661-668.
31. Palomar, J.; Lemus, J.; Alonso-Morales, N.; Bedia, J.; Gilarranz, M. A.; Rodriguez, J. J., Encapsulated ionic liquids (ENILs): from continuous to discrete liquid phase. *Chemical Communications* **2012,** *48* (80), 10046-10048.
32. Lemus, J.; Palomar, J.; A. Gilarranz, M.; J. Rodriguez, J., Characterization of Supported Ionic Liquid Phase (SILP) materials prepared from different supports. *Adsorption* **2011,** *17*, 561-571.
33. Thomassen, P.; Kunov-Kruse, A. J.; Mossin, S.; Kolding, H.; Kegns, S.; Riisager, A.; Fehrmann, R., Separation of Flue Gas Components by SILP (Supported Ionic Liquid-Phase) Absorbers. In *Molten Salts and Ionic Liquids 18*, Reichert, W. M.; Mantz, R. A.; Trulove, P. C.; Ispas, A.; Fox, D. M.; Mizuhata, M.; DeLong, H. C.; Bund, A., Eds. 2012; Vol. 50, pp 433-442.
34. Mehnert, C. P.; Cook, R. A.; Dispenziere, N. C.; Afeworki, M., Supported Ionic Liquid Catalysis − A New Concept for Homogeneous Hydroformylation Catalysis. *Journal of the American Chemical Society* **2002,** *124* (44), 12932-12933.
35. Riisager, A.; Fehrmann, R.; Haumann, M.; Wasserscheid, P., Supported Ionic Liquid Phase (SILP) catalysis: An innovative concept for homogeneous catalysis in continuous fixed-bed reactors. *European Journal of Inorganic Chemistry* **2006,** (4), 695-706.
36. Fehrmann, R.; Riisager, A.; Haumann, M., *Supported Ionic Liquids: Fundamentals and Applications*. 2014; p 1-474.
37. Romanos, G. E.; Schulz, P. S.; Bahlmann, M.; Wasserscheid, P.; Sapalidis, A.; Katsaros, F. K.; Athanasekou, C. P.; Beltsios, K.; Kanellopoulos, N. K., CO2 Capture by Novel Supported Ionic Liquid Phase Systems Consisting of Silica Nanoparticles Encapsulating Amine-Functionalized Ionic Liquids. *The Journal of Physical Chemistry C* **2014,** *118* (42), 24437-24451.
38. Riisager, A.; Jørgensen, B.; Wasserscheid, P.; Fehrmann, R., First application of supported ionic liquid phase (SILP) catalysis for continuous methanol carbonylation. *Chemical Communications* **2006,** (9), 994-996.
39. Lemus, J.; Bedia, J.; Moya, C.; Alonso-Morales, N.; A Gilarranz, M.; Palomar, J.; J Rodriguez, J., Ammonia Capture from Gas Phase by Encapsulated Ionic Liquids (ENILs). *RSC Advances* **2016,** *6*, 61650-61660.

40. Lemus, J.; Da Silva, F. A. F.; Palomar, J.; Carvalho, P. J.; Coutinho, J. A. P., Solubility of carbon dioxide in encapsulated ionic liquids. *Separation and Purification Technology* **2018,** *196*, 41-46.
41. Moya, C.; Alonso-Morales, N.; Gilarranz, M. A.; Rodriguez, J. J.; Palomar, J., Encapsulated Ionic Liquids for CO2 Capture: Using 1-Butyl-methylimidazolium Acetate for Quick and Reversible CO2 Chemical Absorption. *Chemphyschem* **2016,** *17* (23), 3891-3899.
42. Moya, C.; Alonso-Morales, N.; de Riva, J.; Morales-Collazo, O.; Brennecke, J. F.; Palomar, J., Encapsulation of Ionic Liquids with an Aprotic Heterocyclic Anion (AHA-IL) for CO2 Capture: Preserving the Favorable Thermodynamics and Enhancing the Kinetics of Absorption. *The Journal of Physical Chemistry B* **2018,** *122* (9), 2616-2626.
43. Santiago, R.; Lemus, J.; Moya, C.; Moreno, D.; Alonso-Morales, N.; Palomar, J., Encapsulated Ionic Liquids to Enable the Practical Application of Amino Acid-Based Ionic Liquids in CO2 Capture. *ACS Sustainable Chemistry & Engineering* **2018,** *6* (11), 14178-14187.
44. Buchel, G.; Unger, K. K.; Matsumoto, A.; Tsutsumi, K., A novel pathway for synthesis of submicrometer-size solid core/mesoporous shell silica spheres. *Advanced Materials* **1998,** *10* (13), 1036-1038.
45. Alonso-Morales, N.; Gilarranz, M. A.; Palomar, J.; Lemus, J.; Heras, F.; Rodriguez, J. J., Preparation of hollow submicrocapsules with a mesoporous carbon shell. *Carbon* **2013,** *59*, 430-438.
46. Alonso-Morales, N.; Ruiz-Garcia, C.; Palomar, J.; Heras, F.; Calvo, L.; Rodriguez, J. J.; Gilarranz, M. A., Hollow Nitrogen- or Boron-Doped Carbon Submicrospheres with a Porous Shell: Preparation and Application as Supports for Hydrodechlorination Catalysts. *Industrial & Engineering Chemistry Research* **2017,** *56* (27), 7665-7674.
47. Baukal, C. E.; Eleazer, P. B., Quantifying NOx for Industrial Combustion Processes. *Journal of the Air & Waste Management Association* **1998,** *48* (1), 52-58.
48. Sousa, J. P. S.; Pereira, M. F. R.; Figueiredo, J. L., NO oxidation over nitrogen doped carbon xerogels. *Applied Catalysis B: Environmental* **2012,** *125*, 398-408.
49. Mochida, I.; Kisamori, S.; Hironaka, M.; Kawano, S.; Matsumura, Y.; Yoshikawa, M., Oxidation of NO into NO2 over Active Carbon Fibers. *Energy & Fuels* **1994,** *8* (6), 1341-1344.
50. Mochida, I.; Kawabuchi, Y.; Kawano, S.; Matsumura, Y.; Yoshikawa, M., High catalytic activity of pitch-based activated carbon fibres of moderate surface area for oxidation of NO to NO2 at room temperature. *Fuel* **1997,** *76* (6), 543-548.
51. Guo, Z.; Xie, Y.; Hong, I.; Kim, J., *Catalytic oxidation of NO to NO2 on activated carbon*. 2001; Vol. 42, p 2005-2018.
52. Ruggeri, M. P.; Nova, I.; Tronconi, E., Experimental Study of the NO Oxidation to NO2 Over Metal Promoted Zeolites Aimed at the Identification of the Standard SCR Rate Determining Step. *Top. Catal.* **2013,** *56* (1), 109-113.
53. Atkins, P.; de Paula, J., *Atkins' Physical Chemistry*. 9th ed.; OUP Oxford: 2010.
54. Hubbe, M.; D Smith, R.; Zou, X.; Katuscak, S.; Potthast, A.; Ahn, K., *Deacidification of Acidic Books and Paper by Means of Non-aqueous Dispersions of Alkaline Particles: A Review Focusing on Completeness of the Reaction*. 2017; Vol. 12, p 4410-4477.
55. Lyon, R. K.; Cole, J. A.; Kramlich, J. C.; Chen, S. L., The selective reduction of SO3 to SO2 and the oxidation of NO to NO2 by methanol. *Combustion and Flame - COMBUST FLAME* **1990,** *81* (1), 30-39.

56. Zamansky, V. M.; Ho, L. O. C.; Maly, P. M.; Seeker, W. R., Oxidation of NO to NO2 by Hydrogen Peroxide and its Mixtures with Methanol in Natural Gas and Coal Combustion Gases. *Combust. Sci. Technol.* **1996,** *120* (1-6), 255-272.
57. Rasmussen, C. L.; Wassard, K. H.; Dam-Johansen, K.; Glarborg, P., Methanol oxidation in a flow reactor: Implications for the branching ratio of the CH3OH+ OH reaction. *International Journal of Chemical Kinetics* **2008,** *40* (7), 423-441.
58. Taylor, P.; Cheng, L.; Dellinger, B., The influence of nitric oxide on the oxidation of methanol and ethanol. *Combustion and Flame - COMBUST FLAME* **1998,** *115*, 561-567.
59. Alzueta, M. U.; Bilbao, R.; Finestra, M., Methanol Oxidation and Its Interaction with Nitric Oxide. *Energy & Fuels* **2001,** *15* (3), 724-729.
60. Xiao, C.-X.; Yan, N.; Zou, M.; Hou, S.-C.; Kou, Y.; Liu, W.; Zhang, S., NO2-catalyzed deep oxidation of methanol: Experimental and theoretical studies. *Journal of Molecular Catalysis A: Chemical* **2006,** *252* (1), 202-211.
61. Artioli, N.; Lobo, R. F.; Iglesia, E., Catalysis by Confinement: Enthalpic Stabilization of NO Oxidation Transition States by Micropororous and Mesoporous Siliceous Materials. *The Journal of Physical Chemistry C* **2013,** *117* (40), 20666-20674.
62. Loiland, J. A.; Lobo, R. F., Low temperature catalytic NO oxidation over microporous materials. *Journal of Catalysis* **2014,** *311*, 412-423.

Methanol Promoted Oxidation of Nitrogen Oxide (NO_x) by Encapsulated Ionic Liquids (ENILs)

Rubén Santiago[1], Susanne Mossin[2], Jorge Bedia[1], Rasmus Fehrmann[2], and José Palomar[1]

[1]*Chemical Engineering Department. Universidad Autónoma de Madrid. 28049 Madrid. Spain*

[2]*Centre for Catalysis and Sustainable Chemistry, Department of Chemistry, Technical University of Denmark, DK-2800 Kgs. Lyngby (Denmark).*

Supporting Information

Table S1: Elemental composition characterization of ENIL materials involved in the work 5

Figure S1: Pore size distribution of the materials involved in the work. 3
Figure S2: N_2 adsorption/desorption isotherms @ 77 K of all the materials involved in the work. 4
Figure S3: UV-Vis Spectrum of hollow carbon capsules (C_{Cap}) in dry conditions at different oxygen contents. Gas composition: 2,000 ppm NO, 6.3, 10.5 and 16.8% O_2, balance N_2, Flow: 200 mL·min^{-1}, GHSV=10,000 h^{-1}. Experiments conducted at room temperature. 6
Figure S4: UV-Vis Spectrum of 40% [bmim][NO_3] ENIL material (40% ENIL) in dry and 10% Relative Humidity conditions. Gas composition: 2,000 ppm NO, 10.5% O_2, balance N_2, Flow: 200 mL·min^{-1}, GHSV=10,000 h^{-1}. Experiments conducted at room temperature. 7
Figure S5: UV-Vis Spectrum of 20% [bmim][NO_3] ENIL material (20% ENIL) in 50% Relative Humidity and 800 ppm of MeOH conditions. Gas composition: 2,000 ppm NO, 10.5% O_2, balance N_2, Flow: 200 mL·min^{-1}, GHSV=10,000 h^{-1}. Experiments conducted at room temperature. 8
Figure S6: TGA analysis of the materials used in this work: hollow carbon capsules (C_{cap}) and ENIL materials with four different IL loads (20, 40, 60 and 80 % of [bmim][NO_3])

after being used in the catalytic reactions. Analysis carried out with a temperature increase of 10 ºC·min^{-1} under 50 mL·min^{-1} of N_2. 9

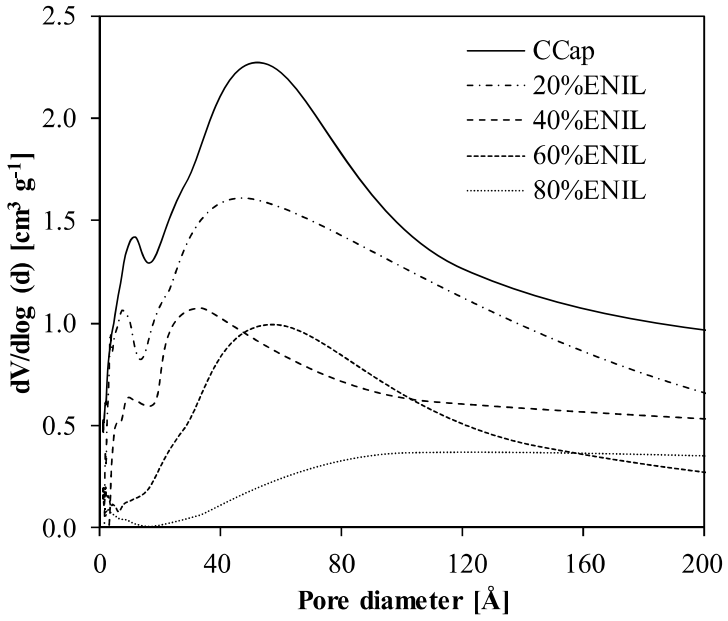

Figure S1: Pore size distribution of the materials involved in the work.

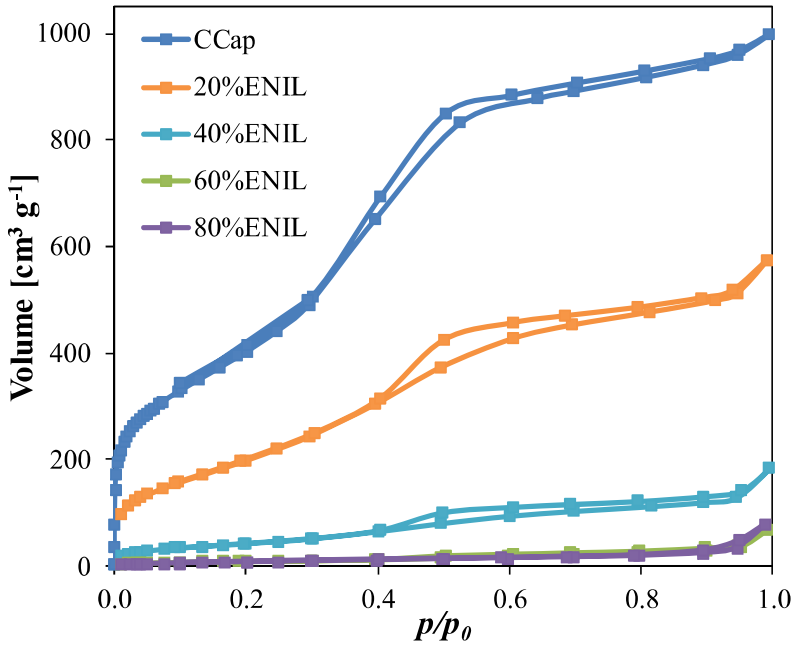

Figure S2: N_2 adsorption/desorption isotherms @ 77 K of all the materials involved in the work.

Table S1: Elemental composition characterization of ENIL materials involved in the work

		20% ENIL	40% ENIL	60% ENIL	80% ENIL
EA	**%C**	81.75	73.86	61.91	53.70
	%H	3.33	3.74	5.83	6.85
	%N	4.18	7.65	11.93	15.66
%IL	**EA**	20.03	36.65	57.16	75.04
	TGA	20.31	35.74	56.14	76.54
BET Area (m^2/g)		761	159	33	< 5
Average pore diameter (Å)		45.41	38.33	49.68	--

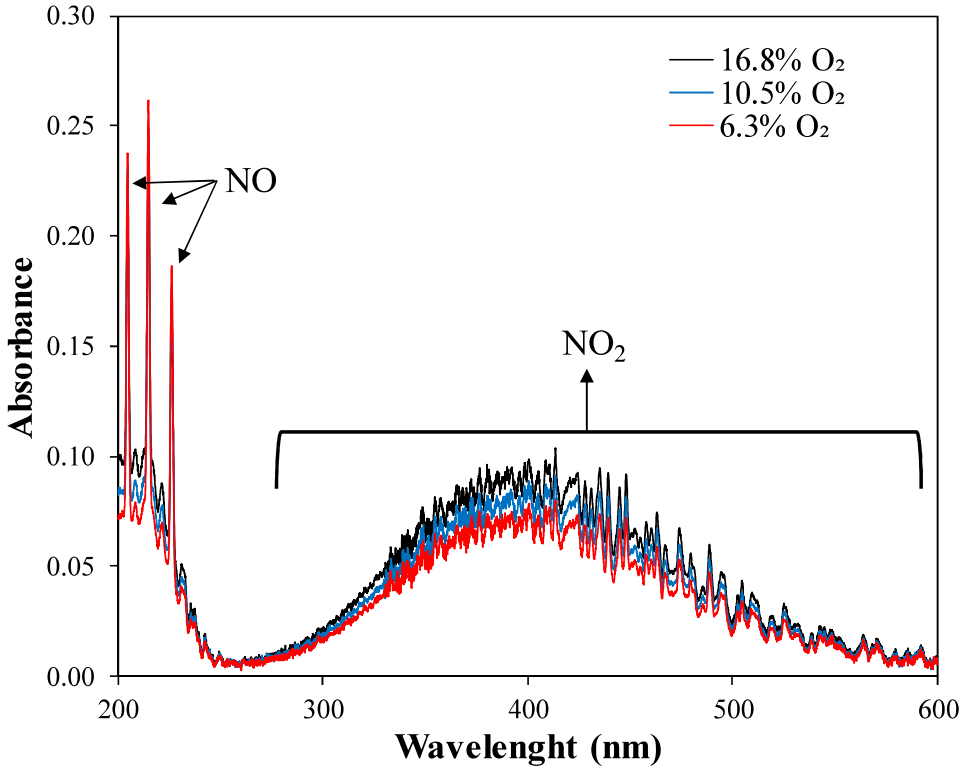

Figure S3: UV-Vis Spectrum of hollow carbon capsules (C_{Cap}) in dry conditions at different oxygen contents. Gas composition: 2,000 ppm NO, 6.3, 10.5 and 16.8% O_2, balance N_2, Flow: 200 mL·min^{-1}, GHSV=10,000 h^{-1}. Experiments conducted at room temperature.

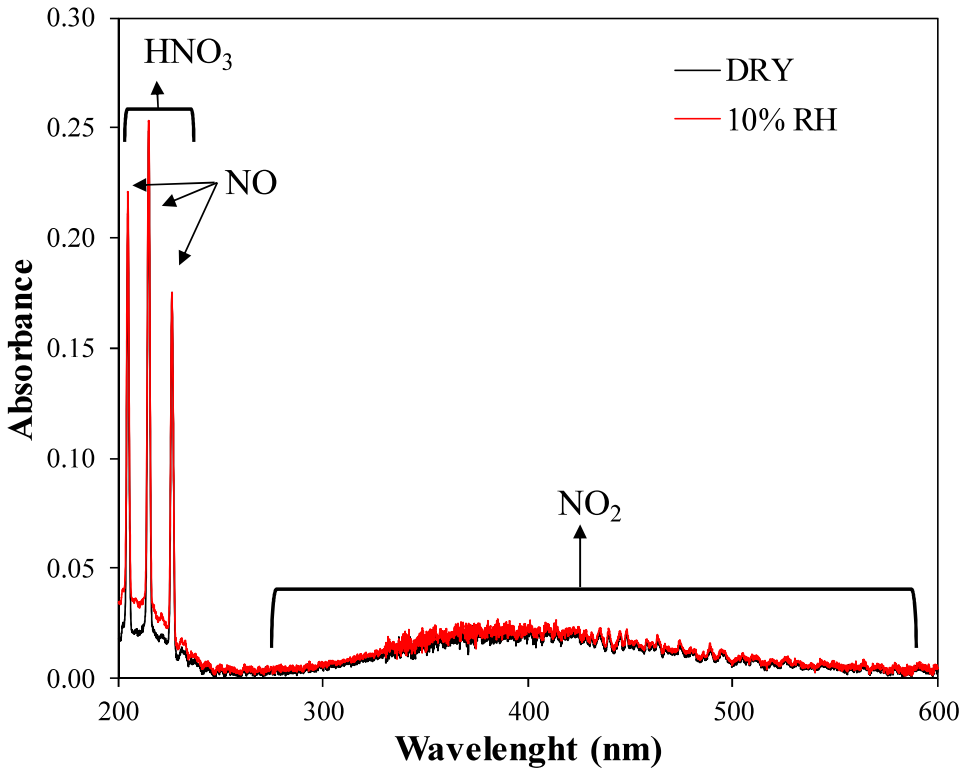

Figure S4: UV-Vis Spectrum of 40% [bmim][NO_3] ENIL material (40% ENIL) in dry and 10% Relative Humidity conditions. Gas composition: 2,000 ppm NO, 10.5% O_2, balance N_2, Flow: 200 mL·min^{-1}, GHSV=10,000 h^{-1}. Experiments conducted at room temperature.

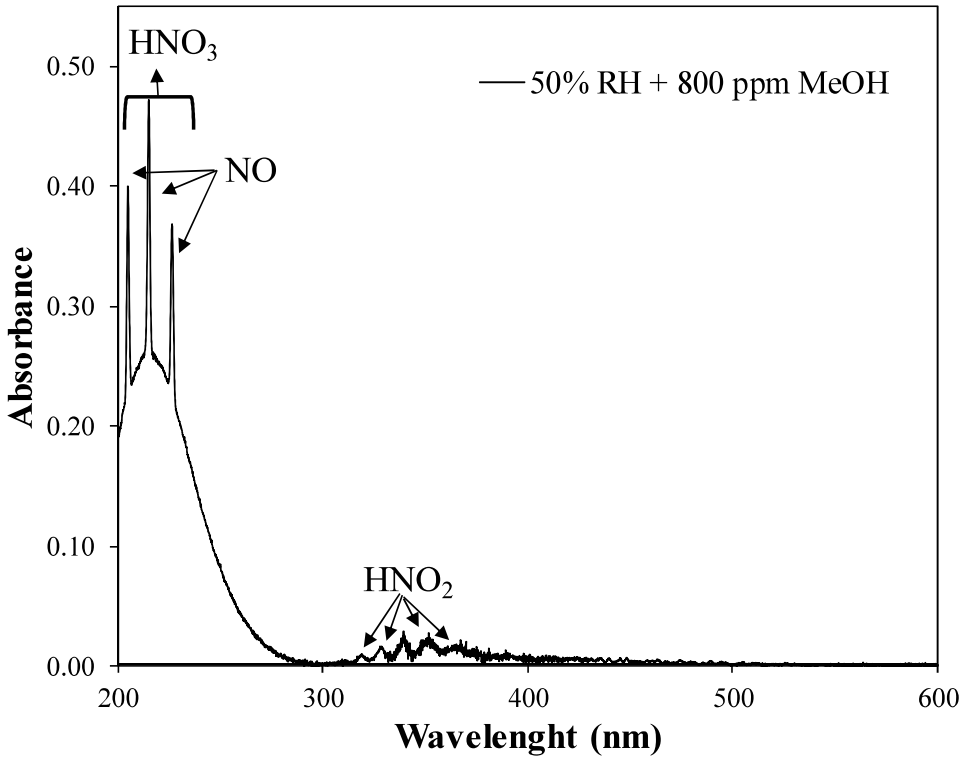

Figure S5: UV-Vis Spectrum of 20% [bmim][NO_3] ENIL material (20% ENIL) in 50% Relative Humidity and 800 ppm of MeOH conditions. Gas composition: 2,000 ppm NO, 10.5% O_2, balance N_2, Flow: 200 mL·min^{-1}, GHSV=10,000 h^{-1}. Experiments conducted at room temperature.

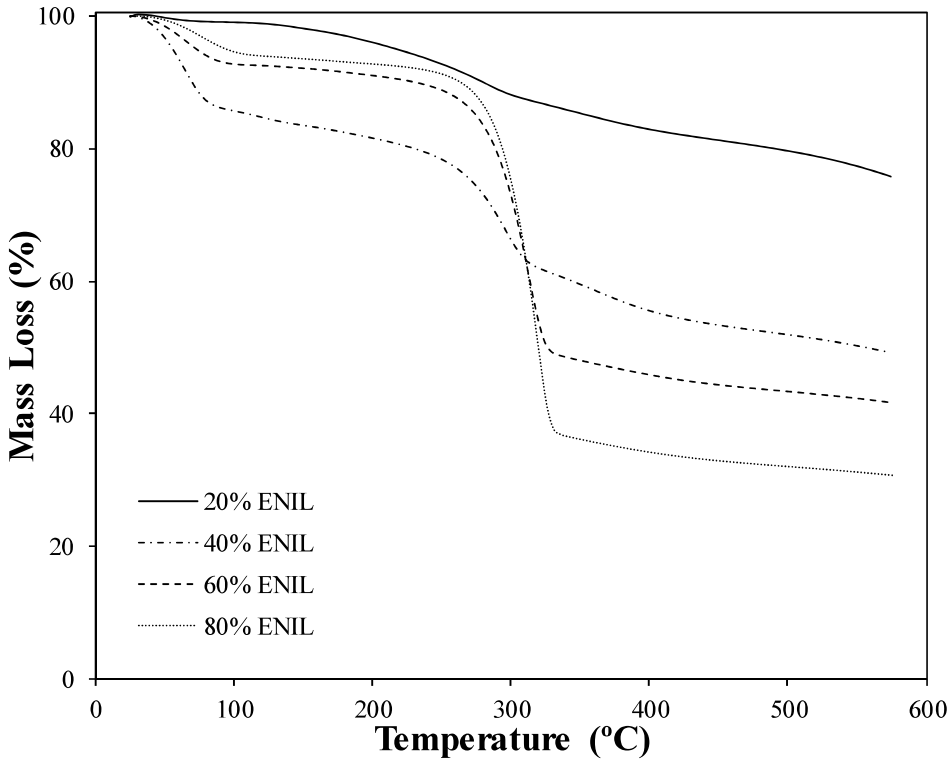

Figure S6: TGA analysis of the materials used in this work: hollow carbon capsules (C_{cap}) and ENIL materials with four different IL loads (20, 40, 60 and 80 % of [bmim][NO_3]) after being used in the catalytic reactions. Analysis carried out with a temperature increase of 10 ºC·min^{-1} under 50 mL·min^{-1} of N_2.

REFERENCES

1. Seddon, K.R., *Ionic liquids for clean technology.* Journal of Chemical Technology & Biotechnology: International Research in Process, Environmental and Clean Technology, **1997**. 68(4): p. 351-356.
2. Welton, T., *Room-Temperature Ionic Liquids. Solvents for Synthesis and Catalysis.* Chemical Reviews, **1999**. 99(8): p. 2071-2084.
3. Wasserscheid, P. and T. Welton, *Ionic liquids in synthesis*. **2008**: John Wiley & Sons.
4. Seddon, K., *Seddon, K. R. Ionic liquids: a taste of the future. Nat. Mater. 2, 363-365*. Vol. 2. **2003**. 363-5.
5. Plechkova, N.V. and K.R. Seddon, *Ionic liquids:"designer" solvents for green chemistry.* Methods and Reagents for Green Chemistry, **2007**: p. 105-130.
6. Rogers, R.D. and K.R. Seddon, *Ionic liquids: Industrial applications for green chemistry*, in *ACS Symposium Series*. **2002**: Washington D.C.
7. Mallakpour, S. and M. Dinari, *Ionic Liquids As Green Solvents: Progress and Prospects*. **2012**. p. 1-32.
8. Bier, M. and S. Dietrich, *Vapour pressure of ionic liquids.* Molecular Physics, **2010**. 108(2): p. 211-214.
9. Heintz, A., *Recent developments in thermodynamics and thermophysics of non-aqueous mixtures containing ionic liquids. A review.* The Journal of Chemical Thermodynamics, **2005**. 37(6): p. 525-535.
10. Rabideau, B.D., et al., *Making good on a promise: ionic liquids with genuinely high degrees of thermal stability.* Chemical Communications, **2018**. 54(40): p. 5019-5031.
11. MacFarlane, D.R., et al., *Ionic liquids based on imidazolium, ammonium and pyrrolidinium salts of the dicyanamide anion.* Green Chemistry, **2002**. 4(5): p. 444-448.
12. D. Holbrey, J. and K. R. Seddon, *The phase behaviour of 1-alkyl-3-methylimidazolium tetrafluoroborates; ionic liquids and ionic liquid crystals.* Journal of the Chemical Society, Dalton Transactions, **1999**(13): p. 2133-2140.
13. de Riva, J., et al., *Statistical Refinement and Fitting of Experimental Viscosity-to-Temperature Data in Ionic Liquids.* Industrial & Engineering Chemistry Research, **2014**. 53(25): p. 10475-10484.
14. Endres, F. and S.Z. El Abedin, *Air and water stable ionic liquids in physical chemistry.* Physical Chemistry Chemical Physics, **2006**. 8(18): p. 2101-2116.
15. Ahosseini, A. and A.M. Scurto, *Viscosity of imidazolium-based ionic liquids at elevated pressures: Cation and anion effects.* International Journal of Thermophysics, **2008**. 29(4): p. 1222-1243.
16. Marsh, K.N., et al., *Room temperature ionic liquids and their mixtures—a review.* Fluid Phase Equilibria, **2004**. 219(1): p. 93-98.
17. Song, D. and J. Chen, *Density and Viscosity Data for Mixtures of Ionic Liquids with a Common Anion.* Journal of Chemical & Engineering Data, **2014**. 59(2): p. 257-262.

18. Huddleston, J.G., et al., *Characterization and comparison of hydrophilic and hydrophobic room temperature ionic liquids incorporating the imidazolium cation.* Green Chemistry, **2001**. 3(4): p. 156-164.
19. Tariq, M., et al., *Surface tension of ionic liquids and ionic liquid solutions.* Chemical Society Reviews, **2012**. 41(2): p. 829-868.
20. Seddon, K., et al., *Influence of Chloride, Water, and Organic Solvents on the Physical Properties of Ionic Liquids*. Vol. 72. **2000**. 2275-2287.
21. Petkovic, M., et al., *Ionic liquids: a pathway to environmental acceptability.* Chemical Society Reviews, **2011**. 40(3): p. 1383-1403.
22. Abrusci, C., et al., *Efficient biodegradation of common ionic liquids by Sphingomonas paucimobilis bacterium.* Green Chemistry, **2011**. 13(3): p. 709-717.
23. Deetlefs, M., et al., *Ionic liquids: the view from Mount Improbable.* RSC Advances, **2016**. 6(6): p. 4280-4288.
24. Qureshi, Z.S., et al., *Applications of ionic liquids in organic synthesis and catalysis.* Clean Technologies and Environmental Policy, **2014**. 16(8): p. 1487-1513.
25. Silveira, E.T., et al., *The partial hydrogenation of benzene to cyclohexene by nanoscale ruthenium catalysts in imidazolium ionic liquids.* Chemistry-a European Journal, **2004**. 10(15): p. 3734-3740.
26. Moya, C., et al., *CO_2 conversion to cyclic carbonates catalyzed by ionic liquids with aprotic heterocyclic anions: DFT calculations and operando FTIR analysis.* Journal of CO_2 Utilization, **2018**. 28: p. 66-72.
27. Li, W., et al., *A short review of recent advances in CO_2 hydrogenation to hydrocarbons over heterogeneous catalysts.* RSC Advances, **2018**. 8(14): p. 7651-7669.
28. Marques Mota, F. and D.H. Kim, *From CO_2 methanation to ambitious long-chain hydrocarbons: alternative fuels paving the path to sustainability.* Chemical Society Reviews, **2019**. 48(1): p. 205-259.
29. Geng, T., et al., *Viscosity, Electrical Conductivity, Density and Surface Tension of Methyltriphenylphosphonium Carboxylate Ionic Liquids.* Bulletin of the Chemical Society of Japan, **2019**. 92(3): p. 578-584.
30. Seki, S., et al., *Densities, Viscosities, and Refractive Indices of Binary Room-Temperature Ionic Liquids with Common Cations/Anions.* Journal of Chemical and Engineering Data, **2019**. 64(2): p. 433-441.
31. Fillion, J.J., et al., *The Viscosity and Density of Ionic Liquid + Tetraglyme Mixtures and the Effect of Tetraglyme on CO_2 Solubility.* Journal of Chemical & Engineering Data, **2017**. 62(2): p. 608-622.
32. Rodil, E., et al., *Measurements of the density, refractive index, electrical conductivity, thermal conductivity and dynamic viscosity for tributylmethylphosphonium and methylsulfate based ionic liquids.* Thermochimica Acta, **2018**. 664: p. 81-90.
33. Tariq, M., et al., *Surface tension of ionic liquids and ionic liquid solutions.* Chemical Society Reviews, **2012**. 41(2): p. 829-868.
34. Sedev, R., *Surface tension, interfacial tension and contact angles of ionic liquids.* Current Opinion in Colloid & Interface Science, **2011**. 16(4): p. 310-316.

35. Calvar, N., et al., *Thermal analysis and heat capacities of pyridinium and imidazolium ionic liquids.* Thermochimica Acta, **2013**. 565: p. 178-182.
36. Karadas, F., et al., *Review on the Use of Ionic Liquids (ILs) as Alternative Fluids for CO_2 Capture and Natural Gas Sweetening.* Energy & Fuels, **2010**. 24(11): p. 5817-5828.
37. Fehrmann, R., et al., *Selective gas absorption by ionic liquids.* Abstracts of Papers of the American Chemical Society, **2015**. 250.
38. Shannon, M.S. and J.E. Bara, *Reactive and Reversible Ionic Liquids for CO_2 Capture and Acid Gas Removal.* Separation Science and Technology, **2012**. 47(2): p. 178-188.
39. Sas, O.G., et al., *Liquid-liquid extraction of phenolic compounds from water using ionic liquids: Literature review and new experimental data using C_2mim FSI.* Journal of Environmental Management, **2018**. 228: p. 475-482.
40. Dominguez, I., et al., *Liquid extraction of aromatic/cyclic aliphatic hydrocarbon mixtures using ionic liquids as solvent: Literature review and new experimental LLE data.* Fuel Processing Technology, **2014**. 125: p. 207-216.
41. Yan, X., et al., *Ionic liquids combined with membrane separation processes: A review.* Separation and Purification Technology, **2019**. 222: p. 230-253.
42. Dai, Z., et al., *Combination of ionic liquids with membrane technology: A new approach for CO_2 separation.* Journal of Membrane Science, **2016**. 497: p. 1-20.
43. Lenca, N. and C.F. Poole, *Liquid Chromatography with Room Temperature Ionic Liquids.* Jpc-Journal of Planar Chromatography-Modern Tlc, **2017**. 30(2): p. 97-105.
44. Martins, M.A.P., et al., *Ionic liquids in heterocyclic synthesis.* Chemical Reviews, **2008**. 108(6): p. 2015-2050.
45. Zhao, H. and S.V. Malhotra, *Applications of ionic liquids in organic synthesis.* Aldrichimica Acta, **2002**. 35(3): p. 75-83.
46. Doherty, A.P., et al., *Application of clean technologies using electrochemistry in ionic liquids.* Asia-Pacific Journal of Chemical Engineering, **2012**. 7(1): p. 14-23.
47. Macfarlane, D.R., et al., *Ionic liquids in electrochemical devices and processes: managing interfacial Electrochemistry.* Accounts of Chemical Research, **2007**. 40(11): p. 1165-1173.
48. Endres, F., *Ionic liquids: Promising solvents for electrochemistry.* Zeitschrift Fur Physikalische Chemie-International Journal of Research in Physical Chemistry & Chemical Physics, **2004**. 218(2): p. 255-283.
49. Lu, J., et al., *Advanced applications of ionic liquids in polymer science.* Progress in Polymer Science, **2009**. 34(5): p. 431-448.
50. Kudasheva, A., et al., *Dehumidification of air using liquid membranes with ionic liquids.* Journal of Membrane Science, **2016**. 499: p. 379-385.
51. Livazovic, S., et al., *Cellulose multilayer membranes manufacture with ionic liquid.* Journal of Membrane Science, **2015**. 490: p. 282-293.
52. Yuan, J., et al., *Poly(ionic liquid)s: An update.* Progress in Polymer Science, **2013**. 38(7): p. 1009-1036.

53. Yuan, K. and H. Ling, *Ionic liquids in green chemistry: Today's solvent or tomorrow's solution?* Progress in Chemistry, **2008**. 20(1): p. 5-10.
54. Welton, T., *Ionic liquids in Green Chemistry.* Green Chemistry, **2011**. 13(2): p. 225-225.
55. Benedetto, A. and P. Ballone, *Room temperature ionic liquids interacting with bio-molecules: an overview of experimental and computational studies.* Philosophical Magazine, **2016**. 96(7-9): p. 870-894.
56. Fukaya, Y., et al., *Bio ionic liquids: room temperature ionic liquids composed wholly of biomaterials.* Green Chemistry, **2007**. 9(11): p. 1155-1157.
57. Sprenger, K.G. and J. Pfaendtner, *Using Molecular Simulation to Study Biocatalysis in Ionic Liquids*, in *Computational Approaches for Studying Enzyme Mechanism, Pt A*, G.A. Voth, Editor. **2016**. p. 419-441.
58. Keaveney, S.T., et al., *Computational approaches to understanding reaction outcomes of organic processes in ionic liquids.* RSC Advances, **2015**. 5(45): p. 35709-35729.
59. Plechkova, N.V. and K.R. Seddon, *Applications of ionic liquids in the chemical industry.* Chemical Society Reviews, **2008**. 37(1): p. 123-150.
60. Siriwardana, A.I., *Industrial Applications of Ionic Liquids*, in *Electrochemistry in Ionic Liquids: Volume 2: Applications*, A.A.J. Torriero, Editor. **2015**, Springer International Publishing: Cham. p. 563-603.
61. Institute Français du Pétrole (IFP), *Anual Report*. **2004**.
62. Volland, M., et al., *Method for the separation of acids from chemical reaction mixtures by means of ionic fluids.* **2005**. BASF. Germany. *US20050020857A1.*
63. Maase, M. and Huttenloch, O., *Method for isolating acids from chemical reaction mixtures by using 1-alkylimidazoles.* **2009**. BASF. Germany. *US20090023933A1.*
64. Abai, M., et al., *An ionic liquid process for mercury removal from natural gas.* Dalton Transactions, **2015**. 44(18): p. 8617-8624.
65. Abbas, T., et al., *Stability and performance of physically immobilized ionic liquids for mercury adsorption from a gas stream.* Industrial & Engineering Chemistry Research, **2015**. 54(48): p. 12114-12123.
66. IoLiTec, et al., *Novel IOnic LIquid and supported ionic liquid solvents for reversible CAPture of CO_2 "IoLiCAP"*. **2011-2015**: Greece.
67. Liu, Z.-C., et al., *Ionic liquid alkylation process produces high-quality gasoline.* Oil & Gas Journal, **2006**. 104(40): p. 52-56.
68. PetroChina. *PetroChina's first ionic liquid alkylation unit*. **2018**; Available from: https://www.hydrocarbonprocessing.com/news/2018/11/petrochinas-first-ionic-liquid-alkylation-unit.
69. Lei, Z., et al., *Gas Solubility in Ionic Liquids.* Chemical Reviews, **2014**. 114(2): p. 1289-1326.
70. Agency, E.E. *Greenhouse gas emissions*. **2018**; Available from: https://www.eea.europa.eu/airs/2018/resource-efficiency-and-low-carbon-economy/greenhouse-gas-emission.
71. Agency of the European Union (EEA). *Climate change, impacts and vulnerability in Europe 2016, European Environment Agency*. **2016**;

Available from: https://www.eea.europa.eu/publications/climate-change-impacts-and-vulnerability-2016.
72. European Environment Agency. *GHG emissions by sector in the EU-28, 1990-2016*. **2016**; Available from: https://www.eea.europa.eu/data-and-maps/daviz/ghg-emissions-by-sector-in#tab-chart_1.
73. Figueroa, J.D., et al., *Advances in CO_2 capture technology—The U.S. Department of Energy's Carbon Sequestration Program.* International Journal of Greenhouse Gas Control, **2008**. 2(1): p. 9-20.
74. Ahn, J.H., et al., *Influence of various carbon capture technologies on the performance of natural gas-fired combined cycle power plants.* Journal of Mechanical Science and Technology, **2019**. 33(3): p. 1431-1440.
75. DOE-NETL, *Current and Future Technologies for Power Generation with Post Combustion Carbon Capture*. **2012**, Pittsburgh, PA.
76. DOE-NETL, *Cost and Performance Baseline for Fossil Energy Plants, Volume 1: Bituminous Coal and Natural Gas to Electricity*. **2010**, Pittsburgh, PA.
77. DOE-NETL, *Cost and Performance Baseline for Fossil Energy Plants Volume 1b: Bituminous Coal (IGCC) to Electricity*. **2015**, U.S. Department of Energy, National Energy Technology Laboratory.
78. Ramdin, M., et al., *State-of-the-Art of CO_2 Capture with Ionic Liquids.* Industrial & Engineering Chemistry Research, **2012**. 51(24): p. 8149-8177.
79. Kohl, A. and R. Nielsen, *Gas purification, 1997.* Houston: Elsevier, **2011**.
80. Luis, P., *Use of monoethanolamine (MEA) for CO_2 capture in a global scenario: Consequences and alternatives.* Desalination, **2016**. 380: p. 93-99.
81. Liang, Z., et al., *Recent progress and new developments in post-combustion carbon-capture technology with amine based solvents.* International Journal of Greenhouse Gas Control, **2015**. 40: p. 26-54.
82. Rangwala, H., et al., *Absorption of CO_2 into aqueous tertiary amine/MEA solutions.* The Canadian Journal of Chemical Engineering, **1992**. 70(3): p. 482-490.
83. Llamas, B., et al., *Greenhouse Gas Emissions–Carbon Capture, Storage and Utilisation*, in *Greenhouse Gases*. **2016**, IntechOpen.
84. DOE, U.S., *Advanced carbon dioxide capture R&D program: Technology update*. **2013**.
85. Keskes, E., et al., *A Physical Absorption Process for the Capture of CO_2 from CO_2-Rich Natural gas Streams*. **2008**.
86. Mumford, K.A., et al., *Review of solvent based carbon-dioxide capture technologies.* Frontiers of Chemical Science and Engineering, **2015**. 9(2): p. 125-141.
87. Yan, S., et al., *CO_2 removal from biogas by using green amino acid salts: Performance evaluation.* Fuel processing technology, **2015**. 129: p. 203-212.
88. Mumford, K.A., et al., *Post-combustion capture of CO_2: results from the solvent absorption capture plant at Hazelwood power station using potassium carbonate solvent.* Energy & fuels, **2011**. 26(1): p. 138-146.

89. Yang, N., et al., *Aqueous ammonia (NH_3) based post combustion CO_2 capture: A review.* Oil & Gas Science and Technology–Revue d'IFP Energies nouvelles, **2014**. 69(5): p. 931-945.
90. Yu, C.H., et al., *A Review of CO_2 Capture by Absorption and Adsorption.* Aerosol and Air Quality Research, **2012**. 12(5): p. 745-769.
91. Choi, S., et al., *Adsorbent materials for carbon dioxide capture from large anthropogenic point sources.* ChemSusChem: Chemistry & Sustainability Energy & Materials, **2009**. 2(9): p. 796-854.
92. Sayari, A., et al., *Flue gas treatment via CO_2 adsorption.* Chemical Engineering Journal, **2011**. 171(3): p. 760-774.
93. Plaza, M., et al., *Post-combustion CO_2 capture with a commercial activated carbon: comparison of different regeneration strategies.* Chemical Engineering Journal, **2010**. 163(1-2): p. 41-47.
94. Wang, Q., et al., *CO_2 capture by solid adsorbents and their applications: current status and new trends.* Energy & Environmental Science, **2011**. 4(1): p. 42-55.
95. Han, Y. and W.S.W. Ho, *Recent advances in polymeric membranes for CO_2 capture.* Chinese Journal of Chemical Engineering, **2018**. 26(11): p. 2238-2254.
96. Bonaventura, D., et al., *Dry carbonate process for CO_2 capture and storage: Integration with solar thermal power.* Renewable & Sustainable Energy Reviews, **2018**. 82: p. 1796-1812.
97. Yu, H., *Recent developments in aqueous ammonia-based post-combustion CO_2 capture technologies.* Chinese Journal of Chemical Engineering, **2018**. 26(11): p. 2255-2265.
98. Aghaie, M., et al., *A systematic review on CO_2 capture with ionic liquids: Current status and future prospects.* Renewable & Sustainable Energy Reviews, **2018**. 96: p. 502-525.
99. Kerlé, D., et al., *Temperature Dependence of the Solubility of Carbon Dioxide in Imidazolium-Based Ionic Liquids.* The Journal of Physical Chemistry B, **2009**. 113(38): p. 12727-12735.
100. Torralba-Calleja, E., et al., *CO_2 capture in ionic liquids: a review of solubilities and experimental methods.* Journal of Chemistry, **2013**. 2013.
101. Sarmad, S., et al., *Carbon Dioxide Capture with Ionic Liquids and Deep Eutectic Solvents: A New Generation of Sorbents.* Chemsuschem, **2017**. 10(2): p. 324-352.
102. Aki, S.N., et al., *High-pressure phase behavior of carbon dioxide with imidazolium-based ionic liquids.* The Journal of Physical Chemistry B, **2004**. 108(52): p. 20355-20365.
103. Zhang, X., et al., *Screening of ionic liquids to capture CO_2 by COSMO-RS and experiments.* AIChE journal, **2008**. 54(10): p. 2717-2728.
104. Carvalho, P.J., et al., *Dispelling some myths about the CO_2 solubility in ionic liquids.* Physical Chemistry Chemical Physics, **2016**. 18(22): p. 14757-14771.
105. Palomar, J., et al., *Demonstrating the key role of kinetics over thermodynamics in the selection of ionic liquids for CO_2 physical*

absorption. Separation and Purification Technology, **2019**. 213: p. 578-586.
106. Bates, E.D., et al., *CO_2 capture by a task-specific ionic liquid.* Journal of the American Chemical Society, **2002**. 124(6): p. 926-927.
107. Shang, D.W., et al., *Ionic liquids in gas separation processing.* Current Opinion in Green and Sustainable Chemistry, **2017**. 5: p. 74-81.
108. Sánchez, L.G., et al., *Solvent properties of functionalized ionic liquids for CO_2 absorption.* Chemical Engineering Research and Design, **2007**. 85(1): p. 31-39.
109. Gurkan, B.E., et al., *Equimolar CO_2 absorption by anion-functionalized ionic liquids.* Journal of the American Chemical Society, **2010**. 132(7): p. 2116-2117.
110. Goodrich, B.F., et al., *Experimental measurements of amine-functionalized anion-tethered ionic liquids with carbon dioxide.* Industrial and Engineering Chemistry Research, **2011**. 50(1): p. 111-118.
111. Sistla, Y.S. and A. Khanna, *CO_2 absorption studies in amino acid-anion based ionic liquids.* Chemical Engineering Journal, **2015**. 273: p. 268-276.
112. Barrosse-Antle, L.E. and R.G. Compton, *Reduction of carbon dioxide in 1-butyl-3-methylimidazolium acetate.* Chemical Communications, **2009**(25): p. 3744-3746.
113. Gurau, G., et al., *Demonstration of chemisorption of carbon dioxide in 1, 3-dialkylimidazolium acetate ionic liquids.* Angewandte Chemie International Edition, **2011**. 50(50): p. 12024-12026.
114. Shiflett, M.B., et al., *Carbon Dioxide Capture Using Ionic Liquid 1-Butyl-3-methylimidazolium Acetate.* Energy & Fuels, **2010**. 24(10): p. 5781-5789.
115. Shiflett, M.B. and A. Yokozeki, *Phase Behavior of Carbon Dioxide in Ionic Liquids: [emim][Acetate], [emim][Trifluoroacetate], and [emim][Acetate] + [emim][Trifluoroacetate] Mixtures.* Journal of Chemical & Engineering Data, **2009**. 54(1): p. 108-114.
116. Gurkan, B., et al., *Molecular Design of High Capacity, Low Viscosity, Chemically Tunable Ionic Liquids for CO_2 Capture.* The Journal of Physical Chemistry Letters, **2010**. 1(24): p. 3494-3499.
117. Seo, S., et al., *Chemically Tunable Ionic Liquids with Aprotic Heterocyclic Anion (AHA) for CO_2 Capture.* The Journal of Physical Chemistry B, **2014**. 118(21): p. 5740-5751.
118. Gohndrone, T.R., et al., *Competing reactions of CO_2 with cations and anions in azolide ionic liquids.* ChemSusChem, **2014**. 7(7): p. 1970-1975.
119. Seo, S., et al., *Effect of cation on physical properties and CO_2 solubility for phosphonium-based ionic liquids with 2-cyanopyrrolide anions.* The Journal of Physical Chemistry B, **2015**. 119(35): p. 11807-11814.
120. Williams, A. and D.B. Smith, *Combustion and oxidation of acetylene.* Chemical Reviews, **1970**. 70(2): p. 267-293.
121. United States Environmental Protection Agency (EPA),. *Assessment of Acetylene as a Potential Air Pollution Problem: Volume I - Final Report*. **1976**.

122. Analysis, Z.R., *Acetylene Gas Market for Chemical Production, Welding & Cutting and Other Applications: Global Industry Perspective, Comprehensive Analysis and Forecast, 2014 – 2020*. **2015**.
123. Pässler, P., et al., *Acetylene*. Ullmann's Encyclopedia of Industrial Chemistry, ed. Wiley-CH. **2011**.
124. Reppe, W., *Vinylierung.* Justus Liebigs Annalen der Chemie, **1956**. 601(1): p. 81-138.
125. Wegner, G., *Polymers with Metal-Like Conductivity—A Review of their Synthesis, Structure and Properties.* Angewandte Chemie International Edition in English, **1981**. 20(4): p. 361-381.
126. Forbath, T., *Acetylene by the BASF process.* Pertol. Refiner, **1954**. 33: p. 160-165.
127. McCue, A.J. and J.A. Anderson, *Recent advances in selective acetylene hydrogenation using palladium containing catalysts.* Frontiers of Chemical Science and Engineering, **2015**. 9(2): p. 142-153.
128. Friedrich, R., *Process for obtaining pure acetylene from a solution containing a solvent and C2 hydrocarbons.* **1961**. Linde AG. United States. *US3279152A.*
129. Palgunadi, J., et al., *Ionic liquids for acetylene and ethylene separation: Material selection and solubility investigation.* Chemical Engineering and Processing: Process Intensification, **2010**. 49(2): p. 192-198.
130. Palgunadi, J., et al., *Correlation between Hydrogen Bond Basicity and Acetylene Solubility in Room Temperature Ionic Liquids.* The Journal of Physical Chemistry B, **2011**. 115(5): p. 1067-1074.
131. Xu, H., et al., *Interface Behaviors of Acetylene and Ethylene Molecules with 1-Butyl-3-methylimidazolium Acetate Ionic Liquid: A Combined Quantum Chemistry Calculation and Molecular Dynamics Simulation Study.* ACS Applied Materials & Interfaces, **2012**. 4(12): p. 6646-6653.
132. Zhao, X., et al., *Differential Solubility of Ethylene and Acetylene in Room-Temperature Ionic Liquids: A Theoretical Study.* The Journal of Physical Chemistry B, **2012**. 116(13): p. 3944-3953.
133. Zhao, X., et al., *Design and screening of ionic liquids for C_2H_2/C_2H_4 separation by COSMO-RS and experiments.* AIChE Journal, **2015**. 61(6): p. 2016-2027.
134. Júlíusson, B.M., et al. *Tackling the challenge of H_2S emissions*. in *Proceedings, World Geothermal Congress*. **2015**.
135. CEIP. Centre on Emission Inventories and Projections. *Officially reported emission data*. **2015**.
136. Petroleum, B., *Statistical review of world energy*. **2018**.
137. Sadegh, N., *Acid Gas Removal from Natural Gas with Alkanolamines. A Modeling and Experimental Study*. **2013**.
138. Dutton, J.A., *Natural Gas Composition and Specifications*. **2007**, Penn State College of Earth and Mineral Sciences.
139. Wiheeb, A.D., et al., *Present technologies for hydrogen sulfide removal from gaseous mixtures.* Reviews in Chemical Engineering, **2013**. 29(6): p. 449-470.

140. Godini, H.R. and D. Mowla, *Selectivity study of H_2S and CO_2 absorption from gaseous mixtures by MEA in packed beds.* Chemical engineering research and design, **2008**. 86(4): p. 401-409.
141. Mohammad, A., *Green solvents II: properties and applications of ionic liquids*. Vol. 2. **2012**: Springer Science & Business Media.
142. Burr, B. and L. Lyddon. *A comparison of physical solvents for acid gas removal*. in *87th Annual Gas Processors Association Convention, Grapevine, TX, March*. **2008**.
143. Doctor, R., et al., *Gasification combined cycle: carbon dioxide recovery, transport, and disposal.* Energy conversion and management, **1993**. 34(9-11): p. 1113-1120.
144. Mansourizadeh, A., et al., *Effect of operating conditions on the physical and chemical CO_2 absorption through the PVDF hollow fiber membrane contactor.* Journal of Membrane Science, **2010**. 353(1-2): p. 192-200.
145. Seredych, M. and T.J. Bandosz, *Adsorption of hydrogen sulfide on graphite derived materials modified by incorporation of nitrogen.* Materials Chemistry and Physics, **2009**. 113(2-3): p. 946-952.
146. Dolan, M.D., et al., *Sulfur removal from coal-derived syngas: thermodynamic considerations and review.* Asia-Pacific Journal of Chemical Engineering, **2012**. 7(1): p. 1-13.
147. Steudel, R. and L. West, *Carl Friedrich Claus (1827-1900) - inventor of the Claus Process for sulfur production from hydrogen sulfide (update December 2015; with patents)*. **2015**.
148. Chiappe, C. and C.S. Pomelli, *Hydrogen Sulfide and Ionic Liquids: Absorption, Separation, and Oxidation.* Topics in Current Chemistry, **2017**. 375(3): p. 52.
149. Jou, F.-Y. and A.E. Mather, *Solubility of Hydrogen Sulfide in [bmim][PF_6].* International Journal of Thermophysics, **2007**. 28(2): p. 490.
150. Jalili, A.H., et al., *Solubility of CO_2, H_2S, and Their Mixture in the Ionic Liquid 1-Octyl-3-methylimidazolium Bis(trifluoromethyl)sulfonylimide.* The Journal of Physical Chemistry B, **2012**. 116(9): p. 2758-2774.
151. Jalili, A.H., et al., *Solubility of H_2S in Ionic Liquids [bmim][PF_6], [bmim][BF_4], and [bmim][Tf_2N].* Journal of Chemical & Engineering Data, **2009**. 54(6): p. 1844-1849.
152. Jalili, A.H., et al., *Solubility of CO_2 and H_2S in the ionic liquid 1-ethyl-3-methylimidazolium tris(pentafluoroethyl)trifluorophosphate.* The Journal of Chemical Thermodynamics, **2013**. 67: p. 55-62.
153. Handy, H., et al., *H_2S–CO_2 Separation Using Room Temperature Ionic Liquid [bmim][Br].* Separation Science and Technology, **2014**. 49(13): p. 2079-2084.
154. Huang, K., et al., *Thermodynamic validation of 1-alkyl-3-methylimidazolium carboxylates as task-specific ionic liquids for H_2S absorption.* AIChE Journal, **2013**. 59(6): p. 2227-2235.
155. United States Environmental Protection Agency (EPA), *Nitrogen Oxides Emissions*. **2015**.
156. Hooftman, N., et al., *Environmental analysis of petrol, diesel and electric passenger cars in a Belgian urban setting.* Energies, **2016**. 9(2): p. 84.

157. Sigal, I.Y., *The development and aims of investigation to study the conditions of formation of Nitrogen Oxides in Furnace Processes.* Thermal Engineering, **1983**. 30(9): p. 499-505.
158. Flamme, M., *Low NOx combustion technologies for high temperature applications.* Energy Conversion and Management, **2001**. 42(15-17): p. 1919-1935.
159. Nagle, L. and D. Probert, *A two-stage burner.* Applied energy, **1992**. 41(4): p. 309-313.
160. Nussbaumer, T., *Combustion and co-combustion of biomass: fundamentals, technologies, and primary measures for emission reduction.* Energy & fuels, **2003**. 17(6): p. 1510-1521.
161. Poole, D.R. and W.M. Graven, *Kinetics of the Reaction of Ammonia and Nitric Oxide in the Region of Spontaneous Ignition.* Journal of the American Chemical Society, **1961**. 83(2): p. 283-286.
162. Chen, K., et al., *Highly Efficient Nitric Oxide Capture by Azole-Based Ionic Liquids through Multiple-Site Absorption.* Angewandte Chemie International Edition, **2016**. 55(46): p. 14364-14368.
163. Roy, S., et al., *Catalysis for NOx abatement.* Applied Energy, **2009**. 86(11): p. 2283-2297.
164. Meier, H. and G. Gut, *Kinetics of the selective catalytic reduction of nitric oxide with ammonia on a platinum catalyst.* Chemical Engineering Science, **1978**. 33(1): p. 123-131.
165. Forzatti, P., *Present status and perspectives in de-NOx SCR catalysis.* Applied catalysis A: general, **2001**. 222(1-2): p. 221-236.
166. Bahrami, B., et al., *NH_3 decomposition and oxidation over noble metal-based FCC CO combustion promoters.* Applied Catalysis B: Environmental, **2013**. 130: p. 25-35.
167. Narkhede, V., et al., *Low temperature selective catalytic reduction of NOx over vanadium-based catalysts.* SAE International Journal of Engines, **2015**. 8(1): p. 380-385.
168. Sun, Y., et al., *Absorption of nitric oxide in simulated flue gas by a metallic functional ionic liquid.* Fuel processing technology, **2018**. 178: p. 7-12.
169. Sun, Y., et al., *Highly Efficient Nitric Oxide Absorption by Environmentally Friendly Deep Eutectic Solvents Based on 1, 3-Dimethylthiourea.* Energy & Fuels, **2017**. 31(11): p. 12439-12445.
170. Kunov-Kruse, A.J., et al., *Absorption and oxidation of nitrogen oxide in ionic liquids.* Chemistry–A European Journal, **2016**. 22(33): p. 11745-11755.
171. Mehnert, C.P., et al., *Supported ionic liquid catalysis– A new concept for homogeneous hydroformylation catalysis.* Journal of the American Chemical Society, **2002**. 124(44): p. 12932-12933.
172. Riisager, A., et al., *Continuous fixed-bed gas-phase hydroformylation using supported ionic liquid-phase (SILP) Rh catalysts.* Journal of Catalysis, **2003**. 219(2): p. 452-455.
173. Klefer, H., et al., *Kontinuierliche Gasreinigung mit SILP-Materialien.* Chemie Ingenieur Technik, **2014**. 86(1-2): p. 92-96.
174. Zhang, M., et al., *One-pot synthesis of ordered mesoporous silica encapsulated polyoxometalate-based ionic liquids induced efficient*

desulfurization of organosulfur in fuel. RSC Advances, **2015**. 5(93): p. 76048-76056.
175. Khan, N.A., et al., *Ionic Liquids Supported on Metal-Organic Frameworks: Remarkable Adsorbents for Adsorptive Desulfurization.* Chemistry – A European Journal, **2014**. 20(2): p. 376-380.
176. Steinrück, H.-P. and P. Wasserscheid, *Ionic Liquids in Catalysis.* Catalysis Letters, **2015**. 145(1): p. 380-397.
177. Erto, A., et al., *Carbon-supported ionic liquids as innovative adsorbents for CO_2 separation from synthetic flue-gas.* Journal of Colloid and Interface Science, **2015**. 448: p. 41-50.
178. Lemus, J., et al., *Characterization of Supported Ionic Liquid Phase (SILP) materials prepared from different supports.* Adsorption, **2011**. 17(3): p. 561-571.
179. Song, T., et al., *Recyclability of Encapsulated Ionic Liquids for Post-Combustion CO_2 Capture.* Industrial & Engineering Chemistry Research, **2019**. 58(12): p. 4997-5007.
180. Kaviani, S., et al., *Enhanced solubility of carbon dioxide for encapsulated ionic liquids in polymeric materials.* Chemical Engineering Journal, **2018**. 354: p. 753-757.
181. Stolaroff, J.K., et al., *CO_2 Absorption Kinetics of Micro-encapsulated Ionic Liquids.* Energy Procedia, **2017**. 114: p. 860-865.
182. Saxena, P., et al., *Ionic Liquid-Encapsulated Zeolite Catalysts for the Conversion of Glucose to 5-Hydroxymethylfurfural.* Chemistryselect, **2017**. 2(32): p. 10379-10386.
183. Alonso-Morales, N., et al., *Preparation of hollow submicrocapsules with a mesoporous carbon shell*. Vol. 59. **2013**. 430–438.
184. Palomar, J., et al., *Encapsulated ionic liquids (ENILs): from continuous to discrete liquid phase.* Chemical Communications, **2012**. 48(80): p. 10046-10048.
185. Lemus, J., et al., *Ammonia capture from the gas phase by encapsulated ionic liquids (ENILs).* RSC Advances, **2016**. 6(66): p. 61650-61660.
186. Moya, C., et al., *Encapsulated Ionic Liquids for CO_2 Capture: Using 1-Butyl-methylimidazolium Acetate for Quick and Reversible CO_2 Chemical Absorption.* ChemPhysChem, **2016**. 17(23): p. 3891-3899.
187. Lemus, J., et al., *Solubility of carbon dioxide in encapsulated ionic liquids*. **2017**.
188. Moya, C., et al., *Encapsulation of Ionic Liquids with an Aprotic Heterocyclic Anion (AHA-IL) for CO_2 Capture: Preserving the Favorable Thermodynamics and Enhancing the Kinetics of Absorption.* The Journal of Physical Chemistry B, **2018**. 122(9): p. 2616-2626.
189. Moya, C., *Captura de CO_2 mediante operaciones de separación basadas en líquidos iónicos*, in *Chemical Engineering Department*. **2017**, Universidad Autónoma de Madrid.
190. Klamt, A., *Conductor-like screening model for real solvents: a new approach to the quantitative calculation of solvation phenomena.* The Journal of Physical Chemistry, **1995**. 99(7): p. 2224-2235.
191. Klamt, A. and G. Schüürmann, *COSMO: a new approach to dielectric screening in solvents with explicit expressions for the screening energy*

and its gradient. Journal of the Chemical Society, Perkin Transactions 2, **1993**(5): p. 799-805.
192. Klamt, A., et al., *Refinement and parametrization of COSMO-RS.* The Journal of Physical Chemistry A, **1998**. 102(26): p. 5074-5085.
193. Lin, S.-T. and S.I. Sandler, *A priori phase equilibrium prediction from a segment contribution solvation model.* Industrial & engineering chemistry research, **2002**. 41(5): p. 899-913.
194. Grensemann, H. and J. Gmehling, *Performance of a conductor-like screening model for real solvents model in comparison to classical group contribution methods.* Industrial & engineering chemistry research, **2005**. 44(5): p. 1610-1624.
195. Palomar, J., et al., *A COSMO-RS based guide to analyze/quantify the polarity of ionic liquids and their mixtures with organic cosolvents.* Physical Chemistry Chemical Physics, **2010**. 12(8): p. 1991-2000.
196. Palomar, J., et al., *Prediction of non-ideal behavior of polarity/polarizability scales of solvent mixtures by integration of a novel COSMO-RS molecular descriptor and neural networks.* Physical Chemistry Chemical Physics, **2008**. 10(39): p. 5967-5975.
197. Lin, S.T., et al., *Prediction of vapor pressures and enthalpies of vaporization using a COSMO solvation model.* Journal of Physical Chemistry A, **2004**. 108(36): p. 7429-7439.
198. Banerjee, T., et al., *Prediction of binary VLE for imidazolium based ionic liquid systems using COSMO-RS.* Industrial & Engineering Chemistry Research, **2006**. 45(9): p. 3207-3219.
199. Diedenhofen, M., et al., *Prediction of infinite dilution activity coefficients of organic compounds in ionic liquids using COSMO-RS.* Journal of Chemical & Engineering Data, **2003**. 48(3): p. 475-479.
200. Diedenhofen, M. and A. Klamt, *COSMO-RS as a tool for property prediction of IL mixtures—A review.* Fluid Phase Equilibria, **2010**. 294(1-2): p. 31-38.
201. Jiang, H., et al., *Vapor-Liquid Phase Equilibrium for Separation of Isopropanol from Its Aqueous Solution by Choline Chloride-Based Deep Eutectic Solvent Selected by COSMO-SAC Model.* Journal of Chemical and Engineering Data, **2019**. 64(4): p. 1338-1348.
202. Salleh, M.Z.M., et al., *Ionic liquids for the separation of benzene and cyclohexane - COSMO-RS screening and experimental validation.* Journal of Molecular Liquids, **2018**. 266: p. 51-61.
203. Larriba, M., et al., *COSMO-based/Aspen Plus process simulation of the aromatic extraction from pyrolysis gasoline using the 1 4empy NTf_2 + emim DCA } ionic liquid mixture.* Separation and Purification Technology, **2018**. 190: p. 211-227.
204. Moreno, D., et al., *Molecular and Thermodynamic Properties of Zwitterions versus Ionic Liquids: A Comprehensive Computational Analysis to Develop Advanced Separation Processes.* Chemphyschem, **2018**. 19(7): p. 801-815.
205. Moya, C., et al., *Non-ideal behavior of ionic liquid mixtures to enhance CO_2 capture.* Fluid Phase Equilibria, **2017**. 450: p. 175-183.

206. Gonzalez-Miquel, M., et al., *Anion Effects on Kinetics and Thermodynamics of CO_2 Absorption in Ionic Liquids.* Journal of Physical Chemistry B, **2013**. 117(12): p. 3398-3406.
207. Gonzalez-Miquel, M., et al., *COSMO-RS Studies: Structure-Property Relationships for CO_2 Capture by Reversible Ionic Liquids.* Industrial & Engineering Chemistry Research, **2012**. 51(49): p. 16066-16073.
208. Calvar, N., et al., *Evaluation of ionic liquids as solvent for aromatic extraction: Experimental, correlation and COSMO-RS predictions.* Journal of Chemical Thermodynamics, **2013**. 67: p. 5-12.
209. Bedia, J., et al., *Optimized Ionic Liquids for Toluene Absorption.* AIChe Journal, **2013**. 59(5): p. 1648-1656.
210. Fallanza, M., et al., *Screening of RTILs for propane/propylene separation using COSMO-RS methodology.* Chemical Engineering Journal, **2013**. 220: p. 284-293.
211. Gonzalez-Miquel, M., et al., *Selection of Ionic Liquids for Enhancing the Gas Solubility of Volatile Organic Compounds.* Journal of Physical Chemistry B, **2013**. 117(1): p. 296-306.
212. Bedia, J., et al., *Screening ionic liquids as suitable ammonia absorbents on the basis of thermodynamic and kinetic analysis.* Separation and Purification Technology, **2012**. 95: p. 188-195.
213. Palomar, J., et al., *Task-specific ionic liquids for efficient ammonia absorption.* Separation and Purification Technology, **2011**. 82: p. 43-52.
214. Rhodes, C.L., *The Process Simulation Revolution: Thermophysical Property Needs and Concerns.* Journal of Chemical & Engineering Data, **1996**. 41(5): p. 947-950.
215. Hendriks, E., et al., *Industrial Requirements for Thermodynamics and Transport Properties.* Industrial & Engineering Chemistry Research, **2010**. 49(22): p. 11131-11141.
216. Bagchi, B., et al., *Modeling solubility of CO_2/hydrocarbon gas in ionic liquid ([emim][FAP]) using Aspen Plus simulations.* Environmental Science and Pollution Research, **2017**. 24(22): p. 18106-18122.
217. Graczova, E., et al., *Design calculations of an extractor for aromatic and aliphatic hydrocarbons separation using ionic liquids.* Chemical Papers, **2013**. 67(12): p. 1548-1559.
218. Fredenslund, A., et al., *Group-contribution estimation of activity coefficients in nonideal liquid mixtures.* AIChE Journal, **1975**. 21(6): p. 1086-1099.
219. Lei, Z., et al., *UNIFAC Model for Ionic Liquids.* Industrial & Engineering Chemistry Research, **2009**. 48(5): p. 2697-2704.
220. Chao, H., et al., *Computer-aided design and process evaluation of ionic liquids for n-hexane-methylcyclopentane extractive distillation.* Separation and Purification Technology, **2018**. 196: p. 157-165.
221. Song, Z., et al., *Computer-Aided Design of Ionic Liquids as Solvents for Extractive Desulfurization.* Aiche Journal, **2018**. 64(3): p. 1013-1025.
222. Ruiz, E., *Multiscale approach for the conceptual development of industrial processes based on ionic liquids*, in *Chemical Engineering Department*. **2013**, Universidad Autónoma de Madrid.

223. de Riva, J., *Aspen Plus/COSMO-RS Multiscale Ionic Liquid Conceptual Process Design*, in *Chemical Engineering Department*. **2017**, Universidad Autónoma de Madrid.
224. Moreno, D., *From quantum chemistry to process engineering: A methodology for the study of properties and applications of ionic liquids in the chemical industry*, in *Chemical Engineering Department*. **2018**, Universidad Autónoma de Madrid.
225. Borghi, D., et al., *Use of COSMO-SAC to Determine the Activity Coefficient and Predict Phase Equilibrium of Binary Systems Involving Methanol, Glycerol and Water.* Chemical Engineering Transactions, **2015**. 43: p. 1879-1884.
226. Ruiz, E., et al., *Evaluation of ionic liquids as absorbents for ammonia absorption refrigeration cycles using COSMO-based process simulations.* Applied Energy, **2014**. 123: p. 281-291.
227. Moreno, D., et al., *Absorption refrigeration cycles based on ionic liquids: Refrigerant/absorbent selection by thermodynamic and process analysis.* Applied energy, **2018**. 213: p. 179-194.
228. Ferro, V., et al., *Conceptual design of unit operations to separate aromatic hydrocarbons from naphtha using ionic liquids. COSMO-based process simulations with multi-component "real" mixture feed.* Chemical Engineering Research & Design, **2015**. 94: p. 632-647.
229. de Riva, J., et al., *Aspen Plus supported analysis of the post-combustion CO2 capture by chemical absorption using the [P_{2228}][CNPyr] and [P_{66614}][CNPyr]AHA Ionic Liquids.* International Journal of Greenhouse Gas Control, **2018**. 78: p. 94-102.
230. de Riva, J., et al., *Ionic liquids for post-combustion CO_2 capture by physical absorption: Thermodynamic, kinetic and process analysis.* International Journal of Greenhouse Gas Control, **2017**. 61: p. 61-70.
231. de Riva, J., et al., *Aspen Plus supported conceptual design of the aromatic–aliphatic separation from low aromatic content naphtha using 4-methyl-N-butylpyridinium tetrafluoroborate ionic liquid.* Fuel Processing Technology, **2016**. 146: p. 29-38.
232. Díaz, I., et al., *Ionic liquids as entrainers for the separation of aromatic–aliphatic hydrocarbon mixtures by extractive distillation.* Chemical Engineering Research and Design, **2016**. 115: p. 382-393.
233. Larriba, M., et al., *COSMO-based/Aspen Plus process simulation of the aromatic extraction from pyrolysis gasoline using the {[4empy][NTf_2] + [emim][DCA]} ionic liquid mixture.* Separation and Purification Technology, **2018**. 190: p. 211-227.
234. Ferro, V.R., et al., *Enterprise Ionic Liquids Database (ILUAM) for Use in Aspen ONE Programs Suite with COSMO-Based Property Methods.* Industrial & Engineering Chemistry Research, **2018**. 57(3): p. 980-989.

Publications related to this PhD thesis

1. Santiago, R., et al., *Acetylene absorption by ionic liquids: A multiscale analysis based on molecular and process simulation.* Separation and Purification Technology, **2018**. 204: p. 38-48.
2. Santiago, R., et al., *From kinetics to equilibrium control in CO_2 capture columns using Encapsulated Ionic Liquids (ENILs).* Chemical Engineering Journal, **2018**. 348: p. 661-668.
3. Santiago, R., et al., *Encapsulated Ionic Liquids to Enable the Practical Application of Amino Acid-Based Ionic Liquids in CO_2 Capture.* ACS Sustainable Chemistry & Engineering, **2018**. 6(11): p. 14178-14187.
4. Santiago, R., et al., *CO_2 capture by Supported Ionic Liquid Phase (SILP): Highlighting the role of the particle size.* ACS Sustainable Chemistry & Engineering, **2019**. 7(15): p. 13089-13097.
5. Santiago, R., et al., *Assessment of Ionic Liquids as H_2S Physical Absorbents by Thermodynamic and Kinetic Analysis based on Process Simulation*. Separation and Purification Technology, **2019. (Submitted).**
6. Santiago, R., et al., *Methanol Promoted Oxidation of Nitrogen Oxide (NOx) by Encapsulated Ionic Liquids (ENILs)*. Enviromental Science & Technology, **2019. (Submitted).**

Other publications

1. Ferro, V.R., Moya, C., Moreno, D., Santiago, R., de Riva, J., Pedrosa, G., Larriba, M., Diaz, I., and Palomar, J., *Enterprise Ionic Liquids Database (ILUAM) for Use in Aspen ONE Programs Suite with COSMO-Based Property Methods.* Industrial & Engineering Chemistry Research, **2018**. 57(3): p. 980-989.
2. Moreno, D., Ferro, V.R., de Riva, J., Santiago, R., Moya, C., Larriba, M., and Palomar, J., *Absorption refrigeration cycles based on ionic liquids: Refrigerant/absorbent selection by thermodynamic and process analysis.* Applied Energy, **2018**. 213: p. 179-194.
3. Palomar, J., Larriba, M., Lemus, J., Moreno, D., Santiago, R., Moya, C., de Riva, J., and Pedrosa, G., *Demonstrating the key role of kinetics over thermodynamics in the selection of ionic liquids for CO_2 physical absorption.* Separation and Purification Technology, **2019**. 213: p. 578-586.
4. Rodríguez-García, S., Santiago, R., López-Díaz, D., Merchán, M.D., Velázquez, M.M., Fierro, J.L.G., and Palomar, J., *Role of the Structure of Graphene Oxide Sheets on the CO_2 Adsorption Properties of Nanocomposites Based on Graphene Oxide and Polyaniline or Fe_3O_4-Nanoparticles.* ACS Sustainable Chemistry & Engineering, **2019**. 7(14): p. 12464-12473.